High-Throughput Dense Wireless Networks in Unlicensed Spectrum

by

Phillip Babatunde Oni

A thesis submitted to the
Department of Electrical and Computer Engineering
in conformity with the requirements for
the degree of Doctor of Philosophy

Queen's University
Kingston, Ontario, Canada
September 2019

Dedication

In memory of my mother, Felicia M. Oni (Oct. 2017).

Abstract

Dense deployment of wireless local area networks (WLANs) will support the prolific data traffic in future wireless networks beyond fifth generation (B5G), either as small cells for cellular data offloading or last-miles for high throughput broadband connectivity. Key technical challenges in dense deployment of WLAN access points (APs) include interference and contention from large numbers of concurrent spectrum sharing nodes, spatial reuse and coexistence of new radio access technologies (RATs), as well as legacy systems in the same bands, which could potentially degrade performance.

This thesis focuses on improving performance of high density WLAN in the presence of interference and contention among densely distributed mobile stations (STAs) and APs. Interference in high density wireless networks is inevitable and inherently depends on the distribution of users among the available APs. To that effect, multiuser (MU) based AP association is proposed to associate groups of users to maximize sum-rate to an AP, as opposed to several single-user (SU) frameworks in existence. The MU-AP association problem is solved using a proposed graph-theoretic polynomial time algorithm and a proposed dual ascent method. The proposed polynomial time algorithm requires channel knowledge to perform MU-AP association. To avert

constant a priori channel information, an alternative framework is proposed to efficiently perform association based on spatial statistics of a network.

Due to the limited number of orthogonal channels in unlicensed spectrum, high density WLAN could suffer from inefficient spatial reuse. Addressing this radio resources shortfall, new approaches are proposed to optimize the network parameters that determine spatial reuse, i.e., separation of multiple concurrent transmissions in space. The optimized network parameters of interest are the physical carrier sensing (PCS) and the energy detection (ED) thresholds. PCS threshold is used by Wireless Fidelity (WiFi) WLAN nodes to detect WiFi-like signals from active transmissions while ED thresholds are used to detect non-WiFi preambles. The proposed frameworks address efficient selection of the PCS and ED thresholds that are network-specific and improve spatial average throughput.

To jointly address the user-AP association and PCS threshold selection problem, a rate-maximizing framework is proposed. A user-AP association solution is first obtained. PCS threshold selection is then optimized based on the achieved user-AP association. The proposed AP association frameworks aim to maximize performance while taking interference into account. By combining the proposed PCS and ED thresholds selection schemes, interference is further reduced through efficient separation of multiple concurrent transmissions of high density WLAN deployments in unlicensed spectrum. Densification, inevitable in future WLANs in improving performance in the presence of large numbers of contending nodes, is critical to delivering the required service level in next generation wireless networks. Analysis of the tradeoffs between densification and overall throughput is provided to determine node densities that achieve maximum rate.

Acknowledgments

Ultimate gratitude goes to Almighty God for the gift of life and sound health to pursue this research and academic goal. My profound gratitude goes to my supervisor Prof. Steven D. Blostein for his amazing guidance and financial support; I really appreciate his unrelenting feedback, patience, and supervision. To my examiners, Prof. Ekram Hossain, Prof. Hossam S. Hassanein and Prof. Saeed Gazor, your time and feedback are greatly appreciated. Also, my sincere appreciation goes the department administrative staffs whose guidance contributed to this academic success. Specifically, Debie Fraser for the amazing supports and guidance that helped in staying on track towards degree completion. To John McKay, Mary Gillespie, Cheryl Wright and Irina Pavich, thank you for your willingness to always help.

Thank you Queen's University and School of Graduate Studies (SGS) for providing an enabling environment, supports and opportunity to pursue graduate studies. To my friends and co-players (especially, Dr. Hesham Farahat and Dr. Ali Ghobadzadeh) in the Queen's Intramural Soccer, the recreational activity was great with you guys. I appreciate my lab colleagues, Dr. Ye Li, Dr. Hongfei Wang and Dr. Majid Bavand for the valuable research discussions. God bless and keep you all. Finally, my heartfelt appreciation goes to my family, especially my parents, Deacon James Oni and Late Mrs. Felicia Oni for their prayers and excellent parenting.

Co-Authorship

This dissertation is written based on the contributions presented in the following co-authored publications with Prof. Steven D. Blostein:

Chapter 3.2 - 3.4 is based in part on:

[1] P.B. Oni and S.D. Blostein, "User-Access Point Association for High Density Uplink MIMO Wireless LANs, submitted to *IEEE Transactions on Wireless Communications*, 2018. (under revision)

Chapter 3.5 - 3.8 is based on

[2] P. B. Oni and S. D. Blostein, "User-AP Association for Performance Gains in Dense Full Duplex CSMA/CA Networks," *Proc. ICC Workshop on Full Duplex Networks*, Kansas City, May 2018.

Chapter 4 is based on:

[3] P. B. Oni and S. D. Blostein, "Optimized Physical Carrier Sensing Threshold in High Density CSMA/CA Networks," *29th Biennial Symposium on Communications*, Toronto, June 2018.

[4] P. B. Oni and S. D. Blostein, "PCS Threshold Selection for Spatial Reuse in High Density CSMA/CA MIMO Wireless Networks," *IEEE Access*, vol. 7, no. 1, pp. 112470 - 112482, December 2019.

Chapter 5 is based on:

[5] P. B. Oni and S. D. Blostein, "Optimal Node Density in 5G NR-U/WiGig Coexistence in Unlicensed mmWave Bands," *Proc. 16th Canadian Workshop on Information Theory* (CWIT), Hamilton, Ontario, Canada, June 2019.

[6] P. B. Oni and S. D. Blostein, "Throughput Maximizing Node Density for 5G NR-U/WiGig Coexistence in Unlicensed mmWave Bands," *in review: IEEE Wireless Communications Letters.*

Chapter 6 is based on:

[7] P. B. Oni and S. D. Blostein, "AP Association Optimization and CCA Threshold Adjustment in Dense WLANs," *Proc. IEEE GLOBECOM Workshop on Enabling Technologies in Future Wireless Local Area Net.*, San Diego, Dec. 2015.

[8] P. B. Oni and S. D. Blostein, "Joint User-AP Association and PCS Threshold Selection in Dense MIMO Full Duplex CSMA/CA Wireless Networks," *in preparation* for submission to *IEEE Transactions on Networking.*

Other co-authored publication:

[9] P. B. Oni and S. D. Blostein, "Decentralized AP Selection in Large-Scale Wireless LANs Considering Multi-AP Interference," *Proc. Int. Conference on Computing, Networking and Commun.* (ICNC), Silicon Valley, CA, Jan. 2017.

Abbreviations

5G	Fifth Generation
ACK	Acknowledgment Frame
AP	Access Point
B5G	Beyond 5G
BEB	Binary Exponential Backoff
BER	Bit Error Rate
BSS	Basic Service Set
CAP	Channel Access Probability
CCA	Clear Channel Assessment
CD	Collision Detection
CSMA/CA	Carrier Sense Multiple Access with Collision Avoidance
CSR	Carrier Sensing Range
CW	Contention Window
CTS	Clear to Send
DCF	Distributed Coordination Function
DIFS	Distributed Interframe Space
DL	Downlink

DSC	Dynamic Sensitivity Control
DS	Distribution System
DWLAN	Dense Wireless Local Area Networks
EIFS	Extended Interframe Space
ESS	Extended Service Set
ET	Experimental Topology
FEP	Frame Exchange Protocol
HEWSG	High Efficiency WLAN Study Group
HTTP	Hypertext Transfer Protocol
IEEE	Institute of Electrical and Electronics Engineers
ISM	Industrial, Scientific and Medical Frequency Band
ITU	International Telecommunication Union
KMA	Kuhn-Munkres Algorithm
LBT	Listen Before Talk
MAC	Medium Access Control Layer
MACh	Multiple Access Channel
mmWave	Millimeter-wave
NAV	Network Allocation Vector
NOMA	Nonorthogonal Multiple Access
OBSS	Overlapped Basic Service Set
OSI	Open System Interconnection
PCF	Point Coordination Function
PCS	Physical Carrier Sensing
PER	Packet Error Rate

PGFL	Probability Generating Functional
PHY	Physical Layer
PIFS	Priority Interframe Space
PLCP	Physical Layer Convergence Procedure
PMD	Physical Medium Dependent
PPP	Poisson Point Process
QoS	Quality of Service
RATs	Radio Access Technologies
RSSI	Received Signal Strength Indicator
RSS	Received Signal Strength
RTS	Request to Send
SIFS	Short interframe Space
SINR	Signal-to-Interference Plus Noise Ratio
SISO	Single Input Single Output
SSF	Strongest Signal First
STA	Station
STP	Successful Transmission Probability
TPC	Transmit Power Control
UL	Uplink
VCS	Virtual Carrier Sensing
VoIP	Voice Over IP
WiFi	Wireless Fidelity
WLAN	Wireless Local Area Network

Notations

Φ	Poisson Point Process
λ	Node density (or intensity of Φ)
γ	SINR threshold
Γ	PCS threshold
$\Upsilon_{\delta}(\cdot)$	Proportional fair throughput function
$U(\cdot)$	Throughput utility function
P_t	Transmit power
P^{rx}	Received power
$\|\cdot\|$	Euclidean distance between nodes
α	Path loss exponent
$\ell(\cdot)$	Path loss
$\mathcal{M}_c$	Optimal graph matching
$\mathcal{F}_i$	Frame size
$G_{(\cdot)}$	Channel gain
$\mathbf{H}$	Channel matrix
$\mathbf{h}$	Channel vector
$\mathbf{R}$	Channel correlation matrix

$\mathbf{W}$	Beamformer matrix
$\|\cdot\|^2$	Frobenius norm
$\mathbf{n}$	Noise vector
Υ	Throughput density
$\mathcal{R}_{\mathrm{SDT}}$	Spatial density of throughput
$\mathcal{P}_{\mathrm{CAP}}$	Chanel access probability
N_o	Noise power
σ_o^2	Noise variance
Ψ	Self-interference channel
$\mathit{\Gamma}(\cdot)$	Gamma function
$[\cdot]^H$	Conjugate transpose (Hermitian)
$[\cdot]^T$	Transpose of a matrix
$\mathrm{tr}(\cdot)$	Self-interference channel
$\mathbf{E}[\cdot]$	Expected value
$[\cdot]_{ii}$	Element in i^{th} row and i^{th} column
$CW_{\max}$	Maximum contention window
$CW_{\min}$	Minimum contention window
$\xi^*_{\vartheta j}$	Optimal association variable
$\mathcal{R}$	Carrier sensing range

Contents

List of Tables

List of Figures

Chapter 1

Introduction

Future wireless networks infrastructure will be deployed to provide coverage and access to a large number and/or high density of mobile devices. These devices include but not limited to wearables, home appliances, connected autonomous vehicles, industrial/manufacturing machines (under Industry 4.0 or smart manufacturing), smart traffic lights, devices for monitoring, analyzing, and treatment of medical conditions and everything Internet of Things (IoTs). With the enormous potential of wireless networking, the number of global connected devices is projected to reach 12.3 billion by 2022, which is 1.5 mobile devices per capita worldwide [3]. This implies that the wireless communication infrastructure including cellular network and networks in the unlicensed spectrum will undergo tremendous expansion and access protocol improvement is required to meet the growing connectivity demand.

It is expected that future wireless networks will provide high reliability, coverage (both *indoor* and *outdoor*) and support at least a data rate of 100 Gbps. To meet these requirements, next generation wireless networking and communication will employ enablers such as massive Multiple Input Multiple Output (MIMO), energy harvesting,

cognitive radios, as well as a full duplex and millimeter-wave (mmWave) physical layer (PHY). Implementation of these technology enablers in wireless networking in unlicensed spectrum is paramount to the provision of high data rate to support high density of mobile stations or users. This is needed because 59% of all mobile data traffic will be offloaded to wireless local area networks (WLANs) or Wireless Fidelity (Wi-Fi) and femtocells on a monthly basis. More precisely, by 2022, 51% of all Internet Protocol (IP) traffic will be Wi-Fi, 29% wired and 20% mobile [3]. This forecast necessitates improvements in wireless networking protocols and radio access technologies (RATs) such as the IEEE 802.11 Wi-Fi protocol operating in unlicensed spectrum.

1.1 Motivation

The unlicensed spectrum consists of frequency bands that are reserved globally and does not require any form of license for operations; it is often referred to as the *Industrial, Scientific and Medical* (ISM) bands. Although, the potential applications of these bands are enormous, two of the major challenges are *interference* and *fair coexistence* among different radio technologies. Since its inception in 1997, WLANs under the IEEE 802.11 standard (a.k.a Wi-Fi) are often deployed in the 2.4 GHz and 5 GHz ISM bands. With the predicted role of Wi-Fi as one of the major enablers of 5G services, spectrum shortfall (between 500 MHz and 1 GHz in some regions) [4] might disrupt or limit its potential as the core of wireless connectivity that provides high data rate for several applications. Hence, new paradigms are needed to improve the efficiency of the limited available spectrum (*spectral efficiency*) to achieve performance gains despite growing network density. This will equally assure Wi-Fi growth and its

associated global economic benefit of $3.47 trillion [5].

Wireless networking in unlicensed spectrum will be an integral part of the future wireless communication infrastructure for fifth generation (5G) and beyond 5G (B5G); serving as small cells for cellular data offloading and providing high data rates to mobile users. In other words, the emerging radio-neutral 5G will be largely supported by the next generations of Wi-Fi standards IEEE 802.11ax [6] and IEEE 802.11ad/ay [7]. Since majority of the mobile data traffic will be offloaded to IEEE 802.11 Wi-Fi or WLAN, its future operation in the 60 GHz mmWave bands is in development to support wireless Gigabits (WiGig) transmissions [7–9]. WLANs are ubiquitous today due to high data rate connectivity at affordable cost, easy deployment and the close proximity of access points (APs) to mobile stations (STAs).

Allowing 51% of future mobile IP traffic to traverse WLAN comes with some technical challenges that need to be addressed in order to leverage its enormous potential. First, is *interference management*, which deals with minimizing the effects of interference from large numbers of concurrent mobile users or nodes sharing the spectrum. Secondly, the issue of *spatial reuse* remains in WLAN due to the large number of APs that are deployed on limited number of orthogonal channels, and with the envisaged high density of future networks, this problem becomes more aggravated. Additionally, separating multiple concurrent transmissions is challenging due to the inherent multiple overlapped Basic Service Set (BSS)[1] in dense WLANs. Third, is the *coexistence* of IEEE 802.11 Wi-Fi RAT with other RATs and technologies that occupy the unlicensed spectrum today. In terms of coexistence, the most challenging part is the fair coexistence of 802.11 WLANs with cellular RATs such as the Long

[1] An AP with its associated STAs within a coverage area is referred to as the *Basic Service Set* (BSS), which is analogous to a *cell* in cellular networks (Discussed later in Section 2.1.1).

term evolution in unlicensed bands (LTE-U) or Licensed Assisted Access (LAA) and its emerging variant known as 5G New Radio in unlicensed bands (5G NR-U).

1.1.1 Challenges and Drawbacks of Channel Access Protocol

The three aforementioned challenges (*interference*, *spatial reuse* and *coexistence*) are rooted in the channel access protocols that govern fair spectrum sharing in WLANs. Inevitably, providing high date rates leads to the deployment of high density APs to support the explosive traffic from densely distributed STAs. Some of the consequences of high density WLAN deployments under the existing channel and users coordination protocols are expatiated as follows.

1.1.2 Spatial Reuse and Interference in High Density WLANs

On the spatial reuse, 802.11 protocol uses the *Carrier Sense Multiple Access with Collision Avoidance* (CSMA/CA) to coordinate access to the channel and forbids two or more nodes within the carrier sensing range (CSR) to transmit concurrently in the same time slot. CSR represents the contention domain and only one node among other nodes within the CSR can transmit in each time slot. CSMA/CA determines the CSR based on the specified Physical Carrier Sensing (PCS) threshold Γ used by the PHY to determine if channel is *idle* or *busy* [10]. CSMA/CA protocol requires that each node checks the channel through the PCS process performed by the PHY, and if the sensed signal power is above the PCS threshold, the PHY reports a busy channel and the node defers transmission until the channel becomes available. This PCS process is primarily used by the CSMA/CA protocol to prevent collisions by permitting only one node in a CSR to transmit per time slot, which means only a

subset of nodes in the network can transmit in each time slot.

Consequently, the PCS threshold determines the number of concurrent transmissions per time slot permitted by the CSMA/CA protocol. Most implementations of CSMA/CA protocol in commercial devices adopt a fixed PCS threshold, which is not optimized for performance in large-scale wireless networks. This important network parameter, especially for high density networks, must be carefully chosen to enhance spatial reuse and performance through real-time adaptation based on measured network parameters [11–14]. On one hand, a lower (or conservative) PCS threshold will permit more concurrent transmissions, and that implies high interference. On the other hand, a higher PCS threshold reduces spatial reuse and degrades aggregate performance in the network. Therefore, the fundamental research questions (RQs) are posed as follows:

RQ.1 How do we select the PCS threshold Γ *to improve performance gains without incurring excessive interference and jeopardizing spatial reuse?*

RQ.2 How to design PCS threshold values taking into account the node density, transmit power, path loss exponent and other network parameters that are usually known a priori?

RQ.3 How do we optimize the PCS threshold Γ *to achieve a balance in the trade off between the hidden terminal problem and the exposed terminal problem?*

More details on this issue of selecting PCS threshold and why it is important for future high density WLANs, are discussed in Section 2.1.4. With high density of APs and STAs transmitting concurrently in the downlink (DL) and uplink (UL), respectively, high interference and contention are among the major issues. Increasing the number

of concurrent transmitters per network area is tantamount to amplifying the interference footprint in the network. Therefore, new interference avoidance techniques are required to improve performance of future high density WLANs. Arguably, the level of interference in a WLAN depends on the distribution of STAs (users) among APs through association (AP selection) and the PCS threshold value that is being used for spatial reuse. This leads to the following RQs:

RQ.4 *What is the optimal user-AP association that guarantees the worst-case interference distribution or footprint in high density WLANs?*

RQ.5 *How to design a framework that jointly considers user-AP association and PCS threshold selection?*

1.1.3 Fair Coexistence in High Density WLANs

Let not forget that WiFi nodes need to share the spectrum with other wireless technologies such as Bluetooth, UWB etc as well as the emerging Long Term Evolution small cells in unlicensed band (LTE-U) [15]. With the emergence of dense 802.11 networks, it is important to consider the coexistence of WiFi systems with other wireless systems or technologies that use the same ISM band (2.4 GHz and 5 GHz) and the mmWave bands for transmission. For improved performance of 802.11 networks, WiFi nodes must be able to coexist in any heterogeneous environment where technologies like Bluetooth, Zig-Bee, and LTE-U exist [16, 17].

The most important coexistence is with LTE-U small cells and its 5G NR-U variant [18–20] that are being deployed at customer premises. Similarly, coexistence of new 802.11 nodes (such as 802.11ac APs) with legacy nodes is very important. This is because *collision* and transmission *deferrals* occur when the 20 MHz primary channel

of a legacy AP is anywhere within the 80 or 160 GHz of an 802.11ac AP, and the clients of 802.11ac APs and legacy AP transmit at the same time. Consequently, in addition to developing new *carrier sensing* scheme for WiFi systems, new coexistence schemes are needed for WiFi nodes to detect the presence of non-WiFi transmissions and make smart decisions; defining a PCS threshold that enables WiFi nodes to optimally detect the presence of non-WiFi transmissions is also of interest. Coexisting multiple RATs in a WLAN increases the interference footprint in the network, thereby degrading the overall performance due to increased interference.

Unlike WiFi (802.11) only WLANs, in a mixed RATs WLANs, WiFi nodes contend with other WiFi and non-WiFi nodes for channel access. Take 5G NR-U and WiGig Coexistence for example, due to the PHY layer discrepancy NR-U nodes are not able to decode WiGig signals and vice versa [21–23]. In such coexisting WLANs, during carrier sensing or PCS process, a WiFi node detects the presence of other WiFi-like signals using *signal detection* and compares the detected signal power to the PCS threshold to determine if the channel is *idle* or *busy*. On the contrary, since 802.11 (WiFi) nodes are unable to decode non-WiFi signals, a WiFi node uses *energy detection* (ED) to detect the presence of active non-WiFi (e.g. 5G NR-U) transmissions and compares the detected energy to a threshold known as the ED threshold to determine a *busy* or *idle* channel. This mandatory *protocol-level* process is aimed at reducing *collision* and ensuring fair channel access among nodes. Therefore

RQ.6 What are the optimal ED and PCS thresholds for fair coexistence and performance maximization in coexisting wireless networks?.

Coexistence of multi-RATs in a WLAN causes the total node density to grow and performance becomes intra-RAT and inter-RAT interference limited. In other words,

increasing network density (*densification*) increases interference and contention, and subsequently degrades aggregate performance. This tradeoff between performance and network *densification* leads to the following RQs:

RQ.7 *What are the optimal node densities to guarantee best performance in high density multi-RAT WLANs?*

RQ.8 *What is the trade-off between the maximum throughput per unit area and the propagation characteristics?*

1.2 Objectives and Thesis Contributions

Motivated by the future impacts of wireless networking in the unlicensed spectrum, this thesis addresses the aforementioned questions. Fundamentally, the above research questions *RQ.1*, *RQ.2*, *RQ.3*, and *RQ.6* are related and herein, the aim is to optimize the PCS and the ED thresholds to maximize spatial average of performance in high density WLANs. The objective is to provide frameworks that guide the PCS and ED thresholds selection that are network specific (in terms of propagation characteristics, node density, antenna configuration and transmit power). That is, adapting the PCS and ED thresholds to other network parameters upon which overall network performance depend on.

Questions *RQ.4* and *RQ.5* are posed to address the issue of inefficient AP selection in high density WLAN. Current strongest signal first (SSF) (a.k.a best receive signal strength (RSS)) scheme used in existing WLAN systems has been shown to be ineffective, and it might worsen performance in interference-dominated high density WLANs. The aim of *RQ.4* and *RQ.5* is primarily to distribute STAs (users) among

APs to tolerate the worst-case interference level in the network. The last set of questions, *RQ.7* and *RQ.8* will lead to answers that provide analytical framework for designing coexisting WLANs. Basically, to address the tradeoff between *densification* and performance, that is, to determine the maximum node density per network area that guarantees best performance.

1.2.1 Thesis Contributions

Consequently, this research addresses scalable design of future high density WLANs to improve performance in the presence of multiple concurrent transmissions and large-number of nodes contending for the limited radio resource in unlicensed spectrum. In addressing the above research questions, the contributions of this thesis are highlighted as follows:

1. On the user-AP association scheme, an efficient distributed framework to associate multi-user (MU) group to an AP is proposed in Chapter 3, as opposed to the several schemes in literature that aimed at single-user (SU) association with the AP. The MU-group-AP association problem is formulated as a *logarithmic* throughput maximization problem, which is solved using a proposed *polynomial-time* graph-based algorithm and a proposed *Dual ascent* method.

2. Since the proposed multiuser-AP association algorithm above requires channel information and network measurement to solve the utility maximization problem, another framework is proposed to efficiently perform association based on *spatial statistics* rather than on deterministic user-AP channels that require constant updates or *a priori* channel information. To that effect, a scheme is proposed to find a set of user-AP associations that maximizes FD mean rate

utility, which represents a spatial average of performance. This is important because spectral efficiency and overall network performance depend on the interference distribution, and the interference distribution somewhat depends on the spatial pattern at which users are distributed among AP.

3. In the above contributions, PCS threshold is fixed regardless of the node density, transmit power and other network parameters. To address the PCS threshold selection problem for WiFi-only WLANs and assuming node locations are realizations of Poisson point process (PPP), closed-form expressions for selecting optimal PCS threshold are proposed in Chapter 4. The PCS threshold value that maximizes the *spatial density of throughput* (SDT) is determined. This important network parameter determines the spatial reuse permitted by the CSMA/CA protocol, which consequently determines the interference level. In contrast to several existing methods that depend heavily on frequent channel measurement, the proposed PCS threshold selection is based mainly on *a-priori* knowledge of the network such as node density, path loss exponent and required minimum SINR.

4. For WLAN coexistence, the above SDT-maximizing PCS threshold selection problem is extended to multi-RATs coexistence WLAN. To address spatial reuse in WLAN coexistence, both the PCS and ED thresholds are optimized. This contribution in Chapter 5 captures the propagation characteristics of the mmWave bands in optimizing the PCS/ED thresholds specific for multi-RAT coexistence WLAN. Unlike existing studies on WLAN multi-RAT coexistence, we propose an analysis of the optimal node density that guarantees minimum tolerable interference in a WLAN coexistence. The proposed analysis shows

that the degree of network *densification* depends on the minimum guaranteed throughput in terms of SINR threshold.

5. Thus far, in existing literature, the AP association and the PCS threshold selection problems are solved independently. Based on our knowledge of the state-of-the-art research on WLAN, for the first time, a new framework is proposed in Chapter 6 to jointly solve the user-AP association and PCS threshold selection problems for future full duplex (FD) MIMO WLANs in the presence of interference and self-interference of FD transmissions.

Considering the PHY characteristics of future WLAN systems equipped with FD capability alongside MIMO at the STAs, the PHY layer model in this thesis considers FD and MIMO. Additionally, uplink seems to be the bottleneck in dense WLAN mainly because large number of users contend for the limited radio resources. Therefore, while the throughput objective is easily generalized to downlink, the performance objective in thesis is centered on enhancing per-user throughput in uplink transmissions.

1.3 Thesis Organization

In Chapter 2, general background on WLAN systems is provided; covering the architecture and channel access protocol (CSMA/CA). Some of the limitations of the existing user-AP association and the PCS threshold selection schemes are also discussed. In addition, *stochastic geometry* properties of the PPP used in this thesis are presented. In Chapter 3, dual-ascent based and graph-theoretic multiuser-AP association frameworks are proposed. The performance and significance of the proposed schemes over the existing strongest signal first (SSF) scheme are discussed. In

addition, the user-AP association problem is reformulated to maximize throughput utility function for future full duplex (FD) WLANs. The framework is developed for FD SISO and MIMO and seeks AP association set that maximizes spatial average of performance. This framework differs from that of the graph-based and dual ascent schemes as it does not require network information but uses the spatial statistics to optimize user-AP association.

In Chapter 4, two frameworks are proposed for PCS threshold selection in SISO and MIMO WLANs with their respective system model, problem formulations and performance evaluation. Chapter 5 is dedicated to the proposed PCS/ED threshold selection schemes for multi-RAT coexistence WLANs. Also, an analysis on the trade-off between densification and performance is provided. To consider a joint solution for the AP association and PCS threshold selection problems addressed in Chapters 3 and 4, respectively, a joint framework is proposed in Chapter 6. To conclude this dissertation, Chapter 7 summarizes the contributions, highlights the main findings in this research, and provides suggestions for future research directions.

Chapter 2

Background

Background on the problems addressed in this thesis is provided in this chapter. It contains related existing studies on the same subject. In Section 2.1, an overview of the is presented; encompassing the WLAN architecture, WiFi protocols and IEEE 802.11 standards with focus on the physical and the data link layer. Section 2.2 discusses the evolution of WLAN and highlights the emerging standard promoting dense WLANs and future applications of WLAN. In Section 2.3, the fundamentals of stochastic geometry tools applied in this thesis are discussed.

2.1 Wireless Local Area Network

Since the inception of wireless communications in the unlicensed spectrum, specifically, the Industrial, Scientific and Medical (ISM) frequency band, wireless connectivity has been enhanced with high speed data rate compared to the traditional cellular systems where packetized traffic is transmitted at lower speed. Wireless networks can be categorized into three types based on their geographical coverage, which are Wireless Local Area Networks (WLANs), Wireless Personal Area Networks (WPANs) and

Wireless Metropolitan Area Networks (WMANs) [24]. WLAN a.k.a wireless fidelity (WiFi) provides local coverage in large indoor environments such as campus buildings, enterprise buildings, multi-tenant apartments, airports, stadium, and private homes using 2.4 GHz and 5 GHz ISM bands, which are globally unlicensed.

As discussed later in this thesis, standards are being developed for future WLAN to allow operation of WLANs in other spectrum such as the 60 GHz millimeter-wave (mmWave), which will deliver gigabit data rates. Since the introduction of wireless connectivity to the ISM bands, standardization bodies such as the Institute of Electrical and Electronics Engineers (IEEE) have developed standards for WLAN operations. The IEEE 802.11 standard developed by IEEE has been the most adopted standard for designing WLAN systems for interoperability. Consequently, the investigation in this thesis is focused mainly on the IEEE 802.11 WLAN systems.

2.1.1 IEEE 802.11 WLAN System Architecture

Interoperability among WLAN devices from different vendors is very important to the entire functionality of WLANs. IEEE 802.11 standards are aimed at ensuring interoperability by defining how WLAN devices such as access points (APs) and user stations (STAs) communicate with one another. IEEE 802.11 standards are based on the conventional layered architecture, the open system interconnection (OSI) model, to specify the lower layers of the OSI model [1], namely, the *Physical Layer* (PHY) and the *Medium Access Control Layer* (MAC) sublayer. More specifically, the IEEE 802.11 standard the MAC sublayer, MAC management protocols and services, and three PHY layers [25], [26]. The MAC sublayer protects data, provides reliable data delivery services and fair control access to the shared spectrum or wireless medium.

Data protection is achieved in the 802.11 protocol through privacy services that encrypt the data sent over the wireless channel. The IEEE 802.11 MAC uses frame exchange protocol at the MAC level to improve the reliability of data.

To control access to the shared channel, two access mechanisms are defined: the *Distributed Coordination Function* (DCF) and the *Point Coordination Function* (PCF). While the DCF access mechanism is distributed at the STAs, the PCF protocol is a centralized access mechanism, which is usually deployed at the APs. The investigation in this thesis considers the DCF channel access mechanism, which uses the *Carrier Sense Multiple Access with Collision Avoidance* (CSMA/CA) to control access to the shared medium. Operation of the CSMA/CA protocol is explained in Section 2.1.3. Figure 2.1 depicts the protocol architecture of IEEE 802.11. The PHY is an interface between the MAC layer and the wireless channel, and mainly responsible for transmitting and receiving data frames over the wireless channel [25], [1], [24].

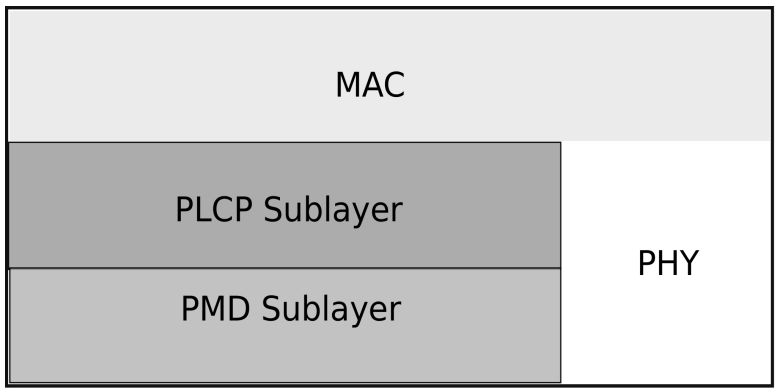

Figure 2.1: IEEE 802.11 Layered Protocol [1].

The PHY layer is consists of two sublayers known as the *Physical Layer Convergence Procedure* (PLCP) and the *Physical Medium Dependent* (PMD). The PLCP is used by the PHY to provide frame exchange between the MAC and PHY. The

transmission of payload is achieved through the PMD sublayer by using signal carrier and spread spectrum modulation [1]. In addition, the PHY provides a carrier sense indication to inform the MAC about the channel activity per time-slot [27], [1]. This carrier sense indication is an integral part of the CSMA/CA protocol and it is performed by the PHY using the *Physical Carrier Sensing* (PCS) process, which is the process whereby the PHY checks the activity of the channel and reports back to the MAC. This process and how it impacts the performance of CSMA/CA protocol is discussed in detail in Section 2.1.4.

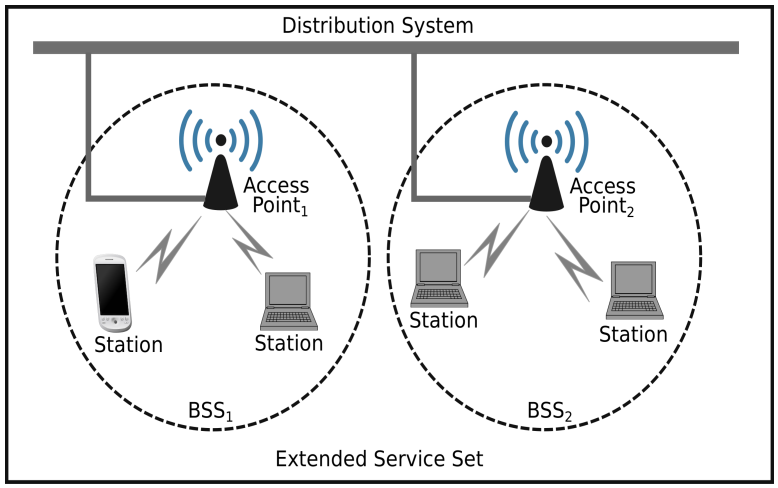

Figure 2.2: An Infrastructure WLAN.

A typical WLAN can be implemented to support two main operating modes specified in the IEEE 802.11 standards, which are infrastructure and ad hoc (or independent) modes. In infrastructure mode depicted in Figure 2.2, a WLAN is made up of the stations (STAs) or user equipment (UEs), access points (APs), wireless medium and the distribution system (DS). As shown in Figure 2.2, an AP with its associated STAs within a coverage area is referred to as the *Basic Service Set* (BSS) and a network with two or more connected BSSs is called the extended service set

(ESS). In practical terms, an ESS belongs to a specific operator and each ESS has a unique identifier known as the Service Set Identifier (SSID). Several APs in the ESS are interconnected through the DS backbone to provide distribution services to STAs. For instance, when an STA roams from one BSS to another, APs use the DS to forward data from one AP to another for the roaming STA. Each BSS controls access to the shared medium using the CSMA/CA with DCF.

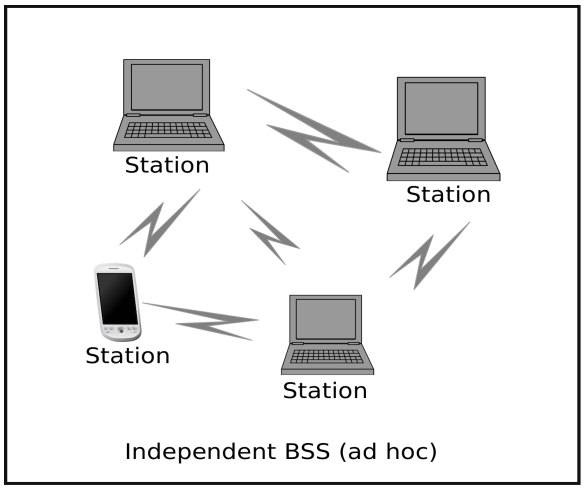

Figure 2.3: An ad hoc (or independent) WLAN.

Figure 2.3 shows the *independent* mode, the nodes can communicate directly with each other without the need for a central node (AP). For one node to communicate with the other, the transmitting STA establishes an ad hoc link with the receiver node before commencing transmission; STAs (or nodes) have direct links with one another for the duration of a communication session. In independent node, there are multiple failure points. Ad hoc mode has found applications in many areas today including military tactic missions for temporary wireless communication, home networks and other types of sensor networks. This thesis focuses on the *infrastructure* WLAN where there are several APs and STAs to form a large or high density network. Next, the

AP selection or association is discussed.

2.1.2 Access Point Association in WLAN

To provide coverage in an infrastructure WLAN, an operator often deploys several APs that are interconnected for seamless service. In some cases such as multi-tenant apartment buildings, several independently controlled APs are deployed by independent owners on the available limited channels. Users arriving to the network need to select an AP among several APs in order to gain access to the network. The procedure to select or associate with an AP is highlighted as follows and depicted in Figure 2.4. When a user (or STA) enters the network, its initial state is State 1, and while in this state, the user attempts to discover APs in the network. Two *management frames* are employed by the STA to discover APs, namely, *Beacon frame* and *Probe request frame* [1].

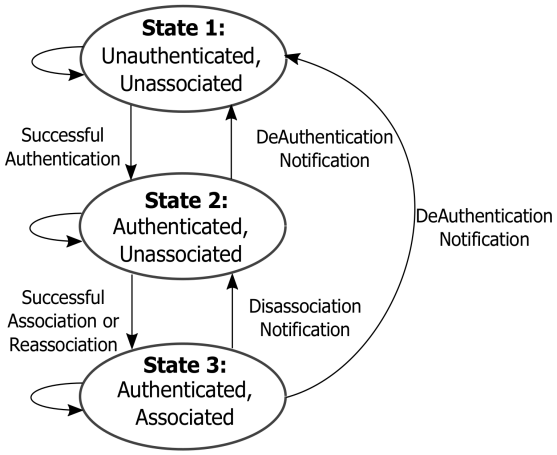

Figure 2.4: Access Point Association Procedure [1].

APs within an ESS periodically broadcast the Beacon frame to allow STAs discover available BSSs. Each AP appends specific information in the Beacon frame such as

the network SSID, supported data rate, timestamp, PHY parameters, Beacon interval and other Quality of Service (QoS) information. STAs continue to monitor or listen on specific channels to capture Beacon frames to discover APs; this method is known as *Passive scanning*. Alternatively, STAs could use the *Probe request frame* in a process known as *Active scanning* to discover APs. Under this Active scanning, a STA broadcasts *Probe request frame* and waits for an AP to respond with a *Probe response frame*. The *Probe response frame* contains similar information conveyed using Beacon frame under the *Passive scanning*. In terms of time to discover an AP, the *Active scanning* is faster than the *Passive scanning* because depending on the Beacon frame interval or loss rate, a STA could spend longer time in the channel in anticipation of a Beacon frame.

Once an STA discovers an AP either through the *Passive scanning* or *Active scanning*, it sends *Authentication request frame* to the AP and upon successful authentication, the STA transits to State 2 as shown in Figure 2.4. Subsequent to the authentication state, the STA sends *Association request frame* to the AP and the AP responds with *Association response frame*. Once a STA is authenticated and associated in State 3, the STA has fully joined the network for access. During the frame exchange procedure for AP association, APs often include information such as supported data rate, QoS, PHY and security settings that facilitate the STA's seamless connectivity. Upon authentication and association, STAs are allowed to contend for transmission opportunity with other STAs associated with the same AP. In the next section, this medium sharing/access procedure is discussed.

2.1.3 IEEE 802.11 Channel Access Protocol

As with other generations of radio access technologies (RATs), WLAN is confronted with spectrum (radio resource) scarcity. Due to the limited number of available orthogonal channels, especially in 2.4 GHz and 5 GHz ISM bands, several nodes contend for transmission opportunity. Access to the channel is controlled by the CSMA/CA with *binary exponential backoff* (BEB), which requires that a STA listen to the channel before commencing a transmission and if the channel is *busy* or occupied by another transmissions, it defers its transmission. In other words, the CSMA/CA protocol is a type of "Listen-Before-Talk" (LBT) protocol. The process of checking if the medium is busy or not, is the CSMA part of this access scheme, and it is coordinated using the PCS mechanism of the PHY; the PCS mechanism is discussed later in Section 2.1.4. Without the channel sensing process, a STA would commence transmission and cause collision with ongoing transmission in the channel; this leads to persistent retransmissions and increased *Packet Error Rate* (PER).

When packets become available in the *buffer*, the MAC informs the PHY to perform the PCS process. In event that the medium is sensed to be *busy* (detecting the presence of an active transmission), the listening STA defers its transmission and waits for a period determined by the BEB algorithm [1]. The BEB algorithm generates a random waiting time *uniformly distributed* in a range known as the contention window (CW), and the CW varies from PHY to PHY. The listening STA defers its transmission and begins transmission after the backoff time elapses [1], [25], [26]. To implement the collision avoidance (CA) part of the CSMA/CA, the MAC layer uses a time value known as the *Network Allocation Vector* (NAV) to inform a STA of the time left until the channel becomes *idle* or available. During the *busy* channel, each

frame in the channel carries the NAV value so that listen STAs become aware of the time. NAV is a *Virtual Carrier Sensing* (VCS) technique and when it is enabled, a STA avoids transmitting even though the PCS indicates that the channel is idle. Combining the PCS with the NAV, unprecedented collision is avoided [26], [25], [1].

Under the CSMA/CA protocol, five timing intervals are very useful in the channel sensing and backoff procedure. There timing intervals are *Slot-time*, *Short interframe Space* (SIFS), *Priority Interframe Space* (PIFS), *Distributed Interframe Space* (DIFS) and *Extended Interframe Space* (EIFS). While *Slot-time* and SIFS are the two basic time intervals determined by the PHY (or PHY-dependent), PIFS, DIFS and EIFS are determined from *Slot-time* and SIFS [1], [26]. Recall that the 802.11 MAC standard specifies DCF and PCF as two medium access configuration in the MAC protocol. The former is distributed at the STAs while the latter is a centrally controlled access mechanism. While DCF guarantees equal access and *best effort* services, PCF is suitable for real-time application/services. Although DCF is a *contention-based* scheme while PCF is *contention-free*, both methods can be combined to implement a hybrid access method. With the hybrid mechanism, a contention-free period is followed by a contention period; that is, DCF is used subsequent to PCF [28].

With PCF, there is a centralized AP coordinating access to the medium. Under the PCF access mechanism, a STA begins to transmit when permission is granted by the AP. When DCF is being used, access to the medium is coordinated using the CSMA/CA. Throughout this thesis, the DCF mechanism (i.e. all STAs on the WLAN are DCF-enabled) is considered mainly because of its distributed nature, which gives STAs the liberty to autonomously make AP association decisions using the CSMA/CA protocol. Under the DCF mechanism, a STA with packets to transmit

sends request to the MAC layer. The MAC then checks if the channel is flagged *idle* or *busy* by both PCS and VCS. If both schemes report an *idle* channel for a time interval of DIFS ($= 2 \times$ Slot-time $+$ SIFS), the MAC proceeds with the transmission. Figure 2.5 depicts this process. At the end of the previous transmission, the MAC checks the channel status and waits for a DIFS and begins the next transmission if the channel remains *idle* for a DIFS. The goal is to prevent collisions with ongoing transmissions or with the acknowledgment (ACK) frame of the previous transmission.

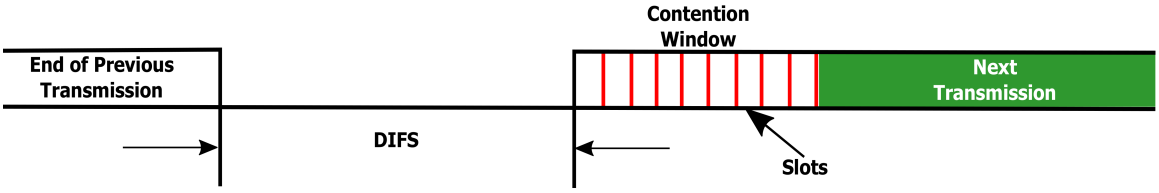

Figure 2.5: DCF timing under CSMA/CA [1].

An ACK frame is used by the receiver to inform the transmitter of a successfully or correctly received frame. If the ACK frame is not received, a collision or an error is deemed to have occurred and the MAC checks with PCS and VCS to see if the channel is idle for EIFS before commencing a new transmission. In the case of a collision, a *retry counter* is initiated and depends on the length of the frame, it indicates the number of times the frame may be retransmitted. If either the PCS or VCS flags the medium as busy during the DIFS, using the BEB algorithm, the MAC chooses a uniformly distributed backoff interval within a range known as the *Contention Window* (CW). For every attempted transmission that is deferred, the CW doubles until the maximum CW (CW_{max}) is reached, and when a frame is successfully transmitted, the CW is reset to the minimum CW (CW_{min}) for the next transmission. The values of CW_{max} and CW_{min} are fixed in PHY but varies from PHY to PHY depending on the supported 802.11 standard or generation [26], [1].

2.1.4 Physical Carrier Sensing (PCS) in WLAN

For an effective CSMA/CA protocol or channel access control in 802.11 WLAN, the PCS and the VCS processes are very important because they report channel status to the MAC and inefficient report is detrimental to overall system performance. The VCS is a supplemental scheme in 802.11 standard aiming to minimize the effect of the *hidden terminal* problem [1]. Herein, the focus is on the PCS process as it forms an integral part of this thesis. In other literature, the PCS process is referred to as the *Clear Channel Assessment* (CCA) process but for easy readability, it is simply called PCS. Since CSMA is a LBT protocol, when the MAC layer receives transmission request from a node, it requests *channel status* from the PHY and in response, the PHY provides CCA signal to MAC indicating an *idle channel* or a *busy channel*. This mainly to indicate whether other nodes are using the channel or not [26], [1].

To determine *channel status*, the PHY interfaces with the wireless channel or air medium and measures the signal power or energy in the channel. If the measured signal or energy is above a threshold known as the PCS or CCA threshold, the PHY flags the channel as busy and reports a *busy channel* back to the MAC. Otherwise, if the measured signal or energy is below the PCS threshold, an *idle channel* is reported back to the MAC. The PCS threshold is an important parameter in WLAN as it determines the degree of spatial reuse and the number of concurrent transmitters in a multi-AP or multi-BSS WLAN, and consequently, it impacts the overall performance. To illustrate, Figure 2.6 depicts a scenario.

In the system scenario of Figure 2.6, the coverage area of an AP (or a BSS) is depicted with a circle. All STAs within the same coverage area of a BSS, compete to access the channel on which the AP is deployed. The major drawback of such a shared

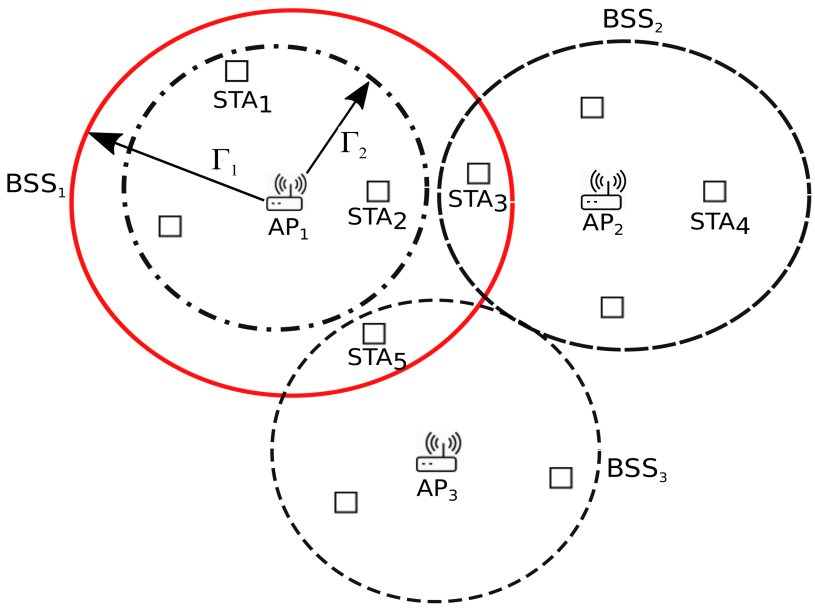

Figure 2.6: Physical carrier sensing under CSMA/CA protocol.

medium is that whenever an STA is transmitting, other STAs defer their transmissions and wait for the STA occupying the channel to finish its transmission. STAs sense the channel using the PCS mechanism at the PHY because the CSMA/CA requires that each node senses the channel before commencing transmission. During this channel assessment period, the *PCS threshold* is used to determine if the channel is busy or idle. If the signal energy sensed during the PCS is above the PCS threshold, the PHY informs the MAC that the channel is busy. Consequently, the node performing the PCS defers its transmission until the channel becomes idle; the channel is idle when the energy sensed on the channel is below the PCS threshold. The deferment of transmissions due to a busy channel could severely impair performance in dense WLAN environments.

To buttress this assertion, let us consider the impact of PCS on AP_1 in Figure 2.6.

Assuming the PCS threshold in BSS_1 to be Γ_1, the solid circle becomes the carrier sensing range of AP_1 and its associated STAs, which cover STA_3 and STA_5 that are associated with AP_2 and AP_3 respectively. Consequently, in compliance with CSMA/CA procedures, AP_1 will always defer its transmission whenever STA_3 in BSS_2 or STA_5 in BSS_3 is transmitting or occupies the channel, assuming that the three APs are deployed on the same channel for spatial reuse. On the other hand, setting the PCS threshold to Γ_2 in BSS_1 alleviates this problem, and thus AP_1 assumes the signals coming from STA_3 and STA_5 as tolerable interferences rather than deferring its transmission.

With Γ_2 as the PCS threshold value, the carrier sensing range (CSR) shrinks as depicted with the dashed circle covering BSS_1, hence, AP_1, STA_3 and STA_5 can transmit simultaneously in their respective BSS, thereby increasing the number of spatially separated concurrent transmissions. For dense deployments, APs are deployed much more closely than the conventional 100 m spatial reuse distance between co-channel APs. As illustrated with Figure 2.6, AP_1 will defer its transmission when STA_3 is transmitting if they are both operating on the same channel and the PCS threshold of AP_1 covers STA_3. Otherwise, AP_1 ignores and treats the signal coming from STA_3 as interference.

2.1.5 Physical Carrier Sensing in Coexisting Networks

The above discussion covers the PCS process in a WLAN where only WiFi RAT exists. The coexistence of WiFi APs with other non-WiFi or WiFi-like signals present new challenges. There are other wireless technologies existing and operating in the ISM unlicensed band. The ability of Wi-Fi nodes to peacefully coexist with these

technologies, would enhance throughput of dense WLAN (DWLAN). A more recent wireless technology that is harnessing the ISM band is the long term evolution in the unlicensed band (LTE-U) around 5 GHz. The goal of the LTE-U is to offload high cellular traffic to the inactive unlicensed band [15], [29], [30]. *Rate diversity and fairness*, *random losses and TCP performance* and *traffic asymmetry* are other factors degrading performance in large Wi-Fi networks [31]. The ongoing 3rd Generation Partnership Project (3GPP) New Radio (NR) access technology standardization for fifth generation (5G) [18], [20] is expected to support variants of unlicensed bands [19], [32], analogous to the 4G Long Term Evolution (LTE) in unlicensed band (LTE-U).

LTE-U systems that coexist with incumbent Wi-Fi systems in the 5 GHz band. In the same vein, the 5G NR in unlicensed band (NR-U) will coexist with the wireless gigabit (WiGig) Wi-Fi (or IEEE 802.11ad/ay) in the 60 GHz band [8], [33]. When WiFi nodes coexist with other RATs such as the 5G NR-U, WiFi nodes are mandated to detect both ongoing WiFi and non-WiFi transmissions. Due to PHY layer differences, WiGig nodes are unable to decode NR-U signals, and vice versa. Therefore, WiGig nodes use coherent *signal detection* to detect active WiFi transmission and use *energy detection* (ED) to detect the presence of an NR-U transmission. A WiGig node detects other WiGig transmissions by comparing the signal level in the channel to a PCS threshold Γ_{WG}, and detects NR-U transmissions by comparing the energy level in the channel to an ED threshold Γ_{WG}^{ed}. If either the signal power or energy is above Γ_{WG} or Γ_{WG}^{ed}, the CSMA/CA protocol reports a *busy* channel.

2.2 Evolution of 802.11 WLAN and the Future WLAN

The first *ratified* standard (IEEE 802.11) released in 1999 [1] contains specifications for the operations of a Wi-Fi network and this standard has passed through some amendments as summarized in Table 1 in [34], which compares the features of the different 802.11 generations. The standard has been modified from generation to generation in order to achieve *gigabit* data rates, with the most recent ratified standard being IEEE 802.11ac, which promises at least 500 Mbps on a 80 MHz channel with 8 *spatial streams*. IEEE 802.11ac inherited certain features from 802.11n, which include static/dynamic channel bonding and multiple simultaneous data streams using multi-user multiple-input multiple-output (MU-MIMO). These new features are mainly PHY layer specifications. However, some changes at the MAC are proposed to ensure that the MAC is compatible with the enhanced PHY. IEEE 802.11ac retains the beamforming capability of 802.11n but extends channelization to a wider channel width [34].

The standard that motivates this research is still ongoing under the High Efficiency WLAN Study Group (HEW SG) and it is scheduled for ratification in 2019. The IEEE 802.11ax standard is aimed at improving spectrum efficiency to enhance the network *throughput per area* in DWLAN [15], [6]. There are other standards in the IEEE 802.11 series, IEEE 802.11ah [35] is another one, which is mainly proposed to allow 802.11ah-enabled nodes to operate in the 1 GHz band as opposed to the conventional 2.4 GHz and 5 GHz bands. IEEE 802.11ah is being developed mainly for IoT devices. The two main specifications in all of these standards are the MAC protocol and the PHY layer. Other functionalities for 802.11 networks are specified in different standards such as security enhancement in 802.11i and quality of service

(QoS) in 802.11e [1]. Other future WLAN systems include IEEE 802.11ad (WiGi) that will operate in the higher frequencies (up to 60 GHz), also known as millimeter wave (mmWae) 60 GHz band to deliver multi-Gb/s data rates. This emerging wireless technology will introduce WiFi tri-band (2.4 GHz, 5 GHz and 60 GHz) products to consumers [36]. Therefore, for B5G, one technique to increase capacity in 5G is the use of small cells, and most femtocells will have WiFi-like ranges [37], [38]. Ultra-densification, mmWave and massive MIMO are the three main 5G technologies [37].

2.2.1 IEEE 802.11ax: High Density WLAN Deployments

Ongoing standardization of IEEE 802.11ax for DWLAN has been initiated by the IEEE *High Efficiency WLAN Study Group* (HEWSG) with the goal of improving per-node throughput of DWLAN in the presence of sources of interference. The ongoing activities to standardize 802.11ax for emerging applications motivates this research. Approaches of the IEEE 802.11ax Task Group to enhance node throughput in DWLAN are *congestion control*, *interference* and *frame conflicts mitigation*. IEEE 802.11ax APs and devices are expected to hit the market in 2019 and 802.11ax is expected to deliver upto 10 Gbps [6], [15]. Reducing the size of control frames (minimizing overhead) and increasing the data frame size aim to resolve the congestion problem in DWLAN by preventing nodes from occupying the channel for a longer period of time. The hidden terminal problem is responsible for frame conflicts in hidden STAs, and frame conflicts can be reduced by modifying the channel access scheme and overlapped BSS (OBSS) management [6], [15]. Interference mitigation in DWLAN is possible through PCS and other interference cancellation schemes.

2.3 Stochastic Geometry Preliminaries

Stochastic geometry is an area of mathematical statistics that provides tools and models for studying and analyzing random spatial patterns. Stochastic geometry tools are suitable in modeling spatial average of performance in wireless communications [28], [39]. This section provides the mathematical preliminaries of the main stochastic geometry principles applied in this thesis. The geographical locations of nodes in wireless networks can be modeled as realizations of a point process. There are different types of point processes, which include *Binomial Point Process* (BPP), *Poisson Point Process* (PPP), *Poisson Cluster Process* (PCP) etc., but in this thesis the PPP is adopted; readers interested in a detailed description are referred to [40]. Generally, a point process on $\mathbb{R}^d$ is a random variable which takes values from the set of simple and finite sequences $\mathbf{X}$; finite number of points in any bounded subset of $\mathbb{R}^d$ [40], [28].

2.3.1 Poisson Point Process (PPP)

PPP is the most studied point process, and because of its ease of analysis, it is used in several studies (e.g. [41], [39], [42], [43], [44],) related to wireless communications. Let Φ represent a stationary PPP of density λ, the number of points in any set $B \subset \mathbb{R}^d$ is a Poisson random variable with mean $\lambda|B|$ and the number of points in disjoint sets are independent random variables [40]. Hence [28]

$$\mathbb{P}\left(\Phi\left(B\right)=k\right)=\exp\left(-\lambda|B|\right)\frac{\left(\lambda|B|\right)^{k}}{k!}, \tag{2.1}$$

where $\exp\left(-\lambda|B|\right)$ is the void probability. Herein, *homogeneous* PPPs are employed and are formally defined as [45]

Definition 2.1. *The Poisson point process* Φ *of intensity measure* Λ *is defined by means of its finite-dimensional distributions:*

$$\mathbb{P}\Big\{\Phi(A_1) = n_1, \cdots, \Phi(A_k) = n_k\Big\} = \prod_{i=1}^{k}\left(e^{\Lambda}(A_i)\,\frac{\Lambda(A_i)^{n_i}}{n_i!}\right), \tag{2.2}$$

for all bounded $k = 1, 2, \cdots$ and mutually disjoint sets A_i for $i = 1, \cdots, k$. If $\Lambda(x) = \lambda \mathrm{d}x$ is a multiple of Lebesgue measure (volume) in $\mathbb{R}^d$, then Φ is a *homogeneous* PPP with density λ (or parameter). The key properties of PPP that are of interest in this thesis are [28]:

1. Given two PPPs Φ_1 and Φ_2 with densities (or intensities) λ_1 and λ_2, respectively, the *superposition* of Φ_1 and Φ_2 results in a new PPP $\Phi_{1,2}$ with density $\lambda_{1,2} = \lambda_1 + \lambda_2$. This property is important in wireless networks, where the AP locations and STA locations are characterized as independent PPPs Φ_a and Φ_s, respectively, the *superposition* property can be used to describe the total density of the whole network. This is for *homogeneous* PPP and realizations of node locations are based on independent *homogeneous* PPPs for receivers and transmitters.

2. The *Thinning* Process deals with the selection of a point from a set of points in Φ with probability p independently of the other points, and the probability $1 - p$ of not selecting the point. Consequently, the two resultant PPPs (one for those points selected and the other for the points not selected from Φ) have density $p\lambda$ and $(1-p)\lambda$. This property is quite useful in modeling the MAC layer activities, specifically, the channel access process. By modeling the node locations as realizations of PPP Φ, the set of active nodes $\tilde{\Phi} \subset \Phi$ permitted by the access protocol such as CSMA/CA or ALOHA can be modeled using the

thinning property. For instance, if all the nodes form a PPP Φ with density λ and each node transmit with probability p, the transmitting nodes form another PPP Φ_{active} with density $\lambda_{active} = p\lambda$ while the nodes that are quiet in that time-slot form a PPP with density $\lambda_{silent} = (1-p)\,\lambda$.

3. The third property is related to the simulation of a PPP. For simulation, the BPP is used conditioned on the fact that the number of points of Φ in a compact set $B \subset \mathbb{R}^d$, the set of points $\Phi \cap B$ form a BPP.

2.3.2 Useful Theorems on PPP Model

Throughout this thesis, it is assumed that node locations are realizations of *homogeneous* PPP characterized by a single density parameter λ. Herein, the performance evaluation based on the PPP model is a statistical average over the points of the PPP. This average can be average sum of a throughput function, interference or any other performance metric related to wireless communication. For example, if active or concurrently transmitting nodes permitted by CSMA/CA protocol form a PPP Φ_{active} with density λ_{active}, the total interference at a typical receiver can be written as $\sum_{x \in \Phi_{active}} R^{-\alpha}$, where R represents the distance between the receiver and a potential interference source, and α is the path loss exponent. The average interference at the receiver from all points in Φ_{active} can be evaluated using [45], [40], [28]

Theorem 2.1. *Campbell's Theorem: Let $f(x) : \mathbb{R}^d \to [0, \infty]$ be a measurable function. Then*

$$\mathbb{E}\left(\sum_{x \in \Phi} f(x)\right) = \int_{\mathbb{R}} f(x)\,\Lambda(dx) \tag{2.3}$$

Proof. *See* [28, Appendix A.1.2] □.

Consequently, assuming node locations in the network follow realizations of *stationary* PPP with density and applying *Campbell's Theorem*, the mean interference in the network can be evaluated as follows

$$\mathbb{E}\left(\sum_{x\in\Phi_{active}} R^{-\alpha}\right) = \lambda_{active}\int_{\mathbb{R}^d} R^{-\alpha}\,\mathrm{d}R, \tag{2.4}$$

which implies that the mean interference depends heavily on the density or intensity of the concurrent transmitters, and two *stationary* node distributions with equal density would generate equal average interference, and the variance is also measurable as [28]:

$$\mathrm{var}\left[\sum_{x\in\Phi_{active}} R^{-\alpha}\right] = \lambda_{active}\int_{\mathbb{R}^d} \left(R^{-\alpha}\right)^2\,\mathrm{d}R. \tag{2.5}$$

The *Probability Generating Functional* (PGFL) of a PPP can defined as [28]

Definition 2.2. *Let* $v(x):\mathbb{R}^d\to(a,b]$ *be measurable, the PGFL of the point process* Φ *is*

$$\mathcal{G}[v] = \mathbb{E}\prod_{x\in\Phi} v(x) \tag{2.6}$$

specifically, if Φ is a PPP,

$$\mathcal{G}[v] = \exp\left(-\int_{\mathbb{R}^d}(1-v(x))\,\Lambda(\mathrm{d}x)\right), \tag{2.7}$$

and the Laplace transform $\mathcal{G}(s)$ of the $\sum_{x\in\Phi} f(x)$ can be evaluated from the PGFL as [28]

$$\mathbb{E}\left[\exp\left(-s\sum_{x\in\Phi} f(x)\right)\right] = \mathbb{E}\left[\prod_{x\in\Phi}\exp\left(-sf(x)\right)\right] = \mathcal{G}\left[\exp\left(-sf(x)\right)\right]. \tag{2.8}$$

Another useful characterization of the PPP is the *Palm Distribution* [45], [28], [40], which arises when the point process is conditioned to have a point at $x \in \mathbb{R}^d$. In other words, the point process has a particular point x that is being excluded from the set (i.e., not being counted). This property is very useful in evaluating mean interference without including the transmission from the desired point x or desired signal. This implies that, only signals from interference sources will be counted while the point transmitting the desired signal is excluded from the interference set. Therefore, the reduced Palm distribution equals the distribution of the original PPP according to

Theorem 2.2. *Slivnyak Mecke Theorem: For a PPP,*

$$\mathbf{P}^{!o} \equiv \mathbf{P}, \tag{2.9}$$

and for a *stationary* PPP Φ, with Slivnyak's theorem,

$$\mathbb{E}\left[\sum_{x\in\Phi} f\left(x, \Phi \setminus \{x\}\right)\right] = \lambda \int_{\mathbb{R}^d} \mathbb{E} f\left(x, \Phi\right)\ \mathrm{d}x. \tag{2.10}$$

2.3.3 Matérn Hard-core Process

A hard-core point process is a point process that forbids two or more points to lie closer together than a minimum distance $\mathcal{R}$ [40]. Such point process is useful in modeling the behavior of the CSMA/CA protocol [39] and the channel contention process discussed earlier in Sections 2.1.3 and 2.1.4. The hard-core point process of interest in this thesis, is the *Matérn hard-core process* [39], [40], which is employed later in subsequent chapters in modeling the CSMA/CA contention process.

Consider a homogeneous Poisson process Φ_u representing users in a WLAN with density λ_u. Assign to each point u, a mark $m\left(u\right)$ that is uniformly distributed over

(0,1). Under *Matérn hard-core process*, the dependent *thinning* retains the point $u \in \Phi_u$ with mark $m(u)$ if no other point within a ball $\mathcal{B}(u, \mathcal{R})$ has a mark lower than $m(u)$. Mathematically, this process is defined as follows

$$\tilde{\Phi}_u = \{u \in \Phi_u : m(u) < m(\tilde{u}) \forall \tilde{u} \in \Phi_u \cup \mathcal{B}(u, \mathcal{R}) \setminus \{u\}\}. \tag{2.11}$$

The intensity, $\tilde{\lambda}_u$ of this resultant point process $\tilde{\Phi}_u$ is written as

$$\tilde{\lambda}_u = p\lambda_u, \tag{2.12}$$

where p is the *Palm* probability of retaining a typical point u and is given by

$$p = \int_0^1 r(t)\, dt = \frac{1 - \exp(-\lambda_u c)}{\lambda_u c}, \tag{2.13}$$

where $r(t) = \exp(-\lambda_u c t)$ denote the retaining probability of a point with mark t [40] and for a 2-D point process, $c = \pi\mathcal{R}^2$.

The *Matérn hard-core process* has been applied to model the mean interference in wireless networks [46]. Herein, it is used in modeling the behavior of the contention process under CSMA/CA protocol. Two or more nodes within the carrier sensing range (CSR) $\mathcal{R}$ contend with one another and only one node wins the contention since CSMA/CA forbids two or more nodes within CSR $\mathcal{R}$ from transmitting concurrently. In this context, the mark $m(u)$ represents the back off time of each STA and only an STA with the lowest back off time is allowed to transmit in the next time slot when the channel becomes idle.

Chapter 3

Decentralized User-AP Association

3.1 Introduction

A new AP association framework is proposed in this chapter for future uplink (UL) multiuser (MU)-MIMO (MU-MIMO) WLANs. As opposed to the existing frameworks of associating single user (SU) to the best serving AP, a MU-AP association is studied in this chapter, primarily to associate group of users with an AP offering the maximum sum rate bound. This is important for future WLANs where MU uplink transmissions or beamforming will be employed to improve throughput of the multiple access channel (MACh). This problem is formulated as a logarithmic utility maximization problem, which takes into account, the sum rate bound of a multiuser group and the MAC protocol effects.

As opposed to the traditional RSS-based scheme, the idea of decoupled user association (DUA) where different APs serve a user in UL and DL transmissions to improve the system performance was investigated for full-duplex (FD) networks in [41]. With DUA, aggregate throughput could be improved if the AP with the best DL channel serves a user and the user has the liberty to choose an AP with the best UL

channel for its UL transmissions. Posing the user-AP association problem as a classical assignment problem, a distributed auction algorithm is used in [47] to jointly solve the AP selection and relaying problem, which yields an optimal client-relay-AP association. Also, in [48], to maximize user utility for UL MU-MIMO WLANs an auction-based AP selection and STA scheduling framework is proposed. The issues of user association and spectrum allocation in heterogeneous networks are coupled in [49] where the joint problem is solved as two sub-problems to maximize sum-rate. The auction-based AP association control algorithms [47], [48], [50] could potentially suffer from lack of fairness.

In addressing the issue of fairness to STAs, formulating the user-AP association as a utility maximization is able to account for fairness [51], [52], [53], [54], [55]. In [51], the issue of proportional fairness in achievable rates of users is addressed by solving the user-AP association problem in multi-rate WLANs. The proposed *best performance first* (BPF) algorithm therein achieves proportionally fair performance for single-input single-output (SISO) links. The authors in [52] solve the user-AP association in massive MIMO wireless networks as a utility maximization problem. Therein, it is assumed that user rates are deterministic under certain channel conditions.

Similarly for massive MIMO systems, a joint user-AP association and power allocation problem is formulated in [55]. From a game theoretic perspective, the user-AP association problem is addressed to improve fairness [53]. When a set of dense WLANs share the same upstream provider, some level of collaboration among the APs could facilitate a proportional-fair user-AP association [54]. However, such AP-to-AP collaboration is not feasible for scenarios such as multi-tenant networks [56], where APs do not belong to the same service provider.

Improving the proportional fairness among STAs through efficient AP selection framework could mitigate starvation, and even the cell-edge users (STAs with low SINR or farther way from the AP) could receive some level of service. On the other hand, efficient use of the large number of deployed APs seems to be a priority in some cases, especially for load balancing [57, 58]. Efficient use of the APs is often achieved through load balancing where the goal is to avoid overloading some APs while having others be lightly loaded or idle; the objective of load balancing is feasible by optimizing the AP association [57, 58]. An example of a load balancing algorithm via AP association is the *greedy algorithm* [57], which allows a user to selfishly associate with an AP with low load upon entering the network and to remain with the same AP for its entire time in the network.

As opposed to the *greedy algorithm* that restricts STAs from switching AP upon association, the *best response algorithm* [57] allows users to switch their AP multiple times and select the least loaded AP. Jointly considering proportional fairness and load balancing in heterogeneous networks, a utility maximization problem is formulated in [59] where using a biasing factor, users associate with lightly loaded small cells as opposed associating with the heavily-loaded macrocells. To minimize AP utilization in millimeter-wave (mmWave) networks, user-AP association problem is formulated with constraints on the demanded user data rate [58].

Although, proportional fairness and load balancing via AP association optimization are important, retransmission resulting from collision and high packet error rate (PER) will be dominance in high density WLANs. Excessive collision is due to high contention among densely distributed STAs sharing the limited orthogonal channels, and the high PER occurs when receivers are unable to decode packets at low SINR

(or high interference). Therefore, neglecting the effect of interference and contention is detrimental to overall system performance of dense WLANs. Decentralizing the user-AP association improves the DL throughput in the presence of multi-AP interference [60], by using pilot signals or preambles to measure inter-BSS interference at the target (or candidate) APs and select the AP that offers the best DL SINR. The ultimate goal of [61] is to minimize the effects of inter-WLAN interference through cooperation between networks using location and channel information from the APs. As demonstrated experimentally in [62], considering interference level could facilitate load balancing at the APs.

The major challenge in dense wireless networks is not necessarily related to load balancing because there is usually a large number of APs to handle heavy traffic and ensure coverage to all users. Using AP load measured in terms of AP utilization [57] - [58], [62] as the AP selection decision metric, could result in STAs associating with AP with other deleterious effects such as high interference and high contention. Therefore, considering interference and contention as factors in performing user-AP association is crucial in enhancing the performance of high density WLANs. Moreso, with the advent of multi-antenna STAs with UL multiuser transmission capability, the multiuser interference pattern is different from that of SISO or SIMO channels considered in most existing frameworks for WLANs. Arguably, user-AP association to suppress multiuser interference resulting from a large number of concurrent transmissions is desirable to improve performance in MU-MIMO WLANs. Thus far, little attention has been given to multi-antenna AP selection in MU-MIMO WLANs except for the specific scenarios [48], [50] where perfect successive interference cancellation exists.

With future nodes equipped with full duplex (FD) capability, there are new challenges. Recent studies (e.g. [47] , [51], [52], [57], [59], [63]) investigate the user-AP association problem for half duplex (HD) WLAN. For general HD communication, a special case of achieving proportional fairness via AP association appears in [51], where the authors study proportional fairness in multi-rate WLANs using AP association based on distributed auction algorithms optimize client-relay-AP association. Two association algorithms are proposed in [57] with performance bounds. In [59], the User-AP Association problem is addressed for heterogeneous cellular networks with the primary objective of load balancing. User-AP association is optimized for load balancing and fairness in millimeter-wave (mmWave) wireless networks in [58]. The association control and relaying problems are jointly addressed in [47].

In FD, the interference experienced by a pair of *primary* (AP) and *secondary* (STA) transmitters depends on AP-STA associations in the network. In FD WLANs, the strongest signal first (SSF) or legacy scheme might not be efficient because it considers only the RSS in the uplink when selecting an AP. Existing schemes for WLAN only take channel condition at one receiver end into account when associating an STA to an AP. For these association schemes to work in FD CSMA/CA networks, both the *primary* (downlink) and the *secondary* (downlink) transmitters would at least experience equal levels of interference, which might not be the case for wireless channels. The MAC layer throughput in FD-enabled WLAN under imperfect collision detection (CD) is analyzed in [64], to demonstrate the performance of a proposed CSMA with imperfect CD over the conventional CSMA/CA protocol in FD WLAN. The most relevant existing study can be found in [41] where the authors aim to maximize the mean rate utility of FD networks by optimizing the user association.

They focus primarily on cellular networks where base stations (BSs) are distributed according to Poisson Point Processes (PPPs) in the in-band FD mode.

In this chapter, boldface uppercase letters represent matrices, for instance, matrix $\mathbf{H}$ represents the channel matrix between a user and an AP. Column vectors are denoted as boldface lowercase letter such as $\mathbf{x}$ representing the transmitted symbol vector. The expected value of any random variable will be denoted as $\mathbb{E}[\cdot]$. While the Frobenius norm of a matrix is denoted as $\|\cdot\|_F^2$, the superscripts $(\cdot)^H$ and $[\cdot]^T$ represent the Hermitian conjugate transpose and the transpose, respectively. The chapter is organized as follows: The UL MU-MIMO system model is presented in Section 3.2.2 while the user-AP association problem is formulated in Section 3.3 alongside with two solution techniques. In Section 3.4, we present the performance evaluation of the proposed MU-AP association algorithm. In Section 3.5, another framework is introduced for AP association in full duplex WLANs with system model, proposed method and performance evaluation presented in Sections 3.6, 3.7 and 3.8, respectively. Section 3.9 concludes this entire chapter.

3.2 Decentralized Multiuser-AP Association

3.2.1 Graph Theory Preliminaries

User-AP association problem is a type of assignment problem whereby users (or STAs) are assigned to the best serving AP based on certain criteria such as received SINR, AP load, RSS etc. Assignment in general can be generalized as graph matching problem, specifically, the *Maximum Weighted Bipartite Matching* [65], and solved in *Polynomial time* using Graph theoretic algorithms. In more general terms, bipartite graph matching deals with the process of assigning a set of jobs to a set of workers;

in this context, a set of STAs is to be assigned to a set of APs with the goal of maximizing an objective function.

A bipartite graph $G = \{V, U, \mathcal{E}\}$ consists of two sets of nodes V and U and a set of edges $\mathcal{E}$ connecting each node in V to each node in U. Each edge connecting a node $i \in V$ to a node $j \in U$ is associated with an edge cost or weight w_{ij}. The edge weights of all outgoing edges can be represented as a matrix $w_{ij} \in \mathbf{W}$. To perform matching or assignment of nodes in V to nodes in U, the graph is partitioned into left and right vertices, and then an algorithm is used to solve the graph matching problem. One renown algorithm that yields optimal matching or assignment is the *Hungarian* or *Kuhn-Munkre* algorithm (KMA) [65], [66]. The operation of the KMA is discussed later in Chapter 3 where it is applied in solving the User-AP association problem as a graph matching or assignment problem.

3.2.2 System and Network Models

Consider a multi-cell WLAN with N STAs transmitting to M APs in multiple access channel (MACh) as depicted in Figure 3.1. Let index i for STA_i belong to $i = 1, \cdots, N$ and let AP_j be indexed as $j = 1, \cdots, M$. An AP and its associated STAs form a basic service set (BSS), analogous to cells in cellular networks. Consequently, we will use AP_j and BSS_j interchangeably to refer to a BSS consisting of STAs being served by AP_j. For simplicity, STAs in Figure 3.1 are single-antenna users transmitting concurrently in MACh to an AP equipped with K receiving antennas. This model of UL multiuser transmission is consistent with the future support for UL beamforming in 802.11ax [67], [68], [69].

Let $k = 1, \cdots, K$ index each receive antenna at the AP and there are N_j users in

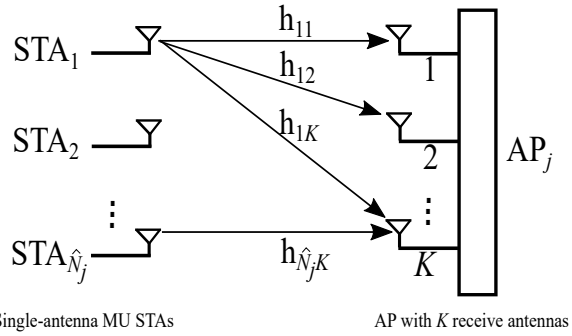

Figure 3.1: Uplink MACh MU-MIMO model with K antennas AP.

BSS$_j$ (or within the transmission range of AP$_j$). Since in most cases, $N_j \geq K$, only $\hat{N}_j \leq K \leq N_j$ STAs could beamform concurrently to AP$_j$ as depicted in Figure 3.1. Therefore, given N single-antenna STAs in the network, let ϑ be the index of each MU group, which consists of $\hat{N}_j$ STAs, i.e., $\vartheta = 1, \cdots, \frac{N}{\hat{N}_j}$. If each STA in MU-group ϑ is denoted as $i = 1, \cdots, \hat{N}_j$, $h_{ik} \sim \mathcal{CN}(0,1)$ represents the narrowband channel complex coefficient between the i^{th} STA$_i$ and the k^{th} receive antenna element of AP$_j$. Each h_{ik} of each transmit-receive antenna pair is the $(i,k)\,th$ entry of the channel matrix $\mathbf{H}_\vartheta \in \mathbb{C}^{K \times \hat{N}_j}$ between a MU-group ϑ ($\hat{N}_j$ STAs) and AP$_j$.

Assuming the channel $\mathbf{H}_\vartheta = [\mathbf{h}_1, \mathbf{h}_2, \cdots, \mathbf{h}_{\hat{N}_j}]$ is a quasi-stationary MIMO channel known at the receiver, whose i^{th} column $\mathbf{h}_i = [h_{1i}, h_{2i}, \cdots h_{Ki}]^T$ denotes the channel vector from ith STA to the K antennas at the receiver AP. Suppressing subscripts, the received signal vector at AP is:

$$\mathbf{y} = \mathbf{H}_\vartheta \mathbf{x}_\vartheta + \mathbf{n} \tag{3.1}$$

where $\mathbf{x}_\vartheta \in \mathbb{C}^{\hat{N}_j \times 1} = [x_1, \cdots, x_{\hat{N}_j}]$ is the uplink transmitted signal vector from the STAs intended for AP$_j$, $\mathbf{n} \sim \mathcal{CN}(0, \sigma_n^2 \mathbf{I}_K)$ represents the $K \times 1$ noise vector at AP$_j$ whose entries are $n_1 \cdots n_K$ zero mean white Gaussian noise with variance σ_n^2. The

transmitted symbols contained in $\mathbf{x}_\vartheta$ can be recovered using linear zero-forcing (ZF) or minimum mean squared error (MMSE) detectors. Under ZF detection, the weight matrix $\mathbf{W}_\vartheta$ designed using the Moore-Penrose pseudoinverse is

$$\mathbf{W}_\vartheta = \mathbf{H}_\vartheta^\dagger = \left(\mathbf{H}_\vartheta^H \mathbf{H}_\vartheta\right)^{-1} \mathbf{H}_\vartheta^H \tag{3.2}$$

consequently, the post-detection signal is

$$\hat{\mathbf{x}} = \mathbf{W}_\vartheta \mathbf{y} = \left(\mathbf{H}_\vartheta^H \mathbf{H}_\vartheta\right)^{-1} \mathbf{H}_\vartheta^H \left(\mathbf{H}_\vartheta \mathbf{x}_\vartheta + \mathbf{n}\right). \tag{3.3}$$

The post-detection signal-to-noise ratio (SNR) of the ith STA at AP_j is given by [70]

$$\gamma_i = \frac{\mathbb{E}\left[|x_i|^2\right]}{\mathbb{E}\left[|n_i|^2\right]} = \frac{\mathbb{E}\left[|x_i|^2\right]}{\left[\left(\mathbf{H}_\vartheta^H \mathbf{H}_\vartheta\right)^{-1}\right]_{ii} \sigma_n^2} = \frac{\gamma_o}{\left[\left(\mathbf{H}_\vartheta^H \mathbf{H}_\vartheta\right)^{-1}\right]_{ii}}, \qquad i = 1, \cdots, \hat{N}_j \tag{3.4}$$

where $\gamma_o = \frac{\mathbb{E}\left[|x_i|^2\right]}{\sigma_n^2}$ and $[\cdot]_{ii}$ represents the element in the ith row and ith column. The bit rate of the channel for the ith concurrent transmission becomes

$$R_i = BW \log_2\left(1 + \gamma_i\right), \qquad i = 1, \cdots, \hat{N}_j \tag{3.5}$$

where BW is channel bandwidth. Herein, we consider only ZF detection and note that the availability of global channel side information (CSI) required to measure SNR in (3.4) by APs in the UL whether via *channel sounding*, transmission of *pilot signals, preambles* or explicit compressed feedback [71] is more practically obtainable at APs than at STAs in the DL. Therefore, considering UL transmissions, we assume

the availability of CSI at the APs.

3.2.3 MAC Layer Saturation Throughput

Next, we determine the user throughputs to capture both the effects of the channel characteristics defined in (3.4) and the MAC layer protocol when the network is in a saturation state. Here, saturation state means that all users have packets in their buffers and are contending for an opportunity to transmit in their respective BSS. IEEE 802.11 WLAN uses the CSMA/CA protocol to govern channel access and prevent collisions using binary exponential backoff. Using the DCF access mechanism, the CSMA/CA protocol requires that each node sense the channel for a period of time known as the DCF interframe space (DIFS) and backoff (or defer transmission) if the channel is idle for an interval of DIFS. If the DIFS elapsed and the channel remains idle, the node in backoff mode could commence transmission. During the backoff procedure, each node randomly chooses a *backoff counter* (an integer value) between 0 and $CW_{\min} - 1$, where $CW_{\min}$ denote the minimum contention window (CW) size.

While in the backoff mode, a node decrements its backoff counter each time the channel is detected to be idle for one *slot-time* and this counter is frozen whenever the shared channel is occupied by other nodes. A node is eligible to transmit its payload when its backoff counter reaches zero, i.e., expires. After transmission of its payload, the node waits for a period of time known as the short interframe space (SIFS), to receive an acknowledgment frame (ACK) from the receiver AP. If no ACK frame is received at the end of SIFS period, a collision is deemed to have occurred. In the event of a collision or failed transmission, the CW is doubled and a new backoff counter is chosen to reinitiate the backoff procedure; this process repeats until a

frame is successfully transmitted. A frame is retransmitted provided that neither the maximum retry limit and the maximum value $CW_{\max}$ of CW have been reached.

The above MAC layer contention process is modeled in [27] (Bianchi Model) as a Discrete Time Markov Chain (DTMC) to determine the saturation throughput in a network with saturated traffic. Similar to [70], [72] we adopt this model to define the *saturation throughput utility* function that captures the impact of the MAC layer protocol on simultaneous transmissions from multiple STAs in a MU-MIMO environment. Subsequent to AP association, there are $N_j\,(< N)$ STAs in BSS j of each AP_j. Under the saturation throughput assumption, for each time-slot, there are N_j-contending STAs (each with packets to send) in BSS j and an AP can support $\hat{N}_j \leq K$ MU transmissions. A collision or failed transmission occurs if there are more than $\hat{N}_j$ simultaneous transmissions in a BSS. User STA_i among N_j STAs transmits with probability

$$\tau = \frac{2\left(1-p^{R+1}\right)}{W\left(1-2^{L}p^{R+1}\right)+Wp\left[\sum_{i=0}^{L-1}(2p)^{i}\right]+\left(1-p^{R+1}\right)}, \tag{3.6}$$

where $W = CW_{\min}$, R is the retry (retransmission) limit, $L = \log_2\left[\frac{(CW_{\max}+1)}{(CW_{\min}+1)}\right]$ is the maximum number of times CW can be doubled and p is the probability that STA_i retransmits its previous frame (due to collision) defined

$$p = 1 - \underbrace{\sum_{n=0}^{\hat{N}_j-1}\binom{N_j-1}{n}\tau^{n}\left(1-\tau\right)^{N_j-1-n}}_{\bar{\mathbf{p}}}, \tag{3.7}$$

where $\bar{\mathbf{p}}$ represents the probability that $\hat{N}_j$ STAs transmit frames concurrently among

N_j contending STAs in BSS_j. The probability of having $\hat{N}_j$ [1] simultaneous transmissions is

$$P_{\hat{N}_j}^{tr} = \binom{N_j}{\hat{N}_j} \tau^{\hat{N}_j} (1-\tau)^{N_j - \hat{N}_j}. \tag{3.8}$$

Assuming each STA transmits a fixed frame size of $\mathcal{F}$ and given the channel rate of an STA_i in (3.5), the transmission time (or data time) of each frame from STA_i is

$$T_i = \frac{\mathcal{F}_i\,(\text{bits})}{R_i\,(\text{bits/s})}, \tag{3.9}$$

where the PHY rate R_i depends on their received SINR given by (3.4). If ACK frame takes time T_{ack} to transmit, the total channel occupancy time of STA_i

$$T_i^{tr} = \text{SIFS} + T_{\text{ack}} + \text{DIFS} + T_i, \qquad i = 1, \cdots, \hat{N}_j \tag{3.10}$$

here, perfect MAC layer synchronization among the users is assumed and STAs start transmissions at the same time. That is, the SIFS and DIFS of the users are synchronized and the receiver AP broadcasts a block of ACK frames to the $\hat{N}_j$ users in the downlink. This assumption is valid because all transmitting clients in a given time slot are expected to end their transmissions simultaneously when time slot elapses. In the event of a collision due to more than $\hat{N}_j$ simultaneous transmissions, the time duration T_i^c exhausted by STA_i as a result of collision is defined as

$$T_i^c = \hat{T}_{\text{ack}} + \text{DIFS} + T_i, \qquad i = 1, \cdots, \hat{N}_j \tag{3.11}$$

[1] Throughout this chapter, it is assumed that each AP selects $\hat{N}_j \leq K$ users for multiuser transmissions using the modified Incremental User Selection Algorithm [73, Alg. I-B] discussed later, and an STA knows the other $\hat{N}_j - 1$ STAs in its MU group.

where $\hat{T}_{\text{ack}}$ is the ACK frame time-out, which represents the time spent by each concurrent user in anticipation of an ACK frame from the AP. If no ACK frame is received at the end of $\hat{T}_{\text{ack}}$, a collision is deemed to have occurred.

Consequently, the expected time to successfully transmit all the frames or channel occupancy time of $\hat{N}_j$ users can be expressed as:

$$\mathbb{E}\left[T_{s|\hat{N}_j}\right] = \left(P^{tr}_{0|N_j} \cdot \eta + P^{tr}_{\hat{N}_j|N_j} \cdot \sum_{i=1}^{\hat{N}_j} T^{tr}_i + P^{tr}_{\hat{N}_j|N_j} \cdot \sum_{i=\hat{N}_j+1}^{\bar{N}_j} T^{c}_i \right) \cdot \xi_{\vartheta j}, \tag{3.12}$$

where $P^{tr}_{0|N_j} = (1-\tau)^{N_j}$ from (3.8), η is the backoff time, $\xi_{\vartheta j}$ is the binary indicator random variable

$$\xi_{\vartheta j} = \begin{cases} 1, & \text{if group } \vartheta \text{ associates with AP}_j \\ 0, & \text{otherwise.} \end{cases} \tag{3.13}$$

The expected MU-MIMO *throughput* of $\hat{N}_j$ STAs in BSS j per slot-time is

$$\mathcal{R}_\vartheta = \frac{\mathbb{E}\left[P_l\right]}{\mathbb{E}\left[T_{s|\hat{N}_j}\right]} = \frac{\sum_{i=1}^{\hat{N}_j} i \cdot \mathcal{F}_i \cdot P^{tr}_{\hat{N}_j}}{\left(P^{tr}_{0|N_j} \cdot \eta + P^{tr}_{\hat{N}_j|N_j} \cdot \sum_{i=1}^{\hat{N}_j} T^{tr}_i + P^{tr}_{\hat{N}_j|N_j} \cdot \sum_{i=\hat{N}_j+1}^{\bar{N}_j} T^{c}_i \right)} \xi_{\vartheta j}, \tag{3.14}$$

where $\mathbb{E}\left[P_l\right]$ is the average payload size from $\hat{N}_j$ concurrently transmitting STAs. The above saturation throughput model in (3.14) assumes that the transmission time of each STA depends on its respective channel rate captured in Eqn. (3.9) and individual payload size.

3.3 Proposed MU-AP Association Framework

In dense or large-scale WLANs, it is quite bandwidth intensive to obtain network-wide information when assigning users to APs, especially in multi-antenna systems where the amount of the CSI is large. Also, using network-wide information is computationally expensive and sometimes impractical to obtain. An STA has lower need for network information of farther away interference sources. In contrast, only nearby interference sources (usually within few tens of meters) could potentially affect a receiver's sensitivity level. Thus, the proposed framework consists of three parts: first is network clustering that divides the network into neighborhood and local contention or interference domains. The second part is the multiuser grouping. The final part involves solving the MU-AP association in each cluster to maximize logarithmic throughput utility per cluster; a cluster in this case consists of several APs to serve STAs in their cluster. This model assumes AP-to-AP coordination to share network information needed to perform clustering and user grouping.

3.3.1 Network Clustering

Since nearby concurrent interfering transmitters are stronger than the interference received from farther nodes, only interference from a "cluster" or "neighborhood" is taken into account in estimating a typical STA's SINR defined by (3.4). We employ the fast local clustering (FLOC) proposed in [74], which is a distributed message-passing and self-healing clustering algorithm. FLOC requires the election of cluster head (CH) and the identification of *in-band* and *out-band* APs. An *in-band* AP is required to be a unit distance from the CH while *out-band* APs can be u units of distance from the CH. In this context, a neighborhood consists of several APs that

are a CSR away from the CH. Partitioning the APs into clusters implies that a typical STA only considers interference from other STAs within its cluster while interference from other clusters is negligible or close to noise level.

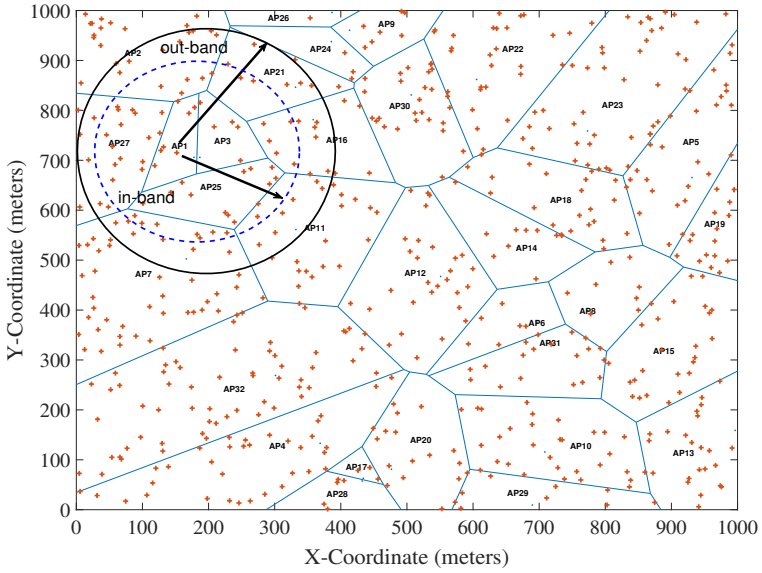

Figure 3.2: An example of FLOC clustering with CSR defining the in-band and out-band regions in PPP Wireless LANs with $M = 32$ APs and $N = 400$ STAs.

APs are randomly chosen to be CHs and the *in-band* distance is defined as 2×CSR while the *out-band* distance is set to 3×CSR. In WLAN, the CSR depends on the PCS threshold, which determines the degree of spatial reuse and interference level from concurrent transmitters [10]. For instance, if the PCS threshold is −70dBm, using power loss law path-loss exponent α, the CSR is approximately 115 meters. With this configuration, an *in-band* AP and *out-band* AP are 115-meters and 230 meters from the CH, respectively. APs located in the *in-band* of cluster c join the cluster while APs in the *out-band* of cluster c and not in the *in-band* of any other cluster also join cluster c. Using the CSR as the clustering metric helps us to capture the regions

where strong interference is expected since the PCS threshold represents the receiver sensitivity in WLANs. Figure 3.2 depicts an example of a clustered WLAN where there are $M = 32$ APs and $N = 400$ STAs. Using AP1 as the CH, APs within the *in-band* region (dotted circle) will join the cluster while APs (e.g. AP21 and AP2) located within the *out-band* region (solid circle) will join AP1's cluster if they are not within the *in-band* of another CH.

3.3.2 Cluster-based Multiuser Grouping

Here, the focus is neither on the efficiency of user selection algorithm nor to propose a new user selection algorithm but on the performance of MU group-AP association. This section mainly describes the algorithm being used in grouping the users prior to performing association of each MU group to an AP. Several multiuser selection algorithms exist in the literature to group users based on users' orthogonality or sum rate bound given full CSI at the transmitter or at the receiver. Subsequent to the network clustering in Section 3.3.1, users are grouped into their respective MU groups based on a minimum-mean-squared-error (MMSE) criterion adopted from [73] and extended to MACh. Let $\mathcal{N}_c = \{1, 2, \cdots, N_c\}$, $N_c = |\mathcal{N}_c|$ be the set of indices of STAs and $\mathcal{A}_c = \{1, 2, \cdots, M_c\}$ $|M_c = |\mathcal{M}_c|$ be the set of indices of APs within a cluster c. Each $\text{AP}_j \in \mathcal{A}_c$ independently performs the grouping of the N_c users using Algorithm 1.

Given that in a dense WLAN, the number of STAs N_c in a typical cluster c is greater than the number of receive antennas, K, at the APs, users are grouped into groups of size K; that is, each MU group size $\hat{N}_j \leq K$ and at the end of the multiuser grouping, each cluster c has N_c/K MU groups per AP prior to association. Therefore,

Algorithm 1: Cluster-based User Grouping Algorithm

Input: $\mathbf{H}_{jc}$, $\eta = \frac{N_c}{\mathcal{E}_x}$, $\mathcal{N}_c = \{1, 2, \cdots, N_c\}$, $\mathcal{N}_j = \emptyset$
Output: $\mathcal{N}_c^{groups}$ {Set of K-users groups in cluster c}
while $\mathcal{N}_c \neq \emptyset$ **do**
  Compute $\mathbf{A} = \eta^{-1}\mathbf{I}_K$
  Select first user $n = \underset{i \in \mathcal{N}_c}{\arg\max} \|\mathbf{h}_i\|^2$
  Add selected user to $\mathcal{N}_j$: $\mathcal{N}_j \cup n$
  Remove selected user: $\mathcal{N}_c = \mathcal{N}_c \setminus n$
  Compute $\mathbf{G}_n = \mathbf{h}_n\mathbf{A}$
  Select next $K-1$ STAs:
  for $\tilde{n} = 1 : K-1$ **do**
    Update $\mathbf{A} \leftarrow \mathbf{A} - \left(1 + \mathbf{G}_n\mathbf{h}_n^H\right)^{-1}\mathbf{G}_n^H\mathbf{G}_n$
    Compute $\mathbf{G}_i = \mathbf{h}_i\mathbf{A} \qquad \forall i \in \mathcal{N}_c$
    Select next user: $n = \underset{i \in \mathcal{N}_c}{\arg\max} \left(1 + \mathbf{G}_i\mathbf{h}_i^H\right)^{-1}\|\mathbf{G}_i\|^2$
    $\mathcal{N}_j = \mathcal{N}_j \cup n$, $\mathcal{N}_c = \mathcal{N}_c \setminus n$
  $\mathcal{N}_c^{groups} \leftarrow \mathcal{N}_j$

the channels of N_c users seen by AP_j in cluster c is denoted as $\mathbf{H}_{jc} \in \mathbb{C}^{K \times N_c} = [\mathbf{h}_1, \mathbf{h}_2, \cdots, \mathbf{h}_{N_c}]$ where the $\mathbf{h}_i = [h_{i1}, h_{i2}, \cdots, h_{iK}], i = 1, \cdots, N_c$. For an AP_j to group the users in its cluster according to the available CSI $\mathbf{H}_{jc}$, the Incremental User Selection algorithm ([73, Alg. I-B]) is being adopted for application in UL users grouping. This algorithm is described as follows and summarized in Algorithm 1. Using matrix inversion lemma [73] for a positive definite matrix, at the start of the algorithm, we compute $\mathbf{A} = \eta^{-1}\mathbf{I}_K$ where $\eta = \frac{N_c}{\mathcal{E}_x}$, the first user is selected such that $n = \underset{i \in \mathcal{N}_c}{\arg\max} \|\mathbf{h}_i\|^2$ and by computing $\mathbf{G}_n = \mathbf{h}_n\mathbf{A}$, the next $K-1$ users are selected and added to group $\mathcal{N}_j$. Once the first K-users are grouped from $\mathbf{H}_{jc}$, the process of selecting K-users repeats until the user set $\mathcal{N}_c$ is empty and no more users to be grouped. At the end of the user grouping algorithm, AP_j has a set $\mathcal{N}_j$ of groups and each group consists of at most K users. If we let $\hat{N}_j \leq K$ represents the number of

users per group, the saturation throughput of a MU group through AP_j is therefore given by Equation (3.14). Algorithm 1 is independently executed and distributed at each AP, and each AP appends its MU groups $\mathcal{N}_j$ to $\mathcal{N}_c^{groups}$, which is broadcasted to other AP members in cluster c.

3.3.3 Multiuser Throughput Utility

The expected throughput expression in Eqn. (3.14) captures the throughput of each multiuser group per time slot. Herein, the primary objective is to find the MU group-AP association set that maximizes the overall throughput utility per cluster (Clusters are formed using the algorithm discussed in Section 3.3.1) using neighbor-to-neighbor (or AP to AP) local information rather than exploiting the global CSI, which could degrade spectral efficiency. Therefore, the clustering algorithm divides the entire network into set $\mathcal{C}$ of clusters and each cluster $c = 1, \cdots, |\mathcal{C}|$ consists of $M_c (< M)$ APs. Let $U(\mathcal{R}_c)$ denote the sum throughput utility in a typical cluster c, using proportional fairness [75], which has been widely used in existing studies (e.g [51], [52], [55]). The expected saturation throughput utility in cluster c per slot-time is

$$U(\mathcal{R}_c) = \sum_{j=1}^{M_c} \sum_{\vartheta=1}^{|\mathcal{N}_c^{groups}|} \Upsilon_\delta(\mathcal{R}_\vartheta), \tag{3.15}$$

where $\mathcal{R}_\vartheta$ is the saturation throughput defined in Eqn. (3.14) for a particular MU group ϑ, $\delta | 0 \leq \delta \leq 1$ is the parameter that determines the degree of fairness among

all MU groups. In particular,

$$\Upsilon_{\delta}\left(\mathcal{R}_{\vartheta}\right) = \begin{cases} \log \mathcal{R}_{\vartheta}\cdot, & \delta = 1 \\ \\ \frac{\left(\mathcal{R}_{\vartheta}\right)^{1-\delta}}{1-\delta}, & \delta \neq 1 | \delta \geq 0 \end{cases} \tag{3.16}$$

which implies that $\delta = 1$ if all multiuser groups achieve equal throughput (100% fairness), and $\delta \neq 1$ for any discrepancy in fairness, i.e., $\delta \neq 1$. Without loss of generality, we consider only the case when $\delta = 1$, which achieves proportional fairness. Therefore, the sum logarithmic throughput objective under consideration can be written as

$$U\left(\mathcal{R}_{\mathcal{C}}\right) = \sum_{c=1}^{|\mathcal{C}|} U\left(\mathcal{R}_{c}\right) = \sum_{c=1}^{|\mathcal{C}|} \sum_{j=1}^{M_c} \sum_{\vartheta=1}^{\left|\mathcal{N}_{c}^{groups}\right|} \log \mathcal{R}_{\vartheta}. \tag{3.17}$$

3.3.4 MU group-AP Association Problem Formulation

Subsequent to the clustering in Section 3.3.1, each AP is a member of a cluster c and each cluster consists of M_c APs. The objective is to assign each MU group ϑ to an AP such that the aggregate throughput utility in each cluster is maximized, and each group can only associate with one AP. Since network nodes are partitioned into local contention and interference domains (clusters), maximizing throughput utility in each cluster is tantamount to maximizing global throughput utility. In other words, the MU group-AP association problem is solved per cluster to simplify the AP selection process whereby each group considers only nearby APs as candidate APs, and therefore, no need for acquisition of global CSI through all the APs. Overall, the goal is to find an optimal set of AP associations that maximizes network-wide aggregate multiuser throughput utility and the problem is formulated mathematically

as:

$$\text{maximize} \qquad U\left(\mathcal{R}_{\mathcal{C}}\right) \tag{3.18a}$$

$$\text{subject to} \qquad \sum_{j=1}^{M_c} \xi_{\vartheta j} = 1, \qquad \forall \vartheta \in \mathcal{N}_c^{groups} \tag{3.18b}$$

$$\xi_{\vartheta j} \in \{0,1\}, \qquad \vartheta \in \mathcal{N}_c^{groups}, \tag{3.18c}$$

$$\sum_{j=1}^{M_c} \xi_{\vartheta j} \cdot \mathcal{R}_{\vartheta} \geq \hat{\mathcal{R}} \qquad \forall \vartheta \in \mathcal{N}_c^{groups}, \tag{3.18d}$$

where constraint (3.18b) ensures that each MU group associates with exactly one AP in one cluster and in (3.18c) $\xi_{\vartheta j} \in \{0,1\} = 1$ if group ϑ is associated with AP_j and zero otherwise, while (3.18d) represents a quality of service (QoS) constraint to guarantee a minimum rate $\hat{\mathcal{R}}$ for multiuser transmissions. In the next two subsections, a solution to this optimization problem is sought for, using two approaches based on a graph theory method and the dual ascent method [76], [77] for solving constrained optimization problems.

3.3.5 Graph Theory-based Solution

The solution to problem (3.18) in Section 3.3.6 is realizable by posing the original problem as a maximum weighted graph matching problem. Based on the clustering algorithm in Section 3.3.1, problem (3.18) decomposes into $C = |\mathcal{C}|$ subproblems and each subproblem can be solved using a graph algorithm. Figure 3.3 represents each subproblem as a bipartite graph, where each cluster (subproblem) consists of M_c APs and $N_g = |\mathcal{N}_c^{groups}|$ MU groups, and each group has an outgoing edge to each AP. From Eqn. (6.44), the weight of an edge connecting MU-group ϑ to an AP $_j$ is defined

as:

$$w_{\vartheta j} = \Upsilon_{\delta}\left(\mathcal{R}_{\vartheta}\right) = \log \mathcal{R}_{\vartheta} \qquad \{(\vartheta, j)\,|i = 1, 2, \cdots, N_g; j = 1, 2, \cdots, M_c\}, \tag{3.19}$$

using graph theory notations, each cluster in Figure 3.3 is a subgraph denoted as $G_c = (\mathcal{N}_c^{groups}, \mathcal{A}_c, \mathcal{E}_c)$ with $\mathcal{N}_c^{groups} = \{1, 2, \cdots, N_g\}$, $\mathcal{A}_c = \{1, 2, \cdots, M_c\}$ and $\mathcal{E}_c \subseteq \mathcal{N}_c^{groups} \times \mathcal{A}_c$ is the set of edge weights $w_{\vartheta j}$ of the outgoing edge from each MU group to each AP.

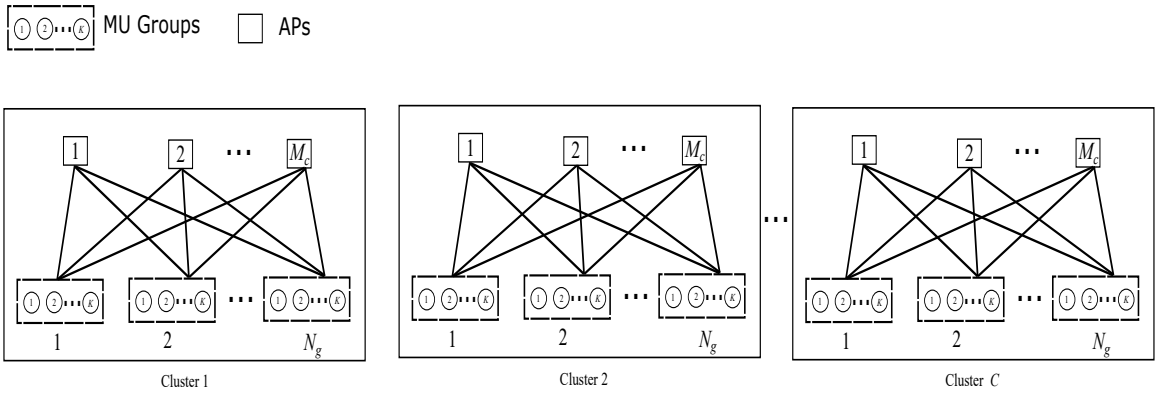

Figure 3.3: Graphical model of the original problem (3.18), showing C clusters to decompose the problem into C subproblems.

Objectively, obtain optimal matching in each cluster using local CSI (CSI of nodes within the cluster) is expected to yield optimal matching across the network. Decomposing the original problem into subproblems or subgraphs, reduces the cost (in terms of spectral efficiency) of obtaining the network-wide CSI. In each subgraph, each group $\vartheta \in \mathcal{N}_c^{groups}$ can be matched to exactly one AP such that the throughput (3.18a) is maximized. Maximizing the throughput objective can be achieved using maximum-weighted graph matching technique such as the KMA defined earlier in Section 3.2.1. For optimal matching in cluster c, $\mathcal{M}_c \subseteq \mathcal{E}_c$ connects each vertex in $\mathcal{N}_c^{groups} \cup \mathcal{A}_c$ such

that each AP in $\mathcal{A}_c$ is an endpoint of at least one edge. In a distributed manner, each STA solves the graph problem G_c and selects an AP based on the following policy:

$$\xi^*_{\vartheta j} = \begin{cases} 1, & j^* = \arg\max_j \left\{ w_{\vartheta j} : j \in \mathcal{A}_c, \mathcal{R}_\vartheta \geq \hat{\mathcal{R}} \right\} \\ 0, & \forall j \in \mathcal{A}_c \setminus \{j^*\} \end{cases}, \tag{3.20}$$

where selecting j^* must satisfy the QoS constraint (3.18d) and improve the multiuser throughput utility of group ϑ. Consequently, satisfying the condition in (3.20) renders problem (3.18) as a combinatorial search for j^* for each $\vartheta \in \mathcal{N}_c^{groups}$, which is achieved using Algorithm 2. Algorithm 2 is based on a modified classical KMA algorithm for solving bipartite graph matching, which has other applications [78], [79], [80].

Algorithm 2: Distributed Graph AP Selection Algorithm (DGAA)

Input: $\mathcal{N}_c^{groups}$, $\mathcal{A}_c$, $\mathcal{E}_c$
Output: Optimal match $\mathcal{M}_c$.
Edge weights estimate at APs:
Let $\boldsymbol{\omega}_j$ represent the $1 \times |\mathcal{N}_c^{groups}|$ vector of edge weight at AP_j
for κ *time-slots* **do**
  for *each MU-group* $\vartheta \in \mathcal{N}_j^{groups}$ **do**
    Compute edge weight $w_{\vartheta j}$ using (3.19)
    $\boldsymbol{\omega}_j \leftarrow w_{\vartheta j}$
AP_j broadcast $\boldsymbol{\omega}_j$ to STAs in cluster c using beacon signal
Distributed AP Selection at the STAs:
Receive $\boldsymbol{\omega}_j$ from each AP $j \in \mathcal{A}_c$ {APs within cluster c}
Construct $N_g \times M_c$ weight matrix $\mathcal{E}_c$
Construct Graph $G_c = (\mathcal{N}_c^{groups}, \mathcal{A}_c, \mathcal{E}_c)$;
Obtain $\mathcal{M}_c$: solve Graph G_c using **KMA Routine** [63, Alg. 2], [78], [79], [80];
Select AP j^* from $\mathcal{M}_c$ using policy in (3.20) and keep group membership ϑ at AP j^*.

Distributed Graph AP Selection Algorithm (DGAA)

Algorithm 2 is based on the KMA, which provides an optimal solution to assignment problems in polynomial time [78], [79], [80]. The problem in (3.18) is equivalent to a maximum weighted bipartite graph matching problem of finding the set of edge weights that maximizes the objective or conforms with (3.20) for all STAs. Subsequent to multiuser grouping, each AP computes the weight matrix $w_{\vartheta j}$ for each group $\vartheta \in \mathcal{N}_c^{groups}$. To better capture the effect of interference (or interference pattern) in the edge weight computation, the computation can be performed by taking a statistical average over a specified number, κ, of time-slots.

Using the regular *beacon signal*, each AP j broadcasts the weight vector $\boldsymbol{\omega}_j$ to the STAs in their respective cluster c. Upon the receipt of $\boldsymbol{\omega}_j$ from each AP, each STA regardless of its group membership, constructs a graph $G_c = (\mathcal{N}_c^{groups}, \mathcal{A}_c, \mathcal{E}_c)$ and the graph problem using the KMA routine to obtain an optimal association j^* according to the AP association policy in (3.20) and a typical STA retains its group *membership* at AP j^*. We remark that the APs do not require global CSI but only the CSI of STAs within their respective cluster. This reduces the computational complexity of the channel measurements and graph matching procedure.

Remark 3.1. ***Updated CSI or Dynamics:*** *Algorithm 2 can be implemented to handle changes in the network due to user mobility, updated CSI and/or arrival of new users. To handle such dynamics, APs can perform measurement periodically or per time-slot and update $\boldsymbol{\omega}_j$ for STAs to construct a new graph $G_c^{'}$ and solve the updated graph problem obtain to new set of associations, which can be achieved using a dynamic (or incremental) version of the KMA [65], [81]. In this case, the existing user-AP associations are not affected, only the users with updated CSI or new entrants*

require new associations and group membership.

Complexity of Algorithm 2

At each STA, the optimal matching is achievable with polynomial complexity $O\left(N_g^3\right)$ with $N_g = |\mathcal{N}_c^{groups}|$ the number of MU groups in each cluster. Efficient implementation of the KMA can be achieved using proper data structures and the computational complexity can be reduced to $O\left(N_g\right)$ with the use of slack variables [82], [83], and [65]. User-AP association is a type of *combinatorial problem* for which KMA achieves optimal matching [82], [83], and [65]. Hence, Algorithm 2 achieves local optimum as it does not take into account the global network information but solves subproblem of the user-AP association problem in a distributed manner, which is preferable to a centralized approach that has global knowledge.

3.3.6 Dual Ascent Approach

In this section, we seek another distributed approach to solving the MU-group-AP association problem. The solution to the Linear programming (LP) problem in (3.18) is realizable by solving its dual using dual decomposition techniques [76], [77] which is suitable for solving LP problem by formulating the dual of the problem. By decomposing the optimization problem in (3.18) into c subproblems (cluster-by-cluster) and substituting Eqn. (3.14) in (3.21a), the zero-one integrality constraint in (3.18c) is relaxed and the problem becomes convex as thus

$$\max_{0\leq\xi_{\vartheta j}\leq 1} \quad \sum_{j=1}^{M_c}\sum_{\vartheta=1}^{N_g}\log\mathcal{R}_\vartheta, \tag{3.21a}$$

$$\text{subject to} \quad \sum_{j=1}^{M_c}\xi_{\vartheta j}=1 \qquad \forall\vartheta\in\mathcal{N}_c^{groups} \tag{3.21b}$$

$$\sum_{\vartheta=1}^{M_c}\xi_{\vartheta j}\cdot\mathcal{R}_\vartheta\geq\hat{\mathcal{R}} \qquad \forall\vartheta\in\mathcal{N}_c^{groups}, \tag{3.21c}$$

where $N_g=|\mathcal{N}_c^{groups}|$ and the decomposition also allows the solution to be obtainable in a distributed manner at the STAs. Introducing the dual variables μ_j and β_ϑ corresponding to the user-AP association constraint (3.21b) and the minimum rate constraint (3.18d), respectively, the Lagrangian function of problem (3.21) is expressed as follows:

$$\mathcal{L}\left(\boldsymbol{\xi},\boldsymbol{\mu},\boldsymbol{\beta}\right)=\sum_{j=1}^{M_c}\sum_{\vartheta=1}^{N_g}\log\mathcal{R}_\vartheta-\left(\sum_{j=1}^{M_c}\mu_j\xi_{\vartheta j}-\mu_j\right)-\left(\sum_{\vartheta=1}^{M_c}\xi_{\vartheta j}\mathcal{R}_\vartheta\beta_\vartheta-\hat{\mathcal{R}}\beta_\vartheta\right), \tag{3.22}$$

where $\boldsymbol{\mu}=\{\mu_j\}$, $\boldsymbol{\beta}=\{\beta_\vartheta\}$ and $\boldsymbol{\xi}=\{\xi_{\vartheta j}\}$. This implies that the dual problem (3.21) is optimized over all APs in each cluster, and its corresponding Lagrange dual function

$$\mathcal{D}\left(\boldsymbol{\mu},\boldsymbol{\beta}\right)=\max_{\boldsymbol{\xi}}\mathcal{L}\left(\boldsymbol{\xi},\boldsymbol{\mu},\boldsymbol{\beta}\right). \tag{3.23}$$

Consequently, due to the convexity of the original problem (3.21), solving its dual is equivalent to solving problem (3.21). Therefore, the corresponding dual problem is

$$\text{minimize} \qquad \mathcal{D}\left(\boldsymbol{\mu}, \boldsymbol{\beta}\right) \tag{3.24a}$$

$$\text{subject to} \qquad \boldsymbol{\mu_1} \geq 0 \tag{3.24b}$$

$$\boldsymbol{\mu_2} \geq 0, \tag{3.24c}$$

this dual problem is convex since $\mathcal{D}\left(\boldsymbol{\mu}, \boldsymbol{\beta}\right)$ is a linear function of $\boldsymbol{\mu}$ and $\boldsymbol{\beta}$. Since the goal is to obtain a distributed AP association solution, we assume that each STA in each MU group, through the APs in their respective cluster, could obtain all the required knowledge to solve (3.24).

Algorithm 3: Dual Ascent Algorithm (DAA)

Input: $\mathcal{R}_\vartheta \qquad \forall \vartheta \in \mathcal{N}_c^{groups}$
Output: AP Association $\xi^*_{\vartheta j}$.
Distributed AP Selection at the STAs:
Initialize $\boldsymbol{\mu} = \{\mu_j\}$ and $\boldsymbol{\beta} = \{\beta_\vartheta\}$
do
Compute $\xi^*_{\vartheta j}$ using (3.26)
Update μ_j and β_ϑ using (3.28) and (3.29), respectively.
$z \leftarrow z + 1$
until $\xi^*_{\vartheta j}$ converges, $\boldsymbol{\xi}^* \leftarrow \xi^*_{\vartheta j}$
Select AP j^* using policy in (3.27) Keep group membership ϑ at AP j^*

To obtain a solution to this problem, the AP association policy can be found by setting $\bigtriangledown_{\boldsymbol{\xi}} \mathcal{L}\left(\boldsymbol{\xi}, \boldsymbol{\mu}, \boldsymbol{\beta}\right) = 0$ to satisfy Karush-Kuhn-Tucker (KKT) conditions [76], [77], which leads to:

$$\sum_{j=1}^{M_c} \sum_{\vartheta=1}^{N_g} \frac{1}{\xi_{\vartheta j} \ln 10} - \sum_{j=1}^{M_c} \mu_j - \sum_{j=1}^{M_c} \mathcal{R}_\vartheta \beta_\vartheta = 0, \tag{3.25}$$

where considering a simple case of one MU-group ϑ and one AP $_j$, the optimal decision

variable

$$\xi^*_{\vartheta j} = \frac{\ln 10}{\mu_j + \mathcal{R}_\vartheta \beta_\vartheta}, \tag{3.26}$$

and since the utility function in (3.21a) is concave in $\xi_{\vartheta j}$, $\xi^*_{\vartheta j}$ achieves the maximum utility given the optimal multipliers μ^*_j and β^*_ϑ. Since, the AP association problem is equivalent to minimizing $\mathcal{L}(\boldsymbol{\xi}, \boldsymbol{\mu}, \boldsymbol{\beta})$, a MU-group ϑ will select an AP_j based on the following AP association policy:

$$j^* = \arg\min_j \left\{ \frac{\ln 10}{\mu_j + \mathcal{R}_\vartheta \beta_\vartheta} \right\}. \tag{3.27}$$

which implies that MU group ϑ associates with AP_j if $j = j^*$. Hence, Algorithm 3 will be executed at each STA to obtain the best serving AP in terms of the solution to problem (3.24) that yields optimal $\xi^*_{\vartheta j}$, and each STA keeps membership with group ϑ at AP j^*. With Algorithm 3, the problem is iteratively solved by updating the Lagrangian multipliers μ_j and β_ϑ using subgradient method [77], [84] as thus:

$$\mu_j^{z+1} = \left[\mu_j^z - \varphi^z_{\mu_j} \left(\sum_{j=1}^{M_c} \xi^*_{\vartheta j} - 1 \right) \right]^+, \tag{3.28}$$

and

$$\beta_\vartheta^{z+1} = \left[\beta_\vartheta^z - \varphi^z_{\beta_\vartheta} \left(\sum_{j=1}^{M_c} \xi^*_{\vartheta j} \mathcal{R}_\vartheta - \hat{\mathcal{R}} \right) \right]^+, \tag{3.29}$$

where $[\cdot]^+ = \max\{\cdot, 0\}$, z is the iteration index while $\varphi^z_{\mu_j}$ and $\varphi^z_{\beta_\vartheta}$ [84] are the positive step-size for μ_j and β_ϑ, respectively.

3.4 Performance Evaluation

3.4.1 Simulation Setup

To evaluate the performance of the proposed algorithms in Section 3.3, we conduct a WLAN simulation based on the distribution coordination function (DCF) MAC protocol. In the simulation, a WLAN with saturated traffic, that is, all STAs have packet to send at each time-slot and the MAC-level saturation throughput is completely based on the Bianchi model in Section 3.2.3. The simulated system consists of N single antenna STAs and M APs each with K receive antennas, randomly distributed in a network area of 800 × 800-m. Since, we only consider the uplink saturation throughput of MU-MIMO, the number of APs $M = 50$ throughout the simulation while N number of STAs is varied to model different network densities.

Table 3.1: Key Simulation parameters

PHY Parameters			**MAC Parameters**	
Network area	800m × 800m		MAC Payload	802.11ac AMPDU
Channel Bandwidth	40 MHz		SIFS	$10\mu s$
OFDM FFT Size	64		ACK time, $\hat{T}_{\text{ack}}$	64 μs
Guard Interval	800 ns		DIFS	SIFS + 2 × Slot-time
SNR thresholds γ_o	0 dB and 15 dB		Slot-time	20 μs
PCS threshold	-70 dBm		Packet arrival rate	1/Slot-time
OFDM FFT Size	64		$CW_{\max}$ and $CW_{\min}$	1024 and 32
			Backoff time	10 μs

For the PHY layer setup, the number of antennas at the APs are equipped with $K = [2, 4, 8, 16]$ receive antennas throughout the simulation. The channel frequency considered for the simulated 802.11 WLAN is the 5-GHz channel, which has 10 non-overlapping 40-MHz channels and in each cluster, APs are deployed on each 40-MHz bandwidth. The parameter for the clustering in Section 3.3.1 is the PCS threshold

value of -70 dBm and carrier sensing range is determined by the path loss exponent $\alpha = 3.4$. The noise floor of the WLAN environment is assumed to be -100 dBm/Hz, the STAs transmit power is 15.85mW (12dBm) while the symbol energy $\mathcal{E}_x$ is normalized to 1. The main PHY layer parameters are based on the 802.11ac OFDM PHY standard and summarized in Table 3.1.

For channel access, a modified DCF MAC protocol is implemented where contention takes place among the groups rather than individual STAs. This implementation assumes some level of synchronization or coordination among STAs who are members of the same multiuser group. Once, a group wins the contention, all members (STAs) of the MU-group transmit concurrently in the uplink; in this implementation, we assume that one STA in a group contends on-behalf of its group. This group-based carrier sensing eliminates the chaotic channel access contention that could occur in high density WLANs where each STA has to contend for transmission opportunity. Other key MAC layer parameters are defined in Table 3.1, specifically, the Slot-time, SIFS, DIFS and ACK time $\hat{T}_{\text{ack}}$ are defined as 20μs, 10μs, SIFS + 2×Slot-time and 64μs respectively. Under the saturation condition, each STA always has a packet to transmit and it is assumed that each STA generates an 802.11ac AMPDU packet size of each STA which is fixed as $\mathcal{F}_i = 11454$ bytes.

In the next section, we compare the performances of the Graph-based algorithm (DGAA) in Section 3.3.5 and the Dual-Ascent algorithm (DAA) in Section 3.3.6 to a baseline strongest signal first (SSF) method use in existing WLAN systems. For the SSF scheme, each STA independently selects an AP that offers the best received signal strength and joins the appropriate MU group at the selected AP. The channel contention under the SSF scheme is the same as the group-based DCF described

earlier. The Dual-Ascent algorithm is intended to serve as an optimal benchmark for the graph-based solution. The performance metric is the proportionally-fair aggregate saturation throughput. In addition, similar to [52], [55], the geometric mean throughput is also measured mainly because there is a relationship between the geometric mean and the logarithmic utility defined in Eqn. (3.16); indicating load balance around throughput utility. Simulation results are averaged over 10^6 channel realizations of the network.

3.4.2 Simulation Results

Figure 3.4 compares the achievable total saturation throughput for various network densities (or number of STAs in the network) and numbers of antennas K at the APs with SNR threshold $\gamma_o = 15$ dB. Throughput utility indicates a proportionally fair performance of the entire network. The proposed graph-based algorithm outperforms the existing SSF scheme for any given network size in terms of N STAs. As the number of contending nodes increases, the graph-based algorithm performance improves while additional gains are achievable by increasing the number of antennas at the APs. An interesting observation in Figure 3.4 is that, increasing the number of K, antennas at the APs yields more DoF, which improves the performance of the proposed algorithms and the existing SSF approach, causing the performance of SSF scheme to asymptotically approach the proposed graph-based and dual ascent algorithms as N increases (more obvious at $N = 600$).

Fig. 3.5 depicts the saturation throughput utility versus the average number of multiuser groups per network size. With more MU groups in the network, the sum throughput utility increases. The geometric mean of the throughput utility is shown

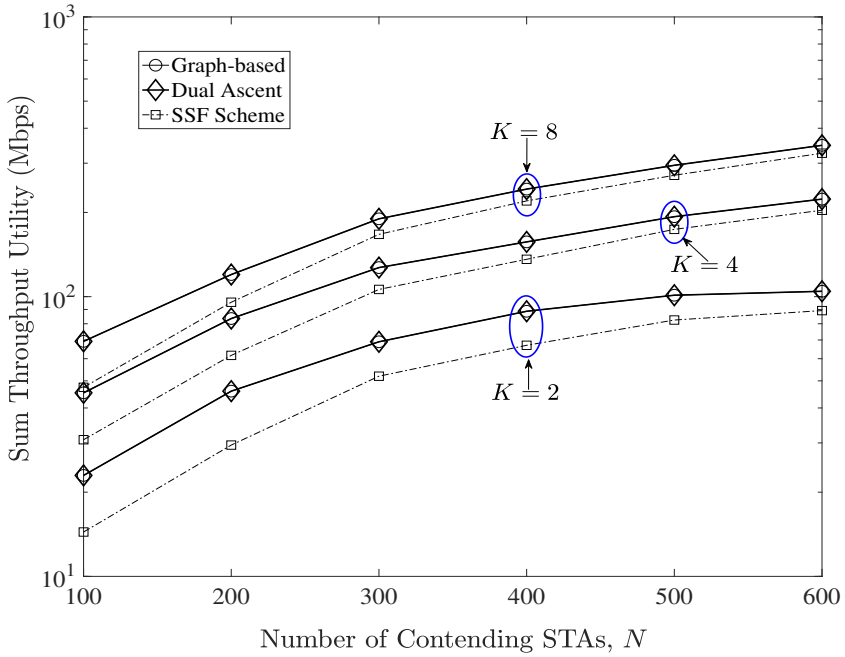

Figure 3.4: Sum throughput utility versus number of contending STAs (Network size) for various K antennas at the APs and SNR $\gamma_o = 15$ dB.

in Figure 3.6, which indicates the achievable proportionally-fair performance with respect to load at the APs. For SNR $\gamma_o = 15$ dB, while increasing the number of AP antennas yields 26.6% gain on average, increasing the number of STAs (network size) consequently decreases the mean utility achieved, which is an indication of the impact of offered load and saturation at the APs on throughput utility. Under such saturation condition, the proposed graph-based and dual ascent algorithms yield performance gains at a large network size of $N = 600$. In both Figures 3.4 and 3.5, the dual ascent algorithm establishes the optimality of the graph-based algorithm as the two algorithms achieve nearly identical performance.

For $N = 100$, 200 and 300, Fig. 3.7 shows the sum throughput utility for different number of antennas at the APs. At $\gamma_o = 0$ dB, the Graph-based method yield

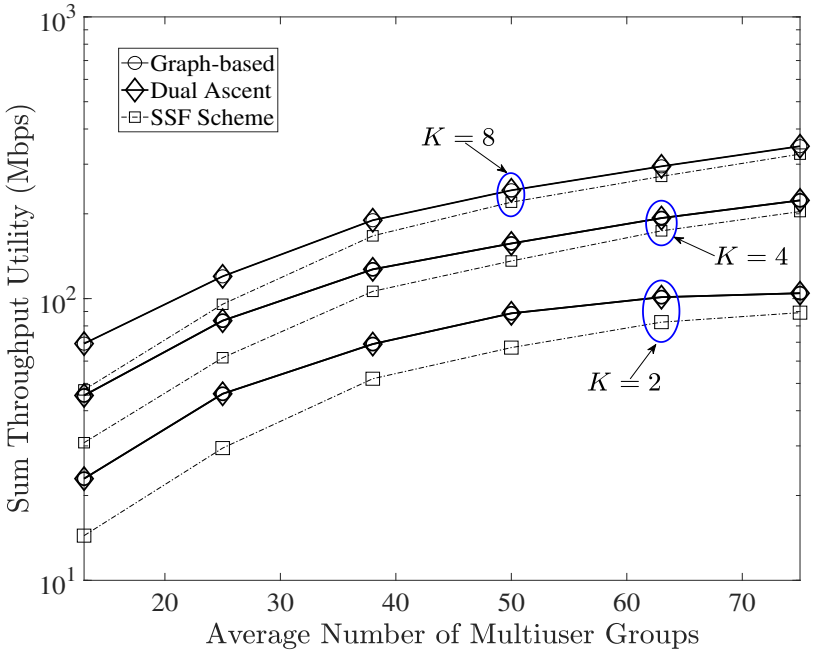

Figure 3.5: Sum throughput utility versus total multiuser groups in the network for various K antennas at the APs and SNR $\gamma_o = 15$ dB.

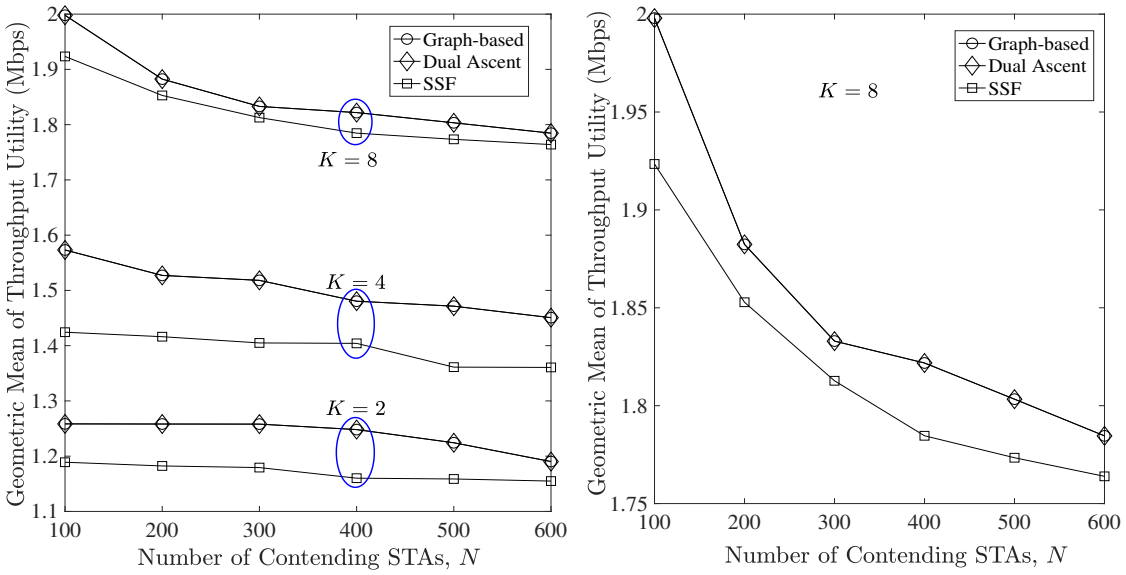

Figure 3.6: Geometric Mean of throughput utility versus number of contending STAs (Network size) for various K antennas at the APs and SNR $\gamma_o = 15$ dB

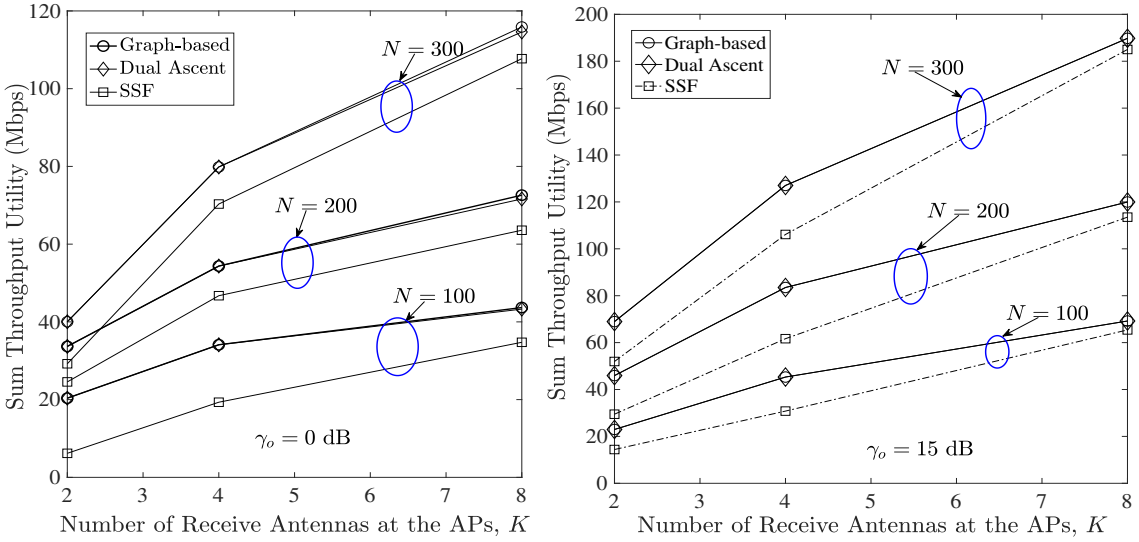

Figure 3.7: Sum throughput utility versus number of AP antennas for various N contending STAs, SNRs $\gamma_o = 0$ dB and $\gamma_o = 15$ dB.

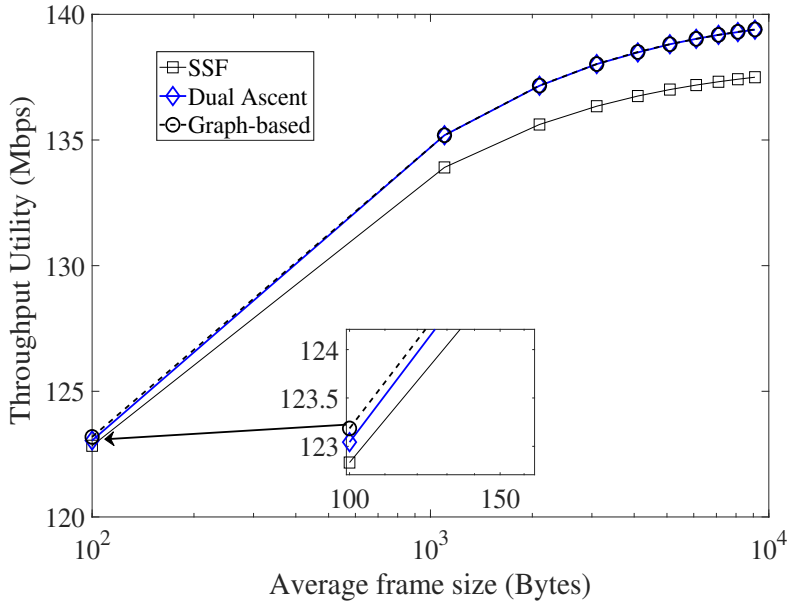

Figure 3.8: Average throughput utility versus average frame size $K = 8$, SNR $\gamma_o = 15$ dB and $N = 300$ STAs

improved throughput utility over the SSF scheme and the DoF of K antenna enhances the performance for any network size. Thus far, the frame size is assumed to be fixed for each STA and all MU groups. Fig. 3.8 shows the throughput performance for different average frame size $\mathcal{F}_i$. Except for a small fraction of discrepancy at low frame size of 100-bytes, the performance of the Dual ascent asymptotically approaches the Graph-based method. While increasing the average transmitted frame size $\mathcal{F}_i$, the proposed framework outperforms the existing baseline SSF scheme.

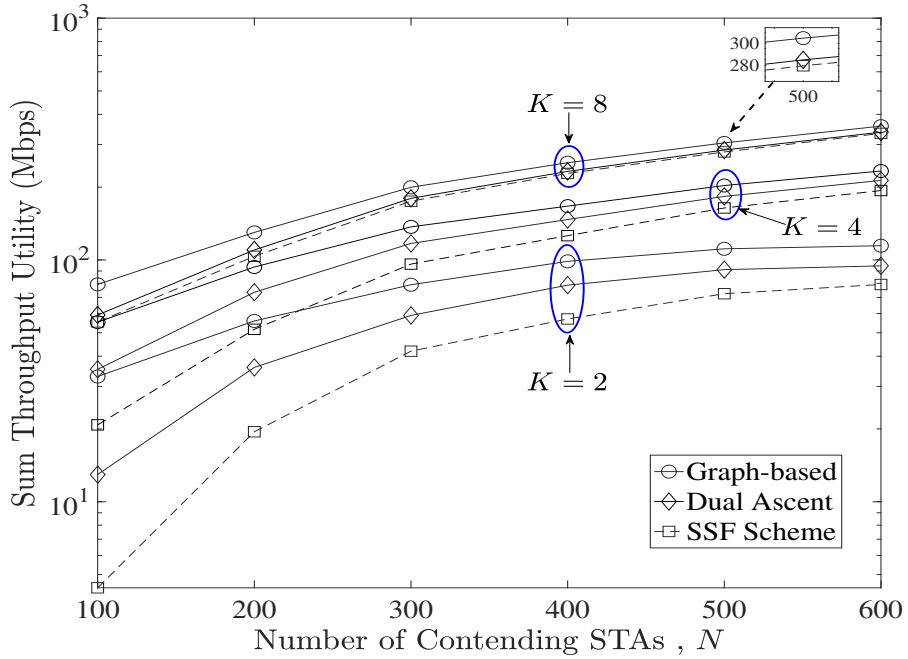

Figure 3.9: Centralized Case: Sum throughput utility versus number of contending STAs (Network size) for various numbers of antennas, K antennas at the APs and SNR $\gamma_o = 15$ dB.

In essence, regardless of the frame size transmitted by the STAs, optimally matching MU group to each AP improves performance. In a centralized case where AP association decision is based on global information, similar to an earlier work in [63],

is shown in Fig. 3.9, the graph-based scheme significantly outperforms the dual ascent method and the SSF scheme; the graph-based algorithm is known to achieve an optimal combinatorial problem solution. For large numbers of contending STAs, complexity becomes the bottleneck for the graph-based scheme. With increasing node density as in Fig. 3.9, performance of the Dual Ascent method approaches that of the graph-based method.

Remark 3.1. *The performance of the dual ascent method in Algorithm 3 asymptotically approaches that of the graph-based solution in Algorithm 2 because solving the AP association problem in a distributed manner, reduces the solution search space, as opposed to a centralized approach where the algorithms have global knowledge of the network. In the centralized case, the graph algorithm will outperform the dual ascent method with some increase in complexity.*

3.5 AP Association in Future Full duplex-WLANs

The proposed multiuser-AP association algorithm discussed above requires channel information and network measurement to solve the utility maximization problem. To this effect, another framework is proposed in this section to efficiently perform association based on *spatial statistics* rather than on deterministic user-AP channels that require constant updates or *a-priori* channel information. The aim of the next sections is to find a set of user-AP associations that maximizes the aggregate FD rate and the mean rate utility. This is important because spectral efficiency and overall network performance depend on the interference distribution, and interference distribution somewhat depends on the spatial pattern at which users are distributed among AP. The analysis of throughput gain when FD is performed in dense WLAN

with an optimized user-AP association and assuming that self-interference (SI) is reduced close to the noise level. Although, SI is ignored in this model, it is considered later in the FD model in Chapter 6.

3.6 FD WLAN System Model

3.6.1 Full-Duplex Communication Mode

In wireless LANs, full-duplex nodes operate in two modes, the *bidirectional transmission mode* and the *cut-through transmission mode* [85], [86]. When full-duplex nodes operate in the *bidirectional transmission mode*, a pair of AP-STA could concurrently transmit to each other while the *cut-through transmission mode* allows an access point (AP) to transmit to two stations (STAs) at the same time. Herein, we will assume that the full-duplex wireless LAN allows only bidirectional transmission mode, as shown in Figure 3.10, where STA y_i and AP x_i transmit concurrently to each other while AP x_i and STA y_i receivers experience interference from AP x_j and STA y_j respectively. This interference model in *bidirectional transmission mode* assumes that the self-interference (SI) can be reduced to the level of the noise floor [41] - we only consider out-of-cell interference as discussed later in Section 3.6.3.

3.6.2 Network Model

We assume a multi-cell WLAN where each AP in each cell or BSS serves its associated STAs, one at a time and only out-of-cell interference is taken into consideration. Subsequently, as shown in Figure 3.10, we will assume that each AP initiates full-duplex communication and is the *primary transmitter* while the STA being served is the *secondary transmitter*. Using the same assumption about transmitter/receiver

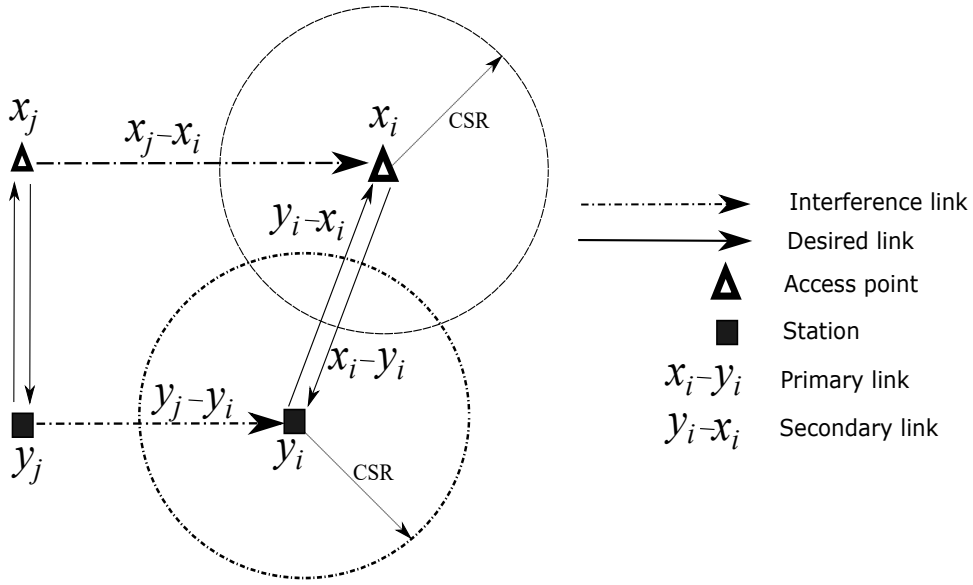

Figure 3.10: Bi-directional Full-duplex mode.

locations in [85], [86], [87], we assume that STAs and APs are distributed randomly according to a *Poisson bipolar model*. Specifically, the locations of the APs follow a homogeneous Poisson point process (PPP) $\Phi_a = \{x_1, x_2, \cdots, x_{|\Phi_a|}\} \subset \mathbb{R}^2$ with density λ_a and likewise, the locations of the STAs follow a homogeneous PPP $\Phi_s = \{y_1, y_2, \cdots, y_{|\Phi_s|}\} \subset \mathbb{R}^2$ with density λ_s. While the density of APs λ_a is fixed, the user density λ_s is *quasi*-static and users could dynamically enter and exit the network. For a pair of FD transmissions in a typical BSS, the path loss in both directions can be modeled as:

$$\ell(x, y) = \|x - y\|^{-\alpha}, \tag{3.30}$$

where α is the path loss exponent, $\|x - y\|$ denotes the *Euclidean* distance between the *primary transmitter* at point x and the *receiver* at point y.

3.6.3 Interference and Contention Model

At any point in time, the interference distribution on the network depends on the number of concurrent transmitters permitted by the CSMA/CA protocol following a contention period. To model the behavior of CSMA/CA protocol and the set of interference sources, the Matèrn hardcore point process (MHC PP) (a.k.a Matèrn Type II point process) [39], [40], [85], [86], [87] is very useful. In the CSMA/CA protocol, a prospective transmitter senses the channel within its carrier sensing range (CSR) and proceeds with its transmission if there is no other active transmitter within the CSR. For a typical *primary transmitter* x_i, the number of active transmitters within its CSR $\mathcal{R}$ is proportional to $\pi\mathcal{R}^2$. Therefore, only a subset of the parent PPP Φ_a will be permitted by the CSMA/CA protocol to transmit concurrently. Let $\tilde{\Phi}_a$ denote the new PPP of primary transmitters permitted by the CSMA/CA protocol on the network.

To obtain the new PPP $\tilde{\Phi}_a$, the MHC *thinning* process [40] is employed, which works as follows. In Fig. 4.6, a desired transmitter x_i forms a circle $b\left(x_i, \mathcal{R}\right)$ with radius $\mathcal{R}$ and contends with other transmitters within its CSR $\mathcal{R}$. Let associate a mark $\kappa \sim U[0,1]$ to each *primary transmitter* (AP) in the contention range (CSR) of x_i, x_i will be retained in $\tilde{\Phi}_a$ if it has the lowest mark, i.e, $\kappa_{x_i} < \kappa_{\bar{x_i}} \forall \bar{x_i} \in \bar{\mathcal{N}}_{x_i}$. In technical terms, this means that transmitter x_i has the lowest CSMA backoff counter among all the transmitters within its CSR. $\tilde{\Phi}_a$ is the new PPP obtained from *thinning* the parent PPP Φ_a and $\bar{\mathcal{N}}_{x_i} \subset \Phi_a$ is the set of transmitters in the contention neighborhood of typical x_i. Hence, density of the resultant CSMA MHC PP $\tilde{\Phi}_a$ for

the primary transmitters becomes:

$$\tilde{\lambda}_a = p_{x_i}\lambda_a = \frac{1 - e^{-\pi\mathcal{R}^2\lambda_a}}{\pi\mathcal{R}^2}, \tag{3.31}$$

where p_{x_i} is the *Palm probability of retaining* x_i in $\tilde{\Phi}_a$ [40], which is given as follows

$$p_{x_i} = \int_{\kappa} \exp\{-\pi\mathcal{R}^2\lambda_a\bar{x_i}\}\ \mathrm{d}\bar{x_i} = \frac{1 - e^{-\pi\mathcal{R}^2\lambda_a}}{\pi\mathcal{R}^2\lambda_a}. \tag{3.32}$$

Applying the same *thinning* process, the PPP of the concurrent *secondary transmitters* $\tilde{\Phi}_s$ has the following density:

$$\tilde{\lambda}_s = p_{y_i}\lambda_s = \frac{1 - e^{-\pi\mathcal{R}^2\lambda_s}}{\pi\mathcal{R}^2\lambda_s}\lambda_s = \frac{1 - e^{-\pi\mathcal{R}^2\lambda_s}}{\pi\mathcal{R}^2}, \tag{3.33}$$

where p_{y_i} is the probability of retaining y_i in $\tilde{\Phi}_s$. Herein, we assume that the CSR $\mathcal{R}$ is fixed globally on the network; this is the case in currently deployed WLAN systems. The received signal-to-interference plus noise (SINR) at receiver y_i from primary transmitter x_i is

$$\mathrm{SINR}_{x_i - y_i} = \frac{h_{x_i y_i} \cdot P_t \cdot \|x_i - y_i\|^{-\alpha}}{\sigma^2 + \sum\limits_{x_j \in \tilde{\Phi}_a, i \neq j} h_{x_j x_i} \cdot P_t \cdot \|x_j - x_i\|^{-\alpha}}, \tag{3.34}$$

and the SINR at receiver x_i from secondary transmitter y_i is

$$\mathrm{SINR}_{y_i - x_i} = \frac{h_{y_i x_i} \cdot P_t \cdot \|y_i - x_i\|^{-\alpha}}{\sigma^2 + \sum\limits_{y_j \in \tilde{\Phi}_s, i \neq j} h_{y_j y_i} \cdot P_t \cdot \|y_j - y_i\|^{-\alpha}}, \tag{3.35}$$

where $h_{x_i y_i}$ is the *Rayleigh* channel fading coefficient between the transmitter x_i and

the receiver y_i, which are set of *i.i.d* exponentially distributed random variables. P_t is the transmit power, which is assumed to be fixed with no power control or allocation, and σ^2 is the additive noise power. In this SINR model, we assume that the self interference (SI) is negligible or at least can be reduced close to the level of the noise floor [41]; this assumption does not affect our proposed association algorithm.

3.6.4 Performance Metric

Throughput Gain

In a half-duplex (HD) CSMA network, the receiver y_i could successfully decode the transmission from the transmitter x_i if the received $\mathrm{SINR}_{x_i-y_i}$ exceeds a threshold $\gamma_{x_i-y_i}$. This is known as the probability of successful transmission, $\mathbb{P}\left(\mathrm{SINR}_{x_i-y_i} > \gamma_{x_i-y_i}\right)$. Hence, the spatial network throughput density becomes

$$\Upsilon_{HD} = \tilde{\lambda}_a \cdot \mathbb{P}\left(\mathrm{SINR}_{x_i-y_i} > \gamma_{x_i-y_i}\right), \tag{3.36}$$

where $\mathbb{P}\left(\mathrm{SINR}_{x_i-y_i} > \gamma_{x_i-y_i}\right)$ is derived as follows (*See proof in* Appendix A.1):

$$\mathbb{P}\left(\frac{h_{x_iy_i}P_t\|x_i-y_i\|^{-\alpha}}{\sigma^2+\sum\limits_{x_j\in\tilde{\Phi}_a,i\neq j} h_{x_jx_i}\cdot P_t\cdot\|x_j-x_i\|^{-\alpha}} > \gamma_{x_i-y_i}\right) =$$

$$\exp\left(-\gamma_{x_i-y_i}\sigma^2\|x_i-y_i\|^{\alpha}P_t^{-1}\right)\exp\left(\tilde{\lambda}_a^{-1}\int_{\mathbb{R}^2}\ln\left(1+\gamma_{x_i-y_i}\left(\frac{\|x_i-y_i\|}{\|x_j-x_i\|}\right)^{\alpha}\right)\right). \tag{3.37}$$

For the full-duplex CSMA network, assuming the *primary transmitters* and the *secondary transmitters* have the same backoff counter, the density of FD transmission

pairs is the joint density of active *primary transmitters* $\tilde{\lambda}_a$ and the density of active *secondary transmitters* $\tilde{\lambda}_s$, which is given as

$$\lambda_{FD} = \frac{2 - e^{-\pi\mathcal{R}^2\lambda_a} - e^{-\pi\mathcal{R}^2\lambda_s}}{\pi\mathcal{R}^2}, \tag{3.38}$$

from (3.37) and (3.38), the spatial network throughput of FD CSMA is

$$\Upsilon_{FD} = \lambda_{FD} \cdot \mathbb{P}\left(\mathrm{SINR}_{x_i-y_i} > \gamma_{x_i-y_i}, \mathrm{SINR}_{y_i-x_i} > \gamma_{y_i-x_i}\right). \tag{3.39}$$

In most cases, the AP receiver (uplink) and the STA receiver (downlink) experience different magnitude of interference power. Therefore, the probability of successful transmission on the *primary link* (downlink) is independent of the probability of successful transmission on the *secondary link* (uplink). Hence, the joint probability $\mathbb{P}\left(\mathrm{SINR}_{x_i-y_i} > \gamma_{x_i-y_i}, \mathrm{SINR}_{y_i-x_i} > \gamma_{y_i-x_i}\right)$ for FD transmission can be written as:

$$\begin{aligned}
&\mathbb{P}\left(\mathrm{SINR}_{x_i-y_i} > \gamma_{x_i-y_i}, \mathrm{SINR}_{y_i-x_i} > \gamma_{y_i-x_i}\right) = \\
&\exp\left(\frac{\gamma_{x_i-y_i} + \gamma_{y_i-x_i}}{2}\sigma^2\|x_i - y_i\|^\alpha P_t + \|y_i - x_i\|^\alpha P_t\right) \\
&\times \left[\exp\left(\tilde{\lambda}_a^{-1}\int_{\mathbb{R}^2} \ln\left(1 + \gamma_{x_i-y_i}\left(\frac{\|x_i - y_i\|}{\|x_j - x_i\|}\right)^\alpha\right)\right)\right. \\
&\left.\exp\left(\tilde{\lambda}_s^{-1}\int_{\mathbb{R}^2} \ln\left(1 + \gamma_{y_i-x_i}\left(\frac{\|y_i - x_i\|}{\|y_j - y_i\|}\right)^\alpha\right)\right)\right].
\end{aligned} \tag{3.40}$$

Mean Full-Duplex Rate

Given the minimum SINR γ required to achieve a target rate, the achievable rate of a full-duplex transmission between STA at location y_i and the AP at location x_i is

defined as:

$$\mathbf{r}_{x_i y_i} = \mathbb{P}\left(\mathrm{SINR}_{x_i - y_i} > \gamma_{x_i - y_i}\right) \cdot \ln\left(1 + \gamma_{x_i - y_i}\right) + \mathbb{P}\left(\mathrm{SINR}_{y_i - x_i} > \gamma_{y_i - x_i}\right) \cdot \ln\left(1 + \gamma_{y_i - x_i}\right). \tag{3.41}$$

For *proportional fairness* among the nodes (i.e. proportionally fair user-AP association), using the mean rate utility model of [41], [88] the mean rate utility of a FD transmission is defined in terms of (3.41) as:

$$\bar{\mathbf{r}} = \mathbb{E}\left[\ln\left[\mathbf{r}_{x_i y_i}\right]\right] \qquad \text{(nats/sec/Hz)} \tag{3.42}$$

given the basic supported rate at SINR thresholds $\gamma_{x_i - y_i}$ and $\gamma_{y_i - x_i}$; for instance, see [51, Table II] for basic rates at different SINR thresholds.

3.7 Proposed User-AP Association Scheme

In this section, we address the user-AP association problem. Finding an optimal set $\mathcal{K}^*$ of user-AP associations is NP-hard and it is combinatorial in nature. Our objective is to find $\mathcal{K}^*$ that maximizes (3.41) for each FD link. From (3.41), it is apparent that any set of associations that maximizes the sum rate (sum of Eqn.3.41 over all possible FD links) will also maximize the mean rate utility (3.42). Therefore, to obtain a network-wide solution, we resort to finding an optimal user association indicator that maximizes the aggregate rate.

3.7.1 Problem Formulation

In a FD WLAN, if STA y_i associates with AP x_i, the rate of the FD link between AP x_i and STA y_i is given in Eqn. (3.41). Hence, given a set $\mathcal{K}$ of all feasible user-AP associations on the network and a subset $\mathcal{F} \subseteq 2^{\mathcal{K}}$ of feasible solutions, our objective is formulated as the following optimization problem:

$$\begin{aligned}
&\text{maximize} && \sum_{x_i \in \Phi_a} \sum_{y_i \in \Phi_s} \mathbf{r}_{x_i y_i} \cdot k_{x_i y_i}, && \text{(3.43a)}\\
&\text{subject to} && \mathcal{K}^* \in \mathcal{F}, && \text{(3.43b)}\\
& && \sum_{x_i \in \Phi_a} k_{x_i y_i} = 1 && \text{(3.43c)}\\
& && k_{x_i y_i} \in \{0, 1\}, && \text{(3.43d)}
\end{aligned}$$

where $k_{x_i y_i} \in \mathcal{K}^*$ is the binary variable defined as

$$k_{x_i y_i} = \begin{cases} 1, & \text{if STA } y_i \text{ associates with AP} x_i \\ 0, & \text{otherwise.} \end{cases} \tag{3.44}$$

3.7.2 Proposed User-AP Association Algorithm

To find a suboptimal solution to problem (6.40), we can relax constraint $k_{x_i y_i} \in \{0, 1\}$ in (6.40c) from a binary value to take on values between 0 and 1. By quantizing this association variable, the Lagrangian dual decomposition technique [49], [59], can be applied to solve problem (3.43). Consequently, the Lagrangian dual problem can be

written as follows:

$$\text{maximize} \qquad \sum_{x_i \in \Phi_a} \sum_{y_i \in \Phi_s} \mathbf{r}_{x_i y_i} \cdot k_{x_i y_i} - \pi_{y_i} \left(\sum_{x_i \in \Phi_a} k_{x_i y_i} - 1 \right) \tag{3.45a}$$

$$\text{subject to} \qquad k_{x_i y_i} \in [0, 1] \qquad \forall y_i \in \Phi_s \tag{3.45b}$$

where π_{y_i} is the Lagrange multiplier associated with the association constraint (6.40b). Then, the optimal user association indicator can be written as:

$$k^*_{x_i y_i} = \begin{cases} 1, & \text{if } x_i = \arg\max\limits_{x_i} \left(\mathbf{r}_{x_i y_i} - \pi_{y_i} \sum\limits_{x_i \in \Phi_a} k_{x_i y_i} - \pi_{y_i} \right) \\ 0, & \text{otherwise.} \end{cases} \tag{3.46}$$

Algorithm 4: User-AP Association for SISO Full-duplex

Initialization
  Set $t = 1$ {number of iteration}
  initialize π_{y_i}
  Set $t_{\max}$ {stopping criterion}
do
  if *(π_{y_i} is optimal)* **then**
    Get optimal association variable $k^*_{x_i y_i}$ according to (3.46)
  else
    Update π_{y_i} using (3.47)
    $t \leftarrow t + 1$
while $t_{\max} > t$;
end

The optimal value of π_{y_i} is realizable with the use of *subgradient method* [49] since the Lagrangian function of the dual problem is non-differentiable. Given a dynamic

step size $\phi(t)$, the optimal Lagrangian multiplier can be obtained as follows:

$$\pi_{y_i}^{t+1} = \left[\pi_{y_i}^{t} - \phi(t) \left(\sum_{x_i \in \Phi_a} k_{x_i y_i}^{t+1} - 1 \right) \right]^{+}, \tag{3.47}$$

the step size $\phi(t)$ is updated at each iteration and the proposed iterative algorithm for user-AP association is summarized in Algorithm 4.

3.7.3 Analysis of Full-Duplex Rate under Conventional Scheme

In this section, we determine the throughput of Algorithm 4 analytically. First, a statistical distribution of the user-AP associations is formulated in 3.7.3. Then, using this distribution, an approximated throughput gain is computed in Section 3.7.3.

User-AP Association Distribution

Let each user-AP pair at distance $\|y_i - x_i\|$ represents a pair of user-AP association on the network. From Algorithm 4, all user-AP association pairs, in $\mathcal{K}^*$ on the network can be described using a probability distribution according to **Proposition** 3.1.

Proposition 3.1. *Choose one of the STAs and one of the APs each with equal probability. The distance $\|y_i - x_i\|$ between STA y_i and its associated AP x_i has a probability distribution given by the following Matern hardcore (MHC) empty space distribution:*

$$f\left(\|y_i - x_i\|\right) = 2\pi\lambda_{as}\|y_i - x_i\| \exp\left(-\pi\lambda_a \|y_i - x_i\|\right), \tag{3.48}$$

where λ_{as} is the density of the user-AP association distribution.

Proof. Provided in Appendix A.2.

Throughput Gain

Therefore, for an STA at point y_i associated with an AP at point x_i, the average rate of its FD transmission is approximated by integrating the rate in (3.41) over the user-AP association distribution on the network as follows:

$$\hat{\mathbf{r}} = \int_{\theta=0}^{2\pi} \int_{\|y_i - x_i\|=0}^{\infty} \frac{f\left(\|y_i - x_i\|\right)}{2\pi} \mathbf{r} \, \mathrm{d}\|y_i - x_i\| \mathrm{d}\theta, \tag{3.49}$$

which is simply a volume integral and the aggregate rate is approximately the product of $\hat{\mathbf{r}}$ and the cardinality of the user-association PPP $|\Phi_{\mathrm{as}}|$ i.e, $\hat{\mathbf{r}} \times |\Phi_{\mathrm{as}}|$.

3.8 Numerical Results: SISO Full Duplex

3.8.1 System Parameters

For performance analysis, a network simulation and analysis was performed under different network densities λ_n. To model AP and STA locations on the WLAN, unique PPPs are generated to represent user and AP locations with densities λ_s and λ_a on a 2D network with an area of 200×200 m^2. The SINR thresholds $\gamma_{y_i - x_i}$ and $\gamma_{x_i - y_i}$ for the uplink and the downlink are chosen for specific rates in WLAN (see [51, Table II]) and are assumed to be the same γ for both UL and DL. The transmit power P_t of the APs and the STAs are 100mW (20 dBm) and 32mW (15 dBm) respectively, and the noise power is $\sigma^2 = -95$ dBm. The path-loss exponent $\alpha = 3.4$, which is the ITU path-loss exponent for rush-hour propagation. To compute the mean rate utility in Eqn.(3.42), the basic rate $\mathbf{r}_o$ is set to 2. The carrier sensing range (CSR) $\mathcal{R}$ depends on the PCS threshold and for a PCS threshold of -70dBm, the CSR is approximately 80m. Consequently, to compute the mean interference in the Monte

Carlo simulation, the number of concurrently active APs and STAs are determined by Eqns. (3.31) and (3.33) respectively.

3.8.2 Validation and Discussion

Figure 3.11 shows the mean rate utility at different SINR thresholds. Here, the same SINR threshold γ is assumed for the bidirectional link. The mean rate utility for half-duplex (HD) cases in the downlink and uplink are plotted. Clearly, Full-duplex (FD) could double the mean rate utility but an additional gain is possible with the proposed user-AP associations framework. In the case of *Legacy Association* (or SSF), STAs select the closest AP without considering the interference level at the selected AP. At low SINR, for instance, -10 dB, performance gain is insignificant but at high SINR regime, the proposed Algorithm 1 offers performance gains over the SSF or legacy association.

Figure 3.12 shows the performance gains as the network density increases. By increasing the network density, both the densities of APs and STAs are increased. Although there is a decline in the mean rate utility as the network density increases, it is likely due to the increasing interference level as the densities of users and APs increase. Looking at network density $\lambda_n = 0.5$, FD doubles the rate and the proposed Algorithm 1 outperforms the conventional nearest AP or legacy association scheme. While increasing the network density, the simulated Algorithm 1 achieves rate close to the analytical rate and outperforms the legacy association. Figure 3.13 shows the sum rate against number of STAs. For 85 STAs and with the proposed framework, the sum rate increases from 15 nats/sec/Hz to 40 nats/sec/Hz when each STA selects the AP that satisfies the minimum SINR threshold rather than selecting nearest AP

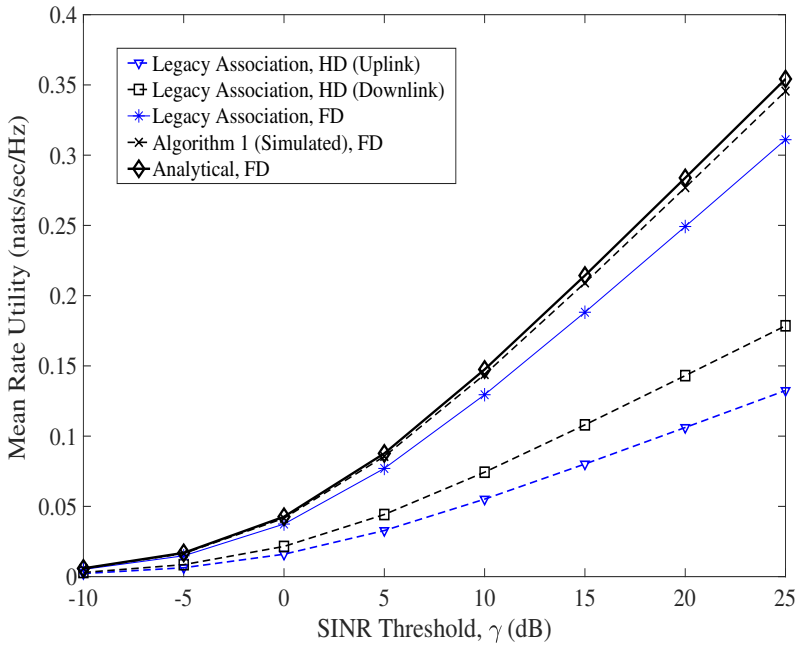

Figure 3.11: Mean rate utility versus SINR threshold, network density $\lambda_n = 0.2$, path-loss $\alpha = 3.4$.

based on signal strength. In the next section, this formulation is extended to FD WLANs with MIMO capability.

3.9 Chapter Summary

An efficient distributed framework to associate multi-user (MU) group to an AP is proposed as opposed to the current single-user AP association. The MU-group-AP association problem is formulated as a *logarithmic* throughput maximization problem, which is solved at each STA using a proposed *polynomial-time* graph-based algorithm and *Dual ascent* method. Simulation results validate the performance of the proposed algorithms over the legacy scheme and provide important conclusions on the MU uplink association in saturated WLAN. With more antennas at the APs, more STAs

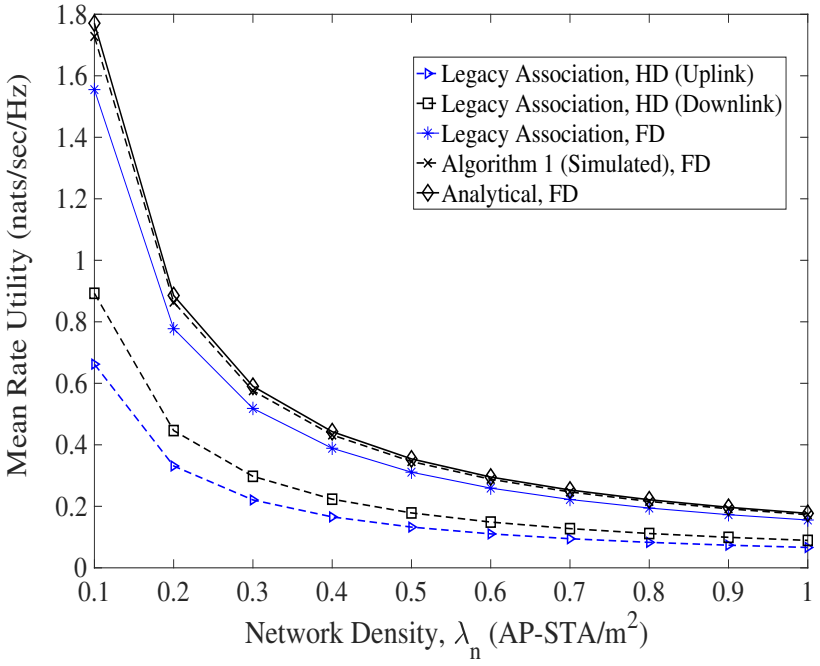

Figure 3.12: Mean rate utility vs network density, SINR $\gamma = 25$dB, path-loss $\alpha = 3.4$.

are grouped into each group, taking advantage of the antennas degrees of freedom. On the other hand, increasing the number of contending STAs, increases the load at the APs and consequently, average proportionally-fair throughput utility decreases, which is an indication of the impact of saturation on the overall performance.

In addition, A new user-AP association framework is proposed for additional performance gains in Full duplex wireless LANs using spatial statistics. For SISO FD systems it is shown that the spatial rate and the aggregate rate of a FD wireless LAN (FD-WLAN) can be improved by effectively distributing STAs among APs. Efficient user-AP association yields pairs of FD links, which improves the overall FD rate and the mean rate utility on the network. The density of future WLANs will require optimal distribution of users among APs such that interference level is minimal in the network; and if FD radio technology will be considered in future WLAN system, this

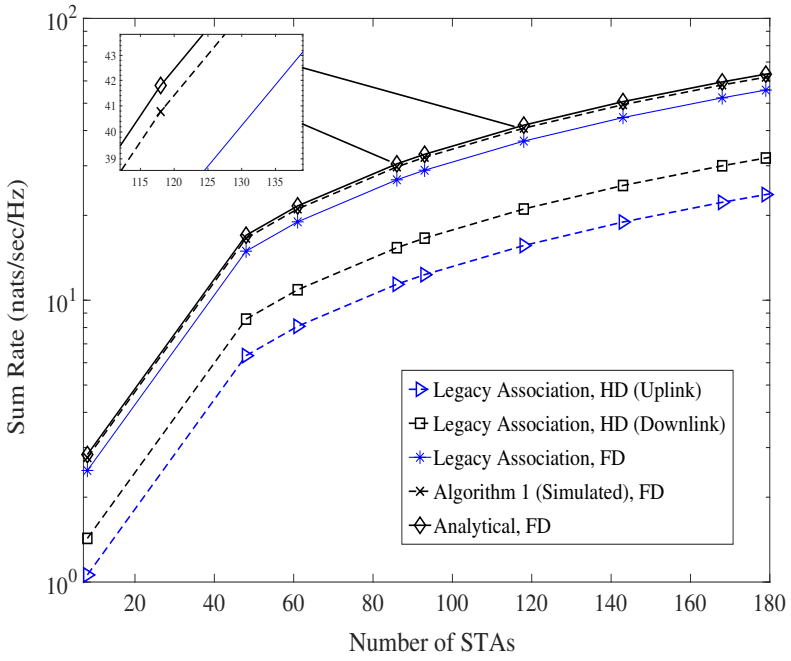

Figure 3.13: Sum rate versus number of STAs, SINR $\gamma = 25$dB, path-loss $\alpha = 3.4$.

evaluation shows that FD has the potential to double WLAN rate and associating STAs with APs satisfying SINR constraint, could yield additional throughput gains over the legacy nearest AP scheme.

Chapter 4

PCS Threshold Selection Frameworks

4.1 Introduction

As discussed in Chapter 2 under Section 2.1.4, the PCS process is an integral part of the WLAN protocol because it determines the effectiveness of the CSMA/CA and the degree of *spatial reuse* in the network. Thus far, in Chapters 3, a fixed or global PCS threshold is assumed. In this chapter, the problem of PCS threshold selection highlighted in Section 2.1.4 is addressed with the goal of optimizing the PCS threshold to maximize performance of high density WLANs. This chapter begins by first discussing the problem with the current system of selecting PCS threshold value to perform PCS process at the PHY and how it impacts spatial reuse and performance. Two different frameworks are proposed in this chapter, the first framework addresses the PCS threshold problem in WLANs with *Single-Input-Single-Output* (SISO) nodes, and the second framework optimizes PCS threshold for MIMO WLAN systems, taking into account the *hidden terminal* and the *exposed terminal* problem. In both cases, the overall objective is to maximize the spatial average of performance.

In current systems, the PCS threshold is static and often vendor dependent, and

is not adaptive to network topologies, fading characteristics, path-loss and other conditions of the wireless network environment. Due to the inevitable increase in network density, wireless networks are becoming increasingly interference-limited, and the ineffectiveness of this static PC threshold selection has long been a subject of investigation [10] (see the references therein). The scale of today's wireless LANs requires adaptive selection of the PCS threshold for the specific network environment where the nodes will operate. Recent approaches mostly assume uniform distribution of nodes, uniform data rates, and single antenna [10]. The reality, however, is that a PCS threshold depends on random node distribution, channel fading characteristics, antenna configuration, path loss, and node density. In [89], it is shown that PCS threshold adaptation enhances WLAN capacity.

As the density of today's WLANs continue to grow, improving spatial reuse becomes more important. Recent research into improving the performance of large-scale CSMA networks includes new CSMA-based protocol designs [90], [91], [92], dynamic tuning of the PCS threshold [11–14] and optimization of the PCS threshold to maximize performance [2], [60], [44, 93]. An enhanced variant of the listen-before-talk (LBT) or CSMA/CA protocol is proposed in [91] to facilitate efficient frequency reuse and interference avoidance when licensed-assisted access (LAA) for LTE systems coexists with 802.11 networks in the unlicensed band. The enhanced LBT schemes incorporate PCS threshold adaptation to avoid interference and increase channel access opportunity. An adaptive channel access scheme is proposed in [92] that exploits the information-theoretic capacity region of a multiple access channel. Exploiting the capacity region to determine the channel access strategy of a node, appears similar to an opportunistic CSMA [90], [94] where nodes with good channels are allowed to

contest for channel access while neglecting to properly choose the PCS threshold, which determines spatial reuse.

Under the 802.11ax working group, dynamic sensitivity control (DSC) [11–14] is recommended as an alternative scheme to the conventional static PCS threshold. The PCS threshold for DSC is implemented by setting a minimum (default sensitivity) and a maximum permissible threshold, usually between -82 and -30 dBm [12], [13], [95], [96] and the PCS threshold is chosen from this range based on transmission loss rate [12], [97], achievable throughput [13], [96], collision rate [95] and the measured received signal strength indicator (RSSI) between the target AP and its neighbor [96]. Since the performance of DSC over the PCS threshold varies from one topology and node density to another [11], it is important to select the PCS threshold margin for DSC based on specific network characteristics such as path loss, node density and fading. The protective clear channel assessment (ProCCA) [98] and fine-grained adaptation of carrier sensing threshold (FACT) [99] aim to improve spatial reuse by setting the PCS threshold according to the network information contained in the PHY header including measured interference.

Similar to [98], [99], using measured network information, [100] and [101] propose a DSC for IEEE 802.11ax APs to dynamically adjust the PCS threshold of an AP based on received signal strength (RSS) from its associated stations and interfering APs. New schemes to configure the PCS threshold based on signal-to-interference-and-noise ratio (SINR) in dense CSMA networks are proposed in [102]. To ensure interference-free transmissions, a static approach to set a global PCS threshold and a dynamic adjustment scheme based on the feedback of nearby transmissions, are proposed. Using the properties of stochastic geometry [44], [103], [93], [104], [105], a PCS

threshold selection rule (DSC scheme) that accounts for the randomness of user locations or node distribution and the channel access behavior, is investigated. Assuming stations (STAs) and APs are distributed according to independent homogeneous Poisson point process (PPP) [44], [103], the PCS threshold can be configured for *cell-edge* STAs by examining the information (link quality, average RSSI from neighbors) in *beacon* frames [44] and provide performance analysis of the DSC scheme given a range of PCS threshold values [103]. For a PPP network, the impact of the CSR on link performance is analyzed in [93], [104] to obtain a bound on the CSR and that bound is used to perform PCS threshold adjustment in a way similar to that of the DSC approaches.

Likewise, [105] provides an analysis of the DSC scheme for Poisson-distributed networks where a default PCS threshold and fixed threshold to update the PCS threshold are known *a priori*. Joint optimization of the PCS threshold and transmission rate for single-input single-out (SISO) Poisson ad hoc networks appears in [106]. Similar to [106], an analytical solution for optimal PCS threshold reveals the relationship between network capacity, PCS threshold and transmit power, and offers a technique to derive the CSR as a function of node density, access probability and duration of each channel state [107]. A host of proposed DSC schemes [12], [13], [95], [96], [97], [108] are based on *probing* procedures where nodes select PCS threshold values from a range of values depending on observed or measured network information. This measurement-based scheme could degenerate spectral efficiency over time as the system needs to keep track of changes in the network to update the PCS threshold. Also, improper PCS threshold margin could jeopardize the advantages of DSC as a result of collisions and disparity in the degree of fairness in accessing the channel [11]. Efficient

implementation of DSC schemes requires an adequate range of threshold values, and there is no consensus on a rule for their selection.

In summary, none of the previous approaches to uplink PCS exploits the multi-antenna nature of current WLANs. Also, the DSC schemes, ProCCA and FACT [12–14] require extensive channel measurement overhead. Adapting the PCS threshold based on this measured network information is further complicated by the CSMA/CA protocol, especially in high-density networks and may not guarantee optimality. The enhanced CSMA protocols proposed and analyzed so far [90], [94], [92] require knowledge of the optimal PCS threshold to guarantee optimal spatial reuse but do not propose methods for PCS threshold optimization. Finally, the PCS threshold should be optimized to prevent the hidden terminal and the exposed terminal problems inherent in the CSMA/CA protocol [10], [2], which are not addressed by the existing schemes [12], [90, 102]. Finally, optimizing the PCS threshold based on prior network information is more practical in large-scale WLAN as it avoids costs associated with persistent network monitoring.

In this chapter, the PCS threshold selection problem is addressed differently by jointly considering density of nodes, antenna configuration, channel fading and path loss. Herein, the performance metric of interest is the *spatial density of throughput* (SDT), which is the average number of successful transmission per unit area [42], [43]. The objective herein is to maximize the SDT by optimizing the PCS threshold for an arbitrary density of nodes, path loss exponent and antenna configuration for SISO and MIMO WLANs. Under the MIMO WLANs, the channel gains of the multi-antenna nodes are characterized by a *one-ring* scattering model [109].

4.2 PCS Threshold Selection in Dense SISO WLAN

In this section, the PCS threshold selection problem is addressed for a SISO dense WLAN. This important network parameter determines the spatial reuse permitted by the CSMA/CA protocol, which consequently determines the interference level and aggregate performance. A closed-form expression for PCS threshold selection is derived for a network where node locations are characterized as PPPs and the channel is Rayleigh fading. The PCS threshold optimization problem is first derived as a throughput function maximization problem, which allows the derivation of the PCS threshold as a function of node density and path loss exponent, parameters that are usually known *a priori*. That is, the optimal PCS threshold is based on the fundamental parameters of the network and does not require channel knowledge of each link.

4.2.1 Network Model

A WLAN with random AP deployment is considered. This choice is motivated by the fact that APs are not usually deployed in a regular grid due to physical and cost constraints; such randomness of AP locations is more common in unplanned networks e.g., the multi-tenant buildings, campus and enterprise networks. Therefore, let STA and AP locations be modeled as realizations of Poisson point processes (PPPs) with intensity λ. A PPP is suitable for modeling dense networks [44], [39], [43].

Both APs and STAs are distributed in the network in a random pattern according to independent homogeneous PPPs Φ_m and Φ_n with *intensities* λ_m and λ_n, respectively. To model AP and STA locations in the network, let $\Phi_m = \{y_1 \dots y_m\}$ denote the set of AP locations and $\Phi_n = \{x_1 \dots x_n\}$ denote the set of STA locations where

$m = |\Phi_m|$ and $n = |\Phi_n|$. Each AP and its associated STAs form a BSS or cell of AP_j centered at point y_j $\forall j \in \Phi_m$ as illustrated in Fig. 4.1. It is assumed that STAs associate with APs using the strong signal first (SSF) association [51]; that is, associate with the AP that offers the strongest beacon signal or closest AP.

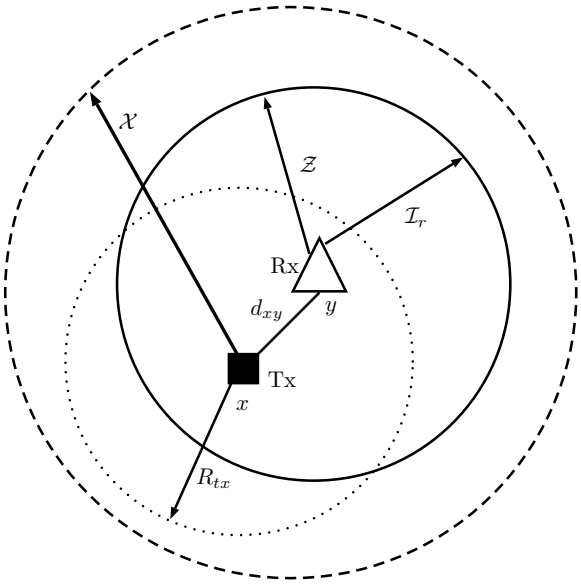

Figure 4.1: System and network model: interference, carrier sensing and transmission ranges.

4.2.2 Channel Model

The received power $P_{d_{xy}}$ at AP_y located at point y from STA_x located at point x is $P_{d_{xy}} = P^t.G_{xy}d_{xy}^{-\alpha}$. Assuming no power control, P^t is the fixed transmit power, α is the path loss exponent, d_{xy} is the distance between point x and point y shown in Figure 4.1 while G_{xy} is the channel gain for an AP-to-STA (or xy-links) links assumed to be Rayleigh fading, i.e $G_{xy} \sim \exp(P^t)$. In the presence of interference, a packet is

successfully received at AP_y from STA_x at an acceptable error rate if:

$$\text{SINR}_{xy} = \frac{P^t G_{xy} d_{xy}^{-\alpha}}{N_o + \sum\limits_{k \in \Phi_n \setminus \{x\}} P^t d_{ky}^{-\alpha} G_{ky}} \geq \gamma, \tag{4.1}$$

where d_{ky} is the distance between the receiving AP and the interference source k, $\sum\limits_{k \in \Phi_n \setminus \{x\}} P^t d_{ky}^{-\alpha} G_{ky}$ is the total interference power received by AP_y from transmitters other than STA_x, N_o is the background noise and γ is the SINR threshold. In a WLAN, we can map γ to different bit rates depending on the standard being supported.

4.2.3 PCS Threshold Constraint

During PCS, a typical STA_x decides to transmit or defer if $\mathbb{I}_c < \Gamma$ where $\mathbb{I}_c$ is the total power sensed on the channel during PCS and Γ is the PCS threshold. The CSR $\mathcal{X}$ is a spatial parameter, which determines the area where a node senses the presence of an active transmission on the channel. In order for a node to detect the presence of an active transmission, the CSR should ideally cover the potential interference range $\mathcal{I}_r$ and the transmission range R_{tx} as illustrated in Figure 4.1. Sensing the interference area and the transmission range during carrier sensing helps nodes to avoid interference prior to transmission. Therefore, as mandated by the CSMA protocol, STA_x defers its transmission to AP_y, if the total power $\mathbb{I}_c$ sensed on the channel exceeds the PCS threshold Γ. The relationship between Γ and $\mathcal{X}$ is that any signal sensed within range $\mathcal{X}$ should not exceed Γ. We can determine Γ when $\mathcal{X}$ is known, by estimating the received signal power at the edge of the CSR area (*the outermost disc* in Fig. 4.1).

4.2.4 Performance Metrics

In this section, we introduce two metrics. First, the probability that a typical node is granted access to the network by the CSMA/CA protocol is derived and this probability is referred to as the *Channel Access Probability* (CAP), $\mathcal{P}_{\mathrm{CAP}}$. The implication of multiple users having high CAPs to use the channel is strong interference in the network as many users will transmit concurrently and strong interference implies low SINRs. To capture the effect of interference, another metric, the *Spatial Density of Throughput* (SDT), [1] is introduced. The SDT measures the average number of users per unit area that *gain access to the medium* and *achieve target SINR* [42].

Channel Access Probability

We derive the CAP of a typical user given that the set Φ_a with density λ_a is known *a priori*. Let $\mathbb{I}_c = P^t_{\bar{x}} G_{x\bar{x}} d^{-\alpha}_{x\bar{x}}$ be the power sensed by STA_x from its neighbor $\bar{x}$ during carrier sensing. The probability that STA_x acquires the channel depends on whether constraint $\mathbb{I}_c < \Gamma$ is satisfied according to the following proposition.

Proposition 4.1. *Given a parent PPP Φ_n of STAs on the network and the channel access constraint $\mathbb{I}_c < \Gamma$, the channel access probability $\mathcal{P}_{CAP}$ of a STA x depends on the contention neighborhood of x :*

$$\bar{\mathcal{N}_x} = \{\bar{x} \in \Phi_n : \mathbb{I}_c > \Gamma\} \tag{4.2}$$

where $\bar{\mathcal{N}_x}$ denotes the set of nodes whose signals could collide with STA x's signal if they transmit concurrently; that is, STA $\bar{x}$ causing interference power of at least Γ

[1] Measures the average throughput of successful transmissions per time slot [42], [43].

to node x's transmission.

$$\mathcal{P}_{\text{CAP}} = 1 - \mathbb{P}\left[P^t_{\bar{x}} G_{x\bar{x}} d^{-\alpha}_{x\bar{x}} > \Gamma\right] \tag{4.3}$$

$$\mathbb{P}\left[G_{x\bar{x}} > \frac{\Gamma}{P^t_{\bar{x}} d^{-\alpha}_{x\bar{x}}}\right] = \mathbb{E}_{\bar{x}\in\Phi_n}\left[\exp\left(-\frac{\Gamma}{P^t_{\bar{x}} d^{-\alpha}_{x\bar{x}}}\right)\right] = \exp\left(-\mathbb{E}_{\bar{x}\in\Phi_n}\left[-\frac{\Gamma}{P^t_{\bar{x}} d^{-\alpha}_{x\bar{x}}}\right]\right) \tag{4.4}$$

$$= \exp\left(-\lambda_n \int_{\mathbb{R}^2} \frac{\Gamma}{P^t_{\bar{x}} d^{-\alpha}_{x\bar{x}}}\right) = \exp\left(-\lambda_n \cdot \frac{d^{\alpha+1}_{x\bar{x}}}{\alpha+1} \cdot \Gamma P^t_{\bar{x}}\right) \tag{4.5}$$

where Eqn. (4.4) is obtained using the independence of the Rayleigh fading channel gains $G_{x\bar{x}}$ and applying Jensen's inequality (($\mathbb{E}[g(x)] \geq g[\mathbb{E}(x)]$)), Eqn. (4.5) is obtained by using *Campbell's Theorem* stated in Eqn. (2.4) under Theorem 2.3 and applying the integral approximation in (Eqn. 2.01.1 in [110]). Figure 4.2 depicts the CAP derived in (4.5). Increasing the density of users, the CAP decreases due to an increase in contention and at high PCS threshold, the STAs becomes more sensitive because the CSR shrinks and an STA's CAP decreases.

Spatial Density of Throughput

As discussed later in Section 4.3, maximizing the CAP derived in Proposition 4.1 could technically increase the number of simultaneous transmissions. However, this is detrimental to achieving higher throughput because the more users that gain access to the channel transmit the stronger the interference. In other words, larger CAP is preferred to increase spatial reuse but the trade-off is strong interference, which prevents the receiver from successfully decoding the packets. To capture the effects of larger CAP and interference, the SDT measures the number of successful

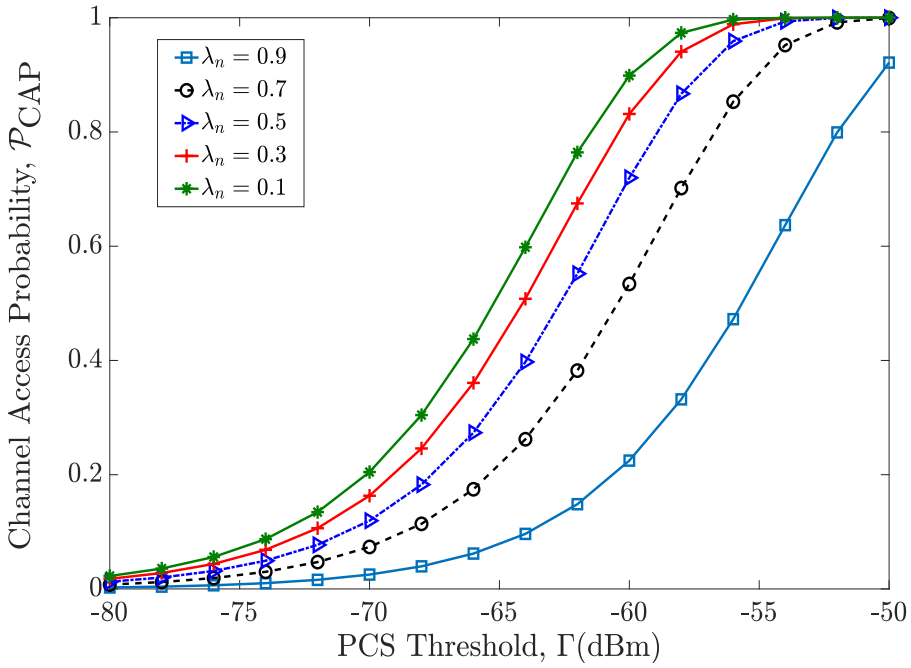

Figure 4.2: Channel access probability given arbitrary PCS threshold values for different STA densities λ_n with path loss exponent $\alpha = 3.4$.

transmissions as thus:

$$\mathcal{R}_{\text{SDT}} = \lambda_n \cdot \mathcal{P}_{\text{CAP}} \cdot \mathbb{E}\left[\sum_{x \in \Phi_n} \mathbb{1}_{\text{SINR}_{xy} > \gamma}\right] \tag{4.6}$$

where, $\mathbb{1}_{\text{SINR}_{xy}>\gamma} = 1$ indicates that STA_x achieves $\text{SINR}_{xy} > \gamma$ at AP_y receiver, the $\mathbb{E}[\cdot]$ term is the well-known coverage probability [42] or technically, the probability that a node achieves SINR above a threshold γ. This probability is:

$$\mathbb{E}\left[\sum_{x \in \Phi_n} \mathbb{1}_{\text{SINR}_{xy}>\gamma}\right] = \mathbb{P}\left(\text{SINR}_{xy} > \gamma\right) = \mathbb{P}\left(P^t G_{xy} d_{xy}^{-\alpha} > \gamma \left(N_o + \sum_{k \in \Phi_n \setminus \{x\}} P^t d_{ky}^{-\alpha} G_{ky}\right)\right)$$

$$\mathbb{E}_{G_{ky}, \Phi_n}\left[\exp\left(-\gamma N_o d_{xy}^{\alpha}\right) \cdot \exp\left(-\gamma N_o d_{xy}^{\alpha} \sum_{k \in \Phi_n \setminus \{x\}} d_{ky}^{-\alpha} G_{ky}\right)\right] \tag{4.7}$$

$$= \exp\left(-\gamma N_o d_{xy}^{\alpha}\right) \cdot \mathbb{E}_{\Phi_n}\left[\prod_{x\in\Phi_n\setminus\{x\}} \frac{1}{1+\gamma\left(\frac{d_{xy}}{d_{ky}}\right)^{\alpha}}\right] \tag{4.8}$$

$$= \exp\left(-\gamma N_o d_{xy}^{\alpha}\right) \cdot \exp\left(\mathbb{E}_{\Phi_n}\left[-\sum_{k\in\Phi_n\setminus\{x\}} \ln\left(1+\gamma\left(\frac{d_{xy}}{d_{ky}}\right)^{\alpha}\right)\right]\right) \tag{4.9}$$

$$= \exp\left(-\gamma N_o d_{xy}^{\alpha}\right) \cdot \exp\left(-\lambda_n \cdot \int_{\mathbb{R}^2} \ln\left(1+\gamma\left(\frac{d_{xy}}{d_{ky}}\right)^{\alpha} \mathrm{d}d_{ky}\right)\right) \tag{4.10}$$

$$\exp\left(-\gamma N_o d_{xy}^{\alpha}\right) \cdot \exp\left(-\lambda_n \Theta \cdot \ln\left(1+\Theta^2\right) 2\gamma d_{xy}^{\alpha} d_{ky}^{-\alpha} + 2\arctan \gamma d_{xy}^{\alpha} d_{ky}^{-\alpha}\right), \tag{4.11}$$

where Eqn. (4.7) follows from the independence of the Rayleigh fading channel gains G_{xy}, Eqn. (4.8) is obtained from taking the expectation w.r.t channel gains G_{ky} of the interference links, (4.9) follows from applying Jensen's inequality ($(\mathbb{E}\left[g(x)\right] \geq g\left[\mathbb{E}(x)\right])$) while (4.10) is obtained from using the property of PPP in Theorem 2.3 and (4.11) follows from the integral transformation of [110, Eqn. 2.733.1]. Fig. 4.3 illustrates Eqn. (4.11) for different network densities where it is observed that the coverage probability of a typical node decreases as the network density increases. This is due to increasing interference that comes with increasing the number of network nodes. For a fixed system bandwidth BW, the *mean rate utility* is

$$\log\left[\left(BW \cdot \log_2\left(1+\gamma\right)\right) \cdot \mathcal{R}_{\mathrm{SDT}}\right], \tag{4.12}$$

which is proportional to the $\mathcal{R}_{\mathrm{SDT}}$ metric as defined in Eq. (4.6).

4.3 Proposed PCS Threshold Optimization for SISO WLAN

In this section, we optimize the PCS threshold to maximize the SDT derived in Eqn. (4.6) under Section 4.2.4 given the CAP derived in Eqn. (4.5) of Proposition (4.1)

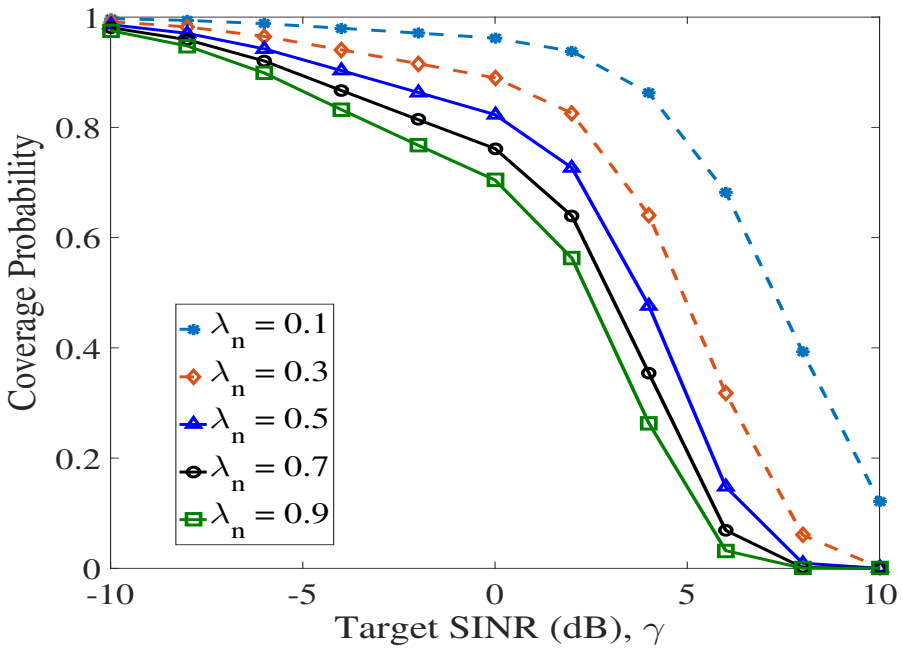

Figure 4.3: Coverage probability versus target SINR for given STA density λ_n, path loss exponent $\alpha = 3.4$ and noise floor $N_o = -100$ dBm.

for a given density of contending STAs λ_n. Since larger CAP implies more concurrent transmissions and strong interference, SDT is being maximized to capture the effect of strong interference due to larger CAP. This helps ensure that we can enhance spatial reuse and at the same time contain the effect of interference. With the constraint imposed by the PCS threshold, the problem is formulated as:

$$\text{maximize} \qquad \mathcal{R}_{\text{SDT}} \tag{4.13a}$$

$$\text{subject to} \qquad \mathbb{I}_c \leq \Gamma \qquad x \in \Phi_n. \tag{4.13b}$$

For a given Lagrangian multiplier ψ, by obtaining the Lagrangian function $\mathcal{L}(\Gamma, \psi)$ of (4.13), satisfying the Karush-Kuhn-Tucker (KKT) conditions [77] and solving $\nabla_{\Gamma,\psi}\mathcal{L}(\Gamma, \psi) = 0$, the PCS threshold that improves spatial re-use and achieves target

SINR to guard against interference is obtained as:

$$\exp\left(-\lambda_n \cdot \frac{d_{x\bar{x}}^{\alpha+1}}{\alpha+1} \cdot \Gamma P_{\bar{x}}^t\right) = \frac{\psi \cdot (\alpha+1)}{\lambda_n^2 \mathbb{P}\left(\mathrm{SINR}_{xy} > \gamma\right) \frac{d_{x\bar{x}}^{\alpha+1}}{\alpha+1} \cdot P_{\bar{x}}^t} \tag{4.14}$$

$$\lambda_n \cdot \frac{d_{x\bar{x}}^{\alpha+1}}{\alpha+1} \cdot \Gamma P_{\bar{x}}^t = \log\left[\frac{\psi \cdot (\alpha+1)}{\lambda_n^2 \mathbb{P}\left(\mathrm{SINR}_{xy} > \gamma\right) \frac{d_{x\bar{x}}^{\alpha+1}}{\alpha+1} \cdot P_{\bar{x}}^t}\right] \tag{4.15}$$

$$\Gamma^* = \log\left[\frac{\psi \cdot (\alpha+1)}{\lambda_n^2 \mathbb{P}\left(\mathrm{SINR}_{xy} > \gamma\right) \frac{d_{x\bar{x}}^{\alpha+1}}{\alpha+1} \cdot P_{\bar{x}}^t}\right]\left(\frac{1}{\lambda_n \cdot \frac{d_{x\bar{x}}^{\alpha+1}}{\alpha+1} \cdot P_{\bar{x}}^t}\right), \qquad \psi > 0, \tag{4.16}$$

given any small value of ψ and unit transmit power, $P_{\bar{x}}^t = 1$ (4.16) can be written as:

$$\Gamma^* = \left[\frac{\mathbf{W}\left[0, -2\pi\lambda_n \Gamma(\alpha)\,\alpha \cdot \frac{\psi}{\lambda_n \mathbb{P}\left(\mathrm{SINR}_{xy}>\gamma\right)}\right]}{-2\pi\lambda_n \Gamma(\alpha)\,\alpha}\right]^{\frac{1}{\alpha-1}},$$

where $\mathbf{W}[\cdot]$ is the Lambert W function [111] and $\Gamma(\cdot)$ is the Gamma function.

4.4 Numerical Results: SISO WLANs

For performance analysis, simulation is performed for different network densities λ_n and different target rates given by SINRs thresholds γ. The realizations of the PPPs with intensity λ_n and λ_m model STAs and APs locations in the WLAN, respectively while the transmit power $P_{\bar{x}}^t$ is normalized to unity. The path loss exponent $\alpha = 3.4$, which is ITU "rush-hour" propagation and $N_o = -100$ dBm. The result obtained by setting the PCS threshold according to (4.16) is compared to the conventional fixed PCS threshold and the Random PCS threshold selection. The results obtained by setting the PCS threshold according to (4.16) is referred to as "Proposed" in the simulation results. The SDT and the rate utility are averaged over 10^4 samples of

the network. For the "Random Selection" method, the PCS thresholds are uniformly distributed between -50 and -100 dBm while in the "Conventional" method, Γ is set to -70 dBm.

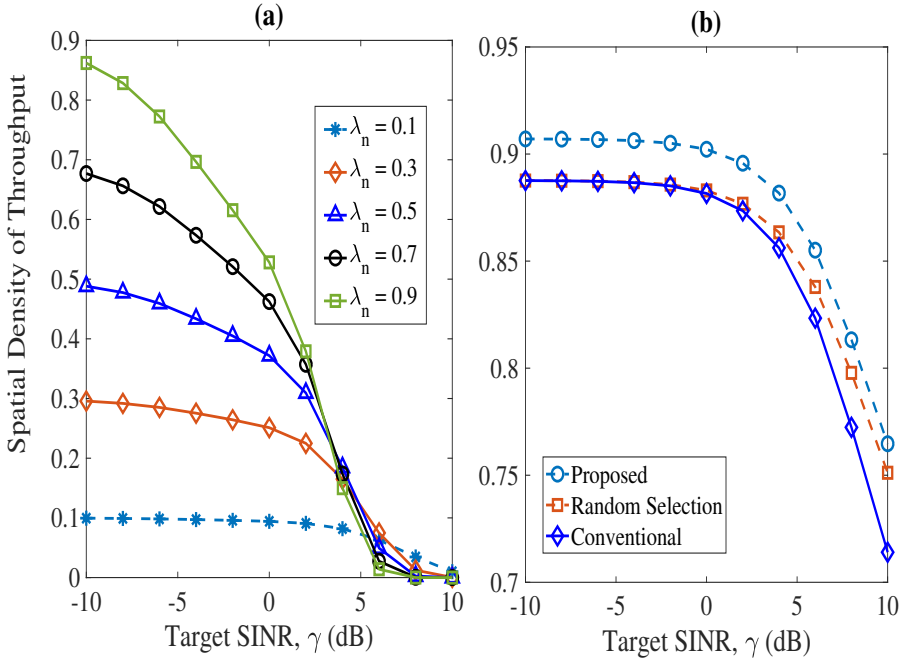

Figure 4.4: (a) SDT for various target SINR γ and node density λ_n given path loss $\alpha = 3.4$ (b) SDT versus target SINR given path loss $\alpha = 3.4$ and $\lambda_n = 0.7$.

Fig. 4.4 (a) depicts the SDT under different target SINRs and node densities. For basic rates at low SINRs, throughput increases with network densification. However, when users require rates at high SINRs, increasing node density decreases the throughput density. Technically, as network density increases, interference increases and it becomes difficult to guarantee high SINRs to users. Performance can be enhanced by tuning the PCS threshold Γ. In Fig. 4.4(b), the performance of the proposed PCS selection in (4.16) over the conventional scheme yields a gain of 0.034 in SDT as observed at 5 dB SINR. Fig. 4.5 depicts the mean rate utility in (4.12) at a high density

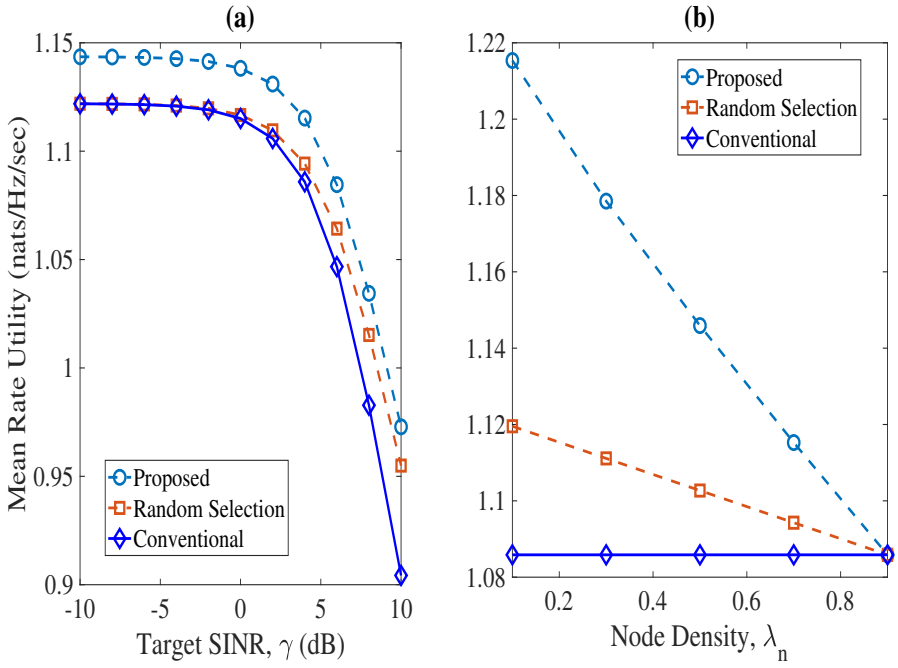

Figure 4.5: Mean rate utility for (a) various target SINR γ given path loss $\alpha = 3.4$ and $\lambda_n = 0.7$ (b) various node density λ_n given $\alpha = 3.4$ and $\gamma = 5$dB.

of $\lambda_n = 0.7$. With increasing the target SINR in Fig. 4.5(a), the proposed method yields significant gain in rate utility. Observing node density $\lambda_n = 0.1$ in Fig. 4.5(b), a gain of 12.5% over the conventional scheme is apparent. As the node density increases, the mean rate utility decreases. This is due to an increase in interference. However, the proposed scheme still provides modest gains as node density increases.

4.5 PCS Threshold Selection in Dense MIMO WLAN

In Section 4.2, the PCS threshold selection problem is addressed under the assumption that nodes are equipped with single antenna. In this section, the problem formulation is extended to a MIMO case where nodes are equipped with multiple antennas. The goal in this section is to examine the impact of multiple antennas on PCS threshold

selection and the PCS process. Two inherent problems in CSMA/CA networks, namely, the *hidden terminal* and the *exposed terminal* problems are also taken into account. Similar to the SISO case in Section 4.2, the performance metric of interest is the SDT, which measures the average number of successful transmission per unit area [42], [43]. That is, the PCS threshold selection problem is formulated as a SDT maximization problem. From the SDT maximization problem, the PCS threshold is optimized for an arbitrary density of nodes assuming a path loss exponent, MIMO capable nodes and channel gains that are characterized by a *one-ring* scattering model [109]. Optimizing the PCS threshold based on prior network information is more practical in large-scale WLAN as it avoids costs associated with persistent network monitoring.

To consider the hidden and the exposed terminal problems, two constraints are introduced into the optimization problem to account for their effects in PCS threshold selection. This is important because the existence of hidden terminals results in collisions at the receiver, causing persistent retransmissions while exposed terminals could depress spectral reuse. The tradeoff is that high PCS threshold allows for the existence of *hidden nodes* while low PCS threshold creates *exposed nodes*. Hence, the fundamental question is *how do we optimize the PCS threshold* Γ *to achieve a balance in the trade off between the hidden terminal problem and the exposed terminal problem?* The impact of our proposed PCS threshold selection method is assessed by comparing its performance to the legacy scheme and the DSC scheme in [112] applied earlier in [103] for stochastic networks. In addition an analysis on the maximum density of nodes that guarantees improved performance, is provided.

Throughout this section, the following notations are used. Boldface uppercase

letters represent matrices. For instance, matrix $\mathbf{H}$ represents the channel matrix between a user and an AP. Column vectors are denoted as boldface lowercase letters such as $\mathbf{x}$ representing the transmitted symbols. The expected value of any random variable will be denoted as $\mathbb{E}[\cdot]$. The Frobenius norm of a matrix is denoted as $\|\cdot\|^2$. Superscripts $[\cdot]^H$ and $[\cdot]^T$ represent Hermitian (conjugate transpose) and transpose, respectively while $\mathrm{tr}(\cdot)$ is the trace of a matrix.

4.5.1 Network Model and Assumptions

We consider a WLAN where STA and AP locations are modeled as independent homogeneous PPPs with respective intensities, λ_n and λ_m. This choice is motivated by the fact that PPPs are suitable for modeling dense networks [39] and STAs/APs are not usually deployed in a regular grid due to physical constraints. Let $\mathcal{N}$ represent the set representing the PPP of STAs and $\mathcal{A}$ represent the set of APs in the network. Subsequently, we focus primarily on deriving the performance metric and the optimal PCS threshold for uplink (UL) transmissions.

This is due to the fact that contention in the UL is usually more severe than that of the downlink (DL), since in most WLANs, there are more user STAs than APs. For example, in Internet of Things (IoT) applications, the UL may be the bottleneck because large numbers of devices that sense the environment need to transmit their information to a central AP. In this sensing scenario, much less information would flow in the DL direction. Herein, based on Assumption 4.1, and we focus primarily on optimizing the PCS threshold selection for the UL:

Assumption 4.1. *While STAs are randomly located in the network, APs are well planned and deployed in such a pattern that allows sufficient separation of multiple*

concurrent downlink transmissions in space. In other words, adequate CSR is achieved for the DL through proper planning of AP deployment, which is achieved through spacing of APs in the network.

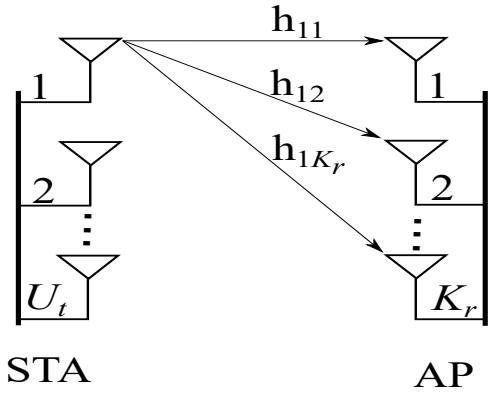

Figure 4.6: Uplink MIMO channel model.

4.5.2 MIMO Channel Model and Assumptions

Figure 4.6 depicts an uplink channel or multiple access channel (MAC) of an STA. The STA is equipped with U_t transmit antennas while the AP receiver has a sectorized linear K_r-element antenna array. For a typical n^{th} STA $n = 1, \cdots, |\mathcal{N}|$ the U_t transmitted signals are modeled as random variables $x_1, \cdots x_{U_t}$ and the signal vector is denoted as $\mathbf{x}_n \in \mathbb{C}^{U_t \times 1} = [x_1, x_2, \cdots x_{U_t}]^T$. The pre-processing received signal $\mathbf{y} \in \mathbb{C}^{K_r \times 1}$ at the AP is:

$$\mathbf{y} = \underbrace{\mathbf{H}_n \mathbf{x}_n}_{\text{desired signal}} + \underbrace{\sum_{\kappa \in \mathcal{K}, \kappa \neq n | \mathcal{K} \subset \mathcal{N}} \mathbf{H}_\kappa \mathbf{x}_\kappa}_{\text{co-channel interference}} + \underbrace{\mathbf{n}_o}_{\text{effective noise}}, \tag{4.17}$$

where $\mathbf{H}_n$ is the $K_r \times U_t$ UL channel coefficient matrix between STA_n and the AP whose entries are circularly symmetric complex Gaussian random variables with zero-mean and unit variance. In (4.17), $\mathbf{H}_\kappa \in \mathbb{C}^{K_r \times U_t}$ represents the channel of concurrent transmitting STA, κ, other than STA n whose signals are received at the AP as interference and $\mathbf{n}_o$ is the $K_r \times 1$ independent and identically distributed (i.i.d) Gaussian noise vector with zero-mean and variance $\sigma^2_{n_o}$.

Therefore, in the presence of interference from other $\mathcal{K}$ STAs (concurrent transmitters), the post-processing signal-to-interference-plus noise (SINR) of STA_n at the AP is written as follows:

$$\text{SINR}_n = \frac{\mathbb{E}\left[\left|\mathbf{W}_n\mathbf{H}_n\mathbf{x}_n\right|^2\right]}{\mathbb{E}\left[\left|\sum\limits_{\kappa\in\mathcal{K},\kappa\neq n|\mathcal{K}\subset\mathcal{N}} \mathbf{W}_n\mathbf{H}_\kappa\mathbf{x}_\kappa + \mathbf{W}_n\mathbf{n}_o\right|^2\right]} = \frac{\left|\mathbf{W}_n^H\mathbf{\Theta}_n\mathbf{R}_n\mathbf{W}_n\right|^2}{\left|\sum\limits_{\kappa\in\mathcal{K},\kappa\neq n|\mathcal{K}\subset\mathcal{N}} \mathbf{R}_{\mathbf{H}_\kappa\mathbf{x}_\kappa+\mathbf{n}_o}\right|^2}, \tag{4.18}$$

where $\mathbf{R}_n = \mathbb{E}\left[\mathbf{H}_n\mathbf{H}_n^H\right]$, $\mathbf{W}_n = \left(\mathbf{H}_n^H\mathbf{H}_n\right)^{-1}\mathbf{H}_n^H$ is the $U_t \times K_r$ receiver beamformer matrix whose column vectors $\mathbf{w}_1, \mathbf{w}_2, \cdots, \mathbf{w}_{K_r}$ represent the block of linear filters at the AP, given symbol energy $\mathcal{E}_x$, for a signal angle of arrival θ_n, the zero mean transmitted signal correlation matrix $\mathbf{\Theta}_n = \mathbb{E}\left[\mathbf{x}_n\mathbf{x}_n^H\right] = e^{j2\theta_n}U_t\mathcal{E}_x\mathbf{I}_{U_t}$, and $\mathbf{R}_{\mathbf{H}_\kappa\mathbf{x}+\mathbf{n}_o}$ is the correlation matrix of the interference-plus-noise at the AP expressed as:

$$\mathbf{R}_{\mathbf{H}_\kappa\mathbf{x}_\kappa+\mathbf{n}_o} = \mathbb{E}\left[\left(\mathbf{W}_n^H\mathbf{H}_\kappa\mathbf{x}_\kappa + \mathbf{n}_o\mathbf{W}_n\right)\left(\mathbf{W}_n^H\mathbf{H}_\kappa\mathbf{x}_\kappa + \mathbf{n}_o\mathbf{W}_n\right)^H\right]. \tag{4.19}$$

By exploiting the fact that $\mathbb{E}\left[\mathbf{n}_o\mathbf{n}_o^H\right] = \sigma^2_{n_o}\mathbf{I}_{K_r}$ and assuming that the transmitted

signals are uncorrelated, we have:

$$\begin{aligned}\mathbf{R}_{\mathbf{H}_\kappa \mathbf{x}_\kappa + \mathbf{n}_o} =& \mathbf{W}_n^H \left(\mathbf{H}_\kappa \mathbf{\Theta}_\kappa \mathbf{H}_\kappa^H + \mathbb{E}\left[\mathbf{n}_o \mathbf{n}_o^H \right] \right) \mathbf{W}_n \\ =& \mathbf{W}_n^H \left(\mathbf{R}_\kappa \mathbf{\Theta}_\kappa + \mathbb{E}\left[\mathbf{n}_o \mathbf{n}_o^H \right] \right) \mathbf{W}_n, \end{aligned} \tag{4.20}$$

where $\mathbf{\Theta}_\kappa = \mathbb{E}\left[\mathbf{x}_\kappa \mathbf{x}_\kappa^H \right] = e^{j2\theta_\kappa} U_t \mathcal{E}_x \mathbf{I}_{U_t}$, $\mathbf{R}_\kappa = \mathbb{E}\left[\mathbf{H}_\kappa \mathbf{H}_\kappa^H \right]$ denotes the spatial correlation of the interference channel $\mathbf{H}_\kappa$ at the receiver AP and $\mathbb{E}\left[\mathbf{n}_o \mathbf{n}_o^H \right] = K_r \sigma_{n_o}^2 \mathbf{I}_{K_r}$. In Assumption 4.2 To obtain an expression for the correlation matrices $\mathbf{R}_\kappa$ and $\mathbf{R}_n$, we employ

Assumption 4.2. *To determine the spatial fading correlation of channels* $\mathbf{H}_n$ *and* $\mathbf{H}_\kappa$*, the one-ring scattering model (a geometry-based stochastic model) [109] is assumed, where both the transmitter and the receiver have the same antenna element spacing.*

The correlation matrix $\mathbf{R}_\kappa$ of the channel $\mathbf{H}_\kappa$ can be described based on a geometrical arrangement of the antenna elements at both the transmitter and the receiver. Under Assumption 4.2, the one-ring model represents a Rayleigh-fading channel where the single-bounce scatterers are located and dominant around the STA provided the AP is elevated and not affected by local scattering. Let R denote the radius of the scattering ring and θ_n denote the angle of arrival at the receiving AP. The angle of the incoming signal is within the range $[\theta_n - \Delta, \theta_n + \Delta]$ where $\Delta = \arcsin\left(\frac{R}{D}\right)$ is the angle spread of the scatterers. The interference channel correlation under the

one-ring channel scattering model [109] is:

$$\begin{aligned}\mathbf{R}_{\kappa} &= \mathbb{E}\left[\mathbf{H}_{\kappa}\mathbf{H}_{\kappa}^{H}\right] \\ &= \frac{1}{2\pi}\int_{0}^{2\pi}\exp\left\{-j\frac{2\pi}{\omega}\left[\psi_x\left(\left(1-\frac{\Delta^2}{4}+\frac{\Delta^2\cos 2\theta_n}{4}\right)+\sin\theta_n\right)\right.\right. \\ &\left.\left.+\psi_y\left(\Delta\sin\theta_n+\cos\theta_n\right)\right]\right\}d\theta_n,\end{aligned} \tag{4.21}$$

where ω is the wavelength of the signal, ψ_x and ψ_y are antenna element spacings on the x-axis and the y-axis, respectively. For tractability, we further assume that the transmitting and the receiving antenna elements are aligned on the y-axis, which implies $\psi_x = 0$ in (4.21). Therefore,

$$\mathbf{R}_{\kappa} = \underbrace{\frac{1}{2\pi}\int_{0}^{2\pi}\exp\left\{-j\frac{2\pi}{\omega}\left[\psi_y\left(\Delta\sin\theta_n+\cos\theta_n\right)\right]\right\}d\theta_n}_{J_0(\cdot)}, \tag{4.22}$$

where $J_0(\cdot)$ is the Bessel function of the first kind of the zeroth order [110], [109]. The value of θ_n depends on the antenna geometry; for details, readers are referred to [109]. Later in Section 4.5.4, $\mathbf{R}_{\kappa}$ is applied to derive the STP of a typical node, and it is shown that the STP (and consequently, PCS threshold selection) in our framework does not require channel sounding but only the knowledge of spatial geometry via θ_n.

4.5.3 CSMA/CA Contention Model and Channel Access Probability

In conventional slotted CSMA wireless networks, nodes are allowed to contend for the shared medium by sensing the channel. The CSMA/CA protocol utilizes physical carrier sensing (PCS) for channel contention. In PCS, a node with a packet in its

buffer senses the channel within its carrier sensing range (CSR) and transmits in a time slot if there are no other transmitting nodes within the CSR. A payload is transmitted if the power sensed in the channel is below the PCS threshold Γ. For the channel to be flagged as idle, the power sensed within the CSR must not exceed the PCS threshold. In other words, the CSR represents a node's contention domain or neighborhood, and a node wins contention in its neighborhood if the power or energy sensed in the channel is below the PCS threshold.

To model the PCS process of the CSMA/CA protocol, let $\tilde{\mathcal{N}_c}$ denote the contention neighborhood of STA_n and let $D_{n\tilde{n}}$ represent the distance between STA_n and any other potential contending $\text{STA}_{\tilde{n}}$ within the contention domain. STA_n in $\tilde{\mathcal{N}_c}$ will transmit if it senses an idle channel for the duration of the contention period. If the power is above the PCS threshold, it backs off by a random amount of time that is uniformly distributed. It transmits in the next time-slot where (i) it has the lowest backoff time in its neighborhood and (ii) the channel remains idle for the contention period. Therefore, at each time slot, a given STA_n contends with other STAs in its neighborhood $\tilde{\mathcal{N}_c}$, given by

$$\tilde{\mathcal{N}_c} = \left\{ \tilde{n} \in \mathcal{N} \text{ s.t. } \left(\|\mathbf{H}_{n\tilde{n}}\|^2 \cdot D_{n\tilde{n}}^{-\alpha} \Theta_{\tilde{n}} + \mathbb{E}\left[\|\mathbf{n}_o\|^2 \right] \right) \geq \Gamma, n \neq \tilde{n} \right\}, \tag{4.23}$$

where the left-hand side of the inequality denotes the total power received by STA_n from a neighboring $\text{STA}_{\tilde{n}}$ during carrier sensing, which is being checked against the PCS threshold to determine an *idle* or *busy* channel. $\|\mathbf{H}_{n\tilde{n}}\|^2 = \text{tr}\left(\mathbf{H}_{n\tilde{n}}\mathbf{H}_{n\tilde{n}}^H\right)$ represents the signal power received from a neighboring STA $\tilde{n}$ during carrier sensing, $D_{n\tilde{n}}$ is the spatial distance between STA_n and its contending neighbor $\text{STA}_{\tilde{n}}$ and α is the path loss exponent. Using spatial information, STA_n is in the contention

neighborhood of $\text{STA}_{\tilde{n}}$, if $\text{STA}_{\tilde{n}}$ is located within the CSR of STA_n, i.e.,

$$\tilde{\mathcal{N}_c} = \left\{ \tilde{n} \in \mathcal{N} \text{ s.t. } D_{n\tilde{n}} \leq \chi, n \neq \tilde{n} \right\}, \tag{4.24}$$

where χ denotes the CSR of STA_n, which is determined based on the chosen PCS threshold. The neighborhood (or contention domain) in (4.24) is next used to derive the CAP of a node.

Channel Access Probability (CAP)

The density of concurrent transmitters permitted by the CSMA/CA protocol to transmit simultaneously per time slot depends on each user's CAP. The CAP or the probability that STA_n transmits or accesses the channel following contention is obtained according to

Lemma 4.1. *STA_n in neighborhood $\tilde{\mathcal{N}_c}$ gains access to the channel with probability*

$$\mathcal{P}_n^c = 1 - \left[\lambda_n \cdot \Gamma\left(\frac{1}{\alpha}\right) \cdot \left(\frac{\Gamma - |U_r \sigma^2 \mathbf{I}_{U_r}|^2}{|\Theta_{\tilde{n}}|} \right)^{-\frac{1}{\alpha}} \cdot \frac{1}{\alpha} \right], \tag{4.25}$$

where λ_n is the density of STAs defined previously in Section 4.5.1, $\Gamma(\cdot)$ is the Gamma function, U_r denotes the number of receiving antenna at the STA performing the PCS process, and $|\Theta_{\tilde{n}}| = \left| e^{j2\theta_{\tilde{n}}} U_t \mathcal{E}_x \mathbf{I}_{U_t} \right|^2$. Eqn. (4.25) reveals that the CAP of a node depends on the path loss exponent α between the sensing node and its neighbors, the number of antennas used for sensing and the node density λ_n, which determines the size of its contention neighborhood or domain.

Proof. The proof follows similar steps of those of Eqns. (4.3)-(4.5). When a packet arrives in STA$_n$'s buffer, it senses the channel for any active transmission in its neighborhood $\tilde{\mathcal{N}}_c$ defined according to (4.23), representing the set of nodes whose signals could collide with STA n's signal if they transmit concurrently; that is, the channel contains signal power above Γ. The CAP that STA n senses an idle channel is:

$$\mathcal{P}_n^c = 1 - \mathbb{P}\left(\|\mathbf{H}_{n\tilde{n}}\|^2 \cdot D_{n\tilde{n}}^{-\alpha}\Theta_{\tilde{n}} + \mathbb{E}\left[\|\mathbf{n}_o\|^2\right] > \Gamma\right) \tag{4.26}$$

$$= 1 - \mathbb{P}\left(\mathrm{tr}\left(\mathbf{H}_{n\tilde{n}}\mathbf{H}_{n\tilde{n}}^H\right) > \frac{\Gamma - |U_r\sigma^2\mathbf{I}_{U_r}|^2}{D_{n\tilde{n}}^{-\alpha}\Theta_{\tilde{n}}}\right) \tag{4.27}$$

$$= 1 - \mathbb{E}_{\mathcal{N}_n}\left[\prod_{\tilde{n}} \exp\left(-\frac{\Gamma - |U_r\sigma^2\mathbf{I}_{U_r}|^2}{D_{n\tilde{n}}^{-\alpha}\Theta_{\tilde{n}}}\right)\right] \tag{4.28}$$

$$= 1 - \exp\left(-\mathbb{E}_{\mathcal{N}_n}\left[\sum_{\tilde{n}\in\mathcal{N}_n} \frac{\Gamma - |U_r\sigma^2\mathbf{I}_{U_r}|^2}{D_{n\tilde{n}}^{-\alpha}\Theta_{\tilde{n}}}\right]\right) \tag{4.29}$$

$$= 1 - \lambda_n \int_{\mathbb{R}^2} \exp\left(-\frac{\Gamma - |U_r\sigma^2\mathbf{I}_{U_r}|^2}{D_{n\tilde{n}}^{-\alpha}\Theta_{\tilde{n}}}\right) \mathrm{d}\ D_{n\tilde{n}} \tag{4.30}$$

$$= 1 - \left[\lambda_n \cdot \Gamma\left(\frac{1}{\alpha}\right) \cdot \left(\frac{\Gamma - |U_r\sigma^2\mathbf{I}_{U_r}|^2}{\Theta_{\tilde{n}}}\right)^{-\frac{1}{\alpha}} \cdot \frac{1}{\alpha}\right], \tag{4.31}$$

where $|U_r\sigma^2\mathbf{I}_{U_r}|^2 = \mathbb{E}\left[\|\mathbf{n}_o\|^2\right]$, (4.28) follows from the fact that $\mathrm{tr}\left(\mathbf{H}_{n\tilde{n}}\mathbf{H}_{n\tilde{n}}^H\right)$ is a sum of exponential random variable and has a Chi-Square distribution with $2U_r$ DoF, (4.29) holds from Jensen's inequality since is a convex function (4.30) is obtained by Campbell's theorem, $\mathbb{E}\left(\sum_{x\in\Phi} f(x)\right) = \lambda\int_{\mathbb{R}^2} f(x)\mathrm{d}x$, defined in Theorem 2.3 and (4.31) follows from applying [110, Eqn. 3.326.1] to prove Eqn. (4.25). □

Figure 4.7(a) depicts the relationship between an arbitrary PCS threshold and the CAP given by Lemma 4.1. The more conservative the PCS threshold, the smaller the probability of a typical node winning the channel contention. At low PCS threshold,

the CSR becomes larger and there are more nodes within the contention neighborhood of a node. On the other hand, as the PCS threshold increases, the CSR of a typical node decreases and its probability of winning the channel contention increases. From Lemma 4.1, the impact of multiple antennas at the sensing node or intended transmitter is apparent in Fig. 4.7(b). It turns out that equipping nodes with MIMO capability could impact their channel access probabilities during the PCS process. For a $U_r = U_t = 8$ MIMO configuration at a node, the power level sensed during the PCS process could be very strong and prevent the node from transmitting if the power sensed is above the PCS threshold. For efficient collision avoidance, using multiple antennas to perform the PCS process enables the sensing node to accurately capture the energy level in the channel from different multipath components.

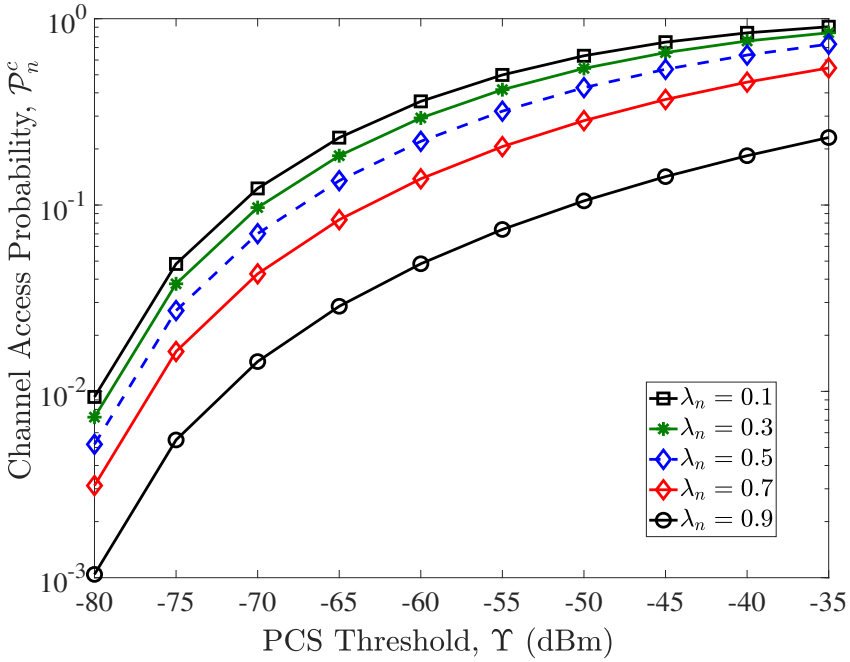

Figure 4.7: Channel access probability versus PCS thresholds (a) for various node densities λ_n and $U_t = U_r = 1$ (b) for varying numbers of antennas at the STAs and node density $\lambda_n = 0.1$.

4.5.4 Successful Transmission Probability (STP)

Next, the *Successful Transmission Probability* (STP) is derived, which is the probability a node achieves SINR above a threshold γ. This is important because gaining access to the channel does not guarantee a target SINR due to interference in large networks, especially in cases where STAs have high CAP; high CAP may cause high interference from densely distributed users, which causes erroneous decoding of transmitted symbols at the receiver AP. Therefore

Lemma 4.2. *STA_n achieves target SINR γ at the receiver AP with probability*

$$\begin{aligned}\mathcal{P}_n^{\gamma} &= \mathbb{E}\left[\sum_{n\in\mathcal{N}} \mathbb{1}_{SINR_n>\gamma}\right] \\ &= \exp\left(-\gamma \left\|\mathbf{W}_n\right\|^2 \left|K_r \sigma_{n_o}^2 \mathbf{I}_{K_r}\right|^2\right) \\ &\cdot \exp\left(-\gamma \left|\mathbf{W}_n^H \left(\left|e^{j2\theta_\kappa} U_t \mathcal{E}_x \mathbf{I}_{U_t}\right|^2 \cdot \lambda_n \cdot \left(\psi_y \frac{2\pi}{\omega}\right)^{-1} e^{-\psi_y \frac{2\pi}{\omega}}\right) \mathbf{W}_n\right|^2\right), \end{aligned} \tag{4.32}$$

where ω is the wavelength of the channel carrier frequency and ψ_y is the antenna spacing aligned on the y-axis at both the transmitter and the receiver.

Proof: see Appendix B.1.

The probability of successful transmission for a particular node depends on the target rate in terms of the SINR threshold γ, the number of antennas at both the transmitters and the receiver, and ultimately the density of nodes that are generating interference through concurrent transmissions. Evaluating the STP predicted in Lemma 4.2, Figure 4.8 provides insight. As expected, increasing the node density

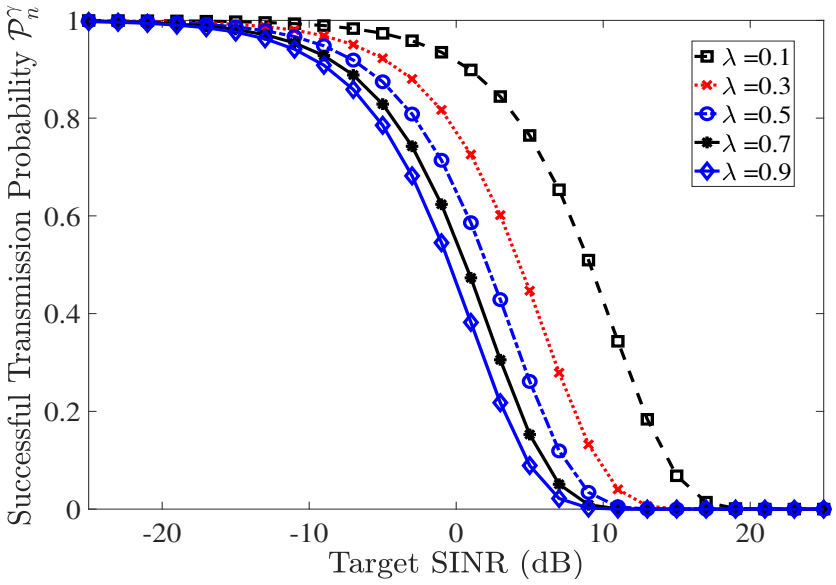

Figure 4.8: Successful transmission probability for various node densities and SINR thresholds given $K_r = K_t = 8$.

could significantly affect the receiver performance in terms of achieving the target SINR. At very low target SINR, for instance, -25 dB, the probability of successful transmission approaches 1 regardless of the node density. This is because targeting such low SINR or rate implies that the interference level is not an issue. However, increasing density increases the interference level due to the large number of concurrent transmitters. This demonstrates that it is imperative to find a tradeoff between increasing node density and achieving high SINR (or rate); this tradeoff can be captured in finding the optimal PCS threshold that maximizes a throughput objective. Since the PCS threshold determines the maximum number of concurrent transmitters per time slot, interference is significantly reduced by optimizing the PCS threshold.

4.5.5 Spatial Density of Throughput (SDT)

The CAP is the probability that a node gains access to the channel under the CSMA/CA protocol following a contention period. On the other hand, STP (also known as the coverage probability [42] or transmission success probability [90]) measures the probability that a node achieves the target SINR at which the receiver is able to successfully decode the transmitted packets. Based on CAP and STP, we define the key performance metric, the spatial density of throughput (SDT) [42], [43], which quantifies the average number of users per unit area that *gain access to the medium* and *achieve the target SINR*

The implication of multiple users having high CAPs to use the channel is strong interference as many users will transmit concurrently and strong interference implies low SINRs. To capture the effect of interference and the CAP, SDT is defined as:

$$\mathcal{R}_{\mathrm{SDT}} = \lambda_n \cdot \mathcal{P}_n^c \cdot \mathcal{P}_n^\gamma \tag{4.33}$$

where $\mathcal{P}_n^c$ is the probability that STA_n gains access to the channel at a given time slot through the PCS process, which is obtained in Lemma 4.1. $\mathcal{P}_n^\gamma$ is the probability that an STA achieves SINR above a threshold γ, for the receiving AP to successfully decode a packet and it is derived in Lemma 4.2. For a fixed system bandwidth B, the *mean rate* $\bar{\mathcal{R}}$ is:

$$\bar{\mathcal{R}} = (B \cdot \log_2(1+\gamma)) \cdot \mathcal{R}_{\mathrm{SDT}}. \tag{4.34}$$

4.6 Proposed PCS Threshold Selection: MIMO WLAN

4.6.1 Problem Formulation

In this section, we optimize the PCS threshold to maximize the SDT defined in Eqn. (4.33) and maximizing $\mathcal{R}_{\text{SDT}}$ also maximizes the mean rate $\bar{\mathcal{R}}$ defined in (4.12). As mentioned earlier, SDT is being maximized to capture the effect of strong interference due to larger CAP. This ensures that we can both enhance spatial reuse and contain the effect of interference. This problem is formulated as follows:

$$\begin{aligned}
&\text{maximize} && \mathcal{R}_{\text{SDT}} && \text{(4.35a)}\\
&\text{subject to} && \mathbb{I}_c \leq \Gamma, && \text{(4.35b)}\\
& && P_I \leq \beta, \text{ and} && \text{(4.35c)}\\
& && \Gamma > 0, \qquad \forall n \in \mathcal{N}, && \text{(4.35d)}
\end{aligned}$$

where constraint (4.35b) represents the PCS threshold constraint that the total power $\mathbb{I}_c$ sensed by a node is below the PCS power threshold Γ. To minimize the effect of inter-BSS interference, the interference power at the AP is constrained by (4.35c) where β is the interference power threshold. That is, for the receiver to successfully decode the packet, the interference power at the AP should not exceed β.

4.6.2 Optimal PCS Threshold for Spatial Reuse

Constraints (4.35b) and (4.35c) are fundamentally important in achieving spatial reuse and high data rate in WLANs, as they are responsible for two phenomena inherent in the CSMA/CA protocol. First, is the *hidden terminal* problem, which occurs when the STA_n senses no active transmission on the channel (i.e. $\mathbb{I}_c < \Gamma$ is

satisfied) but the interference power received at the AP hinders or is too high ($P_I > \beta$) for successful packet reception. The second problem is the *exposed terminal* problem, which results from STA_n sensing a busy channel ($\mathbb{I}_c > \Gamma$) but the interference power at the receiver AP does not affect packet reception ($P_I < \beta$). It is therefore possible that STA_n will defer its transmissions even though the receiver AP could successfully decode its packets. Given the impacts of these events on the system throughput, the goal is to find Γ such that constraints (4.35b) and (4.35c) are satisfied, and achieve spatial reuse by mitigating the hidden terminal and the exposed terminal problems.

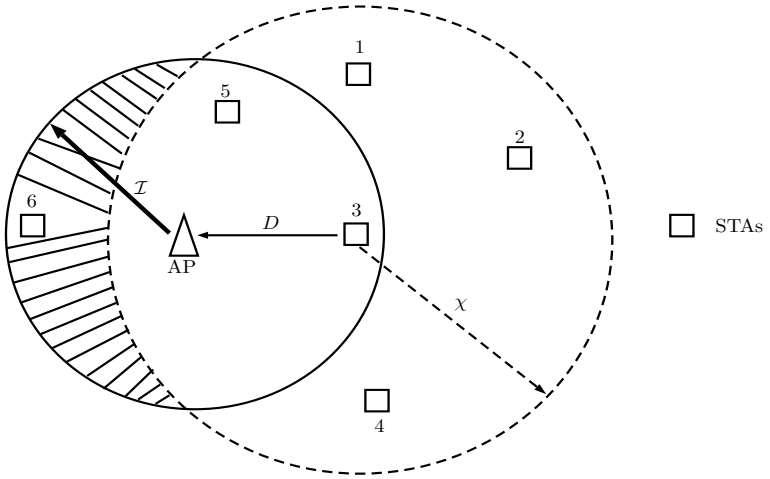

Figure 4.9: Relationships among carrier sensing range χ, the interference range $\mathcal{I}$ and the hidden terminal region [2].

The interference power P_I in constraint (4.35c) can be expressed in terms of the SINR requirement, $\text{SINR}_n \geq \gamma$ as follows:

$$\text{tr}\left(\mathbf{W}_n^H \mathbf{H}_n \mathbf{x}_n\right) \geq \underbrace{\mathbb{E}\left[\left|\sum_{\kappa \in \mathcal{K}, \kappa \neq n | \mathcal{K} \subset \mathcal{N}} \mathbf{W}_n \mathbf{H}_\kappa \mathbf{x}_\kappa\right|^2\right]}_{P_I} \gamma + \mathbb{E}\left[\left|\mathbf{W}_n \mathbf{n}_o\right|^2\right] \gamma \tag{4.36}$$

$$P_I \leq \text{tr}\left(\mathbf{W}_n^H \mathbf{H}_n \mathbf{x}_n\right) \gamma^{-1} - \mathbb{E}\left[\left|\mathbf{W}_n \mathbf{n}_o\right|^2\right]. \tag{4.37}$$

Constraint (4.37) is derived from Eqn. (4.18) assuming that the SINR threshold γ accounts for the minimum tolerable interference power. In other words, Eqn. (4.37) establishes the minimum interference at which a node could decode packets successfully. Additionally, to guard against interference, P_I can be expressed in terms of the PCS threshold Γ as illustrated in Fig. 4.9. In this figure, STA 6 is located in the hidden terminal region and has the potential to interfere with the transmission of STA 3 at the AP. Since STA 6 is outside of the CSR χ of STA 3, STA 3 is completely unaware of STA 6's transmission and a collision is bound to occur. To prevent the hidden terminal, the CSR χ should ideally cover the interference region $\mathcal{I}$ [2], i.e.,

$$\mathcal{I} \leq \chi + D, \tag{4.38}$$

and from this relationship, we can infer that in the worst case scenario $P_I = (\chi + D)^{-\alpha}$. Consequently, (4.37) can be written as:

$$\Gamma \leq \mathrm{tr}\left(\mathbf{W}_n^H \mathbf{H}_n \mathbf{x}_n\right) \gamma^{-1} - \mathbb{E}\left[|\mathbf{W}_n \mathbf{n}_o|^2\right] - D^{-\alpha}. \tag{4.39}$$

By replacing (4.35c) with (4.39), (4.13) is equivalent to the following problem:

Lemma 4.3. *The spatial density of throughput maximization problem in (4.13) is*

$$\begin{aligned}
&\text{maximize} && \mathcal{R}_{\mathrm{SDT}} && (4.40a)\\
&\text{subject to} && \mathbb{I}_c \leq \Upsilon && (4.40b)\\
& && \Upsilon \leq \mathrm{tr}\left(\mathbf{W}_n^H \mathbf{H}_n \mathbf{x}_n\right) \gamma^{-1} - \mathbb{E}\left[|\mathbf{W}_n \mathbf{n}_o|^2\right] - D^{-\alpha}. && (4.40c)
\end{aligned}$$

The solution to (4.40) depends on the selection of the PCS threshold to maximize the throughput density. Here, the Karush-Kuhn-Tucker (KKT) conditions are sufficient to find the optimal PCS threshold. We can obtain a solution to this problem by formulating its Lagrange function

$$\mathcal{L}\left(\Upsilon,\mu_1,\mu_2\right)=\lambda_n\mathcal{P}_n^{\gamma}-\lambda_n^2\mathcal{P}_n^{\gamma}\Gamma\left(\frac{1}{\alpha}\right)\frac{1}{\alpha}\left(\frac{\Gamma-\mathbb{E}\left[\left|\mathbf{W}_n\mathbf{n}_o\right|^2\right]}{\Theta_{\tilde{n}}}\right)^{-\frac{1}{\alpha}}$$
$$+\mu_1\left(\mathbb{I}_c-\Gamma\right)+\mu_2\left(\mathrm{tr}\left(\mathbf{W}_n^H\mathbf{H}_n\mathbf{x}_n\right)\gamma^{-1}-\mathbb{E}\left[\left|\mathbf{W}_n\mathbf{n}_o\right|^2\right]-D^{-\alpha}-\Gamma\right) \tag{4.41}$$

where μ_1 and μ_2 are Lagrange multipliers that penalize the violation of constraints (4.40b) and (4.40c), respectively. Obtaining the optimal $\hat{\mu}_1$ and $\hat{\mu}_2$ from (4.41) by satisfying KKT conditions [77], the optimal PCS threshold that maximizes the spatial density of throughput is obtained as

Theorem 4.1. *The optimal PCS threshold $\hat{\Gamma}$ that maximizes the spatial density throughput under the CSMA/CA protocol is*

$$\hat{\Gamma}=\left[\left(\frac{\hat{\mu}_2-\hat{\mu}_1}{\lambda_n^2\frac{1}{\alpha}\Gamma\left(\frac{1}{\alpha}\right)\cdot\left(\frac{1}{\Theta_{\tilde{n}}}\right)^{-\frac{1}{\alpha}}}\right)^{-\frac{1-\alpha}{2\alpha}}\right]^{+}, \tag{4.42}$$

where $[\cdot]^{+}\equiv\max\{\cdot,0\}$.

Proof. Let $\hat{\mu}_1$ and $\hat{\mu}_2$ represent the optimal Lagrangian multiplier for constraints (4.40b) and (4.40c), respectively, and by taking the derivative of the Lagrangian function of (4.40) given in Equation (4.41) w.r.t Γ, we obtain the KKT conditions as

follows:

$$\frac{\partial \mathcal{L}\left(\Upsilon, \mu_1, \mu_2\right)}{\partial \Gamma} = 0, \hat{\mu}_1 \geq 0, \hat{\mu}_2 \geq 0, \tag{4.43}$$

$$\hat{\mu}_1 \hat{\Gamma} - \hat{\mu}_1 \mathbb{I}_c = 0, \tag{4.44}$$

$$\mu_2 \Gamma - \mu_2 \mathrm{tr}\left(\mathbf{W}_n^H \mathbf{H}_n \mathbf{x}_n\right) \gamma^{-1} - \mu_2 D^{-\alpha} + \mu_2 \left| U_r \sigma^2 \mathbf{I}_{U_r} \right|^2 = 0, \tag{4.45}$$

$$\hat{\Gamma} > 0, \tag{4.46}$$

and from (4.43), the following expression is obtained:

$$-\hat{\Gamma}^{-\frac{1-\alpha}{\alpha}} \mathcal{P}_n^{\gamma} \lambda_n^2 \frac{1}{\alpha} \Gamma\left(\frac{1}{\alpha}\right) \left(\frac{1}{\Theta_{\tilde{n}}}\right)^{-\frac{1}{\alpha}} - \hat{\mu}_1 - \hat{\mu}_2 = 0, \tag{4.47}$$

where it is assumed that noise is negligible during the PCS process. Since the selected PCS threshold value should generate low enough interference such that each node can achieve the desired data rate by satisfying the SINR threshold, setting $\mathcal{P}_n^{\gamma} = 1$ in (4.47), we have

$$\hat{\mu}_2 = \hat{\Gamma}^{-\frac{1-\alpha}{\alpha}} \lambda_n^2 \frac{1}{\alpha} \Gamma\left(\frac{1}{\alpha}\right) \left(\frac{1}{\Theta_{\tilde{n}}}\right)^{-\frac{1}{\alpha}} + \hat{\mu}_1. \tag{4.48}$$

By substituting (4.48) into (4.45), we have the necessary condition and the optimal PCS threshold to maximize the spatial density of throughput is obtained as:

$$\hat{\Upsilon} = \left[\left(\frac{\hat{\mu}_2 - \hat{\mu}_1}{\lambda_n^2 \frac{1}{\alpha} \Gamma\left(\frac{1}{\alpha}\right) \left(\frac{1}{\Theta_{\tilde{n}}}\right)^{-\frac{1}{\alpha}}} \right)^{-\frac{1-\alpha}{2\alpha}} \right]^+, \tag{4.49}$$

where $[\cdot]^+ = \max\{\cdot, 0\}$, which proves Equation (4.42). □

From Equation (4.42), we can infer that the PCS threshold selection that improves spatial reuse depends on network parameters, i.e., path loss, number of transmit antennas at the STAs, the density of nodes. The Lagrange multipliers $\hat{\mu}_2$ and $\hat{\mu}_1$ can be obtained through line search such as the bisection method [77]. Algorithm 1 summarizes the steps in obtaining the optimal PCS threshold according to Theorem 1. Using subgradient update, s^k represents the sequence of positive scalar step sizes [49], [113] to update the Lagrangian multipliers μ_1 and μ_2 using Eqns. (4.50) and (4.51), respectively

$$\mu_1^{k+1} = \left[\mu_1^k + s^k \left(\Upsilon - \mathbb{I}_c\right)\right]^+, \tag{4.50}$$

and

$$\mu_2^{k+1} = \left[\mu_2^k + s^k \left(\mathrm{Tr}\left(\mathbf{W}_n^H \mathbf{H}_n \mathbf{x}_n\right) \gamma^{-1} - \Psi - \Upsilon\right)\right]^+. \tag{4.51}$$

Algorithm 5: Proposed PCS threshold selection

Input: α, λ_n, $\Theta_{\tilde{n}}$, γ
Output: PCS threshold $\hat{\Upsilon}$
Initialize μ_1, μ_2
$k = 1$ (*Number of iterations.*)
repeat
  Calculate $\hat{\Upsilon}$ using (4.42)
  Update $\hat{\mu}_1$ using (4.50)
  Update $\hat{\mu}_2$ using (4.51)
  $k \leftarrow k + 1$
until $\hat{\Upsilon}$ *converges*;
Set $\hat{\Upsilon}$ as PCS threshold for contention.

4.6.3 Optimal Node Density and Throughput

Under the PCS threshold selection framework assumed in Theorem 4.1, the optimal node density that can be supported to mitigate the effect of interference from a large

number of concurrent transmitters can be derived from the mean rate given in (4.12) per unit bandwidth. By substituting Equation (4.42) into (4.12), we have:

$$\begin{aligned}\bar{\mathcal{R}} =&\lambda_n \cdot \log\left(1+\gamma\right)\mathcal{P}_n^{\gamma}\left(1-\left[\lambda_n \Gamma\left(\frac{1}{\alpha}\right)\left(\frac{\hat{\Gamma}}{\Theta_{\tilde{n}}}\right)^{-\frac{1}{\alpha}}\frac{1}{\alpha}\right]\right)\\ =&\lambda_n \log\left(1+\gamma\right)\mathcal{P}_n^{\gamma}-\lambda_n^{2(1-\alpha)}\mathcal{P}_n^{\gamma}\log\left(1+\gamma\right)\left(\frac{\frac{1}{\alpha}\Gamma\left(\frac{1}{\alpha}\right)\left(\frac{1}{\Theta_{\tilde{n}}}\right)^{-\frac{1}{\alpha}}}{\hat{\mu}_2-\hat{\mu}_1}\right)^{\frac{1-\alpha}{2}}, \quad (4.52)\end{aligned}$$

and to evaluate the optimal node density that can be supported with SINR threshold γ, the mean rate can be optimized via:

$$\max_{\lambda_n} \bar{\mathcal{R}}. \quad (4.53)$$

The optimal node density is immediate from

Lemma 4.4. *The optimal node density $\hat{\lambda}_n$ supported by the PCS threshold $\hat{\Upsilon}$ can expressed as*

$$\hat{\lambda}_n = \left[\left(\frac{\frac{1}{\alpha}\Gamma\left(\frac{1}{\alpha}\right)\cdot\left(\frac{1}{\Theta_{\tilde{n}}}\right)^{-\frac{1}{\alpha}}}{\hat{\mu}_2-\hat{\mu}_1}\right)^{\frac{1-\alpha}{2}}(2-2\alpha)\right]^{-\frac{1-2\alpha}{2}}. \quad (4.54)$$

Proof: The proof is obtained by taking the derivative of (4.52) with respect to λ_n. □

In (4.54), $\hat{\lambda}_n$ represents the maximum number of users allowed in the network for the chosen PCS threshold $\hat{\Upsilon}$ to be effective in achieving the optimal target rate, resulting in

Theorem 4.2. *An upper bound mean rate per Hz using the optimal density* $\hat{\lambda}_n$ *is*

$$\bar{\mathcal{R}}\left(\hat{\lambda}_n\right) = \frac{\log\left(1+\gamma\right)}{\left[\left(\frac{\frac{1}{\alpha}\Gamma\left(\frac{1}{\alpha}\right)\cdot\left(\frac{1}{\Theta_{\tilde{n}}}\right)^{-\frac{1}{\alpha}}}{\hat{\mu}_2-\hat{\mu}_1}\right)^{\frac{1-\alpha}{2}}(2-2\alpha)\right]^{\frac{1-2\alpha}{2}}} \tag{4.55}$$

Proof: Substituting $\hat{\lambda}_n$ obtained from Lemma 4.4, $\mathcal{P}_n^c = 1$ and $\mathcal{P}_n^\gamma = 1$ in Equation (4.12), (4.55) is obtained. This implies that under optimal node density $\hat{\lambda}_n$, the optimal mean rate is achievable when each node transmits with probability $\mathcal{P}_n^c = 1$ and achieves SINR above γ with probability $\mathcal{P}_n^\gamma = 1$, which is the ideal case. □

4.7 Numerical Results: MIMO WLAN Systems

4.7.1 Simulation Setup

We assume a 2-D dense WLAN in a 800m×800m plane with varying STA density λ_n and AP density $\lambda_m = 0.2$ throughout the analysis, given different target SINR thresholds γ. The realizations of the PPPs with intensities λ_n and λ_m model STAs and APs locations, respectively while the symbol energy $\mathcal{E}_x$ is normalized to unity. Unless otherwise stated, the path loss exponent $\alpha = 3.4$, which represents the ITU "rush-hour" propagation and $\sigma_{n_o}^2 = \frac{-100}{2}$ dBm. For the MIMO systems, the antenna spacing $\psi_y = 0.1 \cdot \omega$, where the wavelength ω is obtained based on the 5 GHz band for WLAN. For most of the simulations, the numbers of antennas at the APs are $K_r = K_t = \{1, 2, 4, 8\}$ while $U_r = U_t = 2$ for all STAs. Setting the PCS threshold according to Theorem 4.1, the spatial density of throughput and the mean rate are

determined according to Eqn. (4.6) and Eqn. (4.12), respectively. The analysis for each node density λ_n is performed over 10^6 Monte Carlo realizations of the network to measure the density of successful transmissions.

For channel access control under the CSMA/CA protocol, the distributed coordinated function (DCF) is simulated for each of the PCS threshold schemes with a time-slot of $20\mu s$ and other MAC parameters as defined in the 802.11 standard. To determine which STAs are associated with a given AP, that is, belonging to the same BSS, we assume the legacy strongest signal first (SSF) association where STAs associate with their minimum distance AP. For performance benchmarking, the proposed scheme is compared with the legacy fixed threshold and the DSC scheme. For the legacy scheme, the PCS threshold is fixed and identical for all nodes; it is set to -82 dBm [112] while the PCS threshold selection for the DSC scheme is [103]:

$$\Gamma^{'} = \min\left(\max\left(\Gamma_{dsc}, \Gamma_{\min}\right), \Gamma_{\max}\right), \tag{4.56}$$

where, given the RSSI and a constant margin ξ , $\Gamma_{dsc} = \text{RSSI}\,(\text{dBm}) - \xi\,(\text{dB})$, $\Gamma_{\min}$ and $\Gamma_{\max}$ are the minimum and the maximum PCS threshold values allowed, respectively. The parameters for the DSC scheme are as follows: $\Gamma_{\min} = -82$dBm, $\Gamma_{\max} = -30$ dBm, and $\xi = 20$ dB. Basically, the goal is to assess the system performance in terms of the SDT and the mean rate when the proposed PCS threshold framework in Theorem 4.1 is used in defining the PCS threshold versus using the legacy global fixed and the DSC scheme.

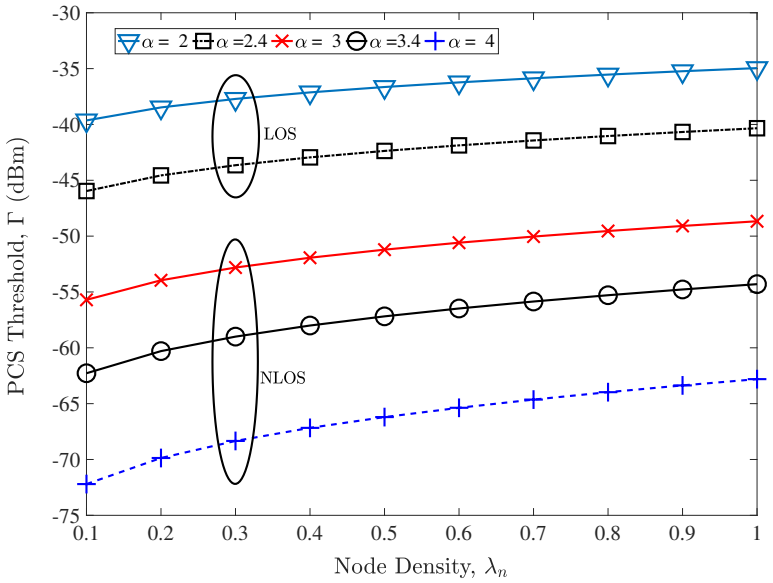

Figure 4.10: PCS Threshold Γ (dBm) obtained from Eqn. (4.42) for various wireless environments α as a function of node density λ_n.

4.7.2 Simulation Results and Performance Benchmarking

First, examining the effectiveness of the proposed PCS threshold selection expressed in Theorem 4.1. In Fig. 4.10, for a given wireless environment, the proposed PCS threshold selection scheme adapts the PCS threshold value to specific node density λ_n and path loss exponent α. As expected, Eqn. (4.42) selects PCS threshold value based on the type of path loss environment and node density. Observing node density $\lambda_n = 0.3$, the PCS threshold for line of sight (LOS), $\alpha = 2$ is higher than that of non-line of sight (NLOS). As expected, the sensing range or CSR needs to be shorter in LOS case than the NLOS case. Also, as the node density increases, regardless of the wireless environment, the PCS threshold needs to scale such that the contention domain or CSR of each node is more conservative. More specifically, higher PCS threshold permits more concurrent transmitters and implies strong interference. Low PCS threshold implies fewer concurrent transmitters and less interference. The proposed

PCS threshold selection scheme finds a balance between these two extreme cases by scaling the PCS threshold based on the path loss environment and node density.

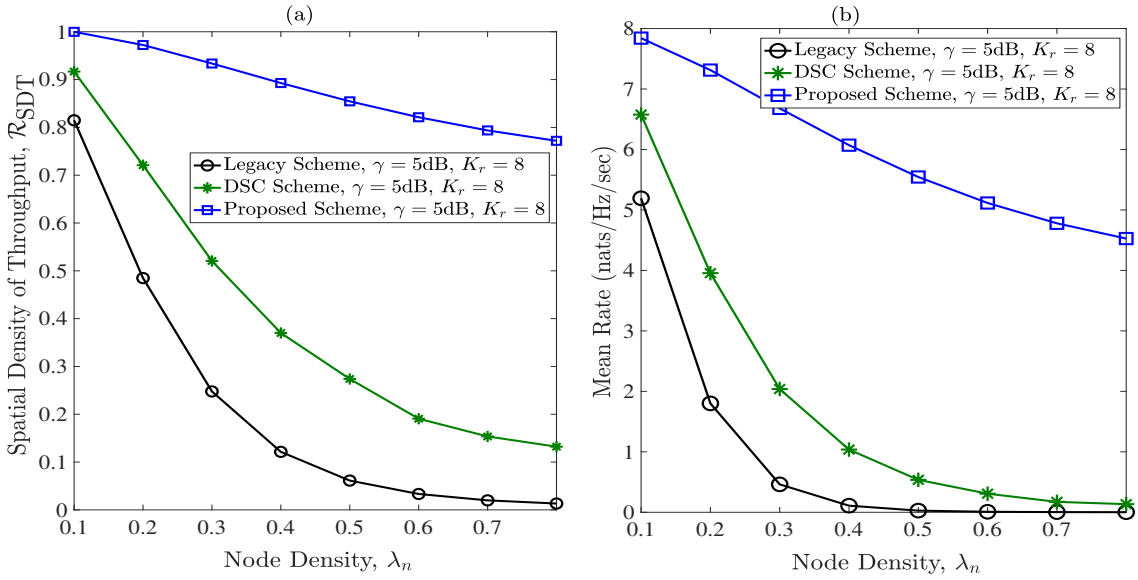

Figure 4.11: (a) Spatial density of throughput versus node density for $K_r = 8$ and $U_t = 2$ (b) Mean rate per node density at SINR $\gamma = 5$dB for $K_r = 8$ and $U_t = 2$.

Given different node densities, the spatial density of throughput (SDT) is plotted in Fig. 4.11(a) for SINR threshold $\gamma = 5$ dB and $K_r = 8$ receiving antennas at the APs. At node density $\lambda_n = 0.2$, the proposed PCS threshold selection scheme increases SDT by 80% over the existing legacy system and by 29% over the DSC scheme; this gain is not surprising as the PCS threshold is chosen for a specific node density rather than setting a globally fixed PCS threshold or performing an update based on some channel measurements. It is apparent that selecting a PCS threshold for each node density becomes more important as the network density increases. Under the same circumstances of $\gamma = 5$ dB and $K_r = 8$, Fig. 4.11(b) depicts the mean rate in nats/Hz/sec, which reveals the significant improved performance of

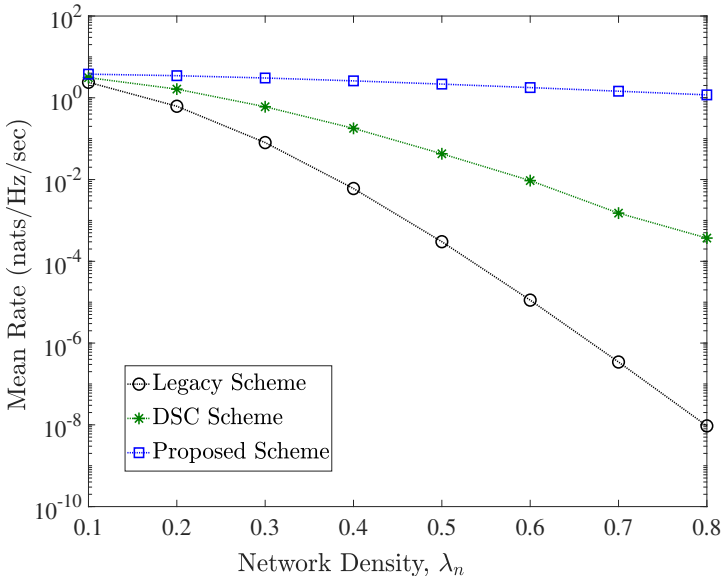

Figure 4.12: Mean Rate per Node Density λ_n given target SINR, $\gamma = -10$ (dB) for $K_r = 8$.

the proposed scheme. As the node density increases, the mean rate under the legacy system and the DSC scheme decreases drastically while the proposed scheme achieves a rate that declines only modestly with increasing node density. The latter is as a result of taking the node density into account when selecting the PCS threshold.

For SINR threshold $\gamma = -10$ dB, Fig. 4.12 depicts the achievable mean rate of the three schemes. The key observation in Fig. 4.12 is that, an improvement in performance is obtainable under the proposed scheme even at high node density. For various SINR thresholds, Fig. 4.13 depicts the mean rate of users achieving different SINRs when node density $\lambda_n = 0.8$. When the PCS threshold is obtained using the proposed scheme, a significant gain is achieved for each antenna setup K_r at the APs. This performance gain over the Legacy and the DSC Schemes is due to the fact that adapting the PCS threshold to specific node density could mitigate excessive interference from concurrent transmitters by allowing the appropriate number of nodes to

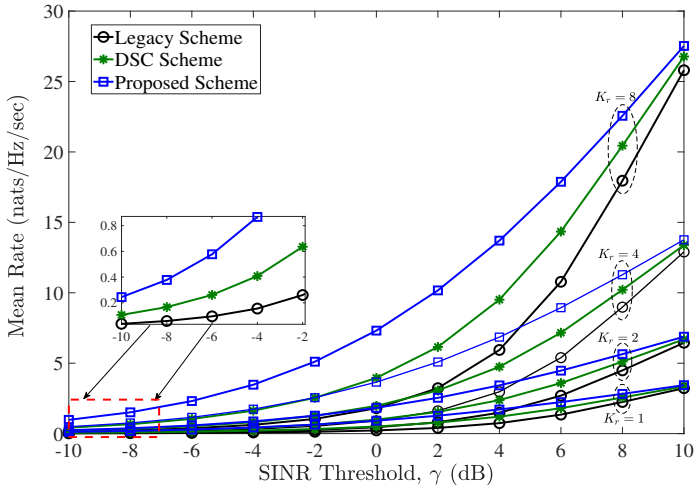

Figure 4.13: Mean Rate per target SINR, γ for various number of receive antennas K_r and given node density $\lambda_n = 0.8$.

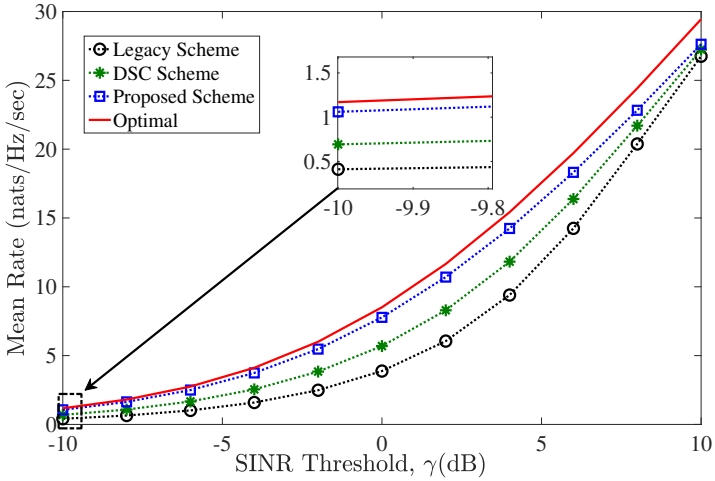

Figure 4.14: Comparing Mean Rate for $K_r = 8$ and $\lambda_n = 0.8$ to Optimal rate for $K_r = 8$ and $\hat{\lambda}_n$.

transmit at each time slot. Fig. 4.14 compares the mean rate of the proposed PCS threshold, the DSC and the Legacy schemes to the optimal rate defined in Theorem 4.2. At low SINR, for instance, $\gamma = -10$ dB, the proposed scheme achieves rate close to the optimal rate obtained at the optimal node density $\hat{\lambda}_n$ from Lemma 4.4. Although, at high SINR, the achievable rate of the proposed scheme slowly diverges

away from the optimum value, it outperforms the DSC and the Legacy schemes.

4.8 Chapter Summary

In this chapter, the PCS threshold selection problem discussed in Section 2.1.4 is addressed for SISO and MIMO WLANs. For SISO systems, a closed-form expression is derived for selecting PCS threshold in CSMA/CA WLANs assuming Rayleigh fading channels and nodes that are distributed according to PPP. The proposed PCS threshold selection method improves the spatial density of throughput over the conventional global PCS threshold and over a random selection method. The proposed framework selects PCS threshold for different target SINR (or rate) given network parameters (path loss exponent and node density), which are global and obtainable during network planning.

For MIMO WLAN environments, the PCS threshold is optimized to take several network parameters such as node density, antenna configuration, path loss and target rates into account. That is, a closed-form expression for selecting PCS threshold in CSMA/CA MIMO-WLANs assuming nodes that are randomly distributed according to PPP. The essence of optimizing the PCS threshold is that this important network parameter scales with the node density and is selected for specific wireless network environment; thereby improving overall system performance. For future WLANs, the proposed scheme can be implemented in such a manner that allows nodes to capture the path loss, supported rate, node density of their host wireless environment in order to adjust the PCS threshold based on this information.

Chapter 5

Spatial Reuse and Coexistence in Unlicensed mmWave Bands

5.1 Introduction

In all the previous chapters, performance improvement is investigated for WLANs with single radio access technology (RAT), specifically, 802.11 or WiFi protocol. However, the future WLANs will continue to support multi-RATs. For instance, the ongoing 3GPP New Radio (NR) access technology standardization for fifth generation (5G) [18], [20] is expected to support variants of unlicensed bands [19], [32], analogous to the 4G Long Term Evolution (LTE) in unlicensed band (LTE-U); that is, LTE-U systems that coexist with incumbent Wi-Fi systems in the 5 GHz band. In the same vein, the 5G NR in unlicensed band (NR-U) will coexist with the wireless gigabit (WiGig) Wi-Fi (or IEEE 802.11ad/ay) in the 60 GHz band [8], [33].

As discussed in Section 2.1.5, the PCS threshold selection problem could affect wireless networks with multi-RATs. In Chapter 4, the PCS threshold selection problem for carrier sensing is addressed for wireless networks with single RAT (IEEE

802.11 or Wi-Fi only). In this chapter, this problem is extended to a multi-RAT wireless network where Wi-Fi WiGig coexists with the emerging 5G NR-U in the millimeter-wave (mmWave) band. Networks deployed in the mmWave band could achieve multi-gigabit data rates due to wide available spectrum [114]. To this point, three issues are identified. First, the underlying parameter that determines spatial reuse or efficient transmissions separation in space is assumed to be fixed. In addition, no insight exists on the relationship between the maximum throughput per unit area and the mmWave propagation characteristics. Thirdly, increasing node density in a multi-RAT network degrades the overall performance due to increased interference. Therefore, *we need to determine the optimal node density to guarantee best performance in a multi-RAT mmWave network.*

Beyond 5G (B5G), network *densification* is important to provide coverage to densely distributed mobile users or stations (STAs) and increase the overall system capacity supporting 1000-fold in user traffic demand [115]. This paradigm involves deployment of a large number of access points (APs) or base stations (BSs) to meet the prolific data traffic demand of users. *Densification* provides the advantage of reducing load-factor if all users are evenly distributed among BSs and/or APs. It reduces the path loss between user stations (STAs) or user equipments (UEs) and the BSs/APs, thereby increasing both the desired and interference signal powers [115]. Hence, interference mitigation is important in providing the required capacity.

Additional spectrum can be exploited to increase system capacity in proportion to increasing signal bandwidth. Using more spectrum requires the integration of different radio access technologies (RATs) that will enable seamless connectivity and mobility, delivering flexible architecture for B5G use cases and service requirements

[116]. Future STAs or UEs will be equipped with multi-RAT capability that enable seamless mobility from one RAT to the other. A typical deployment of a multi-RAT network allows UEs to connect to multiple radios to benefit from different services. Consider the network in Fig. 5.1 where UE_1 and UE_2 could transmit and receive using two different radios, RAT_1 and RAT_2. Depending on the requested service each UE could be served by RAT_1 APs or RAT_2 BSs.

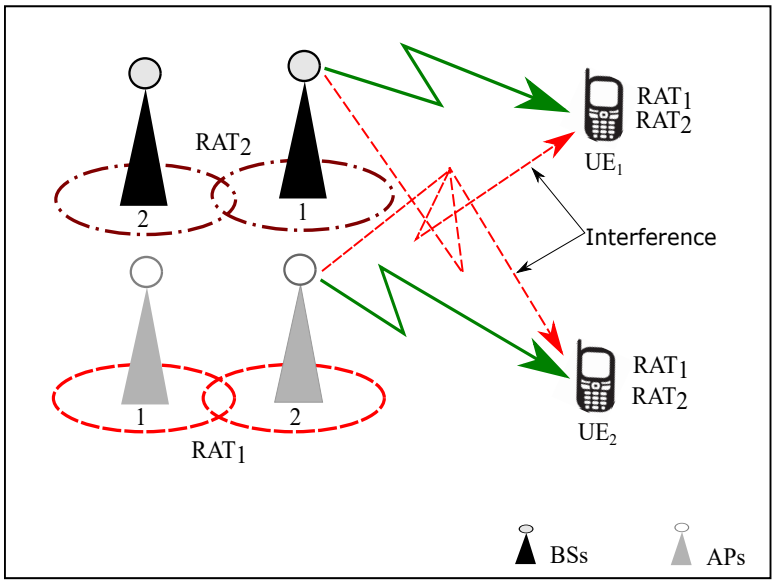

Figure 5.1: A typical network deployment with multiple RATs.

Although a multi-RAT network exploits a wide range of carrier frequencies to improve performance and overall user experience, interference and contention between RATs using the same carrier frequency become severe. While contention level depends on the medium access control (MAC) protocol being used, the density (or number) of concurrent transmitters determines the interference level; both depend on the total density of nodes in the network. With the expected high density of future networks, high contention and interference may result from large numbers of concurrent spectrum-sharing nodes [22], [117]. Increasing node density arbitrarily could

degrade performance due to high contention and interference. In essence, there is a tradeoff between aggregate performance and network densification. This becomes critical when multi-RATs coexist in a spectrum, because the overall performance is impaired by high intra-system and inter-system interference, which jeopardize the overall goal of *densification*.

To take advantage of *spatial densification*[1] in providing high capacity and coverage, the number of BSs and APs deployed per network area could be optimized to find a good balance between interference and densification. In other words, we intend to control *network densification* to maximize throughput performance. Examining the scenario in Fig. 5.1, given the density of RAT_1 APs, we could determine the density of RAT_2 BSs to coexist with RAT_1 in the spectrum such that the minimum tolerable interference exists in the network and performance is improved. Although for simplicity we consider the case of two RAT coexisting in the unlicensed spectrum, this analysis is easily applied to scenarios where there are more than two RATs sharing the same spectrum.

As a special case of the scenario in Fig. 5.1, let us consider a coexistence network with two RATs deployed in the 60 GHz millimeter-wave (mmWave) band where RAT_1 is the wireless gigabit (WiGig) Wi-Fi (or IEEE 802.11ad/ay) [8], [33] while the RAT_2 is the emerging 3rd Generation Partnership Project (3GPP) New Radio (NR) access technology for fifth generation (5G) [18], [20]. The motivation to consider NR-U and WiGig coexistence is that networks deployed in mmWave could achieve multi-gigabit data rates due to widely available spectrum [114]. Existing studies on WiFi/LTE-U coexistence [117], [118], [119] are not easily generalizable to mmWave networks for two reasons. First, the mmWave propagation characteristics differ from

[1]Dense deployment of small cells [115].

those of LTE-U/Wi-Fi in 5 GHz spectrum. Secondly, the spatial interference layout in mmWave network differs from that of LTE-U/Wi-Fi due to the use of directional transmissions [22].

To combat interference in a NR-U/WiGig coexisting network, the listen-before-receive (LBR) spectrum sharing technique is proposed in [22]. With LBR, a receiver defers or allows transmission based on its perceived interference. With LBR, receivers could persistently defer transmissions in high density networks when large numbers of nodes are concurrently active; it is rather a reactive than proactive interference avoidance scheme. Proactively, optimizing the total node density in the network is synonymous to minimizing the overall interference footprint in the system. Herein, the spatial density of throughput (SDT) is the performance metric of interest [2]. By formulating a SDT maximization problem, we derive the optimal density of NR-U nodes that should coexist with WiGig nodes to maximize aggregate SDT in high density WLANs. The key observation is that when the NR-U node density is optimized, aggregate throughput improves and performance gain occurs even at high density of incumbent WiGig nodes.

This chapter is organized as follows. The system model and assumptions are discussed in Section 5.2. In Section 5.3, the channel access probability and the interference model are presented while the performance metric of interest (SDT) is discussed in Section 5.4. The proposed PCS and ED thresholds selection framework is presented in Section 5.5 while in Section 5.6, a rate maximizing node density is derived to unravel the optimal node density that guarantees best performance. The numerical results are discussed in Section 5.7 and this chapter is concluded in Section 5.8.

[2]Measures the average number of successful transmissions per unit area [117].

5.2 Network and System Model

5.2.1 Node Spatial Locations

Without loss of generality, we consider the case of coexistence of two RATs. Consider a WLAN with several 5G NR-U gNBs (a.k.a base stations (BSs)) and WiGig access points (APs) in the 60 GHz unlicensed mmWave spectrum where directional transmissions are used to mitigate propagation limitations. The locations of nodes are modeled as realizations of homogeneous PPP because of the unplanned nature of deployment in today's WLANs where AP and BS locations are not optimized. The locations of 5G NR gNBs and WiGig APs follow realizations of two independent PPPs. Let Φ_{NR} represent the PPP of the 5G NR-U gNBs with density λ_{NR} while the PPP of the WiGig APs is denoted as Φ_{WG} with density λ_{WG}. Specifically, $\Phi_{NR} = \{y_i\}_i$ and $\Phi_{WG} = \{x_j\}_j$. Assuming the WiGig stations (STAs) and NR-U user equipments (UEs) are located at the origin of an AP-STA and gNB-UE pair, respectively, we simply refer to Φ_{WG} as the PPP of AP-STA pairs while the PPP of gNB-UE pairs is denoted as Φ_{NR}.

5.2.2 System Model

Each gNB and WiGig AP uses M transmit antennas while the STAs and the UEs are equipped with N receive antennas. Each gNB aligns its beam $\mathbf{w}_{y_i} \in \mathbb{C}^{M\times 1}$ towards a UE while the AP aligns its beam $\mathbf{w}_{x_j} \in \mathbb{C}^{M\times 1}$ towards its associated STA. The receiver beam vectors at the UE and STA are denoted as $\mathbf{v}_{y_i} \in \mathbb{C}^{N\times 1}$ and $\mathbf{v}_{x_j} \in \mathbb{C}^{N\times 1}$,

respectively. The received power at the UE and STA located at the origin is [22]:

$$P^{rx}_{(o,y_i)} = P_{y_i} G_{o,y_i} \underbrace{\left(\frac{c}{4\pi f_c}\right)^2 \cdot \frac{1}{\|y_i\|^{\alpha}}}_{\ell(o,y_i)}, \tag{5.1}$$

and

$$P^{rx}_{(o,x_j)} = P_{x_j} G_{o,x_j} \underbrace{\left(\frac{c}{4\pi f_c}\right)^2 \cdot \frac{1}{\|x_j\|^{\alpha}}}_{\ell(o,x_j)} \tag{5.2}$$

respectively, where P_{y_i} and P_{x_j} represent the transmit power of the gNBs and the APs, respectively, which are assumed fixed with no power control. and $\ell(\cdot)$ denotes the path loss between the transmitter-receiver pairs given that the UE is located at the origin at distance $\|y_i\|$ from the gNB while the STA is located at the origin at distance $\|x_j\|$ from the AP. α is the path loss exponent, $f_c = 60$ GHz denotes the carrier frequency and c is the speed of light. G_{o,y_i} is the beamforming gain for each gNB-UE pair while G_{o,x_j} is the beamforming gain for the AP-STA pair, which are:

$$G_{o,y_i} = \left|\mathbf{v}^H_{y_i} \mathbf{H}_{y_i} \mathbf{w}_{y_i}\right|^2, \text{ and } G_{o,x_j} = \left|\mathbf{v}^H_{x_j} \mathbf{H}_{x_j} \mathbf{w}_{x_j}\right|^2, \tag{5.3}$$

and where $\mathbf{H}_{y_i}$ and $\mathbf{H}_{x_j}$ represent channels of the gNB-UE and AP-STA pairs, respectively, modeled as [120], [22]:

$$\mathbf{H}_{y_i} = \sqrt{MN\ell(o,y_i)^{-1}} \sum_{k=1}^{K} \beta_k \mathbf{e}_0\left(\theta^k_0\right) \mathbf{e}^H_{y_i}\left(\theta^k_{y_i}\right) \tag{5.4}$$

and

$$\mathbf{H}_{x_j} = \sqrt{MN\ell(o,x_j)^{-1}} \sum_{k=1}^{K} \beta_k \mathbf{e}_0\left(\theta^k_0\right) \mathbf{e}^H_{x_j}\left(\theta^k_{x_j}\right) \tag{5.5}$$

given K resolvable paths, β_k represents the complex gain of the kth path, $\theta^k_{y_i}$ and

$\theta_{x_j}^k$ denote the angles of departure at the transmitters x_i and y_j, respectively, while θ_0^k represents the angle of arrival at UE and STA. $\theta_{y_i}^k$, $\theta_{x_j}^k$ and θ_0^k are assumed to be realizations of uniformly distributed random variables between 0 and 2π. The antenna array responses are [22], [120]:

$$\mathbf{e}_{y_i}\left(\theta_{y_i}^k\right) = \begin{bmatrix} 1 \\ e^{-j\pi \sin\theta_{y_i}^k} \\ \vdots \\ e^{-j\pi(M-1)\sin\theta_{y_i}^k} \end{bmatrix}, \mathbf{e}_{x_j}\left(\theta_{x_j}^k\right) = \begin{bmatrix} 1 \\ e^{-j\pi \sin\theta_{x_j}^k} \\ \vdots \\ e^{-j\pi(M-1)\sin\theta_{x_j}^k} \end{bmatrix}, \mathbf{e}_0\left(\theta_0^k\right) = \begin{bmatrix} 1 \\ e^{-j\pi \sin\theta_0^k} \\ \vdots \\ e^{-j\pi(N-1)\sin\theta_0^k} \end{bmatrix}. \tag{5.6}$$

this model assumes *linear* antenna arrays as opposed to *planar* arrays because the problem formulation considers a 2D network area.

5.3 Channel Access Probability and Interference

In WLANs, nodes must be able to detect the presence of an ongoing transmission and back-off until the transmission is completed. Assume 5G NR-U nodes use the listen-before-talk (LBT) protocol to detect ongoing NR-U and WiGig transmissions, while WiGig nodes employ the carrier sense multiple access collision avoidance (CSMA/CA) protocol. Both LBT and CSMA/CA require nodes to sense the channel through physical carrier sensing (PCS) processes before transmitting and defer transmission if the power or energy in the channel is above a threshold. The probability that a node transmits after the PCS process is termed the channel access probability (CAP), which is derived for WiGig APs and NR-U gNBs.

5.3.1 Medium Access Control for WiGig Systems

WiFi (or 802.11) systems employ the CSMA/CA protocol to coordinate access to the shared medium. Each node contends for a transmission opportunity by sensing the channel to detect the presence of an active transmission through the PCS process and if the power or energy sensed in the channel is below a threshold, the node commences transmission. When WiFi nodes coexist with other RATs such as the 5G NR-U, WiFi nodes are mandated to detect both ongoing WiFi and non-WiFi transmissions. Due to PHY layer differences, WiGig nodes are unable to decode NR-U signals, and vice versa. Therefore, WiGig nodes use *signal detection* to detect active WiFi transmission and use *energy detection* (ED) to detect the presence of an NR-U transmission.

A WiGig node detects other WiGig transmissions by comparing the signal level in the channel to a PCS threshold Γ_{WG}, and detects NR-U transmissions by comparing the energy level in the channel to an ED threshold Γ_{WG}^{ed}. If either the signal power or energy is above Γ_{WG} or Γ_{WG}^{ed}, the CSMA/CA protocol reports a *busy* channel. Otherwise, an *idle* status is reported and the node could begin transmission. The PCS process is performed within a contention domain or radius known as the carrier sensing range (CSR) $\mathcal{R}$, which is usually determined from the PCS threshold Γ_{WG}, and a node transmits if there is no other active transmitter within the CSR. In other words, it is forbidden for two nodes to transmit simultaneously if one lies within the CSR of the other.

To model this behavior of the CSMA/CA protocol, the Matèrn hardcore point process (MHC PP) [40], [117] is very useful. A MHC PP of radius CSR associated with the parent homogeneous PPP Φ_{WG} is obtained through a non-independent *thinning* of Φ_{WG} [40]. When packet arrives at the buffer of AP $x_j \in \Phi_{WG}$, to perform PCS, x_j

forms a circle $\mathcal{B}(x_j, \mathcal{R})$ with radius $\mathcal{R}$ centered at x_j. Assign a uniformly distributed mark $m \in [0,1]$ to each AP x_j within the CSR. An AP with the lowest mark $m(x_j) < m(\tilde{x}_j) \forall \tilde{x}_j \in \Phi_{WG} \setminus x_j$ wins the contention. Technically, in terms of the back-off procedure, x_j wins the contention if it has the lowest back-off counter. Let $\tilde{\Phi}_{WG}$ denote the set of APs that won contention, which represents the Matèrn thinning of the WiGig APs PPP Φ_{WG} with intensity $\tilde{\lambda}_{WG}$. The CAP of a typical WiGig AP is

Lemma 5.1. *A WiGig AP wins contention in its contention domain and transmits with probability:*

$$p_{WG} = \mathbb{P}\left\{x_j \in \tilde{\Phi}_{WG} \middle| m(x_j) < m(\tilde{x}_j) \forall \tilde{x}_j \in \Phi_{WG} \setminus x_j\right\} \mathbb{P}\left\{P^{rx}_{(y_i,x_j)} < \Gamma^{ed}_{WG}\right\} \tag{5.7}$$

$$= \frac{1 - e^{-\lambda_{WG}\Theta}}{\lambda_{WG}\Theta} \exp\left(-\lambda_{NR} \frac{1}{2} \sqrt{\pi \left(\frac{\Gamma^{ed}_{WG}}{P_{y_i}\left(\frac{c}{4\pi f_c}\right)^2} \right)^{-1}} erf\left(\sqrt{\frac{\Gamma^{ed}_{WG}}{P_{y_i}\left(\frac{c}{4\pi f_c}\right)^2}} \|x_j - y_i\| \right) \right),$$

where the first term $\mathbb{P}\{x_j \in \tilde{\Phi}_{WG} | m(x_j) < m(\tilde{x}_j) \forall \tilde{x}_j \in \Phi_{WG} \setminus x_j\}$ and the second term $\mathbb{P}\{P^{rx}_{(y_i,x_j)} < \Gamma^{ed}_{WG}\}$ represent the probabilities of not detecting any ongoing WiGig transmission and NR-U transmission, respectively.

Proof. See Appendix C.1.

5.3.2 Medium Access Control for 5G NR-U Systems

Since discussion is ongoing within the 3GPP group (Rel-16) on NR operating in unlicensed spectrum, similar to LTE-U in 5 GHz band, we assume that the 5G NR-U uses the LBT protocol, which is currently used for unlicensed spectrum for LTE-U channel access. This assumption is consistent with [33] where the LBT specifications

for wireless equipment operating in the 60 GHz band are defined. LBT is a channel access procedure that requires a transmitter to sense the channel and transmit only if there is no ongoing transmission in the channel. Unlike WLAN where channel access control is governed by the CSMA/CA protocol, the LBT for NR-U should be designed for fair coexistence with WLANs.

With LBT for 5G NR-U, gNBs having packets to transmit are required to sense the channel for any active transmission and proceed with the transmission if the NR-U signal detected in the channel is below a detection threshold Γ_{NR}. Similarly, gNBs use ED to detect the presence of an ongoing WiGig transmissions (WiFi signals) above an energy threshold Γ_{NR}^{ed}. This simply implies that the CAP of a gNB depends on the events that it does not detect any NR-U signal (another gNB) and WiGi signal above the detection threshold Γ_{NR} and Γ_{NR}^{ed}, respectively. That is, the sensed NR-U power $P_{(\tilde{y}_i,y_i)}^{rx}$ is below Γ_{NR} and the WiFi energy $P_{(x_j,y_i)}^{rx}$ is below Γ_{NR}^{ed}. The CAP of a typical gNB can be formulated in terms of signal and energy detection according to

Lemma 5.2. *The CAP of a gNB under LBT protocol is:*

$$p_{NR} = \mathbb{P}\left\{ P_{(\tilde{y}_i,y_i)}^{rx} < \Gamma_{NR}, P_{(x_j,y_i)}^{rx} < \Gamma_{NR}^{ed}; \forall \tilde{y}_i \neq y_i \in \Phi_{NR}, x_j \in \Phi_{WG} \right\} \tag{5.8}$$

$$p_{NR} = \exp\left(-\frac{\lambda_{NR}}{2} \sqrt{\frac{\pi}{\Gamma_{NR}/P_{\tilde{y}_i}\left(\frac{c}{4\pi f_c}\right)^2}} erf\left(\sqrt{\Gamma_{NR}/P_{\tilde{y}_i}\left(\frac{c}{4\pi f_c}\right)^2} \|\tilde{y}_i - y_i\| \right) \right) \tag{5.9}$$

$$\cdot \exp\left(-\frac{\lambda_{WG}}{2}\sqrt{\frac{\pi}{\Gamma_{NR}^{ed}/P_{x_j}\left(\frac{c}{4\pi f_c}\right)^2}}\operatorname{erf}\left(\sqrt{\Gamma_{NR}^{ed}/P_{x_j}\left(\frac{c}{4\pi f_c}\right)^2}\,\|x_j - y_i\|\right)\right)$$

Proof. Similar to the Proof of Eq. (C.4) in Appendix C.1 for the case of WiGig access probability.

5.3.3 Density of Active Nodes and Achievable SINRs

Given the CAPs of WiGig APs and NR-U gNBs in Section 5.3.1 and 5.3.2, respectively, we can proceed to determine the density of active transmitters (both APs and gNBs) in the entire network per time-slot. The interference level in the network per time-slot depends greatly on the number concurrently transmitting nodes, that is, the densities of simultaneously active gNBs and WiGig APs. According to the derivation in Section 5.3.1, the PPP $\tilde{\Phi}_{WG}$ of active APs yields the following density of simultaneously transmitting APs:

$$\tilde{\lambda}_{WG} = \lambda_{WG} \cdot p_{WG} \tag{5.10}$$

and if $\tilde{\Phi}_{NR}$ is the resultant PPP of active gNBs per time-slot, the corresponding density is:

$$\tilde{\lambda}_{NR} = \lambda_{NR} \cdot p_{NR}, \tag{5.11}$$

where p_{WG} represents the CAP of a WiGig AP according to Lemma 5.1 and p_{NR} represents channel access probability of the NR-U gNB obtained from Lemma 5.2.

Technically, $\tilde{\Phi}_{WG} \subset \Phi_{WG}$ is the set of concurrently transmitting APs permitted by the CSMA/CA protocol across the network in a given time-slot. Consequently, the signal-to-interference-plus noise of a typical AP x_j at its associated STA is:

$$\text{SINR}_{WG} = \frac{P^{rx}_{(o,x_j)}}{BWN_o + \sum\limits_{\hat{x}_j \in \tilde{\Phi}_{WG} \setminus x_j} P^{rx}_{(\hat{x}_j,x_j)} + \sum\limits_{y_i \in \tilde{\Phi}_{NR}} P^{rx}_{(y_i,x_j)}} \tag{5.12}$$

where $P^{rx}_{(\hat{x}_j,x_j)} = \frac{P_{\hat{x}_j} G_{\hat{x}_j,x_j} \left(\frac{c}{4\pi f_c}\right)^2}{\|\hat{x}_j - x_j\|^{\alpha}}$ and $P^{rx}_{(y_i,x_j)} = \frac{P_{y_i} G_{y_i,x_j} \left(\frac{c}{4\pi f_c}\right)^2}{\|y_i - x_j\|^{\alpha}}$ are the interference power received at x_j from other transmitting APs and gNBs, respectively. BW is the channel bandwdith and N_o is the noise power spectral density. Thus, the SINR_{WG} yields transmission rate:

$$R_{WG} = BW \cdot \log_2 \left(1 + \text{SINR}_{WG}\right). \tag{5.13}$$

Similarly, $\tilde{\Phi}_{NR} \subset \Phi_{NR}$ denotes the set of active gNBs permitted by the LBT protocol and given the PPP $\tilde{\Phi}_{NR}$ of active gNBs per time-slot. The SINR of a typical gNB is:

$$\text{SINR}_{NR} = \frac{P^{rx}_{(o,y_i)}}{BWN_o + \sum\limits_{\hat{y}_i \in \tilde{\Phi}_{NR} \setminus y_i} P^{rx}_{(\hat{y}_i,y_i)} + \sum\limits_{x_j \in \tilde{\Phi}_{WG}} P^{rx}_{(x_j,y_i)}}, \tag{5.14}$$

where $P^{rx}_{(\hat{y}_i,y_i)} = \frac{P_{\hat{y}_i} G_{\hat{y}_i,y_i} \left(\frac{c}{4\pi f_c}\right)^2}{\|\hat{y}_i - y_i\|^{\alpha}}$ and $P^{rx}_{(x_j,y_i)} = \frac{P_{x_j} G_{x_j,y_i} \left(\frac{c}{4\pi f_c}\right)^2}{\|x_j - y_i\|^{\alpha}}$ are the interference power received at y_i from other gNBs and APs, respectively, and the transmission rate is:

$$R_{NR} = BW \cdot \log_2 \left(1 + \text{SINR}_{NR}\right). \tag{5.15}$$

5.4 Performance Metric

The performance metric of interest is the spatial density of throughput (SDT) [117], which measures the average number of users per unit area that *gain access to the medium* and *achieve a target SINR*. The successful transmission probability (STP) is first derived, then the SDT is defined in terms of the CAP and the STP.

5.4.1 Successful Transmission Probability (STP)

Gaining access to the channel based on high CAP does not guarantee a target SINR due to interference in large networks, especially in cases where a large number of nodes have high CAP. High CAP may cause high interference from large numbers of concurrently transmitting nodes, which causes erroneous decoding of transmitted symbols due to low SINRs. Therefore, the STP captures the tradeoff between high CAP and SINR. More concurrent transmitters implies high interference and low SINR while fewer concurrent transmitters improves the SINRs. For a given SINR threshold, a transmission is successful with probability defined in

Lemma 5.3. *A typical gNB and a WiGig AP independently achieves target SINR γ with probability:*

$$\mathcal{P}_{NR} = \mathbb{E}\left[\sum_{y_i \in \Phi_{NR}} \mathbb{1}_{SINR_{NR}>\gamma}\right] = \exp\left(-\gamma BW N_o\right) \tag{5.16}$$

$$\cdot \exp\left(-\frac{\tilde{\lambda}_{NR}}{2}\sqrt{\frac{\pi}{\gamma P_{\hat{y}_i} G_{\hat{y}_i,y_i}\left(\frac{c}{4\pi f_c}\right)^2}}\, erf\left(\sqrt{\gamma P_{\hat{y}_i} G_{\hat{y}_i,y_i}\left(\frac{c}{4\pi f_c}\right)^2}\right)\right) \tag{5.17}$$

$$\cdot \exp\left(-\frac{\tilde{\lambda}_{WG}}{2}\sqrt{\frac{\pi}{\gamma P_{x_j} G_{y_i,x_j}\left(\frac{c}{4\pi f_c}\right)^2}}\operatorname{erf}\left(\sqrt{\gamma P_{x_j} G_{y_i,x_j}\left(\frac{c}{4\pi f_c}\right)^2}\right)\right)$$

and

$$\mathcal{P}_{WG} = \mathbb{E}\left[\sum_{x_j \in \Phi_{WG}} \mathbb{1}_{\mathrm{SINR}_{WG}>\gamma}\right] = \exp\left(-\gamma BW N_o\right) \tag{5.18}$$

$$\cdot \exp\left(-\frac{\tilde{\lambda}_{WG}}{2}\sqrt{\frac{\pi}{\gamma P_{\hat{x}_j} G_{\hat{x}_j,x_j}\left(\frac{c}{4\pi f_c}\right)^2}}\operatorname{erf}\left(\sqrt{\gamma P_{\hat{x}_j} G_{\hat{x}_j,x_j}\left(\frac{c}{4\pi f_c}\right)^2}\right)\right) \tag{5.19}$$

$$\cdot \exp\left(-\frac{\tilde{\lambda}_{NR}}{2}\sqrt{\frac{\pi}{\gamma P_{x_j} G_{y_i,x_j}\left(\frac{c}{4\pi f_c}\right)^2}}\operatorname{erf}\left(\sqrt{\gamma P_{x_j} G_{y_i,x_j}\left(\frac{c}{4\pi f_c}\right)^2}\right)\right),$$

The STP for a particular node (gNB or WiGig AP) depends on the target rate in terms of the SINR threshold γ and ultimately the density of active nodes $\tilde{\lambda}_{WG}$ and $\tilde{\lambda}_{NR}$ defined in Eqns. (5.11) and (5.10), respectively, that are generating interference through concurrent transmissions.

Proof. See Appendix C.2.

5.4.2 Spatial Density of Throughput (SDT)

When multiple nodes have high CAP per time-slot to transmit, interference becomes dominant and low SINRs are inevitable. Therefore, the measure of successful transmissions per unit area becomes important as it capture the effect of interference and the CAP on the achievable SINR. Therefore, SDT for the NR-U gNBs and the WiGig

APs is defined as:

$$\text{SDT}_{NR} = \tilde{\lambda}_{NR}\mathcal{P}_{NR}R_{NR} \qquad \text{and} \qquad \text{SDT}_{WG} = \tilde{\lambda}_{WG}\mathcal{P}_{WG}R_{WG}, \tag{5.20}$$

and the aggregate SDT is

$$\text{SDT} = \text{SDT}_{NR} + \text{SDT}_{WG} \tag{5.21}$$

where $\tilde{\lambda}_{NR}$ and $\tilde{\lambda}_{WG}$ are the densities of active NR-U gNBs and WiGig APs,respectively, permitted by the channel access protocols to transmit simultaneously, $\mathcal{P}_{NR}$ and $\mathcal{P}_{WG}$ from Lemma 4.2 are the probabilities of successful transmissions in the gNB and the WiGig case respectively, while R_{NR} and R_{WG} are the respective channel rates defined in Eqns (5.15) and (5.13), respectively.

5.5 PCS/ED Thresholds for Spatial Reuse

As discussed earlier, an important component of designing the LBT is the PCS threshold, which is the level of sensitivity to detect the existence of ongoing transmissions. While the PCS threshold for LBT by gNBs needs to be set appropriately to effectively protect nearby WLAN transmissions, the energy detection threshold used by WLAN system must be adequately define to detect gNB signals. Therefore, given the performance quantities in Eqns. (5.20) and (5.21), the objective is to tune the PCS threshold such that the aggregate throughput density is improved. That is, choosing the PCS threshold values that maximize the aggregate throughput density.

The transmission probabilities of gNBs and APs depend on the PCS threshold and energy detection threshold being used for LBT and CSMA/CA protocol, and in turn,

they determine the densities of active gNBs and APs as given in Eqns. (5.11) and (5.10), respectively. Therefore, the PCS/ED thresholds can be optimized to maximize the aggregate throughout density. For any given density of gNBs and WiGig APs, putting Eqns. (5.20) and (5.21) together, the aggregate throughput density in the network is:

$$\Upsilon = \mathrm{SDT}_{NR} R_{NR} + \mathrm{SDT}_{WG} R_{WG} \tag{5.22}$$

this aggregate throughput density for the network assumes that the SINR threshold γ sufficiently achieves the spectral efficiencies R_{nr} and R_{wg}. For simplicity, we assume that the SINR threshold γ is identical for both WiGig nodes and gNBs; that is, the target rate of WiGig nodes is similar to that of gNBs.

5.5.1 PCS/ED Threshold Values for NR-U Nodes

The spatial reuse in coexisting NR-U gNBs with WiGig APs can be improved by appropriately defining the PCS threshold or energy detection (ED) threshold in the case of WiGig APs detecting NR-U signals. Increasing the PCS threshold for LBT leads to PCS that protects smaller area around the gNB. Similarly for WiGig APs detecting gNB signals, high detection threshold is quite ineffective as it decreases the sensitivity region of the AP. On the contrary, low threshold values allow nodes to sense a wider area and thereby preventing more concurrent transmissions that have potential to be successful at the receiver.

Considering the case of the NR-U gNBs, gNBs require a PCS threshold Γ_{nr} to detect ongoing transmissions from other gNBs and an ED threshold Γ_{nr}^{ed} to detect WiFi signals during the LBT process; the ED threshold is used because the gNBs are not able to decode WiFi signals. Therefore, to define Γ_{nr} and Γ_{nr}^{ed} for gNBs to

maximize the aggregate throughput density, the problem is formulated as

$$\Upsilon_{\max}\left(\Gamma_{nr}, \Gamma_{nr}^{ed}\right) = \max_{\Gamma_{nr}, \Gamma_{nr}^{ed}} \Upsilon, \tag{5.23}$$

and the solution to this optimization problem is immediate from Theorem 5.1 as follows:

Theorem 5.1. *The PCS and ED thresholds* Γ_{nr} *and* Γ_{nr}^{ed} *that maximize the throughput density are:*

$$\Gamma_{nr} = \frac{6\sqrt{\pi} P_{\tilde{y}_i} \left(\frac{c}{4\pi f_c}\right)^2 \sqrt{\lambda_{nr}}}{\pi \frac{4}{\sqrt{\pi}}} \tag{5.24}$$

and

$$\Gamma_{nr}^{ed} = \frac{6\sqrt{\pi} P_{x_j} \left(\frac{c}{4\pi f_c}\right)^2 \sqrt{\lambda_{wg}}}{\pi \frac{4}{\sqrt{\pi}}}. \tag{5.25}$$

Proof. Since the objective function in Eqn. (5.23) is differentiable, the solution to the problem is feasible by taking the derivative of Eqn. (5.22) w.r.t Γ_{nr} and Γ_{nr}^{ed} to satisfy the necessary condition, i.e., $\frac{\partial \Upsilon}{\partial \Gamma_{nr}} = 0$ and $\frac{\partial \Upsilon}{\partial \Gamma_{nr}^{ed}} = 0$, respectively. Therefore, by first

establishing $\frac{\partial \Upsilon}{\partial \Gamma_{nr}} = 0$, the following key algebraic steps establish Eqn. (5.24):

$$\lambda_{nr}\mathcal{P}_{nr}\mathcal{R}_{nr}\exp\left(-\lambda_{nr}\frac{1}{2}\sqrt{\pi\Xi_{nr}}\Gamma_{nr}^{-\frac{1}{2}}\mathrm{erf}\left(\sqrt{\frac{\Gamma_{nr}\left\|\tilde{y}_i-y_i\right\|}{\Xi_{nr}}}\right)\right) \tag{5.26}$$

$$\cdot\left[\frac{1}{4}\lambda_{nr}\sqrt{\pi\Xi_{nr}}\Gamma_{nr}^{-\frac{3}{2}}\mathrm{erf}\left(\sqrt{\frac{\Gamma_{nr}\left\|\tilde{y}_i-y_i\right\|}{\Xi_{nr}}}\right)-\lambda_{nr}\sqrt{\pi\Xi_{nr}\Gamma_{nr}}\frac{2}{\sqrt{\pi}}\exp\left(-\Gamma_{nr}\frac{\left\|\tilde{y}_i-y_i\right\|}{\Xi_{nr}}\right)\right]=0$$

$$\frac{1}{2}\Gamma_{nr}^{-1}\mathrm{erf}\left(\Gamma_{nr}^{\frac{1}{2}}\left(\frac{\left\|\tilde{y}_i-y_i\right\|}{\Xi_{nr}}\right)^{\frac{1}{2}}\right)=\frac{2}{\sqrt{\pi}}\exp\left(-\Gamma_{nr}\frac{\left\|\tilde{y}_i-y_i\right\|}{\Xi_{nr}}\right)$$

$$\Gamma_{nr}^{-1}\lambda_{nr}\mathrm{erf}\left(\Gamma_{nr}^{\frac{1}{2}}\left(\frac{\left\|\tilde{y}_i-y_i\right\|}{\Xi_{nr}}\right)^{\frac{1}{2}}\right)=\frac{4}{\sqrt{\pi}}\exp\left(-\Gamma_{nr}\frac{\left\|\tilde{y}_i-y_i\right\|}{\Xi_{nr}}\right) \tag{5.27}$$

$$\lambda_{nr}\frac{2}{\sqrt{\pi}}\exp\left(-\frac{\Gamma_{nr}\left\|\tilde{y}_i-y_i\right\|}{\Xi_{nr}}\right)=\frac{4}{\sqrt{\pi}}\exp\left(-\frac{\Gamma_{nr}\left\|\tilde{y}_i-y_i\right\|}{\Xi_{nr}}\right)\left[1-\frac{\Gamma_{nr}\left\|\tilde{y}_i-y_i\right\|}{\Xi_{nr}}\right] \tag{5.28}$$

where $\Xi_{nr}=P_{\tilde{y}_i}\left(\frac{c}{4\pi f_c}\right)^2$ and Eqn. (5.28) is obtained by taking the derivative of both sides of Eqn. (5.27) and using the fact that the $\frac{\partial}{\partial z}\mathrm{erf}\left(z\right)=\frac{2}{\sqrt{\pi}}e^{-z^2}$ [121]. Solving for Γ_{nr} in Eqn. (5.28), the following equation is obtained

$$\Gamma_{nr}=\frac{6\sqrt{\pi}}{\pi}\frac{P_{\tilde{y}_i}\left(\frac{c}{4\pi f_c}\right)^2}{\frac{4}{\sqrt{\pi}}\left\|\tilde{y}_i-y_i\right\|}. \tag{5.29}$$

Eqn (5.29) provides PCS threshold values in complex domain, and as predicted in Lemma 5.2, Eqn (5.29) requires the distances $\|\tilde{y}_i - y_i\|$ between the sensing node y_i and all its neighbors $\tilde{y}_i$, which depends on the *directionality* (in terms of the signal angle θ of arrival) of the carrier sensing. For a 2-D random network, the distance between two points in a sector θ can be characterized as a distribution. Let θ represent the directionality of the sensed signal, the Euclidean distance between NR-U node y_i

and the nth contender $\tilde{y}_i$, is characterized as [122, Corollary 3]

$$f\left(\|\tilde{y}_i - y_i\|\right) = \exp(-\lambda_{nr}\theta\|\tilde{y}_i - y_i\|^2)\frac{2\left(\lambda_{nr}\theta\|\tilde{y}_i - y_i\|^2\right)^n}{\|\tilde{y}_i - y_i\|\beta\left(n\right)}, \tag{5.30}$$

where $\beta(\cdot)$ is the Gamma function. For a 2-D random network, $\theta = \frac{\pi}{4}$, and assuming node y_i contends with $n = 1$ node $\tilde{y}_i$ according to Lemma 5.2, $\|\tilde{y}_i - y_i\|$ is Rayleigh distributed with expected value $\mathbb{E}\left[\|\tilde{y}_i - y_i\|\right] = \frac{1}{\sqrt{\lambda_{nr}}}$. Thus, Eqn. (5.29) is equivalent to

$$\Gamma_{nr} = \frac{6\sqrt{\pi}P_{\tilde{y}_i}\left(\frac{c}{4\pi f_c}\right)^2\sqrt{\lambda_{nr}}}{\pi\frac{4}{\sqrt{\pi}}}, \tag{5.31}$$

which proves Eqn. (5.24). This represents a spatial average over all the potential contending nodes and reveals that the PCS threshold depends on the propagation characteristics of mmWave signal, the density of nodes in the network, and a geometric factor. The propagation profile in turns depend on the transmit power and the carrier frequency; it is generalizable to other mmWave bands. By establishing $\frac{\partial\Upsilon}{\partial\Gamma_{nr}^{ed}} = 0$ and following similar procedure, Eqn. (5.25) is obtained. □

5.5.2 PCS/ED Threshold Values for WiGig Nodes

WiGig nodes require an appropriately defined PCS threshold Γ_{wg} to detect ongoing WiFi signals and ED threshold Γ_{wg}^{ed} to detect non-WiFi signals such as NR-U signals. If Γ_{wg} and Γ_{wg}^{ed} are properly designed, they could significantly improve spatial reuse because efficient separation of multiple concurrent transmissions in space depends on these two parameters. For WiGig signal and NR-U signal detection at the WiGig

APs, problem (5.23) is reformulated as:

$$\Upsilon_{\max}\left(\Gamma_{wg}, \Gamma_{wg}^{ed}\right) = \max_{\Gamma_{wg}, \Gamma_{wg}^{ed}} \Upsilon, \tag{5.32}$$

from which the PCS threshold Γ_{wg} and the ED threshold Γ_{wg}^{ed}, respectively are obtained from Theorem 5.2.

Theorem 5.2. *For WiGig nodes, the PCS and ED thresholds* Γ_{wg} *and* Γ_{wg}^{ed} *that maximize the throughput density are*

$$\Gamma_{wg} = \log\left(\frac{\ln\lambda_{wg} - \frac{\left(\sqrt{\lambda_{wg}}\right)^{-\alpha}}{P_{\tilde{x}_j}\left(\frac{c}{4\pi f_c}\right)^2}}{2\lambda_{wg}\frac{P_{\tilde{x}_j}\left(\frac{c}{4\pi f_c}\right)^2}{\alpha}}\right) \cdot \frac{P_{\tilde{x}_j}\left(\frac{c}{4\pi f_c}\right)^2}{\left(\sqrt{\lambda_{wg}}\right)^{-\alpha}} \tag{5.33}$$

and

$$\Gamma_{wg}^{ed} = \frac{6\sqrt{\pi}P_{y_i}\left(\frac{c}{4\pi f_c}\right)^2\sqrt{\lambda_{nr}}}{\pi\frac{4}{\sqrt{\pi}}}. \tag{5.34}$$

Proof. The proof of Eqn. (5.33) follows from establishing the necessary condition for problem (5.32) by setting the derivative of the objective function w.r.t Γ_{wg} to zero,

i.e., $\frac{\partial \Upsilon}{\partial \Gamma_{wg}} = 0$, leads to the following to solve for Γ_{wg}:

$$\lambda_{wg} \exp\left(-\Gamma_{wg} \frac{\|\tilde{x}_j - x_j\|^{\alpha}}{P_{\tilde{x}_j}\left(\frac{c}{4\pi f_c}\right)^2}\right) \frac{P_{\tilde{x}_j}\left(\frac{c}{4\pi f_c}\right)^2}{\alpha \Gamma_{wg}} \exp\left(-\lambda_{wg} \exp\left(-\Gamma_{wg} \frac{\|\tilde{x}_j - x_j\|^{\alpha}}{P_{\tilde{x}_j}\left(\frac{c}{4\pi f_c}\right)^2}\right) \cdot \frac{P_{\tilde{x}_j}\left(\frac{c}{4\pi f_c}\right)^2}{\alpha \Gamma_{wg}}\right)$$

$$= 1 - \exp\left(-\lambda_{wg} \exp\left(-\Gamma_{wg} \frac{\|\tilde{x}_j - x_j\|^{\alpha}}{P_{\tilde{x}_j}\left(\frac{c}{4\pi f_c}\right)^2}\right) \cdot \frac{P_{\tilde{x}_j}\left(\frac{c}{4\pi f_c}\right)^2}{\alpha \Gamma_{wg}}\right) \tag{5.35}$$

$$\ln\left[\lambda_{wg} \exp\left(-\Gamma_{wg} \frac{\|\tilde{x}_j - x_j\|^{\alpha}}{P_{\tilde{x}_j}\left(\frac{c}{4\pi f_c}\right)^2} - \lambda_{wg} \exp\left(-\Gamma_{wg} \frac{\|\tilde{x}_j - x_j\|^{\alpha}}{P_{\tilde{x}_j}\left(\frac{c}{4\pi f_c}\right)^2}\right) \cdot \frac{P_{\tilde{x}_j}\left(\frac{c}{4\pi f_c}\right)^2}{\alpha \Gamma_{wg}}\right) \cdot \frac{P_{\tilde{x}_j}\left(\frac{c}{4\pi f_c}\right)^2}{\alpha \Gamma_{wg}}\right]$$

$$= \ln 1 - \ln\left[\exp\left(-\lambda_{wg} \exp\left(-\Gamma_{wg} \frac{\|\tilde{x}_j - x_j\|^{\alpha}}{P_{\tilde{x}_j}\left(\frac{c}{4\pi f_c}\right)^2}\right) \cdot \frac{P_{\tilde{x}_j}\left(\frac{c}{4\pi f_c}\right)^2}{\alpha \Gamma_{wg}}\right)\right] \tag{5.36}$$

$$\ln \lambda_{wg} - \frac{\|\tilde{x}_j - x_j\|^{\alpha}}{P_{\tilde{x}_j}\left(\frac{c}{4\pi f_c}\right)^2} - \lambda_{wg} \exp\left(-\Gamma_{wg} \frac{\|\tilde{x}_j - x_j\|^{\alpha}}{P_{\tilde{x}_j}\left(\frac{c}{4\pi f_c}\right)^2}\right) \cdot \frac{P_{\tilde{x}_j}\left(\frac{c}{4\pi f_c}\right)^2}{\alpha}$$

$$= \lambda_{wg} \exp\left(-\Gamma_{wg} \frac{\|\tilde{x}_j - x_j\|^{\alpha}}{P_{\tilde{x}_j}\left(\frac{c}{4\pi f_c}\right)^2}\right) \cdot \frac{P_{\tilde{x}_j}\left(\frac{c}{4\pi f_c}\right)^2}{\alpha} - \ln\left(\frac{P_{\tilde{x}_j}\left(\frac{c}{4\pi f_c}\right)^2}{\alpha \Gamma_{wg}}\right) \Gamma_{wg} \tag{5.37}$$

$$\ln \lambda_{wg} - \frac{\|\tilde{x}_j - x_j\|^{\alpha}}{P_{\tilde{x}_j}\left(\frac{c}{4\pi f_c}\right)^2} = 2\lambda_{wg} \exp\left(-\Gamma_{wg} \frac{\|\tilde{x}_j - x_j\|^{\alpha}}{P_{\tilde{x}_j}\left(\frac{c}{4\pi f_c}\right)^2}\right) \cdot \frac{P_{\tilde{x}_j}\left(\frac{c}{4\pi f_c}\right)^2}{\alpha}. \tag{5.38}$$

Without loss of generality, Eqn. (5.38) is obtained from Eqn. (5.37) by normalizing the term $\frac{P_{\tilde{x}_j}\left(\frac{c}{4\pi f_c}\right)^2}{\alpha \Gamma_{wg}}$ to a unit value since it represents the ratio of the propagated power to the PCS threshold scaled by the path loss exponent. Obtaining a closed-form expression from Eqn. (5.38) and applying the distance law in Eqn. (5.30) to determine $\|\tilde{x}_j - x_j\|$, proves Eqn. (5.33) while the proof of Eqn. (5.34) is similar to the proof of Eqn. (5.24). □

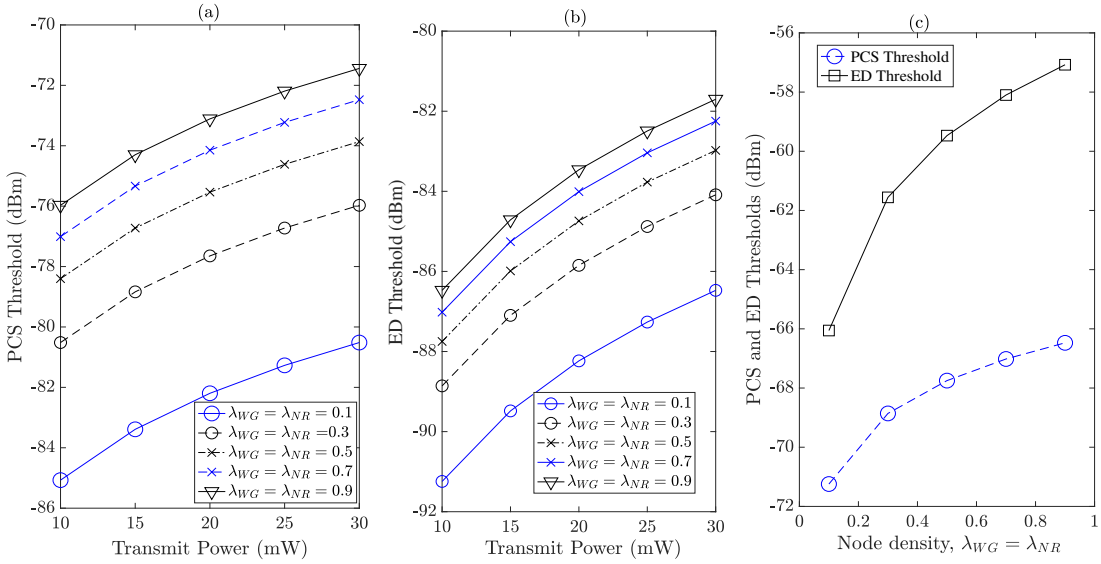

Figure 5.2: As predicted in Theorems 5.1 and 5.2 for various network densities $\lambda_{WG} = \lambda_{NR}$: (a) PCS thresholds vs. node transmit power (b) ED thresholds vs. node transmit power (c) ED and PCS thresholds vs. node density with normalized transmit power of 1.

The optimal PCS and ED thresholds obtained from Theorems 5.1 and 5.2 depend on the mmWave propagation characteristic, path loss exponent, node density, transmit power and spatial information for 2-D wireless network. The dependency on the node density is rooted in the behavior of the channel access protocols discussed earlier in Sections 5.3, and the chances of a node winning contention depends on the number of nodes in its contention domain. Fig. 5.2 illustrates the predictions from Theorems 5.1 and 5.2 that PCS and ED thresholds should be adaptive to changes in node density and transmit power. With lower node density, the PCS/ED thresholds are less sensitive (conservative) and more sensitive at high node density.

5.6 Optimal Node Density for Rate Maximization

Given the performance metric in Eqn. (5.22), the objective is to tune the density of nodes in the network such that the aggregate throughput density is maximized. In practical terms, we tend to answer the question of *how dense should a network be to guarantee the optimal performance in terms of throughput*? This question is valid because as the density of nodes deployed in a network increases, the interference domain of each node increases and such network would inevitably generate high interference that deteriorates the overall performance.

5.6.1 Optimal NR-U Node Density

Here, the goal is to find the optimal density of NR-U nodes to coexist with WiGig nodes such that the aggregate throughput density is maximized. This problem is formulated as

$$\max_{\lambda_{WG},\lambda_{NR}} \Upsilon. \tag{5.39}$$

From a design and performance constraint, there is a tradeoff between increasing the density of nodes per network and throughput. Given the density λ_{WG} of WiGig APs, the density of gNBs to coexist with WiGig APs such that aggregate throughput density Υ is maximized, is obtained by

Theorem 5.3. *The density of NR-U gNBs coexisting with WiGig APs in a mmWave wireless network to maximize aggregate throughput is*

$$\lambda_{NR}^{*}=\frac{R_{WG}\left(1-\frac{\lambda_{WG}}{2}\sqrt{\frac{\pi}{P_{\hat{y}_i}G_{\hat{y}_i,y_i}\left(\frac{c}{4\pi f_c}\right)^2\gamma}}\mathrm{erf}\left(P_{\hat{y}_i}G_{\hat{y}_i,y_i}\left(\frac{c}{4\pi f_c}\right)^2\gamma\right)\right)}{\frac{R_{NR}}{2}\sqrt{\frac{\pi}{P_{x_j}G_{y_i,x_j}\left(\frac{c}{4\pi f_c}\right)^2\gamma}}\mathrm{erf}\left(P_{x_j}G_{y_i,x_j}\left(\frac{c}{4\pi f_c}\right)^2\gamma\right)} \tag{5.40}$$

Proof. Substitute $\mathcal{P}_{NR}$ and $\mathcal{P}_{WG}$ from Lemma 5.3 into (5.22), and replace $\tilde{\lambda}_{WG}$ and $\tilde{\lambda}_{NR}$ with Eqns. (5.10) and (5.11),

$$\Upsilon=\left(\lambda_{WG}\cdot p_{WG}\right)\mathcal{P}_{WG}R_{WG}+\left(\lambda_{NR}\cdot p_{NR}\right)\mathcal{P}_{NR}R_{NR}. \tag{5.41}$$

Setting the derivative of Eqn. (5.41) with respect to the node density λ_{NR} to zero and solving, Eqn. (5.40) is obtained. □

From Eqn. (5.40), we can infer that if gNBs and WiGig APs transmit at equal power and channel rates with equal channel gains and SINR threshold, $\lambda_{NR}^{*}=1-\lambda_{WG}$, which is an ideal case where the maximum normalized total node density is 1. Assuming fixed λ_{NR}, the optimal WiGig node density λ_{WG}^{*} follows similar steps.

5.6.2 Throughput Upper Bound

Thus far, results depend on protocols, which determine p_{WG} and p_{NR}. If ideal protocols exist, we obtain

Theorem 5.4. *The throughput density in coexisting 5G NR-U gNBs with WiGig APs*

in a Poisson mmWave wireless network is upper bounded by

$$\Upsilon_{\max}\left(\lambda_{WG}, \lambda^{*}_{NR}\right) = \frac{1 + R_{WG}\lambda_{WG}\frac{1}{2}\sqrt{\frac{\pi}{\left(\frac{c}{4\pi f_c}\right)^2\gamma}}\, erf\left(\left(\frac{c}{4\pi f_c}\right)^2\gamma\right)}{\frac{1}{2}\sqrt{\frac{\pi}{\left(\frac{c}{4\pi f_c}\right)^2\gamma}}\, erf\left(\left(\frac{c}{4\pi f_c}\right)^2\gamma\right)}\Delta. \tag{5.42}$$

where $\Delta = \lambda_{WG}\mathcal{P}_{WG} + \mathcal{P}_{NR}$.

Proof. Assume all active nodes must have accessed the channel with probabilities $p_{NR} = p_{WG} = 1$ in that time-slot. In (5.22), replace $\tilde{\lambda}_{NR}$ and $\tilde{\lambda}_{WG}$ with Eqns (5.11) and (5.10), respectively, and set $p_{NR} = p_{WG} = 1$ and fix $\mathcal{P}_{NR}$ and $\mathcal{P}_{WG}$, Eqn. (5.42) is obtained, which implies that the above upper-bound throughput depends on the target rate, density of the WiGig nodes and mmWave propagation characteristics □.

5.7 Numerical Results

It is assumed that WiGig nodes are the incumbents while 5G NR-U nodes are being deployed to coexist with the incumbents in 2-D space WLAN. All nodes operate at $f_c = 60$ GHz carrier frequency with channel bandwidth $BW = 1$ GHz, path loss exponent $\alpha = 2$, which is the LOS path loss model for 802.11ad [22]. Transmit powers are normalized to 1 and noise $N_o = -100$ dBm while the PCS and the ED are -70 dBm and -60 dBm, respectively, used in the simulation. We consider $M = 64$ transmit and $N = 16$ receive linear antennas array for a 2-D WLAN. The channel matrix $\mathbf{H}_{y_i}$ and $\mathbf{H}_{x_j}$ are modeled based on Eqs. (5.4) and (5.5), respectively. The beam vectors $\mathbf{v}$ and $\mathbf{w}$ in Eq. (5.3) are computed using channel inversion to obtain the beamforming gains G_{o,y_i} and G_{o,x_j}. The transmitter's beamwidths $\theta^k_{y_i}$ and $\theta^k_{x_j}$ are randomly selected at each time-slot from a $U \sim [0, 360^\circ]$, while the receiver beamwidth

$\theta_0^k = 60°$.

The performance of the proposed optimized PCS and ED thresholds in Theorems 5.1 and 5.2 is compared to the conventional baseline fixed PCS and ED thresholds. Consequently, in the performance benchmarking, the result obtained from Theorems 5.1 and 5.2 is referred to as "Proposed Method" while that of the fixed PCS/ED threshold is called "Conventional Fixed," which emulates the current WLAN systems in use. In simulating contention under the CSMA/CA and the LBT protocols, the conventional fixed PCS and ED thresholds are defined as -70 dBm and -60 dBm, respectively. The proposed method adapts the PCS and ED thresholds to node density and transmit power according to Theorems 5.1 and 5.2. Performance is measured in terms of the SDT and the throughput per unit area defined in Eqns. (5.21) and (5.22), respectively. Simulation results are averaged over 10^6 channel realizations of the network.

Figure 5.3 illustrates a snapshot of the active gNBs and WiGig APs at a time-slot in the simulation under the proposed PCS/ED threshold selection. The circled nodes represent gNBs and APs that successfully acquire the channel in their contention domain as established in Lemmas 5.1 and 5.2. Figure 5.3 shows that the proposed PCS/ED threshold selection method forbids overlapped BSSs or cells under both CSMA/CA and LBT protocols. The proposed scheme allows subset of nodes to transmit concurrently per time-slot such that interference is minimized. Fig. 5.4 illustrates performance as predicted in Lemmas 5.1, 5.2 and 5.3, showing that as the node densities λ_{WG} and λ_{NR} increase, interference and contention become dominant. This degrades both the channel access probability (CAP) and the successful transmission probability (STP). Hence, it is important to optimize PCS and ED thresholds with

respect to known network parameters (node density, transmit power and path loss exponent etc.), to maximize performance rather than arbitrarily fixing the thresholds.

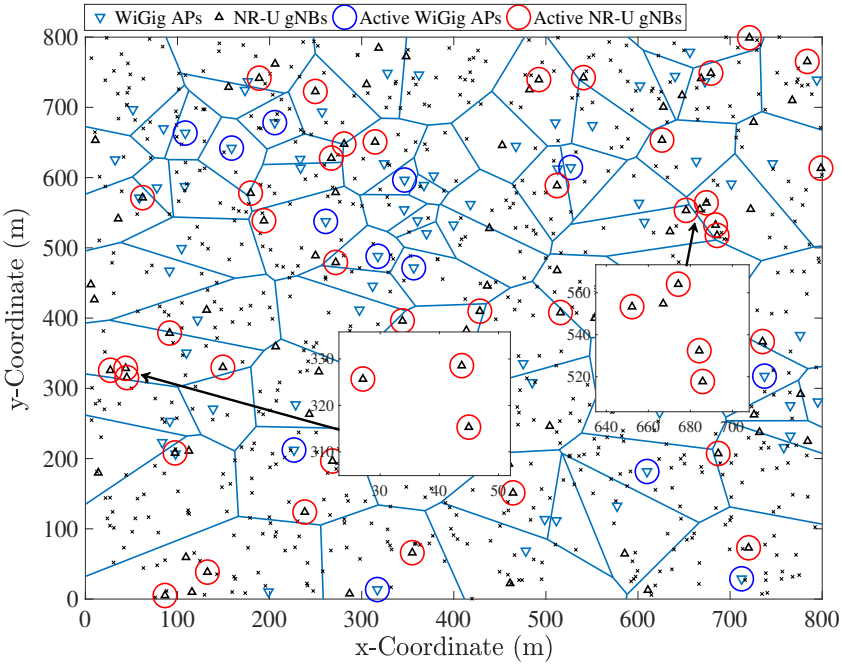

Figure 5.3: Snapshot of a 2-D network showing active WiGig APs and NR-U gNBs at a given time-slot and $\lambda_N R = \lambda_W G = 0.1$ under the proposed PCS and ED thresholds in Theorems 5.1 and 5.2.

Figures 5.5 and 5.6 further buttress the interaction between PCS/ED thresholds and performance in WLAN at high node density $\lambda_{WG} = \lambda_{NR} = 0.9$. In Fig. 5.5, the CAP is plotted against arbitrary PCS/ED thresholds. At highly sensitive PCS/ED thresholds (-80 to -100 dBm), the WiGig nodes are more likely to encounter persistent backoff (due to low CAP) while the NR-U nodes transmit with higher probability. While WiGig APs are more likely to acquire the channel at less sensitive thresholds (-70 to -55 dBm), both gNBs and APs have equal transmission opportunity at -75 dBm. Intuitively, nearly half of the combined density gNBs ($\lambda_{NR} = 0.9$) and APs ($\lambda_{WG} = 0.9$) will transmit at -75 dBm. While this seems like an equilibrium point in

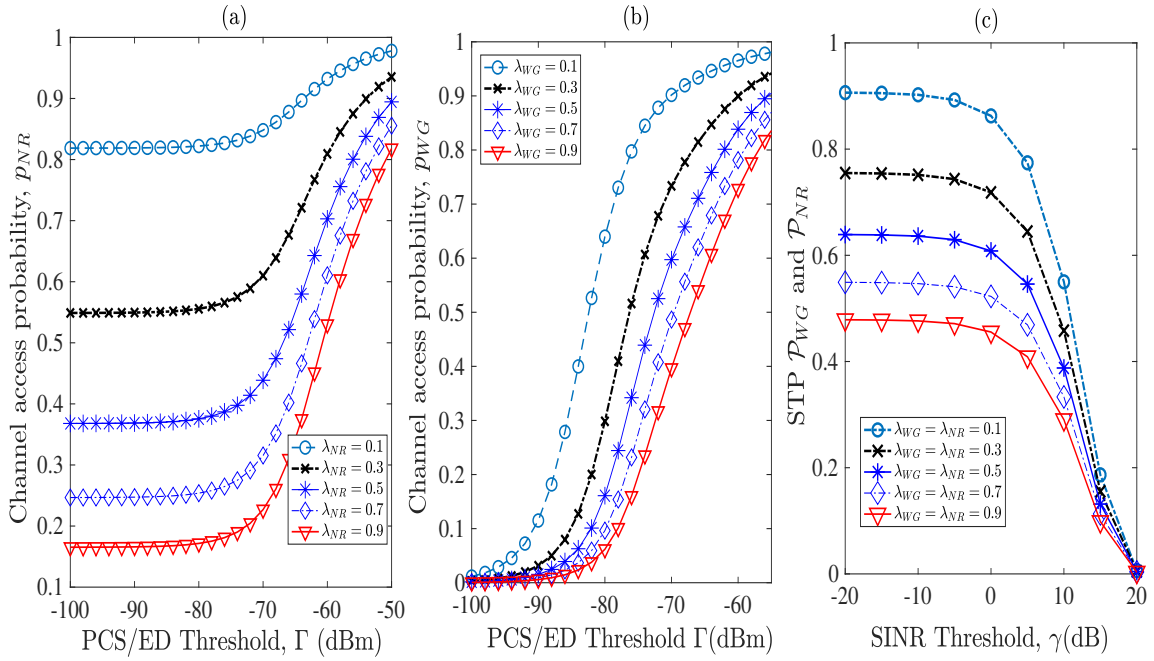

Figure 5.4: (a) CAP versus PCS/ED thresholds for various NR-U node densities λ_{NR} (b) CAP versus PCS/ED thresholds for various WiGig node densities λ_{WG} (c) STP versus SINR threshold for various node densities.

terms of the CAP, allowing more nodes to transmit concurrently reduces the number of successful transmissions in each time-slot. As evident from Fig. 5.6, interference affects STP of nodes in high density networks. While increasing the number of receive antennas from $N = 4$ to $N = 64$ could increase STP gains, high CAP yields more concurrent transmissions, which implies high interference. Under such situation, it is difficult to achieve better STP or the required SINR threshold γ for successful packets decoding. Therefore, we argue that PCS and ED thresholds should be optimized to maximize the interaction between CAP and STP; that is, the trade-off between high CAP and achieving more successful transmission measured in terms of spatial density of throughput (SDT).

Subsequent to the knowledge acquired from the analysis in Figures 5.5 and 5.6, the

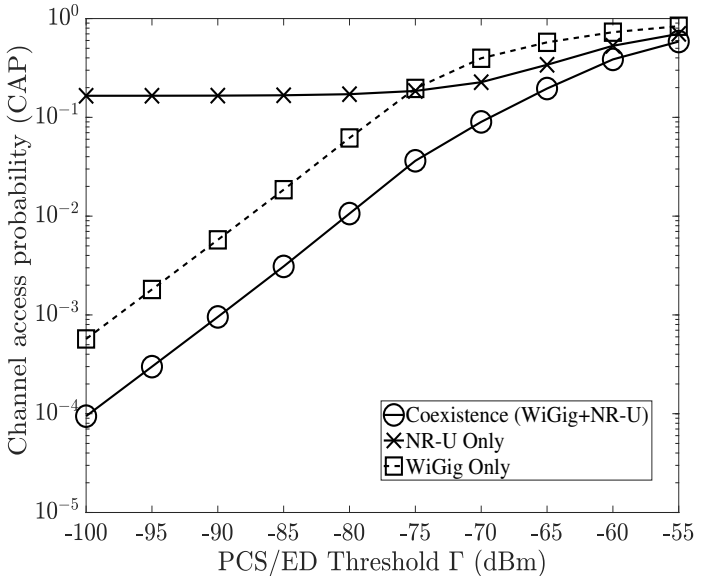

Figure 5.5: Channel access probability versus PCS thresholds for Coexistence, WiGig only and NR-U only cases, $\lambda_N R = \lambda_W G = 0.9$.

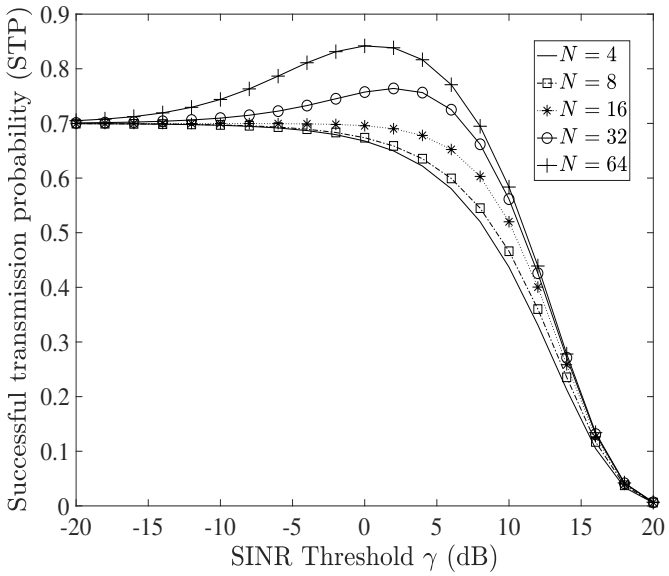

Figure 5.6: Successful transmissions probability versus SINR threshold γ for various receive antenna array sizes N, $M = 64$, transmit beamwidths $\theta_{y_i}^k = \theta_{x_j}^k = 60^\circ$ and receiver beamwidths $\theta_0^k = 60^\circ$ WiGig only and NR-U only cases, $\lambda_N R = \lambda_W G = 0.9$.

PCS and ED thresholds are optimized to account for the tradeoff between CAP and STP, in terms of maximizing the throughput density function that depends on both CAP and STP according to Eqn. (5.22). Figure 5.7 captures the SDT, measuring the proportion of nodes that gained access to the channel (based on CAP) and achieve target SINR (based on STP) at the same time. This is important because not all active transmissions in Fig. (5.3) will be successful; some end up in collisions or are subject to interference that degrades SINRs. At high density of 0.9 and beamwidths of $\theta_{y_i}^k = \theta_{x_j}^k = \theta_0^k = 60°$, the Proposed Method achieves better performance when compared to the Conventional scheme of fixed thresholds. For instance, at 0 dB SINR, the SDT proportion increases from 0.66 under Conventional method to 0.73 under the Proposed method; an additional 7% successful transmissions, which is several Gigabits of throughput in terms of actual transmission rates as shown later.

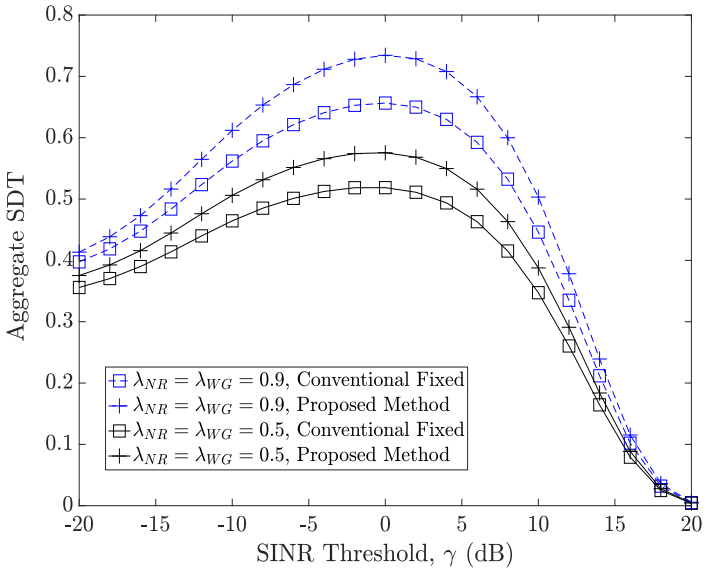

Figure 5.7: Successful transmissions probability versus SINR threshold γ for various receive antenna array sizes N, $M = 64$, transmit beamwidths $\theta_{y_i}^k = \theta_{x_j}^k = 60°$ and receiver beamwidths $\theta_0^k = 60°$ WiGig only and NR-U only cases, $\lambda_N R = \lambda_W G = 0.9$.

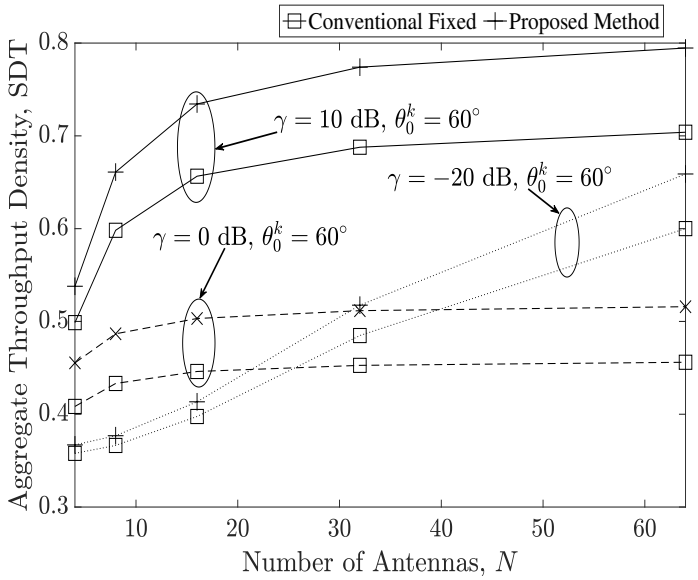

Figure 5.8: Aggregate SDT of coexistence versus SINR threshold for optimized NR-U node density λ^*_{NR} and non-optimized (conventional) λ_{NR} with WiGig densities $\lambda_{WG} = 0.5$ and $\lambda_{WG} = 0.9$.

Fig. 5.8 shows the performance with respect to the numbers of receive antennas $N = 4, 8, 16, 32$ and 64 at the mobile users. Although, increasing the number of receive antenna yields additional gain, throughput converges steadily at high SINR 10 dB and 0 dB to the point where additional receive antenna does not improve the received SINR. At low target SINR $\gamma = -20$ dB, the throughput density increases with increasing number of antennas, N at the receiver. The proposed method yields an improved performance over the conventional scheme. Finally, Figure 5.9 depict performance in terms of throughput per unit area, representing the achievable throughput of each successful transmission in Fig. 5.7 for various target SINR thresholds. At 10 dB SINR in Fig. 5.9, with $N = 32$ antennas at the receiver, the proposed method achieves 10.4% gain in throughput per area over the conventional scheme. These performance gains are spatial averages taken over the entire network.

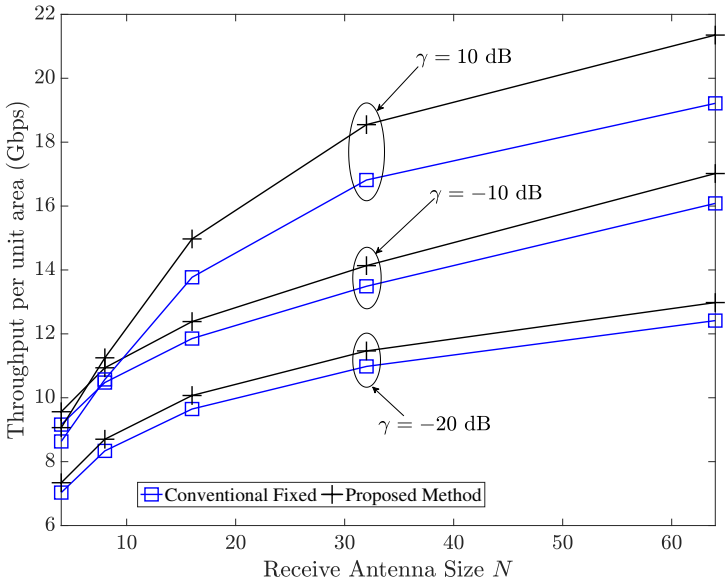

Figure 5.9: Throughput per unit area versus receive antenna size with transmit-receive beamwidths $\theta_{y_i}^k = \theta_{x_j}^k = 60°$ and $\theta_0^k = 120°$, and node density $\lambda_{NR} = \lambda_{WG} = 0.5$, at SINR threshold $\gamma = -20$ dB, $\gamma = -10$ dB and 10 dB.

For a given density λ_{WG}, two cases of selecting the density of NR-U nodes are considered. First, the "Proposed" case where λ_{NR} is defined as the optimized density $\tilde{\lambda}_{NR}$ in Eq. (5.40) of Theorem 5.3. In the "Conventional" case, node density λ_{NR} is not optimized. The "Proposed" and the "Conventional" throughput results are based on simulations averaged over 10^6 realizations of the network, and compared to the upper bound throughput derived in Theorem 5.4 for benchmarking. Given a high density $\lambda_{WG} = 0.9$ of WiGig nodes, Fig. 5.10 compares the throughput obtained from optimizing NR-U node density (Theorem 5.3) to the upper bound (Theorem 5.4) and the *Conventional* scheme of no optimization. At -20 dB SINR, 37.1% gain is observed with the proposed scheme over the conventional method, and the achievable throughput of the proposed densification control asymptotically approaches the upper bound. At high SINR of 10 dB, a gain of 35.2% (≈ 3 Gbps) is obtained when compared

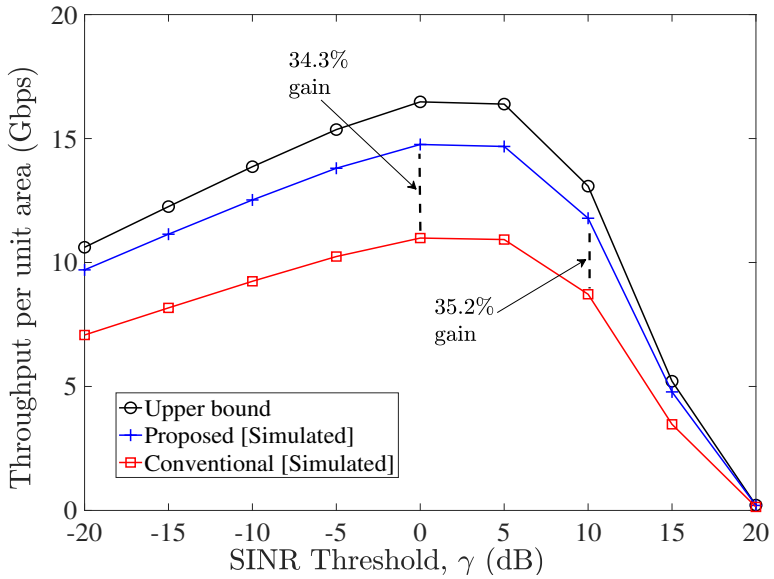

Figure 5.10: Throughput per unit area versus SINR threshold for WiGig node density $\lambda_{WG} = 0.9$, optimized λ^*_{NR} and non-optimized (conventional) $\lambda_{NR} = 0.9$. $M = 64 \times N = 16$.

with the case of no optimization.

5.8 Chapter Summary

The future generations of WLANs will involve deployment of multi-RATs to provide coverage to mobile devices that are capable of operating different access technologies. Although, 5G NR-U/WiGig coexistence will be useful for new applications such as IoT, home/industrial automations and autonomous vehicles. The inability to separate multiple concurrent NR-U and WiGig transmissions is detrimental to performance. Since the PCS and ED thresholds determine the separation of concurrent transmissions in space, closed-form expressions are proposed for selecting PCS and ED threshold in 5G NR-U/WiGig coexistence to improve spatial reuse. This proposed framework is generalizable to other carrier frequencies in the mmWave bands.

In addition, a method is proposed to control node density in high density coexisting network with the objective of maximizing performance. Although, densification provides coverage, optimizing the maximum number of nodes in a coexisting network improves performance. From the simulated scenario, an average performance gain of 36% is achieved at high network density. It is observed that the density of 5G NR-U nodes to coexist with WiGig nodes (incumbents) depends on the density of the incumbents, the mmWave propagation, and the target rates for both NR-U and WiGig nodes. Conclusively, high interference and contention from large number of nodes reduce throughput, and not enough density reduces coverage and aggregate throughput; the proposed optimization finds a good balance for performance gains.

Chapter 6

Joint AP Association and PCS threshold Selection

6.1 Introduction

Thus far, the AP association and the PCS threshold selected problems have been formulated as being decoupled and solved independently in Chapters 3 and 4, respectively. In this chapter, the PCS threshold selection and AP association are jointly considered to further improve performance in high density WLANs. To the best of our knowledge, and judging from the large literature on AP association and PCS threshold selection problems discussed in Chapters 3 and 4, the AP association and PCS threshold selection problems are jointly considered here for the first time, and certainly for the case of full-duplex WLANs with self-interference (SI).

From the existing works discussed in Chapter 3, the closely related works on user-AP association proposed frameworks for joint AP association and spectrum allocation [49,123], joint user-AP association and power allocation [55,124,125], user-AP association and user scheduling [48,50], AP association and load balancing [59,126–128],

and joint AP association and proportional fairness [51, 58]. From Chapter 4, [106] proposes a joint optimization of PCS threshold and transmission rate for wireless Ad Hoc networks. In dense WLANs, transmit power and PCS threshold could be jointly controlled to enhance throughput and fairness [108]. Assuming dense SISO systems, an algorithm is proposed in [13] to select an AP and adjust the PCS threshold. As opposed to the existing schemes [10] and those discussed in Chapters 3 and 4 that decouple the AP association and PCS threshold selection problem, a new framework is proposed in this chapter to jointly consider AP association and PCS threshold selection for future FD WLANs.

In this chapter, the following notation is used. Boldface uppercase letters represent matrices. For instance, matrix $\mathbf{H}$ represents the channel matrix between a user and an AP. Column vectors are denoted as boldface lowercase letters such as $\mathbf{x}$ representing the transmitted symbols. The expected value of any random variable will be denoted as $\mathbb{E}[\cdot]$. The Frobenius norm of a matrix is denoted as $\|\cdot\|^2$. Superscripts $[\cdot]^H$ and $[\cdot]^T$ represent Hermitian (conjugate transpose) and transpose, respectively while $\mathrm{tr}(\cdot)$ is the trace of a matrix. This chapter is organized as follows. The system model under consideration is presented in Section 6.2. Section 6.3 discusses the CSMA/CA protocol and interference model while the performance metric is formulated in Section 6.4. The proposed joint AP association and PCS threshold selection framework is introduced in Section 6.5 while an analysis of SSF association is presented in Section 6.5.5. Section 6.6 contains numerical results and discussions while Section 6.7 concludes this chapter.

6.2 System and Network Model

6.2.1 Network Model

We assume a multi-cell WLAN where the AP in each cell or BSS serves its associated STAs, one at a time in the presence of self-interference and out-of-cell interference. As shown in Figure 6.1, we will assume that each AP initiates FD communication to serve the STA. Due to the unplanned nature of AP deployments in multi-tenant WLANs, we will further assume that locations of APs and STAs follow independent realizations of Poisson point process (PPP). Let $\Phi_a = \{x_1, x_2, \cdots, x_{|\Phi_a|}\} \subset \mathbb{R}^2$ denote the distribution of APs with intensity λ_a. Similar to [85], [86], [87], where random locations of nodes are modeled using PPP, the locations of the STAs follow a homogeneous PPP $\Phi_s = \{y_1, y_2, \cdots, y_{|\Phi_s|}\} \subset \mathbb{R}^2$ with density λ_s. Assuming *bi-directional* FD communication mode (discussed later in Section 6.2.2) in a typical BSS, the received power for a pair of FD transmissions in each direction is:

$$\ell\left(x_i, y_j\right) = P^t \cdot \|x_i - y_j\|^{-\alpha}, \qquad i = 1, \cdots, |\Phi_a|, j = 1, \cdots, |\Phi_s| \tag{6.1}$$

where P^t is the fixed transmit power without power control, α is the path loss exponent, and $\|x_i - y_j\|$ denotes the *Euclidean* distance between the *primary transmitter* at point x and the *receiver* at point y.

6.2.2 Full-Duplex Communication Mode

In wireless LANs, full-duplex nodes operate in two modes, *bidirectional transmission mode* and *cut-through transmission mode* [85], [86]. When full-duplex nodes operate in *bidirectional transmission mode*, an AP-STA pair is able to concurrently transmit

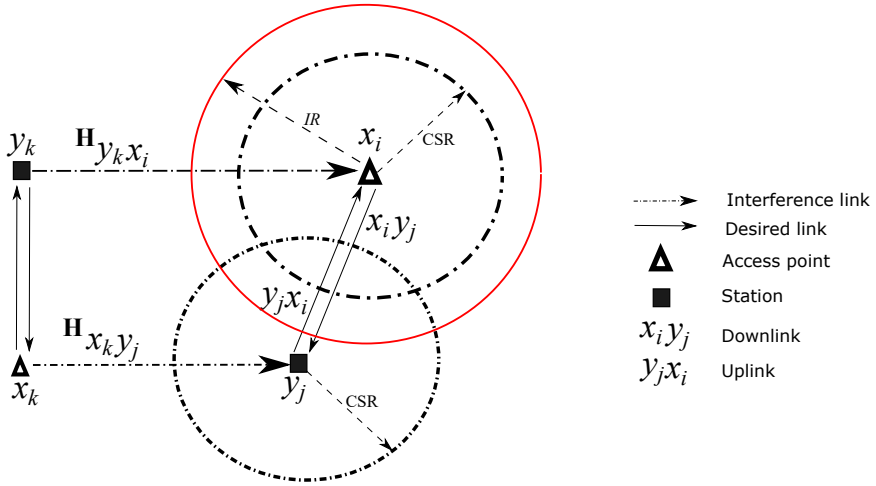

Figure 6.1: Bi-directional FD mode.

to each other while the *cut-through transmission mode* allows an access point (AP) to transmit to two stations (STAs) at the same time; one uplink and one downlink transmission [86]. Herein, we will assume that the full-duplex wireless LAN allows only bidirectional transmission mode, as shown in Figure 6.1, where STA $y_j|j = 1, \cdots, |\Phi_s|$ and AP $x_i|i = 1, \cdots, |\Phi_a|$ transmit concurrently to each other while AP x_i and STA y_j receivers experience interference from STA $y_k|k = 1, \cdots, |\tilde{\Phi}_s|$ and AP $x_k|k = 1, \cdots, |\tilde{\Phi}_a|$, respectively, where $\tilde{\Phi}_s$ and $\tilde{\Phi}_a$ are the set of concurrently active STAs and APs, which are defined later in Section 6.3. This interference model in *bidirectional transmission mode* assumes the presence of SI and out-of-cell interference as discussed later in Section 6.3.

6.2.3 FD-MIMO Channel Model

AP $x_i|i = 1, \cdots, |\Phi_a|$ and STA $y_j|j = 1, \cdots, |\Phi_s|$ are equipped with transceivers having M transmit antennas and N receive antennas. From Fig. 4.6, let $\mathbf{H}_{x_i y_j} \in \mathbb{C}^{M \times N}$ denote the channel of the path from AP x_i to STA y_j and $\mathbf{H}_{y_j x_i} \in \mathbb{C}^{M \times N}$

denote the channel from STA y_j to AP x_i. We assume that both $\mathbf{H}_{x_i y_j} \in \mathbb{C}^{M\times N}$ and $\mathbf{H}_{y_j x_i} \in \mathbb{C}^{M\times N}$ channels are Rayleigh fading with independent and identically distributed (i.i.d) elements with zero mean and unit variance, i.e., $\mathcal{CN}(0,1)$. With imperfect self-interference (SI) cancellation in the system, the SI channel of STA y_j and AP x_i are denoted as $\mathbf{H}_{y_j y_j} \in \mathbb{C}^{M\times N}$ and $\mathbf{H}_{x_i x_i} \in \mathbb{C}^{M\times N}$, respectively. These SI channels are Rician with i.i.d elements with mean μ and standard deviation ψ^2 [129], that is, $\mathbf{H}_{y_j y_j} \in \mathbb{C}^{M\times N} \sim \mathcal{CN}(\mu,\psi^2)$ and $\mathbf{H}_{x_i x_i} \in \mathbb{C}^{M\times N} \sim \mathcal{CN}(\mu,\psi^2)$. The K-factor and the SI attenuation factor Ω [130], μ and ψ^2 of the SI channels are, respectively, [130], [131]:

$$\mu \triangleq \sqrt{\frac{K\Omega}{K+1}} \text{ and } \psi^2 \triangleq \sqrt{\frac{\Omega}{K+1}}. \tag{6.2}$$

The received signal at the desired STA y_j is given as:

$$\mathbf{y}_{y_j} = \ell(x_i, y_j)\cdot \mathbf{H}_{x_i y_j}\mathbf{s}_{x_i} + \sum_{x_k\in\tilde{\Phi}_a, i\neq k} \underbrace{\ell(x_k, y_j)\,\mathbf{H}_{x_k y_j}\mathbf{s}_{x_k}}_{I_o} + \underbrace{\ell(y_j, y_j)\cdot \mathbf{H}_{y_i y_i}\mathbf{s}_{y_i}}_{\text{SI}} + \mathbf{n}_{y_i}, \tag{6.3}$$

where $\ell(x,y)$ is the signal strength of the desired channel defined in Equation (6.1), $\mathbf{s}_{x_i}$ is the desired downlink transmitted symbol from AP x_i to STA y_i, I_o is the out-of-cell interference from other transmitting APs x_k in set $\tilde{\Phi}_a$ of concurrently active transmitters, $\ell(y_j, y_j)$ represents the signal strength of the SI channel and $\mathbf{n}_{y_i}$ is complex additive white Gaussian noise (AWGN) with zero mean and covariance, $\sigma^2\mathbf{I}_N$. The received signal at the desired AP x_i is:

$$\mathbf{y}_{x_i} = \ell(y_j, x_i)\cdot \mathbf{H}_{y_i x_i}\mathbf{s}_{y_i} + \sum_{y_k\in\tilde{\Phi}_s, j\neq k} \underbrace{\ell(y_k, x_i)\,\mathbf{H}_{y_k x_i}\mathbf{s}_{y_k}}_{I_o} + \underbrace{\ell(x_i, x_i)\cdot \mathbf{H}_{x_i x_i}\mathbf{s}_{x_i}}_{\text{SI}} + \mathbf{n}_{x_i}, \tag{6.4}$$

where $\ell(y_j, x_i)$ is the signal strength from STA y_i to AP x_i, $\mathbf{s}_{y_i}$ is the uplink transmitted symbol from STA y_i, I_o is the out-of-cell interference from other transmitting STAs y_k in set $\tilde{\Phi}_s$ of concurrently active transmitters, $\mathbf{H}_{x_i x_i} \in \mathbb{C}^{N \times N}$ is the SI channel of AP x_i and $\mathbf{n}_{x_i} \sim \mathcal{CN}(0, \sigma^2 \mathbf{I}_N)$ is receiver noise at the AP.

6.3 Interference and Contention Model under CSMA/CA Protocol

Under the carrier sense multiple access collision avoidance (CSMA/CA) protocol, each node competes for a transmission opportunity by sensing the channel for an active transmission. If no active transmission is detected during the physical carrier sensing (PCS) process, the node performing the PCS is allowed to transmit if the energy level detected on the channel is below a threshold Γ known as the PCS threshold. The interference distribution on the network depends on the number of concurrent transmitters permitted by the CSMA/CA protocol following a contention period. In other words, a prospective transmitter senses the channel within its carrier sensing range (CSR) $\mathcal{R}$ [1] and proceeds with its transmission if there is no other active transmitter within the CSR; two nodes will transmit concurrently if they are not within the same contention domain or CSR. To model this behavior of the CSMA/CA protocol to determine the set of concurrent transmitters [2], the Matèrn hardcore point process (MHC PP) (a.k.a Matèrn Type II point process) [85], [86], [87], [39], [40] is very useful.

Considering the definition of MHC PP provided in [39], [40], a MHC PP of radius CSR (*see* Fig.4.6) associated with homogeneous PPP Φ is obtained through a non-independent *thinning* of Φ. To perform the *thinning* process, let us assign a uniformly

[1] CSR is the contention domain of each node.

[2] This set determines the amount of interference seen by a desired receiver.

distributed mark $m \sim U[0,1]$ to each point x in Φ. Then point x will be selected if it has the lowest mark among other points within the radius, i.e., $m_x < m_{\bar{x}} \forall \bar{x} \in \Phi \setminus x$. The CSMA/CA permits node x to transmit if the node has the minimum back-off time (or mark m) among other nodes in the contention region or domain CSR and every other node within the contention domain will back-off while node x completes its transmission. Although this model does not account for collisions, the exponential back-off and other delay-induced aspects of CSMA/CA, gives an accurate approximation of a node's transmission probability [39]. In sections that follow, we describe this MHC PP model of the CSMA/CA protocol for HD and FD transmissions.

6.3.1 Half-Duplex (Uplink or Downlink) CSMA/CA

Let $\tilde{\Phi}_s$ denotes the Matèrn thinning of the STAs PPP Φ_s and let $\tilde{\lambda}_s$ denote the intensity of $\tilde{\Phi}_s$. In set terms, $\tilde{\Phi}_s \subset \Phi$ is the set of concurrently transmitting STAs permitted by the CSMA/CA protocol. Using *thinning process* discussed above to obtain $\tilde{\Phi}_s$ and $\tilde{\lambda}_s$, which defines the interference set in Eqn. (6.4), we refer to Fig. 6.1. A desired transmitter y_j forms a circle $b(x_i, \mathcal{R})$ with radius $\mathcal{R}$ as shown in Fig. 6.1 and contends with other transmitters within CSR $\mathcal{R}$. Let us associate a mark $m \sim U[0,1]$ to each contending STA within $\mathcal{R}$ centered at y_j. Transmitter y_i will be retained in $\tilde{\Phi}_s$ if it has the lowest mark, i.e., $m_{y_j} < m_{\bar{y}_j} \forall \bar{y}_j \in \tilde{\Phi}_{\mathcal{R}}^{y_j} \setminus y_j$. In other words, this means that transmitter y_j has the lowest CSMA backoff counter among all the transmitters within its CSR. $\tilde{\Phi}_s$ is the new PPP obtained from *thinning* the parent PPP Φ_s and $\tilde{\Phi}_{\mathcal{R}}^{y_j} \subset \Phi_a$ is the set of transmitters that lie within the contention neighborhood of y_j.

Supposed there are two transmitters y_j and $\tilde{y}_j$ within $\mathcal{R}$, and the PCS threshold

that determines the CSR $\mathcal{R}$ is given as Γ. Then y_j and $\tilde{y}_j$ will transmit concurrently if $\ell\left(y_j, \tilde{y}_j\right) \cdot \left\|\mathbf{H}_{y_j \tilde{y}_j}\right\|^2 < \Gamma$ and $\ell\left(\tilde{y}_j, y_j\right) \cdot \left\|\mathbf{H}_{\tilde{y}_j, y_j}\right\|^2 < \Gamma$. This implies that the energy detected by each node during the carrier sensing is below threshold Γ; i.e., y_j and $\tilde{y}_j$ are each far enough apart to have a successful transmission with their respective receiver APs. Therefore, the *Palm probability of retaining* y_i in $\tilde{\Phi}_s$ [40], that is, the transmission probability that y_j having the lowest backoff time is permitted by the CSMA/CA protocol and is given by

$$p_{y_j} = \int_0^1 \mathbb{P}\left\{ y_j \in \tilde{\Phi}_s \middle| m_{y_j} = t \right\} \mathrm{d}t = \frac{1 - \exp\left(-\lambda_s \Theta_s\right)}{\lambda_s \Theta_s} \tag{6.5}$$

where $\mathbb{P}\{y_j \in \tilde{\Phi}_s | m_{y_j} = t\}$ represents the probability of retaining a mark t (or a backoff time value) as the lowest among other marks, which in terms of signal detection threshold during the PCS process, can be expressed as

$$\mathbb{P}\left\{ y_j \in \tilde{\Phi}_s \middle| m_{y_j} = t \right\} = \mathbb{P}\left\{ y_j \in \tilde{\Phi}_s \middle| m_{y_j} < m_{\bar{y}_j} \forall \bar{y}_j \in \tilde{\Phi}_{\mathcal{R}}^{y_j} \setminus y_j \right\} \tag{6.6}$$

$$= \mathbb{P}\left\{ \ell\left(y_j, \tilde{y}_j\right) \cdot \left\|\mathbf{H}_{y_j \tilde{y}_j}\right\|^2 < \Gamma \right\} \tag{6.7}$$

$$= 1 - \exp\left(-\frac{\Gamma}{\ell\left(y_j, \tilde{y}_j\right)} \right) = 1 - \exp\left(-\Gamma \left\| y_j - \tilde{y}_j \right\|^{\alpha}\right), \tag{6.8}$$

which follows using the exponential property of the Chi-Square distribution with $2N$ degrees of freedom of $\left\|\mathbf{H}_{y_j \tilde{y}_j}\right\|^2 = \mathrm{Tr}\left(\mathbf{H}_{y_j \tilde{y}_j} \mathbf{H}_{y_j \tilde{y}_j}^H\right)$, the channel power between y_j and a contender $\tilde{y}_j$. Given volume b_2 of a unit ball in $\mathbb{R}^2$, $\Theta_s = b_2 \cdot \mathcal{R}^2$ is a volume integral

over polar coordinates and can be written as

$$\Theta_s = 2\pi \int_{\mathbb{R}^+} 1 - \mathbb{P}\left\{ y_j \in \tilde{\Phi}_s \middle| m_{y_j} = t \right\} \cdot \|y_j - \tilde{y}_j\| \ \mathrm{d}\,\|y_j - \tilde{y}_j\| \tag{6.9}$$

$$= 2\pi \int_{\mathbb{R}^+} \exp\left(-\Gamma \|y_j - \tilde{y}_j\|^{\alpha}\right) \cdot \|y_j - \tilde{y}_j\| \ \mathrm{d}\,\|y_j - \tilde{y}_j\| \,. \tag{6.10}$$

Without loss of generality, using [110, Eqn 2.33.16], Eqn. (6.10) is simplified to

$$\Theta_s = \pi \sqrt{\frac{\pi}{\Gamma}} \mathrm{erf}\left(\sqrt{\Gamma} \ell\left(y_j, \tilde{y}_j\right)\right). \tag{6.11}$$

where $\mathrm{erf}(\cdot)$ is the error function and $\ell\left(y_j, \tilde{y}_j\right)$ is defined in Eqn. (6.1) in terms of path loss exponent α.

Hence, applying [40, Eqn. 5.55], the density of the resultant CSMA MHC PP $\tilde{\Phi}_s$ of the concurrently transmitting STAs permitted by the protocol becomes

$$\tilde{\lambda}_s = p_{y_j} \lambda_s = \frac{1 - \exp\left(-\lambda_s \Theta_s\right)}{\Theta_s}. \tag{6.12}$$

Therefore, by substituting Eqn. (6.11) into Eqn. (6.12), given a PCS threshold value Γ and capturing the distance between a desired node y_j and a potential interference source $\tilde{y}_j$, the density of active or concurrently transmitting STAs is expressed as

$$\tilde{\lambda}_s = \frac{1 - \exp\left(-\lambda_s \pi \sqrt{\frac{\pi}{\Gamma}} \mathrm{erf}\left(\sqrt{\Gamma} \ell\left(y_j, \tilde{y}_j\right)\right)\right)}{\pi \sqrt{\frac{\pi}{\Gamma}} \mathrm{erf}\left(\sqrt{\Gamma} \ell\left(y_j, \tilde{y}_j\right)\right)}. \tag{6.13}$$

By applying the same *thinning* process, the PPP of the concurrent APs $\tilde{\Phi}_a$ has the

following density:

$$\tilde{\lambda}_a = p_{x_i}\lambda_a = \frac{1-\exp\left(-\lambda_a\Theta_a\right)}{\Theta_a} = \frac{1-\exp\left(-\lambda_a\pi\sqrt{\frac{\pi}{\Gamma}}\mathrm{erf}\left(\sqrt{\Gamma}\ell\left(x_i,\tilde{x}_i\right)\right)\right)}{\pi\sqrt{\frac{\pi}{\Gamma}}\mathrm{erf}\left(\sqrt{\Gamma}\ell\left(x_i,\tilde{x}_i\right)\right)}. \quad (6.14)$$

Since the goal is to improve the spatial average of performance through user-AP association distribution, the average path loss $\ell\left(y_j,\tilde{y}_j\right)$ and $\ell\left(x_i,\tilde{x}_i\right)$ in Eqns. (6.13) and (6.14), respectively, can be computed using a distance probability distribution. For STAs within the CSR $\mathcal{R}$, the distance $\|y_j-\tilde{y}_j\|$ between STA y_j and its contending neighbor $\tilde{y}_j$ has a probability distribution characterized as

Lemma 6.1. *The Euclidean distance $\|y_j-\tilde{y}_j\|\leq\mathcal{R}$ between STA y_j and the nearest nth STA $\tilde{y}_j$ has a probability distribution given by:*

$$f\left(\|y_j-\tilde{y}_j\|\right) = \frac{\left(2\lambda_s\pi\mathcal{R}^2\right)^n}{\mathcal{R}\beta(n)}e^{-\lambda_s\pi\mathcal{R}^2} \quad (6.15)$$

Proof. Assume that STA y_j is at the origin of a 2-D ball with radius $\mathcal{R}$ to point $\tilde{y}_j$, the rest of the proof follows from [122, Theorem 1]. □

If STA y_j contends with $n=1$ STA $\tilde{y}_j$, the separation distance $\|y_j-\tilde{y}_j\|$ is Rayleigh distributed with expected value

$$\mathbb{E}\left[\|y_j-\tilde{y}_j\|\right] = \frac{1}{\lambda_s\pi}, \quad (6.16)$$

and consequently,

$$\ell\left(y_j,\tilde{y}_j\right) = \left(\frac{1}{\lambda_s\pi}\right)^{-\alpha}. \quad (6.17)$$

Similarly for the contending APs, the average path loss is

$$\ell\left(x_i, \tilde{x}_i\right) = \left(\frac{1}{\lambda_a \pi}\right)^{-\alpha}. \tag{6.18}$$

6.3.2 Full-Duplex (Bidirectional) CSMA/CA

In Section 6.3.1, the CSMA/CA model only considers winning contention for a single node among other nodes within the CSR. For a FD transmission to occur, the two nodes (in this case, one AP and one STA) must be permitted by the CSMA/CA protocol in the same time-slot. That is, a successful FD transmission depends on the probability of STA y_j and AP x_i being permitted concurrently by the CSMA/CA in the same time-slot. It is also assumed that nodes could switch between HD and FD transmissions depending on whether both nodes are granted transmission opportunity at the same time or not; that is, they transmit in FD mode if they both have access to the channel. Otherwise, either of the nodes operate in HD mode.

By the *superposition* principle [40], given the two independent PPPs Φ_s and Φ_a of STAs and APs, respectively, for a FD setting in our network let Φ_{FD} denote the combined PPP of Φ_s and Φ_a. The combined PPP has intensity

$$\lambda_{\text{FD}} = \lambda_s + \lambda_a. \tag{6.19}$$

Therefore, using the same *thinning* process in Section 6.3.1, the probability $p_{x_i y_j}^{FD}$ of retaining both nodes y_j and x_i in Φ_{FD} can be determined. In protocol terms, this probability $p_{x_i y_j}^{FD}$ represents the probability of FD transmission involving AP x_i and STA y_j been granted simultaneous access by the CSMA/CA protocol. Without loss of generality, considering the independence of Φ_s and Φ_a, and their independent *thinning*

processes

$$p_{x_i y_j}^{FD} = \frac{1 - \exp\left(-\lambda_{\mathrm{FD}}\pi\sqrt{\frac{\pi}{\Gamma}}\mathrm{erf}\left(\sqrt{\Gamma}\left(\lambda_{\mathrm{FD}}\pi\right)^{\alpha}\right)\right)}{\lambda_{\mathrm{FD}}\pi\sqrt{\frac{\pi}{\Gamma}}\mathrm{erf}\left(\sqrt{\Gamma}\left(\lambda_{\mathrm{FD}}\pi\right)^{\alpha}\right)}. \tag{6.20}$$

For the FD CSMA network, when a typical AP and its STA jointly win the contention period in the same time slot and activate the FD mode, the density of the FD transmissions in the network is given as

Lemma 6.2. *The density of concurrent FD transmissions in the network is*

$$\tilde{\lambda}_{FD} = p_{x_i y_j}^{FD} \cdot \lambda_{FD} = \frac{1 - \exp\left(-\lambda_{FD}\pi\sqrt{\frac{\pi}{\Gamma}}erf\left(\sqrt{\Gamma}\left(\lambda_{FD}\pi\right)^{\alpha}\right)\right)}{\pi\sqrt{\frac{\pi}{\Gamma}}erf\left(\sqrt{\Gamma}\left(\lambda_{FD}\pi\right)^{\alpha}\right)}. \tag{6.21}$$

Proof. The density of FD transmission pairs is the joint density of active APs with density $\tilde{\lambda}_a$ and the density of active STAs, $\tilde{\lambda}_s$, in Eqs. (6.14) and (6.13), respectively. Therefore, by multiplying the joint density λ_{FD} of the PPPs Φ_s and Φ_a by the probability of FD transmissions in Eqn. (6.20), Eqn. (6.21) is obtained. This yields the proportion $\tilde{\lambda}_{\mathrm{FD}}$ of FD links permitted by CSMA/CA protocol for FD transmissions. □

6.3.3 Signal-to-Interference Plus Noise (SINR) Model

The above CSMA/CA model is a spatial average over all the nodes (STAs or APs) whose spatial distribution is defined by the homogeneous PPPs. Herein, we assume that the PCS threshold Γ is fixed globally on the network; this is the case in currently deployed WLAN systems. From defining the densities $\tilde{\lambda}_s$ (of PPP $\tilde{\Phi}_s$) and $\tilde{\lambda}_a$ (of PPP

$\tilde{\Phi}_a$) of concurrently transmitting STAs and APs, respectively, the received signal-to-interference plus noise (SINR) at receiver y_i from primary transmitter x_i is

$$\mathrm{SINR}_{DL} = \frac{\xi_{x_i y_j} \ell\left(x_i, y_j\right) \cdot |\mathbf{v}_{y_j}^H \mathbf{H}_{x_i y_j} \mathbf{s}_{x_i} \mathbf{w}_{x_i}^H|^2}{\|\mathbf{n}_{y_i}\|^2 + \underbrace{\ell\left(y_j, y_j\right) \cdot |\mathbf{v}_{y_j}^H \mathbf{H}_{y_i y_i} \mathbf{s}_{y_i} \mathbf{w}_{x_i}^H|^2}_{\text{SI}} + \underbrace{\sum_{x_k \in \tilde{\Phi}_a, i \neq k} \ell\left(x_k, y_j\right) |\mathbf{v}_{y_j}^H \mathbf{H}_{x_k y_j} \mathbf{s}_{x_k} \mathbf{w}_{x_i}^H|^2}_{\text{out-of-cell interference}}}, \tag{6.22}$$

where $\mathbf{v}_{y_j}^H$ is the receive combining vector at receiver y_j and $\mathbf{w}_{x_i}^H$ represents the transmit beamforming vector at transmitter x_i, $\xi_{x_i y_j}$ is a binary variable, which indicates that STA y_j is associated with AP x_i, i.e.,

$$\xi_{x_i y_j} = \begin{cases} 1, & \text{if STA } y_j \text{ associates with AP } x_i \\ 0, & \text{otherwise.} \end{cases} \tag{6.23}$$

The SINR at receiver x_i from transmitter y_j is

$$\mathrm{SINR}_{UL} = \frac{\xi_{x_i y_j} \ell\left(y_j, x_i\right) \cdot |\mathbf{v}_{x_i}^H \mathbf{H}_{y_j, x_i} \mathbf{s}_{y_j} \mathbf{w}_{y_j}^H|^2}{\|\mathbf{n}_{x_i}\|^2 + \underbrace{\ell\left(x_i, x_i\right) \cdot |\mathbf{v}_{x_i}^H \mathbf{H}_{x_i x_i} \mathbf{s}_{x_i} \mathbf{w}_{y_j}^H|^2}_{\text{SI}} + \underbrace{\sum_{y_k \in \tilde{\Phi}_s, j \neq k} \ell\left(y_k, x_i\right) |\mathbf{v}_{x_i}^H \mathbf{H}_{y_k x_i} \mathbf{s}_{y_k} \mathbf{w}_{y_j}^H|^2}_{\text{out-of-cell interference}}}, \tag{6.24}$$

where $\mathbf{v}_{x_i}^H$ is the receive combining vector at the receiver x_i and $\mathbf{w}_{y_j}^H$ represents the transmit beamforming vector at the transmitter y_j. These are the SINRs of HD transmissions in both uplink and downlink. The distribution of the desired signal powers $|\mathbf{v}_{y_j}^H \mathbf{H}_{x_i y_j} \mathbf{s}_{x_i} \mathbf{w}_{x_i}^H|^2$ and $|\mathbf{v}_{x_i}^H \mathbf{H}_{y_j, x_i} \mathbf{s}_{y_j} \mathbf{w}_{y_j}^H|^2$ in Eqs. (6.22) and (6.24), respectively, are given by Chi-square distribution with $2M$ DoF. On the other hand, the SI powers $|\mathbf{v}_{y_j}^H \mathbf{H}_{y_i y_i} \mathbf{s}_{y_i} \mathbf{w}_{x_i}^H|^2$ and $|\mathbf{v}_{x_i}^H \mathbf{H}_{x_i x_i} \mathbf{s}_{x_i} \mathbf{w}_{y_j}^H|^2$ are characterized by a Gamma distribution

with shape parameter κ and scale parameter ρ defined as [131, Lemma 1]:

$$f(x) = \frac{x^{\kappa-1}}{\Gamma(\kappa)\rho^{\kappa}} e^{-\frac{x}{\rho}}, \qquad \kappa \triangleq \frac{(\mu^2+\psi^2)^2}{\Xi\mu^4+2\mu^2\psi^2+\psi^4}, \qquad \rho \triangleq \frac{\Xi\mu^4+2\mu^2\psi^2+\psi^4}{\mu^2+\psi^2}, \tag{6.25}$$

where

$$\Xi \triangleq \frac{4MN-(N+1)(M+1)}{(N+1)(M+1)}. \tag{6.26}$$

6.3.4 PCS Threshold Constraint

Consider the system model in Figure 6.1, the dotted circles represent the CSR, which is a guard zone where it is forbidden for two transmitters to transmit concurrently. The CSR determines spatial reuse and it is important to efficiently separate multiple concurrent transmissions in space. From Eqn. (6.1), the CSR depends on the PCS threshold with the following relationship

$$\Gamma = \mathrm{CSR}^{-\alpha}, \tag{6.27}$$

and desirably, the PCS threshold should be chosen to permit simultaneous spatially separated transmissions while keeping UL SINR above a threshold, γ. Similar to [132], assuming wireless links in Figure 6.1 are *homogeneous* with identical interference and noise levels, The CSR can be enlarged to cover the entire potential interference range IR (solid circle in Figure 6.1) as:

$$\mathrm{CSR} \geq \xi_{x_i y_j}\|x_i - y_j\| + IR \tag{6.28}$$

$$\geq \xi_{x_i y_j}\|x_i - y_j\|\left(1 + P^t\gamma^{\frac{1}{\alpha}}\right) \tag{6.29}$$

where IR is defined as a function of the transmission range $\|x_i - y_j\|$ and SINR threshold γ. Consequently, the constraint in Eqn. (6.27) can be written as

$$\Gamma \leq \xi_{x_i y_j} \|x_i - y_j\|^{-\alpha} \frac{1}{\left(1 + P^t \gamma^{\frac{1}{\alpha}}\right)^{\alpha}}. \tag{6.30}$$

6.4 Performance in High Density WLANs

One of the most important performance metrics in future high density WLAN will be the density (or the number) of successful transmissions or spatial density of throughput (SDT). The throughput density is an indicator that represents the network performance per unit area, and is a function of the density of active nodes granted access by the CSMA/CA protocol (discussed in Section 6.3) and the successful transmission probability (STP). STP is the probability that a node achieves a target SINR, which indicates successful signal reception at the receiver [90]. Having derived the densities of active transmissions in both HD and FD cases in Section 6.3, this section introduces the derivation of the STP in Section 6.4.1 followed by the formulation of the SDT in Section 6.4.2. The SDT is a suitable performance metric because it captures the magnitude of interference from simultaneously active transmitters and the number of those transmitters with successful transmissions.

6.4.1 Successful Transmission Probability (STP)

A transmission is successful if the received SINR at the receiver is above a threshold γ. Under the bidirectional FD mode in Section 3.6.1, the AP receiver in the uplink (UL) and the STA receiver in the downlink (DL) experience different interference power levels. This is expected because the number of interference points in the UL

is not usually the same as in the DL, and *channel reciprocity* does not hold. That is, the UL interference depends on the set $\tilde{\Phi}_s$ while the DL interference depends on the set $\tilde{\Phi}_a$ of concurrently transmitting APs. Therefore, the probability of successful transmission of the DL is independent of the probability of successful transmission of the UL. For the UL signal received at the AP, we have

$$\mathbb{P}\left(\mathrm{SINR}_{UL} \geq \gamma\right) = \frac{\xi_{x_i y_j} \ell\left(y_j, x_i\right) \cdot |\mathbf{v}_{x_i}^H \mathbf{H}_{y_j, x_i} \mathbf{s}_{y_j} \mathbf{w}_{y_j}^H|^2}{\left\|\mathbf{n}_{x_i}\right\|^2 + \ell\left(x_i, x_i\right) \cdot |\mathbf{v}_{x_i}^H \mathbf{H}_{x_i x_i} \mathbf{s}_{x_i} \mathbf{w}_{y_j}^H|^2 + \sum\limits_{y_k \in \tilde{\Phi}_s, j \neq k} \ell\left(y_k, x_i\right) |\mathbf{v}_{x_i}^H \mathbf{H}_{y_k x_i} \mathbf{s}_{y_k} \mathbf{w}_{y_j}^H|^2} \geq \gamma, \tag{6.31}$$

while for the DL signal received at the STA

$$\mathbb{P}\left(\mathrm{SINR}_{DL} \geq \gamma\right) = \frac{\xi_{x_i y_j} \ell\left(x_i, y_j\right) |\mathbf{v}_{y_j}^H \mathbf{H}_{x_i y_j} \mathbf{s}_{x_i} \mathbf{w}_{x_i}^H|^2}{\left\|\mathbf{n}_{y_i}\right\|^2 + \ell\left(y_j, y_j\right) |\mathbf{v}_{y_j}^H \mathbf{H}_{y_i y_i} \mathbf{s}_{y_i} \mathbf{w}_{x_i}^H|^2 + \sum\limits_{x_k \in \tilde{\Phi}_a, i \neq k} \ell\left(x_k, y_j\right) |\mathbf{v}_{y_j}^H \mathbf{H}_{x_k y_j} \mathbf{s}_{x_k} \mathbf{w}_{x_i}^H|^2} \geq \gamma, \tag{6.32}$$

given the uniqueness of the interference pattern (due to the independent set of interference sources) and the SI in the UL and the DL, a FD transmission is successful with probability $\mathbb{P}_{FD}$ according to

Lemma 6.3. *The successful transmission probability of a bidirectional FD transmission is*

$$\mathbb{P}_{FD} = \mathbb{P}\left(\text{SINR}_{DL} \geq \gamma\right)\mathbb{P}\left(\text{SINR}_{UL} \geq \gamma\right)$$
$$= \exp\left(-2\frac{\gamma\left\|\mathbf{n}_{x_i}\right\|^2}{\xi_{x_iy_j}\ell\left(y_j,x_i\right)} - \frac{1}{\pi}\left[\ln\left(1+\frac{\gamma\left(\frac{1}{\tilde{\lambda}_s\pi}\right)^{-\alpha}}{\xi_{x_iy_j}\ell\left(y_j,x_i\right)}\right) - \ln\left(1+\frac{\gamma\left(\frac{1}{\tilde{\lambda}_a\pi}\right)^{-\alpha}}{\xi_{x_iy_j}\ell\left(y_j,x_i\right)}\right)\right]\right)$$
$$\exp\left(-2\left(\frac{1}{\tilde{\lambda}_s\pi}+\frac{1}{\tilde{\lambda}_a\pi}\right) + 2\left[\left(\frac{\gamma\left(\frac{1}{\tilde{\lambda}_s\pi}\right)^{1-\alpha}}{\xi_{x_iy_j}\ell\left(y_j,x_i\right)}\right)^2 \arctan\frac{\frac{1}{\tilde{\lambda}_s\pi}}{\left(\frac{\gamma\left(\frac{1}{\tilde{\lambda}_s\pi}\right)^{1-\alpha}}{\xi_{x_iy_j}\ell(y_j,x_i)}\right)^2}\right.\right.$$
$$\left.\left. + \left(\frac{\gamma\left(\frac{1}{\tilde{\lambda}_a\pi}\right)^{1-\alpha}}{\xi_{x_iy_j}\ell\left(y_j,x_i\right)}\right)^2 \arctan\frac{\frac{1}{\tilde{\lambda}_a\pi}}{\left(\frac{\gamma\left(\frac{1}{\tilde{\lambda}_a\pi}\right)^{1-\alpha}}{\xi_{x_iy_j}\ell(y_j,x_i)}\right)^2}\right]\right). \tag{6.33}$$

Proof. The proof follows similar steps as Eqns. (4.7)-(4.11). Since the UL and DL channels are independent, the STP in the UL is also independent of the STP in the DL. Therefore, we proceed by first proving the STP in Eqn. (6.31) for the case of UL transmission. From Eqn. (6.31), let $P^t = 1$, $\Psi_{x_i,x_i} = |\mathbf{v}_{x_i}^H\mathbf{H}_{x_ix_i}\mathbf{s}_{x_i}\mathbf{w}_{y_j}^H|^2$, $\Psi_{y_k,x_i} = |\mathbf{v}_{x_i}^H\mathbf{H}_{y_kx_i}\mathbf{s}_{y_k}\mathbf{w}_{y_j}^H|^2$, $\mathbb{P}\left(\text{SINR}_{UL} \geq \gamma\right)$ is written as:

$$|\mathbf{v}_{x_i}^H\mathbf{H}_{y_j,x_i}\mathbf{s}_{y_j}\mathbf{w}_{y_j}^H|^2 \geq$$
$$\frac{\gamma}{\xi_{x_iy_j}\ell\left(y_j,x_i\right)}\left(\left\|\mathbf{n}_{x_i}\right\|^2 + \ell\left(x_i,x_i\right)\cdot|\mathbf{v}_{x_i}^H\mathbf{H}_{x_ix_i}\mathbf{s}_{x_i}\mathbf{w}_{y_j}^H|^2 + \sum_{y_k\in\tilde{\Phi}_s,j\neq k}\ell\left(y_k,x_i\right)|\mathbf{v}_{x_i}^H\mathbf{H}_{y_kx_i}\mathbf{s}_{y_k}\mathbf{w}_{y_j}^H|^2\right) \tag{6.34}$$

$$\exp\left(-\frac{\gamma\left\|\mathbf{n}_{x_i}\right\|^2}{\xi_{x_iy_j}\ell\left(y_j,x_i\right)}\right)\mathbb{E}\left[\exp\left(-\frac{\gamma\ell\left(x_i,x_i\right)}{\xi_{x_iy_j}\ell\left(y_j,x_i\right)}\Psi_{x_i,x_i}\right)\right]\mathbb{E}\left[\exp\left(-\sum_{y_k\in\tilde{\Phi}_s,j\neq k}\frac{\gamma\ell\left(y_k,x_i\right)}{\xi_{x_iy_j}\ell\left(y_j,x_i\right)}\Psi_{y_k,x_i}\right)\right] \tag{6.35}$$

$$\exp\left(-\frac{\gamma\left\|\mathbf{n}_{x_i}\right\|^2}{\xi_{x_iy_j}\ell\left(y_j,x_i\right)}\right)\exp\left(-\frac{\gamma\ell\left(x_i,x_i\right)}{\xi_{x_iy_j}\ell\left(y_j,x_i\right)}\mathbb{E}\Psi_{x_i,x_i}\right)\exp\left(-\mathbb{E}_{\tilde{\Phi}_s}\left[\sum_{y_k\in\tilde{\Phi}_n,j\neq k}\frac{\gamma\ell\left(y_k,x_i\right)}{\xi_{x_iy_j}\ell\left(y_j,x_i\right)}\mathbb{E}\Psi_{y_k,x_i}\right]\right) \tag{6.36}$$

$$=\exp\left(-\frac{\gamma\left\|\mathbf{n}_{x_i}\right\|^2}{\xi_{x_iy_j}\ell\left(y_j,x_i\right)}\right)\exp\left(-\frac{\gamma\ell\left(x_i,x_i\right)}{\xi_{x_iy_j}\ell\left(y_j,x_i\right)}\kappa\rho\right)\exp\left(-\mathbb{E}_{\tilde{\Phi}_s}\left[\prod_{y_k\in\tilde{\Phi}_s,j\neq k}\frac{1}{1+\frac{\gamma\ell(y_k,x_i)}{\xi_{x_iy_j}\ell(y_j,x_i)}}\right]\right)$$

$$=\exp\left(-\frac{\gamma\left\|\mathbf{n}_{x_i}\right\|^2}{\xi_{x_iy_j}\ell\left(y_j,x_i\right)}\right)\exp\left(-\frac{\gamma\ell\left(x_i,x_i\right)}{\xi_{x_iy_j}\ell\left(y_j,x_i\right)}\kappa\rho\right)\exp\left(-\mathbb{E}_{\tilde{\Phi}_s}\left[\sum_{y_k\in\tilde{\Phi}_s,j\neq k}\ln\left(1+\frac{\gamma\ell\left(y_k,x_i\right)}{\xi_{x_iy_j}\ell\left(y_j,x_i\right)}\right)\right]\right)$$

$$=\exp\left(-\frac{\gamma\left\|\mathbf{n}_{x_i}\right\|^2}{\xi_{x_iy_j}\ell\left(y_j,x_i\right)}\right)\exp\left(-\frac{\gamma\ell\left(x_i,x_i\right)}{\xi_{x_iy_j}\ell\left(y_j,x_i\right)}\kappa\rho\right)\exp\left(-\tilde{\lambda}_s\int_{\mathbb{R}^d}\ln\left(1+\frac{\gamma\|y_k-x_i\|^{-\alpha}}{\xi_{x_iy_j}\ell\left(y_j,x_i\right)}\right)\,\mathrm{d}\|y_k-x_i\|\right)$$

$$=\exp\left(-\frac{\gamma\left\|\mathbf{n}_{x_i}\right\|^2}{\xi_{x_iy_j}\ell\left(y_j,x_i\right)}\right)\exp\left(-\frac{\gamma\ell\left(x_i,x_i\right)}{\xi_{x_iy_j}\ell\left(y_j,x_i\right)}\kappa\rho\right)\exp\left(-\tilde{\lambda}_s\|y_k-x_i\|\ln\left(1+\frac{\gamma\|y_k-x_i\|^{-\alpha}}{\xi_{x_iy_j}\ell\left(y_j,x_i\right)}\right)\right.$$

$$\left.-2\|y_k-x_i\|+2\left(\frac{\gamma\|y_k-x_i\|^{1-\alpha}}{\xi_{x_iy_j}\ell\left(y_j,x_i\right)}\right)^2\arctan\frac{\|y_k-x_i\|}{\left(\frac{\gamma\|y_k-x_i\|^{1-\alpha}}{\xi_{x_iy_j}\ell(y_j,x_i)}\right)^2}\right),$$

where (a) follows from the exponential property of the signal power $|\mathbf{v}_{x_i}^H\mathbf{H}_{y_j,x_i}\mathbf{s}_{y_j}\mathbf{w}_{y_j}^H|^2$, (b) holds by taking the expectation with respect to the SI channel Ψ_{x_i,x_i} and the interference channel Ψ_{y_k,x_i}, (c)-(d) deal with taking the expectation of the interference terms over the PPP $\tilde{\Phi}_n$ of active transmitters, (e) is obtained by applying Campbell's theorem $\mathbb{E}\left[\sum_{x\in\Phi}f\left(x\right)\right]=\lambda\int_{\mathbb{R}^2}f\left(x\right)dx$ [40] and (f) follows from the integral transformation of [110, Eqn. 2.733.1]. The proof of the DL STP $\mathbb{P}\left(\mathrm{SINR}_{DL}\geq\gamma\right)$ follows the same procedures. By combining $\mathbb{P}\left(\mathrm{SINR}_{UL}\geq\gamma\right)$ and $\mathbb{P}\left(\mathrm{SINR}_{DL}\geq\gamma\right)$, Eqn. (6.33) is obtained where it is assumed that the target SINR γ and noise are identical for both UL and DL, causing the SI at both UL and DL to cancel out. □

6.4.2 Spatial Density of Throughput (SDT)

Spatial density of throughput (SDT) measures the average throughput performance per unit area [117], [42]. In other words, it captures the tradeoff between channel access probabilities (CAPs) p_{y_j} and p_{x_i} defined in Eqs. (6.5) and (6.14), respectively, and STP. When more nodes have high CAP to transmit, interference increases and the probability (or STP) of achieving SINR threshold γ decreases. On the other hand, when fewer users transmit concurrently, interference is less of a concern and that implies high SINR. To capture this tradeoff, the SDT for a HD transmission mode in the DL, the throughput per unit area is

$$\Upsilon_{HD}^{DL} = \tilde{\lambda}_a \cdot \log(1+\gamma) \cdot \mathbb{P}\left(\text{SINR}_{DL} \geq \gamma\right) \qquad \text{nats/sec/Hz}, \tag{6.37}$$

where $\tilde{\lambda}_a$ is the density of concurrently transmitting APs according to Equation (6.14), $\mathbb{P}\left(\text{SINR}_{DL} \geq \gamma\right)$ is derived in Lemma 6.3. Similarly, for UL HD transmission, we have

$$\Upsilon_{HD}^{UL} = \tilde{\lambda}_s \cdot \log(1+\gamma) \cdot \mathbb{P}\left(\text{SINR}_{UL} \geq \gamma\right) \qquad \text{nats/sec/Hz}. \tag{6.38}$$

Given the probability of successful transmission $\mathbb{P}_{FD}$ of a FD transmission, the spatial density of network throughput of the FD transmission can be written as

$$\Upsilon_{FD} = \tilde{\lambda}_{FD} \log(1+\gamma) \mathbb{P}_{FD} \qquad \text{nats/sec/Hz}, \tag{6.39}$$

where λ_{FD} is given in Eqn. (6.19).

6.5 Joint User-AP Association and PCS Threshold Framework

In this section, we address the user-AP association problem with the objective of maximizing the throughput per network area given in Eqn. (6.39) for FD networks. The overall goal here is to find both an optimal association and a PCS threshold Γ that maximizes the average throughput in the entire network. Generally, user-AP association is a NP-hard combinatorial problem, herein, we seek a solution via Lagrangian duality theory by relaxing the binary association variable. Once a solution is realized for the user-AP association, the PCS threshold is then optimized. However, the overall joint solution may not be optimal.

6.5.1 Joint User-AP Association and PCS Threshold Optimization (JAPO)

In a FD WLAN, if STA y_j associates with AP x_i, the mean throughput per unit area of the FD transmissions is given by Eqn. (6.39). To improve average performance by optimally selecting an AP, the optimization problem is formulated as follows:

$$\text{maximize} \quad \Upsilon_{FD}, \tag{6.40a}$$

$$\text{subject to} \quad \sum_{x_i \in \Phi_a} \xi_{x_i y_j} = 1. \qquad \forall y_j \in \Phi_n \tag{6.40b}$$

$$\xi_{x_i y_j} \in \{0, 1\} \tag{6.40c}$$

$$\Gamma \leq \xi_{x_i y_j} \|x_i - y_j\|^{-\alpha} \frac{1}{\left(1 + P^t \gamma^{\frac{1}{\alpha}}\right)^{\alpha}} \qquad \forall y_j \in \Phi_a, \forall x_i \in \Phi_n \tag{6.40d}$$

The objective in Eqn. (6.40a) indicates that when an STA y_j associates with AP x_i, the expected rate is Υ_{FD}. The solution to this problem is realizable by finding the optimal association $\xi^*_{x_i y_j}$ and optimal PCS threshold Γ that maximize the spatial

density of FD throughput Υ_{FD}. To obtain a solution that jointly assign STAs to the APs and design the PCS threshold such that the average performance is maximized, the original problem in (6.40) is decomposed into two coupled subproblems addressing the user-AP association and the PCS threshold selection as

$$\max_{\xi_{x_i y_j}} \quad \tilde{\lambda}_{FD} \log(1+\gamma) \mathbb{P}_{FD}, \tag{6.41a}$$

$$\text{subject to} \quad \sum_{x_i \in \Phi_a} \xi_{x_i y_j} = 1. \qquad \forall y_j \in \Phi_n \tag{6.41b}$$

$$\xi_{x_i y_j} \in \{0,1\} \tag{6.41c}$$

$$\Gamma \leq \xi_{x_i y_j} \|x_i - y_j\|^{-\alpha} \frac{1}{\left(1 + P^t \gamma^{\frac{1}{\alpha}}\right)^{\alpha}} \qquad \forall y_j \in \Phi_a, \forall x_i \in \Phi_n \tag{6.41d}$$

and

$$\max_{\Gamma} \quad \tilde{\lambda}_{FD} \log(1+\gamma) \mathbb{P}_{FD}, \tag{6.42a}$$

$$\text{subject to} \quad \Gamma \leq \xi_{x_i y_j} \|x_i - y_j\|^{-\alpha} \frac{1}{\left(1 + P^t \gamma^{\frac{1}{\alpha}}\right)^{\alpha}} \qquad \forall y_j \in \Phi_a, \forall x_i \in \Phi_n, \tag{6.42b}$$

respectively. Subsequently, solutions to the above subproblems are sought for respectively in the following subsections. The overall goal of decomposing the problem into subproblems is to first obtain a solution for the optimal user-AP association under a globally fixed PCS threshold Γ. Then, given the optimal association factor $\xi^*_{x_i y_j}$, the PCS threshold is optimized.

6.5.2 User Association Problem

To find an optimal solution to problem (6.41), we can relax constraint $\xi_{x_i y_j} \in \{0, 1\}$ in (6.41c) from a binary value to take on continuous values between 0 and 1, primarily due to the complexity of solving this type of combinatorial problem. Therefore, by setting $\|x_i - y_j\| = \frac{1}{\lambda_{FD}\pi}$ based on Lemma 6.1, Problem (6.41) is reformulated as

$$\max_{0 \le \xi_{x_i y_j} \le 1} \quad \tilde{\lambda}_{FD} \log(1+\gamma) \mathbb{P}_{FD}, \tag{6.43a}$$

$$\text{subject to} \quad \sum_{x_i \in \Phi_a} \xi_{x_i y_j} = 1. \qquad \forall y_j \in \Phi_n \tag{6.43b}$$

$$\Gamma \left(\frac{1 + P^t \gamma^{\frac{1}{\alpha}}}{\lambda_{FD}\pi} \right)^{\alpha} \le \xi_{x_i y_j} \qquad \forall y_j \in \Phi_a, \forall x_i \in \Phi_n, \tag{6.43c}$$

and using Lagrangian dual technique [59], [49] a solution is feasible. The solution is given by

Theorem 6.1. *The optimal user-AP association policy that maximizes FD throughput* Υ_{FD} *is*

$$\xi^*_{x_i y_j} = \arg\max_{y_j} \left\{ \tilde{\lambda}_{FD} \log(1+\gamma) \mathbb{P}_{FD} + \left(\sum_{x_i \in \Phi_a} \xi_{x_i y_j} - 1 \right) \delta + \left(\Gamma \left(\frac{1 + P^t \gamma^{\frac{1}{\alpha}}}{\lambda_{FD}\pi} \right)^{\alpha} - \xi_{x_i y_j} \right) \eta \right\}. \tag{6.44}$$

Proof. Let δ and η be the Lagrangian multipliers associated with constraints (6.43b)

and (6.43c), respectively, the Lagrangian dual of problem (6.40) is

$$\mathcal{L}\left(\xi_{x_iy_j},\delta,\eta\right)=\tilde{\lambda}_{FD}\log(1+\gamma)\mathbb{P}_{FD}+\left(\sum_{x_i\in\Phi_a}\xi_{x_iy_j}-1\right)\delta+\left(\Gamma\left(\frac{1+P^t\gamma^{\frac{1}{\alpha}}}{\lambda_{FD}\pi}\right)^{\alpha}-\xi_{x_iy_j}\right)\eta, \tag{6.45}$$

and the dual objective becomes

$$g\left(\delta,\eta\right)=\max_{\xi_{x_iy_j}}\mathcal{L}\left(\xi_{x_iy_j},\delta,\eta\right), \tag{6.46}$$

which results to the dual optimization problem

$$\begin{aligned} &\text{minimize} && g\left(\delta,\eta\right)\\ &\text{subject to} && \delta,\eta\geq 0. \end{aligned} \tag{6.47}$$

The user association is obtained by iterating the *necessary conditions* until the rate utility (6.43a) stops improving. The optimal value of δ and η can be obtained via *subgradient method* [49] since the Lagrangian function of the dual problem is non-differentiable. Given a dynamic step size $\phi(k)$, the Lagrangian multipliers are updated as:

$$\delta^{k+1}=\left[\delta^k-\phi(k)\left(\sum_{x_i\in\Phi_a}\delta^{k+1}-1\right)\right]^+, \tag{6.48}$$

and

$$\eta^{k+1}=\left[\eta^k-\phi(k)\left(\Gamma\left(\frac{1+P^k\gamma^{\frac{1}{\alpha}}}{\lambda_{FD}\pi}\right)^{\alpha}-\xi_{x_iy_j}\right)\right]^+, \tag{6.49}$$

the step size $\phi(k)$ is updated at each iteration.

6.5.3 Optimal PCS Threshold Selection

With the AP association solution $\xi^*_{x_i y_j}$ obtained in (6.5.2), the next objective is to solve the PCS threshold selection problem in (6.42). Since $\xi^*_{x_i y_j}$ is obtained, the PCS threshold selection subproblem (6.42) is reformulated as

$$\max_{\Gamma} \quad \tilde{\lambda}_{FD} \log(1+\gamma)\mathbb{P}_{FD}, \tag{6.50a}$$

$$\text{subject to} \quad \Gamma \leq \xi^*_{x_i y_j} \left(\frac{1 + P^t \gamma^{\frac{1}{\alpha}}}{\lambda_{FD}\pi} \right)^{-\alpha} \qquad \forall y_j \in \Phi_a, \forall x_i \in \Phi_n. \tag{6.50b}$$

Let $\Upsilon(\Gamma)$ denote the objective function in (6.50a). Since the density of active FD nodes $\tilde{\lambda}_{FD}$ obtained in **Lemma 6.2** is an increasing function of Γ, we obtain the first-order and the second-order partial derivatives of $\Upsilon(\Gamma)$ with respect to Γ:

$$\frac{\partial \Upsilon(\Gamma)}{\partial \Gamma} = -\frac{\Pi e^{-\pi\lambda_{FD}\sqrt{\pi/\Gamma}\text{erf}\left(\zeta\sqrt{\Gamma}\right)} \left(\frac{\pi^2 \lambda_{FD} \text{erf}\left(\zeta\sqrt{\Gamma}\right)}{2\Gamma^2\sqrt{\frac{\pi}{\Gamma}}} - \frac{\zeta\pi\lambda_{FD} e^{-\zeta^2\Gamma}\sqrt{\frac{\pi}{\Gamma}}}{\sqrt{\pi}\sqrt{\Gamma}} \right)}{\pi\sqrt{\frac{\pi}{\Gamma}}\text{erf}\left(\zeta\sqrt{\Gamma}\right)}$$
$$- \frac{\zeta\Pi e^{-\zeta^2\Gamma}\left(1 - e^{-\pi\lambda_{FD}\sqrt{\pi/\Gamma}\text{erf}\left(\zeta\sqrt{\Gamma}\right)}\right)}{\sqrt{\pi}\pi\sqrt{\Gamma}\sqrt{\frac{\pi}{\Gamma}}\text{erf}\left(\zeta\sqrt{\Gamma}\right)^2} + \frac{\Pi\left(1 - e^{-\pi\lambda_{FD}\sqrt{\pi/\Gamma}\text{erf}\left(\zeta\sqrt{\Gamma}\right)}\right)}{2\Gamma^2\left(\frac{\pi}{\Gamma}\right)^{3/2}\text{erf}\left(\zeta\sqrt{\Gamma}\right)} \tag{6.51}$$

and

$$\frac{\partial^2 \Upsilon(\Gamma)}{\partial \Gamma^2} = -2\Pi \left(\frac{\pi}{2\Gamma^2\left(\frac{\pi}{\Gamma}\right)^{3/2}\text{erf}\left(\zeta\sqrt{\Gamma}\right)} - \frac{\zeta e^{-\zeta^2\Gamma}}{\sqrt{\pi}\sqrt{\Gamma}\sqrt{\frac{\pi}{\Gamma}}\text{erf}\left(\zeta\sqrt{\Gamma}\right)^2} \right)$$
$$e^{-\pi\lambda_{FD}\sqrt{\pi/\Gamma}\text{erf}\left(\zeta\sqrt{\Gamma}\right)} \left(\frac{\pi^2\lambda_{FD}\text{erf}\left(\zeta\sqrt{\Gamma}\right)}{2\Gamma^2\sqrt{\frac{\pi}{\Gamma}}} - \frac{\zeta\pi\lambda_{FD}e^{-\zeta^2\Gamma}\sqrt{\frac{\pi}{\Gamma}}}{\sqrt{\pi}\sqrt{\Gamma}} \right)$$

$$+\Pi\left(-\frac{\zeta\pi e^{-\zeta^2\Gamma}}{\sqrt{\pi}\Gamma^{5/2}\left(\frac{\pi}{\Gamma}\right)^{3/2}\mathrm{erf}\left(\zeta\sqrt{\Gamma}\right)^2}+\frac{\frac{\zeta e^{-\zeta^2\Gamma}}{2\sqrt{\pi}\Gamma^{3/2}\mathrm{erf}\left(\zeta\sqrt{\Gamma}\right)^2}+\frac{2\zeta^2e^{-2\zeta^2\Gamma}}{\pi\Gamma\mathrm{erf}\left(\zeta\sqrt{\Gamma}\right)^3}+\frac{\zeta^3e^{-\zeta^2\Gamma}}{\sqrt{\pi}\sqrt{\Gamma}\mathrm{erf}\left(\zeta\sqrt{\Gamma}\right)^2}}{\sqrt{\frac{\pi}{\Gamma}}}\right.$$
$$\left.+\frac{\frac{3\pi^2}{4\Gamma^4\left(\frac{\pi}{\Gamma}\right)^{5/2}}-\frac{\pi}{\Gamma^3\left(\frac{\pi}{\Gamma}\right)^{3/2}}}{\mathrm{erf}\left(\zeta\sqrt{\Gamma}\right)}\right)\left(1-e^{-\pi\lambda_{FD}\sqrt{\pi/\Gamma}\mathrm{erf}\left(\zeta\sqrt{\Gamma}\right)}\right)$$
$$+\Pi\left(-e^{-\pi\lambda_{FD}\sqrt{\pi/\Gamma}\mathrm{erf}\left(\zeta\sqrt{\Gamma}\right)}\left(\frac{\pi^2\lambda_{FD}\mathrm{erf}\left(\zeta\sqrt{\Gamma}\right)}{2\Gamma^2\sqrt{\frac{\pi}{\Gamma}}}-\frac{\zeta\pi\lambda_{FD}e^{-\zeta^2\Gamma}\sqrt{\frac{\pi}{\Gamma}}}{\sqrt{\pi}\sqrt{\Gamma}}\right)^2-e^{-\pi\lambda_{FD}\sqrt{\pi/\Gamma}\mathrm{erf}\left(\zeta\sqrt{\Gamma}\right)}\right.$$
$$\left.\frac{\left(\frac{\zeta\pi^2\lambda_{FD}e^{-\zeta^2\Gamma}}{\sqrt{\pi}\Gamma^{5/2}\sqrt{\frac{\pi}{\Gamma}}}+\frac{\zeta\pi\lambda_{FD}e^{-\zeta^2\Gamma}\sqrt{\frac{\pi}{\Gamma}}}{2\sqrt{\pi}\Gamma^{3/2}}+\frac{\zeta^3\pi\lambda_{FD}e^{-\zeta^2\Gamma}\sqrt{\frac{\pi}{\Gamma}}}{\sqrt{\pi}\sqrt{\Gamma}}+\frac{\pi^3\lambda_{FD}\mathrm{erf}\left(\zeta\sqrt{\Gamma}\right)}{4\Gamma^4\left(\frac{\pi}{\Gamma}\right)^{3/2}}-\frac{\pi^2\lambda_{FD}\mathrm{erf}\left(\zeta\sqrt{\Gamma}\right)}{\Gamma^3\sqrt{\frac{\pi}{\Gamma}}}\right)}{\sqrt{\frac{\pi}{\Gamma}}\mathrm{erf}\left(\zeta\sqrt{\Gamma}\right)}\right), \tag{6.52}$$

respectively, where $\zeta=(\lambda_{FD}\pi)^{\alpha}$, $\Pi=\log(1+\gamma)\mathbb{P}_{FD}$.

Since the objective function $\Upsilon(\Gamma)$ is twice differentiable and $\frac{\partial^2\Upsilon(\Gamma)}{\partial\Gamma^2}$ is continuous in Γ^*, the solution to the PCS threshold selection objective $\Upsilon(\Gamma)$ is numerically obtained using the truncated Newton's Method (also known as *line search conjugate gradient* method) [133] with incremental Newton search direction [134], [135], which leads to the search iteration policy:

$$\Gamma^{(k+1)}=\Gamma^{(k)}+\epsilon_k\underbrace{\frac{\partial\Upsilon(\Gamma)}{\partial\Gamma}\Big/\left\|\frac{\partial^2\Upsilon(\Gamma)}{\partial\Gamma^2}\right\|}_{\varpi}, \tag{6.53}$$

where ϵ_k is the step length and ϖ is the Newton ascent search direction. The step length is chosen through the well-known *backtracking* approach [134], [133]. To terminate the Newton iteration at an approximate (or inexact) solution [133], we define

the termination criterion

$$\left\| \frac{\partial^2 \Upsilon(\Gamma_k)}{\partial \Gamma_k^2} \varpi + \frac{\partial \Upsilon(\Gamma_k)}{\partial \Gamma_k} \right\| \leq \nu_k \left\| \frac{\partial \Upsilon(\Gamma_k)}{\partial \Gamma_k} \right\|, \tag{6.54}$$

where $\nu_k, 0 \leq \nu_k < 1$ is the *forcing sequence*, which can be chosen to achieve "super-linear" convergence rate as thus [133]:

$$\nu_k = \min \left(0.5, \sqrt{\left\| \frac{\partial \Upsilon(\Gamma_k)}{\partial \Gamma_k} \right\|} \right). \tag{6.55}$$

Finally, since Γ is bounded by $\xi^*_{x_i y_j} \left(\frac{1+P^t \gamma^{\frac{1}{\alpha}}}{\lambda_{FD} \pi} \right)^{-\alpha}$ according to constraint (6.50b), the solution obtained from the above Newton iterative method is verified against constraint (6.50b). Therefore, the PCS threshold selection step is terminated when either termination criterion in Eqn. (6.54) or the following necessary condition is satisfied:

$$\Gamma_k - \xi^*_{x_i y_j} \left(\frac{1 + P^t \gamma^{\frac{1}{\alpha}}}{\lambda_{FD} \pi} \right)^{-\alpha} = 0, \tag{6.56}$$

which is introduced as an additional criterion without loss of generality, to ensure that Γ_k satisfies the constraint. In general, a solution based on Newton's method may not necessarily converge.

6.5.4 Joint User-AP Association and PCS Threshold Selection Algorithm

The proposed algorithm to jointly solve user-AP association and PCS threshold selection is presented in Algorithm 6. First the user-AP association problem is solved iteratively to obtain $\xi^*_{x_i y_j}$, and once $\xi^*_{x_i y_j}$ is determined, the PCS threshold Γ selection problem is solved using the Newton iteration method in Eqn. (6.53).

Remark 6.1. *In wireless networks, user association with the APs takes place before PCS threshold selection. Performing the user-AP association first is to ensure that users are distributed among best serving APs. Then, by further optimizing the PCS threshold, interference from concurrent transmitters is reduced because the PCS threshold determines the degree of spatial reuse and the number of concurrent transmitters per time-slot.*

Algorithm 6: Joint User-AP Association and PCS Threshold Optimization (JAPO)

Initialize Γ, $k = 0$, $\phi(k)$, η, and δ
For fixed Γ, obtain association variable $\xi^*_{x_i y_j}$:
repeat
  Calculate $\xi^*_{x_i y_j}$ using (6.44)
  Update $\delta(k+1)$ using (6.48)
  Update $\eta(k+1)$ using (6.49)
  $k \leftarrow k+1$
until $\xi^*_{x_i y_j}$ *converges*;
For a given $\xi^*_{x_i y_j}$ solve for Γ^*:
Set $k = 0$
Calculate ϖ
repeat
  Compute Eqn. (6.53)
  Update Γ_k and $k = k+1$
until *(6.54) or (6.56) is satisfied*;

6.5.5 User-AP Association under Strongest Signal First (SSF)

Under the SSF association scheme currently used in WLAN [51] , the user selects the AP that offers strongest received signal strength (RSS). Given the path loss model in Eqn. (6.1), it is apparent that selecting an AP based on the SSF (or strongest RSS) means that an STA selects the closest AP. Let each user-AP pair be at distance $\|y_j -$

$x_i\|$ (i.e., distance between one STA and one AP) in the network. From Lemma 6.1, it is established that $\|y_j - x_i\|$ has a probability distribution characterized as

$$f\left(\|y_j - x_i\|\right) = \frac{2\lambda_{\mathrm{FD}}\pi\|y_j - x_i\|^2}{\|y_j - x_i\|} \exp\left(-\lambda_{\mathrm{FD}}\pi\|y_j - x_i\|^2\right) \tag{6.57}$$

where λ_{FD} represents the density of FD points in the network, which is obtained through *superposition* of the two independent node densities λ_s and λ_a in Eqn. (6.19). Since under the SSF association scheme, an STA y_j forms a FD pair with the closest AP x_i, Eqn. (6.57) is the distribution of SSF association in the network.

Consequently, for an STA at point y_j associated with an AP at point x_i according to Lemma 6.1, the spatial average of the FD rate is immediate from

Theorem 6.2. *Achievable spatial mean rate of FD links under SSF association is*

$$\Lambda_{FD}^{ssf} = \int_{\|y_j - x_i\|=0}^{\infty} \Upsilon_{FD}\, \mathrm{d}\|y_j - x_i\| = \tilde{\lambda}_{\mathrm{FD}} \log\left(1+\gamma\right)$$
$$\int_{\|y_j - x_i\|=0}^{\infty} \exp\left(-2\frac{\gamma\left\|\mathbf{n}_{x_i}\right\|^2}{\ell\left(y_j, x_i\right)} - \frac{1}{\pi}\left[\ln\left(1+\frac{\gamma\left(\frac{1}{\tilde{\lambda}_s\pi}\right)^{-\alpha}}{\ell\left(y_j, x_i\right)}\right) - \ln\left(1+\frac{\gamma\left(\frac{1}{\tilde{\lambda}_a\pi}\right)^{-\alpha}}{\ell\left(y_j, x_i\right)}\right)\right]\right)$$
$$\exp\left(-2\left(\frac{1}{\tilde{\lambda}_s\pi} + \frac{1}{\tilde{\lambda}_a\pi}\right) + 2\left[\left(\frac{\gamma\left(\frac{1}{\tilde{\lambda}_s\pi}\right)^{1-\alpha}}{\ell\left(y_j, x_i\right)}\right)^2 \arctan\frac{\frac{1}{\tilde{\lambda}_s\pi}}{\left(\frac{\gamma\left(\frac{1}{\tilde{\lambda}_s\pi}\right)^{1-\alpha}}{\ell(y_j, x_i)}\right)^2}\right.\right.$$
$$\left.\left. + \left(\frac{\gamma\left(\frac{1}{\tilde{\lambda}_a\pi}\right)^{1-\alpha}}{\ell\left(y_j, x_i\right)}\right)^2 \arctan\frac{\frac{1}{\tilde{\lambda}_a\pi}}{\left(\frac{\gamma\left(\frac{1}{\tilde{\lambda}_a\pi}\right)^{1-\alpha}}{\ell(y_j, x_i)}\right)^2}\right]\right) \mathrm{d}\|y_j - x_i\| \tag{6.58}$$

Proof. Setting $\xi_{x_i y_j} = 1$ and substituting Eqn. (6.33) from Lemma 6.3 in Eqn. (6.39) and integrating the resultant mean rate utility function over the SSF association distribution in Eqn. (6.57), Eqn. (6.58) is obtained. □

Remark 6.2. *Eqn. (6.58) is not solved in closed form, it is solved numerically with* $\ell\left(y_j, x_i\right) = \|y_j - x_i\|^{-\alpha}$.

6.6 Numerical Analysis and Observations

6.6.1 System Setup and Parameters

For simulation purposes, we consider a 2D wireless network where AP and STA locations are generated as realizations of independent PPPs denoted as λ_s and λ_a, respectively. Simulation is performed for various STA densities λ_s while the density of APs is fixed at $\lambda_a = 0.3$. The path loss exponent $\alpha = 3.4$, and the noise variance $\sigma^2 = -100$ dBm throughout the simulation. For the fixed PCS threshold case, $\Gamma = -70$ dBm and the CSR is computed based on Γ. The transmit power P_t of APs and the STAs is fixed as 100mW (20 dBm) and APs and STAs are equipped with $M = 4$ and $N = 2$ antennas, respectively. The SINR threshold γ is assumed identical for both the UL and the DL transmissions, and it is chosen for specific WLAN transmission rates (see [51, Table II]). For the FD self-interference (SI) power, the shape parameter κ and the scale parameter ρ are computed according to Eqn. (6.25) with mean μ and variance ψ^2 obtained from Eqn. (6.2) for Ricean K-factor $K = 1$ [129] and SI attenuation factor $\Omega = -80$ dB [131].

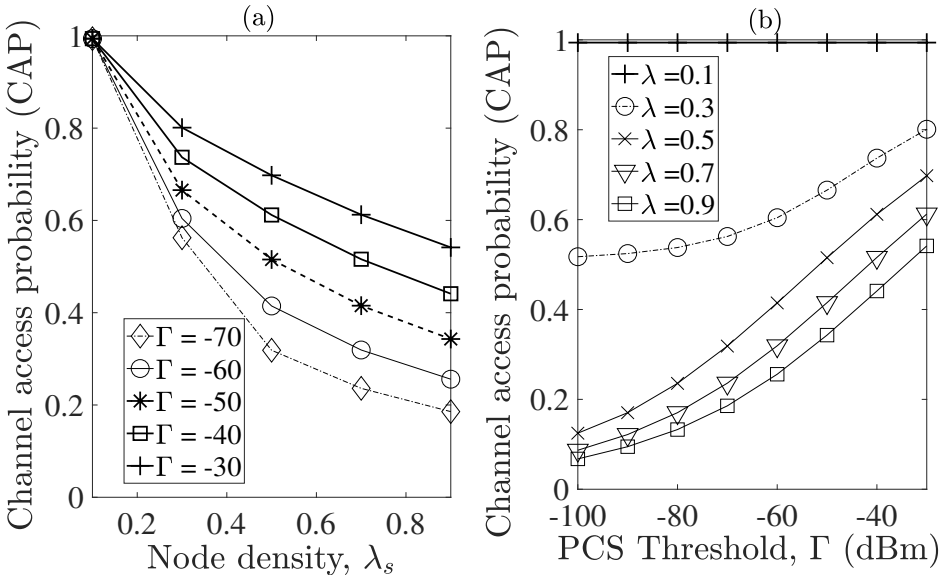

Figure 6.2: Channel access probability, p_{yi} versus (a) Node density λ_s for various PCS threshold Γ and (b) PCS threshold Γ for various node density λ_s.

6.6.2 Validation, Performance Gains and Discussion

For each node density λ_s, the simulation results are averaged over 10^4 network realizations. To evaluate the performance of the proposed joint AP association and PCS threshold selection algorithm (JAPO) in Algorithm 6, its performance is compared to the strongest signal first (SSF) scheme, which is the default AP association scheme in current WLAN systems [51] and analyzed in Theorem 6.2. The second scheme considered is the case of optimizing the AP association according Theorem 6.1 without PCS threshold optimization and it termed "FD Assoc. with fixed PCS threshold (FD Assoc. w/fixed PCS)." The other scenario considered is the half-fuplex case of the proposed JAPO algorithm. The performance metric of interest according to the objective in Eqn. (6.40a), is the spatial average throughput measured in nats/sec/Hz.

Figures 6.2 and 6.3 plot the channel access probability (CAP) defined in Eqn. (6.20)

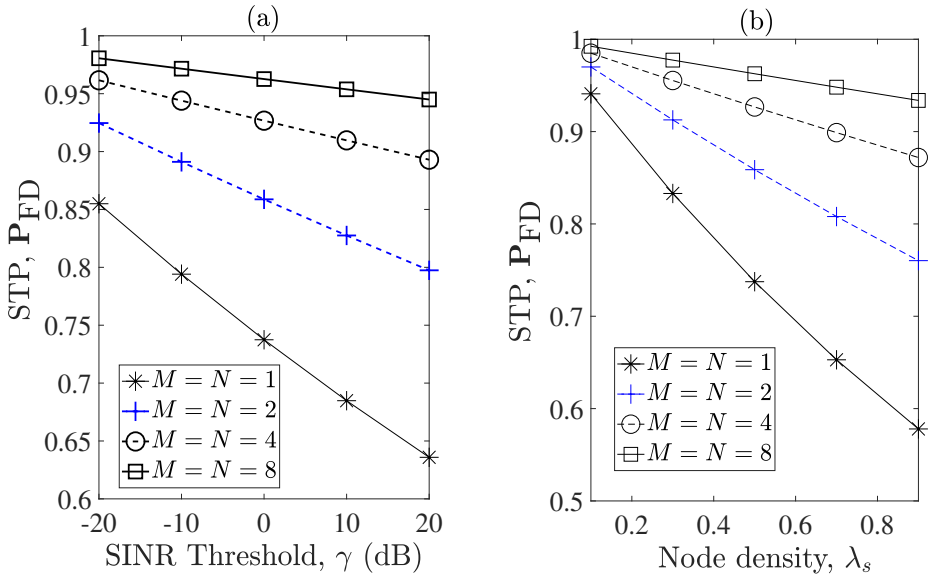

Figure 6.3: Successful transmission probability (STP) versus (a) SINR values at node density $\lambda_s = 0.5$ and $\lambda_a = 0.3$ (b) various node density $\lambda_s = 0.9$, SINR $\gamma = 0$ dB and $\lambda_a = 0.3$.

and the successful transmission probability (STP) in Lemma 6.3, respectively. Figure 6.2(a) depicts the CAP versus node density, increasing node density decreases CAP due to high contention among nodes in high density scenarios. As observed in Fig. 6.2(b), with less sensitive PCS threshold $\Gamma = -30$ dBm, more FD transmissions are likely to occupy the channel as opposed to a more conservative PCS threshold $\Gamma = -70$ dBm, which reduces the number of concurrent FD transmitters per time slot. A less sensitive PCS threshold value increases the number of concurrent transmission and consequently, high interference is inevitable. This behavior of the channel access protocol necessitates the need for efficient PCS threshold selection. Figs. 6.3(a) and (b) depict the STP versus SINR and node density, respectively, for different numbers of antennas. The STP is much lower at the high SINR of 20 dB compared with the low SINR regime (e.g. -20 dB) due to high interference in large-scale networks.

This is compensated for using multi-antenna transmissions. Similarly, at high node density $\lambda = 0.9$, high SINR regime is difficult to achieve due to increased number of concurrent transmissions generating high interference.

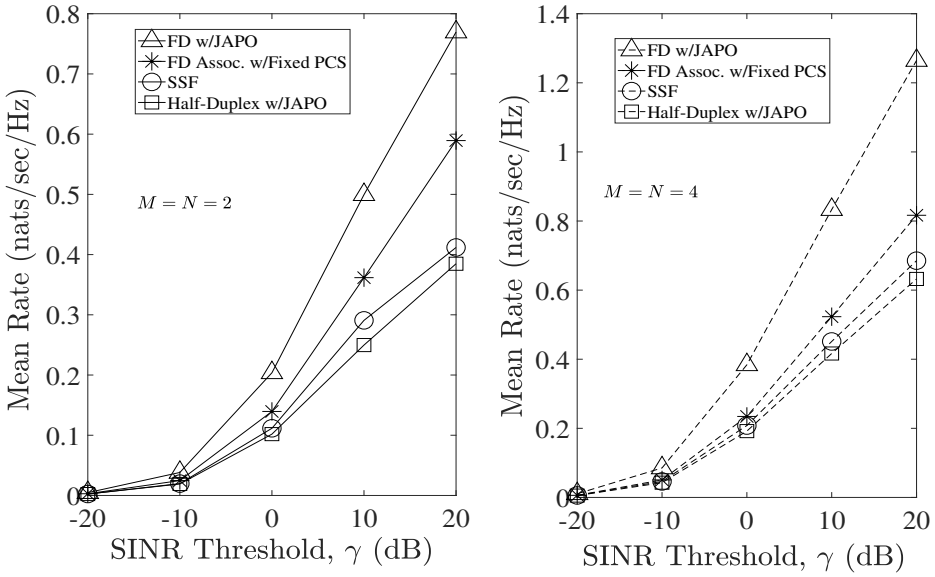

Figure 6.4: Mean rate versus SINR threshold γ for node density $\lambda_s = 0.9$, $\lambda_a = 0.3$, $M = N = 2$ and $M = N = 2$.

In the presence high interference in large-scale networks, Figure 6.4 shows the performance gains at high STA density $\lambda_s = 0.9$ and fixed AP density $\lambda_a = 0.3$. Observing Fig. 6.4 at SINR $\gamma = 0$ dB and $M = N = 2$, the proposed algorithm JAPO doubles the mean rate (0.2 nats/sec/Hz) over the other scheme. The AP association optimization with fixed PCS threshold offers performance gains over the existing SSF scheme, and in all cases, the mean rate is improved with multiple antennas. Fig. 6.5 shows the mean rate versus SINR for $M = N = 8$ and $\lambda_s = 0.9$. Under the FD Association with PCS threshold, the mean rate improves at high SINR and by jointly optimizing the AP association with PCS threshold, a further improvement is achievable. This additional gain is possible by optimizing the PCS threshold to

guarantee that multiple concurrent transmissions are well separated in space to reduce the interference level in the network.

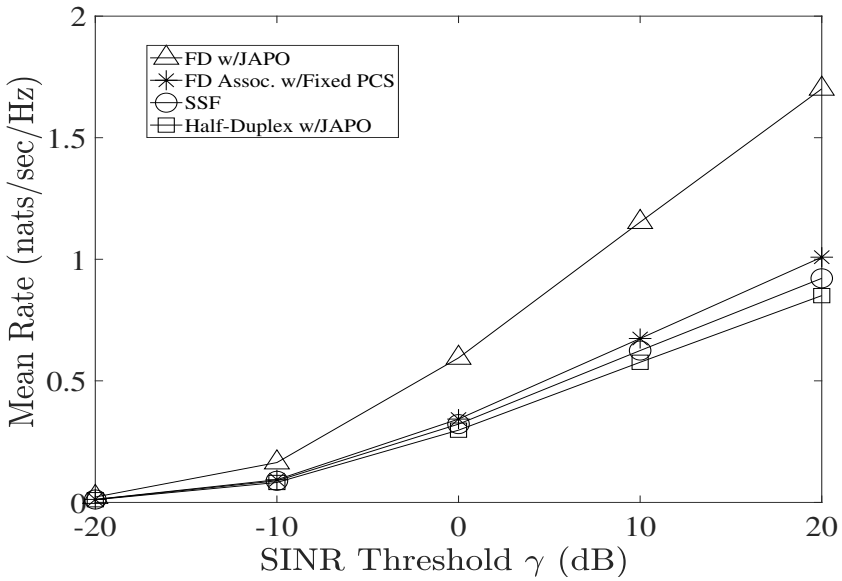

Figure 6.5: Mean rate versus SINR thresholds for $M = N = 8$, node density $\lambda_s = 0.9$ and $\lambda_a = 0.3$.

As shown in Fig. 6.6, increasing to high node density $\lambda_s = 0.9$ is detrimental to the overall system performance because interference and contention tend to be more severe as node density increases. However, the proposed joint AP association and PCS threshold framework offers improvement in performance for mid to high node density over the case of optimizing only AP association and no AP association optimization. Taking a node density $\lambda_s = 0.9$ for example, an additional gain of 0.25 nats/sec/Hz is obtained over the AP association with fixed PCS threshold. Lastly, Fig. 6.7 compares the case of association optimization and the joint association with PCS threshold optimization for various numbers of antennas. Ultimately, with increasing numbers of antennas from $M = N = 1$ to $M = N = 8$, the joint optimization framework furthers improve performance over AP association optimization with fixed PCS threshold

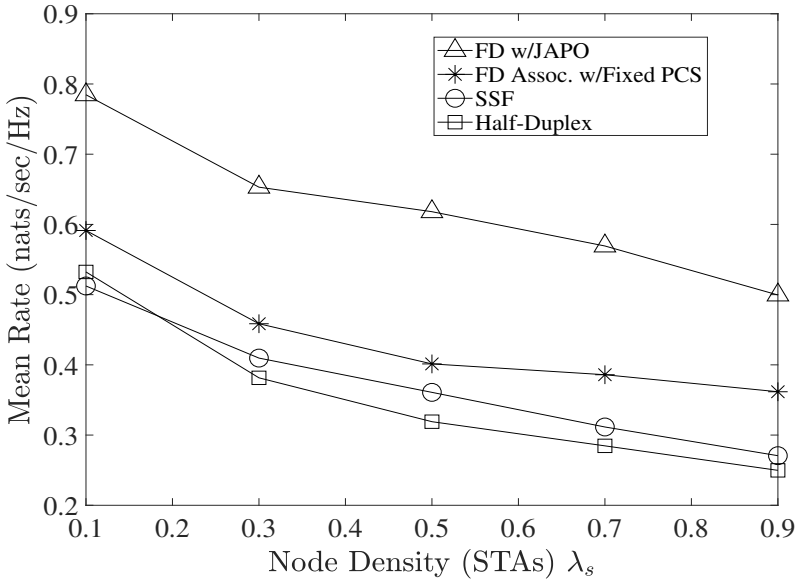

Figure 6.6: Mean rate versus node density λ_s for user association with fixed PCS threshold and joint association and PCS threshold optimization given SINR threshold $\gamma = 10$ dB, $M = 2$ and $\lambda_a = 0.3$.

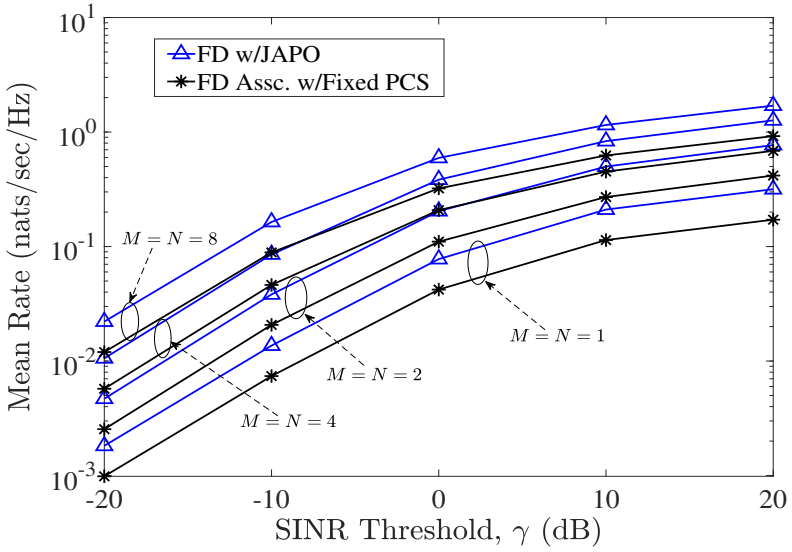

Figure 6.7: Mean rate versus SINR threshold for user association with fixed PCS threshold and joint association and PCS threshold optimization for various antenna sizes, node density $\lambda_s = 0.9$ and $\lambda_a = 0.3$.

$\Gamma = -70$ dBm, which might not efficiently guard against interference and contention.

6.7 Chapter Summary

In this chapter, the impact of jointly optimizing the user-AP association and PCS threshold selection in high density wireless networks is studied. The density of future WLANs will require optimization of the distribution of users among APs to improve performance. The key observation in this contribution is that optimizing AP association yields performance gains for low to high node density in large-scale wireless networks. Adding PCS threshold optimization to the AP association framework further improves performance significantly.

Additional performance gain is achieved because PCS threshold is an important network parameter that determines the degree of spatial reuse among nodes that are being served by the best AP (in terms of achievable rate). On one hand, a user associated with the best serving AP expects better performance. On the other hand, performance loss due to high contention and interference among nodes could be averted via PCS threshold optimization. Hence, the proposed joint AP association and PCS threshold selection framework becomes effective in achieving improved performance in high density networks.

Chapter 7

Conclusions and Future Directions

7.1 Summary and Conclusions

The problem of performance degradation in high density WLANs is addressed through efficient AP association and improved spatial reuse among densely distributed users. In contrast to existing studies [47] - [51], [57, 58], we proposed new AP association schemes that consider traffic saturation, contention and interference in high density WLANs. Two AP association schemes are proposed for performance gains in dense WLANs. The first variant groups users into multi-user (MU) groups based on sum rate determined by a minimum-mean-squared-error (MMSE) criterion. Once users form MU groups, each group is assigned to an AP that offers best throughput utility. The throughput utility maximization problem is solved via two solution techniques, namely, a graph matching polynomial-time algorithm and linear programming (dual ascent). The dual ascent solution is a very good approximation to the optimal graph matching for distributed MU-AP association. From all simulated scenarios under saturation, optimizing the AP association provides a typical improvement of 55.7% in sum throughput over the legacy strongest signal first (SSF) association.

As opposed to several algorithms in the literature that focus primarily on assigning single-user (SU) to an AP, MU group based AP selection not only reduces the complexity of maintaining association for large number of users at each AP, but it also groups users into contention domains and maximizes overall system throughput by accounting for interference. Since the above MU-AP association framework requires channel measurements or CSI, an alternative scheme is proposed to perform user association based on spatial statistical averaging of performance assuming full duplex (FD) capable future WLANs. Performing AP association based on spatial statistics (via stochastic geometry) of the network eliminates the need for channel sounding and global channel knowledge, and potentially improves the average throughput for each user. Without CSI, the stochastic geometry based AP association offers a typical improvement of 166.67% (from 15 nats/sec/Hz to 40 nats/sec/Hz) in sum throughput rate when compared with the legacy SSF scheme.

For spatial reuse of the limited orthogonal channels in WLAN, new schemes are proposed to guide the selection of the PCS threshold parameter that separates multiple concurrent transmissions. In current WLAN systems, the PCS threshold is fixed regardless of the node density, transmit power and other network parameters. Since this important network parameter determines the spatial reuse permitted by the CSMA/CA protocol, which consequently determines the interference level, an efficient framework is proposed for PCS threshold selection. Considering node density, path loss, and the PHY layer characteristics for SISO and MIMO WLANs, closed-form optimum PCS threshold expressions are proposed to improve spatial average of throughput under no power control. The proposed closed-form expressions depend on user density, fixed transmit power, path loss exponent and other

PHY layer parameters, which are usually known a priori. As opposed to existing schemes [11–14], [98–101], [103–105] that require extensive channel measurements to determine a threshold value, the proposed schemes require only network parameters such as node density, transmit power, antenna sizes and path loss. Results from performance benchmarking reveals that the proposed PCS threshold optimization based on a priori information significantly improves throughput at mid to high network densities. For a specific simulated scenario, it achieved 80% gain in throughput over the existing legacy fixed PCS threshold and 29% gain over the existing DSC scheme.

For WLANs where multiple radio access technologies (RATs) coexist, the above rate-maximizing PCS threshold selection is extended to multi-RATs coexistence WLAN. Ultimately, the goal is to optimize both the PCS and energy detection (ED) thresholds require by a node to detect preambles of its kind and other signal types, respectively. It is revealed that the PCS and ED thresholds specific to multi-RAT coexistence WLAN depend on the path loss exponent, node density, transmit power and propagation characteristics. Optimizing the PCS and the ED thresholds based on stochastic geometry of the network yields a typical improvement of 37.1% in spatial average of throughput for coexistence WLANs. In addition to optimizing parameters for spatial reuse and coexistence, a thorough analysis on the optimal throughput-maximizing node density is provided, mainly to obtain an insight on how dense a network needs to be to prevent performance loss arising from high node contention and interference. The main observation from the analysis is that, not enough density reduces coverage and throughput per area, and too high a density increases coverage and interference thereby reducing throughput per area.

Having addressed the AP association and PCS threshold selection problems independently, a new method is proposed to jointly solve the user-AP association and PCS threshold selection problems assuming full duplex (FD) MIMO WLANs in the presence of interference and self-interference of FD transmissions. Performance of this joint optimization reveals that average throughput is improved by 24.4% by AP association optimization alone. By combining AP association with PCS threshold optimization, a total throughput gain of 71.65% is achieved for high node density. This additional 47.25% gain is achievable by further optimizing the PCS threshold subsequent to AP association optimization. Existing methods in the literature either consider AP association or PCS threshold selection, and for the first time, these two WLAN problems are considered jointly for more performance gains. The proposed application frameworks considered are techniques for improving performance of future high density wireless networks in the unlicensed spectrum. They enhance coverage, increase node density and simultaneously improve capacity in the presence of high interference and contention.

7.2 Future Directions

Intelligent use of the limited radio resources will be important in future wireless networks. Some of the possible areas of research towards interference avoidance and/or minimization could include the following:

1. **Multiple User-AP Associations:** The MU-AP association algorithm proposed in thesis assigns each MU group to only one AP. A future work that allows users to have association with multiple APs might be worthwhile to investigate. Performance improvements might be feasible if each user or MU

group is allowed to associate with multiple APs within the same network. That way, a user can seamlessly switch between APs depending on the perceived or anticipated performance.

2. **Learning-based Dynamic AP Selection** Since user-AP association is often formulated as zero-one integer linear program, the primal-dual problems can be solved via *recurrent neural networks*. By casting the user-AP association problem as a discrete-time assignment network, a global solution that converges to an exact solution can be achieved. In future work, the proposed MU-group algorithm in this thesis could be extended to a neural network model and a global solution might be sought.

3. **Learning-based PCS threshold Selection** Similar to developing dynamic AP selection frameworks, the PCS threshold that determines spatial reuse in WLANs could be determined via learning algorithms. For instance, using *Reinforcement learning*, users could aim at maximizing a global utility function by selecting actions based on a predefined PCS threshold value. The PCS threshold could either be estimated per time-slot using some parameters gathered from channel activities and user traffic. Under the *reinforcement learning* framework, the *actions* could include *back-off*, *transmit*, *retransmit* etc. while the *states* could include channel states such as *idle*, *success*, *fail* and *deferring*.

4. **Frame error rate minimization:** Thus far, the main focus is to improve the spatial average of throughput and sum throughput utility. However, the impact of the schemes on frame error rate needs to be investigated. This is important because nodes in WLANs often transmit variable frame sizes depending on

the traffic types (videos, data etc.). The proposed frameworks herein could be extended to cases where the objective is to minimize the frame error rate in the network. Alternatively, we could seek a solution that jointly maximizes user throughput and minimize frame error rate. This may be feasible by formulating a multi-objective optimization problem.

5. **Joint PCS threshold selection and Power control:** All the proposed schemes in thesis assume a fixed transmit power at both the APs and the STAs. An interesting future work will consider power control or at least incorporate a power constraint in the optimization problem formulation. This will capture the additional performance gains possible when users select a PCS threshold value in a power controlled system.

Bibliography

[1] B. O'Hara, *IEEE 802.11 handbook: a designer companion.* IEEE Standards Information Network, IEEE Press, NY, USA,, 2005.

[2] Z. Yangfeng, Q. Zhang, Z. Niu, and J. Zhu, "On optimal QoS-aware physical carrier sensing for IEEE 802.11 based WLANs: theoretical analysis and protocol design," IEEE Trans. on Wireless Comm., vol. 7, no. 4, pp. 1369 – 1378, April 2008.

[3] CISCO. (2017, 06) Cisco visual networking index: Global mobile data traffic forecast update, 2016-2021. Cisco Systems. Accessed: 2019-02-15. [Online]. Available: http://www.cisco.com/c/en/us/solutions/collateral/serviceprovider/visual-networking-index-vni/mobile-white-paper-c11-520862.html.

[4] K. Raul and F. Callorda. (2018, 10) The economic value of WI-FI: A global view (2018 and 2023). Wi-Fi Alliance and Telecom Advisory Services. Accessed: 2019-02-15. [Online]. Available: https://www.wi-fi.org/file/the-economic-value-of-wi-fi-a-global-view-2018-and-2023

[5] M. Steve and W. Webb. (2017, 02) WIFI spectrum needs study. Quotient Associates Ltd. Accessed: 2019-02-15. [Online]. Available: https://www.wi-fi.org/file/wi-fi-spectrum-needs-study

[6] HEWSG. (2016, 05) Status of project IEEE 802.11ax High Efficiency WLAN (HEW). IEEE 802.11 Group. Accessed: 2019-03-01. [Online]. Available: http://www.ieee802.org/11/Reports/tgax_update.htm

[7] IEEE. (2016) Ieee 802.11ad specific requirements part 11: Wireless LAN medium access control. Accessed: 2019-03-01. [Online]. Available: https://standards.ieee.org/standard/802_11ad-2012.html

[8] Y. Ghasempour and et. al., "IEEE 802.11ay: Next-generation 60 GHz communication for 100 GB/S WI-FI," *IEEE Comm. Magazine*, vol. 55, no. 12, pp. 186–192, Oct. 2017.

[9] L. Pengru, D. Liu, and F. Yu, "Joint directional LBT and beam training for channel access in unlicensed 60 GHz mmwave," in *IEEE Globecom Workshops*, Abu Dhabi, UAE, Dec. 2018.

[10] C. Thorpe and L. Murphy, "A survey of adaptive carrier sensing mechanisms for IEEE 802.11 wireless networks," IEEE Commun. Surveys & Tutorials, 3rd Qrt, vol. 16, no. 3, pp. 1266–1293, October 2014.

[11] Z. Z, F. C., P. K., and Z. F., "Promise and perils of dynamic sensitivity control in IEEE 802.1ax WLANs," in *Wireless Comm. Sys. (ISWCS)*, Poznan, Poland, Sept. 2016.

[12] K. P and F. C., "Taming the densification challenge in next generation wireless LANs: an investigation into the use of dynamic sensitivity control," in Proceedings, IEEE 11th WiMob, Abu Dhabi, UAE, Oct. 2015, pp. 860 – 867.

[13] K. Yena, M. Kim, S. Lee, D. Griffith, and N. Golmie, "AP selection algorithm with adaptive for dense wireless networks," in Proceedings, IEEE WCNC, San Francisco, CA, U.S.A, March 2017.

[14] S. Ioannis, M. Filo, S. Vahid, J. Rodriguez, and R. Tafazolli, "Evaluation of the DCS algorithm and the BSS color scheme in dense cellular-like IEEE 802.11ax deployments," in Proceedings, PIMRC, 2016.

[15] K. Shin, I. Park, J. Hong, D. Har, and D. Cho, "Per-node throughput enhancement in WiFi densenets," IEEE Comm. Magazine, vol. 53, no. 1, pp. 118 – 125, January 2015.

[16] Z. Haijun and et. al., "Coexistence of Wi-Fi and heterogeneous small cell networks sharing unlicensed spectrum," *IEEE Comm. Magazine*, vol. 53, no. 3, pp. 158–164, Mar. 2015.

[17] Z. Ran and et. al., "LTE-unlicensed: the future of spectrum aggregate for cellular networks," *IEEE Trans. on Wireless Comm.*, vol. 22, no. 3, pp. 150–159, Jun. 2015.

[18] G. T. 38.300, *TSG RAN: NR overall description. Stage 2.* Release 15, v15.1.0, Apr., 2018.

[19] L. Xi and et. al., "Integrated use of licensed-and unlicensed-band mmwave radio technology in 5G and beyond," *IEEE Access*, vol. 7, pp. 24 376 – 24 391, Feb. 2019.

[20] S. Parkvall and et. al., "NR: the new 5G radio access technology," *IEEE Comm. Standards Magazine*, vol. 1, no. 4, pp. 24–30, Dec. 2017.

[21] J. Jeongho and et. al., "LTE with listen-before-talk in unlicensed spectrum," in *IEEE ICC - Workshop on LTE in Unlicensed Bands: Potential and Challenges*, London, United Kingdom, Jun. 2015.

[22] L. Sandra and L. Giupponi, "Listen before receive for coexistence in unlicensed mmwave bands," in *IEEE WCNC.*, Barcelona, Spain, April 2018.

[23] L. Sandra and et. al., *New radio beam-based access to unlicensed spectrum: design challenges and solutions.* arXiv:1809.10443v1, Sept. 2018.

[24] B. Walke, S. Mangold, and L. Berlemann, *IEEE 802 wireless systems.* John Wiley & Sons West Sussex, England, 2006.

[25] IEEE/ANSI, *Wireless LAN MAC and PHY Layer Specifications.* IEEE Std 802-11-1999,, 1999.

[26] ——, *IEEE Standard for Information Technology- Telecommunications and Information Exchange Between Systems-Local and Metropolitan Area Networks-Specific Requirements-Part 11: Wireless LAN Medium Access Control (MAC) and Physical Layer (PHY) Specifications.* IEEE Std 802-11-1997, pages i 445,, 1997.

[27] B. Giuseppe, "Performance analysis of the IEEE 802.11 distributed coordination function," IEEE Journal on Selected Areas in Communications, vol. 18, no. 3, pp. 535 –547, March 2000.

[28] H. Martin and K. G. Radha, "Interference in large wireless networks," Foundations and Treands in Net., vol. 3, no. 2, pp. 127 – 248, 2008.

[29] F. M. Abinader and et. al., "Enabling the coexistence of LTE and Wi-Fi in unlicensed bands," *Future of WiFi, IEEE Comm. Magazine*, vol. 52, no. 11, pp. 54 – 60, Nov. 2014.

[30] S. C. Yang and P. Winter, "LTE-advanced and IEEE 802.11ac: a new network architecture and opportunity for higher-education institutions," *Int'l Journal of Info.and Learning Tech.*, vol. 32, no. 4, pp. 221 – 234, 2015.

[31] A. Gupta, J. Min, and I. Rhee, "WiFox: Scaling WiFi performance for large audience environment," in *Proc., CoNEXT*, Nice, France, December 2012.

[32] G. T. 38.805, *Study on New Radio access technology: 60 GHz unlicensed spectrum (Release 14)*. V14.0.0, Mar. 2017.

[33] E. E. . 567, *Harmonised European Standard: Multiple-Gigabits/s radio equipment operating in the 60 GHz band: Harmonised standard covering the essential requirements of article 3.2 of Directive 2014/53/EU*. v.2.1.1, July 2017.

[34] O. Bejarano and E. W. Knightly, "IEEE 802.11ac: from channelization to multi-user MIMO," IEEE Comm. Magazine, vol. 35, no. 9, pp. 116 – 126, September 1997.

[35] IEEE. (2016) Status of project IEEE 802.11ah. Accessed: 2017-06-25. [Online]. Available: http://www.ieee802.org/11/Reports/tgah_update.htm

[36] A. Moussa and et. al., "Coexistence of WiFi and LiFi toward 5G: concepts, opportunities, and challenges," *IEEE Comm. Magaz.*, vol. 54, no. 2, pp. 64 – 71, Feb. 2016.

[37] J. G. Andrews and et. al., "What will 5G be?" *IEEE J. Sel. Area in Comm.*, vol. 32, no. 6, pp. 1065 – 1081, Jun. 2014.

[38] O. Galinina and et. al., "5G multi-RAT LTE-WiFi ultra-dense small cells: performance dynamics, architecture, and trends," *IEEE J. Sel. Area in Comm.*, vol. 33, no. 6, pp. 1224 – 1240, Jun. 2015.

[39] H. Q. Nguyen, F. Baccelli, and D. Kofman, "A stochastic geometry analysis of dense IEEE 802.11 networks," in Proceedings, IEEE INFOCOM, Anchorage , Alaska , USA, 2007, pp. 1199 – 1207.

[40] S. N. Chiu, D. Stoyan, W. S. Kendall, and J. Mecke, *Stochastic geometry and its applications, 3rd ed.* John Wiley & Sons Ltd, 2013.

[41] H. S. Ahmed and E. Hossain, "On user association in multi-tier full-duplex cellular networks," IEEE Trans. on Commun., vol. 65, no. 9, pp. 4080 – 4095, Sept. 2017.

[42] N. V. Tien and F. Baccelli, "On the spatial modeling of wireless networks by random packing models," in Proceedings, IEEE INFOCOM, Orlando, FL, U.S.A, Oct. 2012, pp. 28 – 36.

[43] L. Yingzhe, F. Baccelli, J. G. Andrews, T. D. Novlan, and J. C. Zhang, "Modeling and analyzing the coexistence of WI-FI and LTE in unlicensed spectrum," IEEE Trans. Wireless Comm., vol. 15, no. 9, pp. 6310 – 6323, September 2016.

[44] Z. Zhiwei, Y. Li, K. Huang, and C. Liang, "On stochastic geometry modeling of WLAN capacity with dynamic sensitivity control," in Proceedings, Int'l Workshop on Resource Allocation, Cooperation and Competition in Wireless Networks, 2015.

[45] F. Baccelli and B. Blaszczyszyn, "Stochastic geometry and wireless networks, volume i - theory," *NoW Publishers, 1, pp.150, 2009, Foundations and Trends in Networking; 978-1-60198-264-3, 978-1-60198-265-0.*, vol. 3, no. 3-4, pp. 249–449, 2009.

[46] H. Martin, "Mean interference in hard-core wireless networks," *IEEE Communications Letters*, vol. 15, no. 8, pp. 792–794, Aug. 2011.

[47] Y. Xu, G. Anthanasiou, C. Fischione, and L. Tassiulas, "Distributed association control and relaying in millimeter wave wireless networks," in IEEE ICC, Kuala Lumpur, Malaysia, May 2016.

[48] X. Mengjie and T. M. Lok, "Access point selection and auction-based scheduling in uplink MU-MIMO WLANs," in IEEE Proc., ICC, Kuala Lumpur, Malaysia, May 2016.

[49] L. Yinjun, L. Lu, L. Y. Geoffrey, Q. Cui, and W. Han, "Joint user association and spectrum allocation for small cell networks with wireless backhauls," IEEE Wireless Communications Letters, vol. 5, no. 5, pp. 496 – 499, October 2016.

[50] X. Mengjie, T. M. Lok, and Q. Yang, "User association and scheduling based on auction in multi-cell MU-MIMO systems," IEEE Trans. on Wireless Communications, vol. 17, no. 6, pp. 4150 – 4162, June 2018.

[51] W. Li, S. Wang, Y. Ciu, X. Cheng, R. Xin, M. A. Al-Rodaan, and A. Al-Dhelaan, "AP association for proportional fairness in multirate WLANs," IEEE/ACM Trans. on Net., vol. 22, no. 1, pp. 191 – 202, Feb. 2014.

[52] D. Bethanabhotla, O. Y. Bursalioglu, H. Papadopoulos, and G. Caire, "Optimal user-cell association for massive MIMO wireless networks," IEEE Transactions on Wireless Communications, vol. 15, no. 3, pp. 1835 – 1850, March 2016.

[53] L. Yen, J. Li, and C. Lin, "Stability and fairness of AP selection games in IEEE 802.11 access networks," IEEE Trans. on Vehicular Tech., vol. 60, no. 3, pp. 1150 – 1160, March 2011.

[54] O. B. Karimi, J. Liu, and J. Rexford, "Optimal collaborative access point association in wireless networks," in IEEE Infocom, Toronto, Canada, April 2014, pp. 1141 – 1149.

[55] Y. Lin, Y. Wang, C. Li, Y. Huang, and L. Yang, "Joint design of user association and power allocation with proportional fairness in massive MIMO HetNets," IEEE Access, pp. 6560 – 6569, April 2017.

[56] W. Zhang, W. Hardjawana, and B. Vucetic, "User-base stations association in multi-tenant base station networks," in IEEE GLOBECOM, Singapore, Dec. 2017.

[57] Y. Zhang, D. Bethanabhotla, T. Hao, and K. Psounis, "Near-optimal user-cell association schemes for real-world networks," in Information Theory and Applications Workshop (ITA), San Diego, CA, 2015.

[58] G. Athanasiou, P. Weeraddana, C. Fischione, and L. Tassiulas, "Optimizing client association for load balancing and fairness in millimeter-wave wireless networks," IEEE/ACM Trans. on Net., vol. 23, no. 3, pp. 836 – 850, June 2015.

[59] Q. Ye, B. Rong, Y. Chen, M. Al-Shalash, C. Caramanis, and J. G. Andrews, "User association for load balancing in heterogeneous cellular networks," IEEE Trans. on Wireless Communications, vol. 12, no. 6, pp. 2706 – 2716, June 2013.

[60] P. B. Oni and S. D. Blostein, "Decentralized AP selection in large-scale wireless LANs considering multi-AP interference," in Int'l Conference on Computing, Net. and Comm. (ICNC), 2017: Wireless Net. Track, Silicon Valley, CA, USA, Jan. 2017.

[61] B. Akash, S. Michael, S. Ivan, R. Jennifer, and R. Dipankar, "Network cooperation for client-AP association optimization," in Proc., 10th WiOpt, Germany, 2012.

[62] F. Xu, X. Zhu, C. Tan, Q. Li, G. Yan, and J. Wu, "Smartassoc: Decentralized access point selection algorithm to improve throughput," IEEE Trans. on Parallel and Distr. Syst., vol. 24, no. 12, pp. 2482–2491, Dec. 2013.

[63] P. B. Oni and S. D. Blostein, "AP association optimization and CCA threshold adjustment in dense WLANs," in IEEE Globecom 2015 Workshop on Enabling

Technologies in Future Wireless Local Area Network (ETFWLALN), San Diego, CA, USA, Dec. 2015.

[64] K. Megumi, "Throughput analysis of CSMA with imperfect collision detection in full duplex-enabled WLAN," IEEE Wireless Comm. Letters, vol. 6, no. 4, Aug. 2017.

[65] G. A. Mills-Tettey, A. Stentz, and M. B. Dias, *The dynamic Hungarian algorithm for the assignment problem with changing costs.* Robotics Inst., School of Comp. Sci., Carnegie Mellon Univ., PA: CMU-RI-TR-07-27, July 2007.

[66] J. C. Setubal, *Sequential and parallel experimental results with bipartite matching algorithms.* Technical Report IC-96-09: Institute of Computing, State University of Campinas, Brazil, 1996.

[67] T. Nguyen, L. Lanante, H. Ochi, T. Uwai, and Y. Nagao, *Uplink multi-user MAC protocol for 11ax.* IEEE P802.11 Wireless LANs, 2014.

[68] Z. Lan, Y. Li, D. Yang, J. Zhang, R. Luo, P. Loc, and P. Bareber, *Frame exchange control for uplink multi-user transmission.* IEEE P802.11 Wireless LANs, 2014.

[69] I. HEWSG-Group. (2016) Status of project IEEE 802.11ax high efficiency WLAN (HEW). Accessed: 2019-03-29. [Online]. Available: http://www.ieee802.org/11/Reports/tgax_update.htm

[70] J. Hu, B. C. Jung, and D. K. Sung, "A tradeoff between single-user and multi-user MIMO schemes in multi-rate uplink WLANs," IEEE Trans. on Wireless Communications, vol. 10, no. 10, pp. 3332 –3342, October 2011.

[71] J. Kim and C. Aldana, "Efficient feedback of the channel information for closedloop beamforming in WLAN," in *Proceedings, IEEE VTC*, Melbourne, Australia, May 2006.

[72] S. Wu, W. Mao, and X. Wang, "Performance study on a CSMA/CA-based MAC protocol for multi-user MIMO wireless LANs," *IEEE Trans. on Wireless Communications*, vol. 13, no. 6, pp. 3153–3166, June 2014.

[73] D. Ngoc-Dung and Y. Sun, "User-selection algorithms for multiuser precoding," *IEEE Trans. on Vehicular Tech.*, vol. 59, no. 7, pp. 3617–3622, Sept. 2010.

[74] M. Demirbas, A. Arora, V. Mittal, and V. Kulathumani, "A fault-local self-stabilizing clustering service for wireless Ad hoc networks," IEEE Trans. on Parallel Distrib. System, vol. 17, no. 9, pp. 912–922, September 2006.

[75] M. Jeonghoon and J. Walrand, "Fair end-to-end window-based congestion control," IEEE/ACM Trans. on Networking, vol. 8, no. 5, pp. 556 –567, October 2000.

[76] A. M. Emin and T. C. Fogarty, "A distributed evolutionary simulated annealing algorithm for combinatorial optimization problems," Journal of Heuristics, vol. 10, no. 3, pp. 269 – 292, July 2003.

[77] S. Boyd and L. Vandenberghe, *Convex Optimization*. Cambridge University Press, 2004.

[78] R. E. Burkard and E. Cela, *Handbook of combinatorial optimization, supplement volume A. ch. Linear assignment problems and extensions*. Kluwer Academic Publishers, 1999.

[79] J. C. Setubal, *Sequential and parallel experimental results with bipartite matching algorithms*. Technical Report IC-96-09, Institute of Computing, State University of Campinas, Brazil, 1996.

[80] N. J. A. Harvey, R. E. Ladner, L. Lovasz, and T. Tamir, "Semi-matchings for bipartite graphs and load balancing," Journal of Algorithms, Academic Press, vol. 59, no. 1, pp. 53–78, April 2006.

[81] I. H. Toroslu and G. Üçoluk, "Incremental assignment problem," J. of Inform. Sci., vol. 117, no. 6, April 2007.

[82] L. E. L., *Combinatorial Optimization: Networks and Matroids*. Holt, Reinhart and Winston, New York, USA,, 1976.

[83] C. H. Papadimitriou and S. K., *Combinatorial Optimization: Algorithms and Complexity*. Dover Publications, USA, 1998.

[84] W. Yu and R. Lui, "Dual methods for nonconvex spectrum optimization of multicarrier systems," IEEE Trans. Commun., vol. 54, no. 7, pp. 1310 – 1322, July 2006.

[85] W. Shu, V. Vignesh, and X. Zhang, "Exploring full-duplex gains in multi-cell wireless networks: A spatial stochastic framework," in *Proc. IEEE Conf. Comput. Commun. (INFOCOM15)*, Hong Kong, China, April 2015, p. 855863.

[86] ——, "Fundamental analysis of full-duplex gains in wireless networks," *IEEE/ACM Trans. on Networking*, vol. 25, no. 3, pp. 1401–1416, June 2017.

[87] L. Chia-han and M. Haenggi, "Interference and outage in poisson cognitive networks," *IEEE Trans. on Wireless Commun.*, vol. 11, no. 4, pp. 1392–1401, April 2012.

[88] L. Yicheng, W. Bao, W. Yu, and B. Liang, "Optimizing user association and spectrum allocation in HetNets: A utility perspective," *IEEE JSAC*, vol. 33, no. 6, pp. 1025–1039, June 2015.

[89] I. Jamil, L. Cariou, and J. Hélard, "Improving the capacity of future IEEE 802.11 high efficiency WLANs," in Proceedings, IEEE Intl. Conf. on Telecom., Portugal, May 2014, pp. 303 – 307.

[90] Y. Kim, F. Baccelli, and G. de Veciana, "Spatial reuse and fairness of AD hoc networks with channel-aware CSMA protocols," IEEE Trans. on Information Theory, vol. 60, no. 7, pp. 4139 – 4157, July 2014.

[91] L. Yuan, J. Zhang, and Q. Li, "Enhanced listen-before-talk scheme for frequency reuse of licensed-assisted access using LTE," in Proceedings, IEEE PIMRC, Hong Kong, April 2015, pp. 1918 – 1923.

[92] Y. Liou and et. al., "Dynamically tuning aggression levels for capacity-region-aware medium access control in wireless networks," IEEE Trans. Wireless Comm., vol. 13, no. 4, pp. 1766 – 1778, April 2014.

[93] D. Zhaoming, S. Xing, F. Yan, S. Deng, and L. Shen, "Correlation analysis and adaptive carrier sensing adjustment in dense random wireless networks," in Proceedings, 9th Int'l Conf. on Wireless Communications and Signal Processing (WCSP), Nanjing, China, 2017.

[94] K. T. Phan and et. al., "Near-optimal deviation-proof medium access control designs in wireless networks," IEEE/ACM Trans. on Net., vol. 20, no. 5, pp. 1581 – 1594, October 2012.

[95] J. Imad, L. Cariou, and J. Hélard, "Carrier sensing-aware rate control mechanism for future efficient WLANs," in Proceedings, Int'l Conf. and Workshop on the Network of the Future, 2014.

[96] W. Yun, H. Fujita, and D. Kimura, "Throughput-aware dynamic sensitivity control algorithm for next generation WLAN system," in Proceedings, PIRMC, 2017.

[97] K. Parag and F. Cao, "Dynamic sensitivity control to improve spatial reuse in dense wireless LANs," in Proceedings, MSWiM, 2016, pp. 323 – 329.

[98] Y. Seungmin, S. Kim, J. Yi, Y. Son, and S. Choi, "ProCCA: Protective clear channel assessment in IEEE 802.11 WLANs," IEEE Communications Letters, vol. 20, no. 5, pp. 958 – 961, May 2016.

[99] Y. Seungmin and et. al., "FACT: Fine-grained adaptation of carrier sense threshold in IEEE 802.11 WLANs," IEEE Trans. on Vehicular Technology, vol. 66, no. 2, pp. 1886 – 1891, February 2017.

[100] M. S. Afaqui, G. Eduard, L. Elena, and C. Daniel, "Evaluation of dynamic sensitivity control algorithm for IEEE 802.11ax," in Proceedings, IEEE WCNC, 2015, pp. 1060 – 1065.

[101] M. S. Afaqui and et. al., "Dynamic sensitivity control of access points for IEEE 802.11ax," in Proceedings, IEEE ICC, 2016.

[102] C. Chau, W. H. Ivan, S. Zhenhui, and C. L. Soung, "Effective static and adaptive carrier sensing for dense wireless CSMA networks," IEEE Trans. on Mobile Computing, vol. 16, no. 2, pp. 355 – 366, February 2017.

[103] Z. Zhenzhe and F. Cao, "Stochastic analysis of 802.11 uplink with dynamic sensitivity control," in Proceedings, IEEE GLOBECOM, 2016.

[104] D. Zhaoming, S. Xing, F. Yan, Z. Li, and L. Shen, "Impact of adaptive carrier-sensing range on the performance of dense wireless networks," in Proceedings, 9th Int'l Conf. on Wireless Communications and Signal Processing (WCSP), Nanjing, China, 2017.

[105] A. Adnan and P. Kulkarni, "On performance evaluation of dynamic sensitivity control techniques in next-generation WLANS," IEEE Systems Journal, vol. PP, no. 99, 2018.

[106] Z. Yongping, B. Li, Z. Yan, and X. Zuo, "Joint optimization of carrier sensing threshold and transmission rate in wireless AD hoc networks," in Proceedings, IEEE QSHINE, 2015, pp. 210 – 215.

[107] K. Park and et. al., "Optimal physical carrier sensing in wireless networks," Ad Hoc Networks, vol. 9, no. 1, pp. 16 – 27, January 2011.

[108] R. Irda, T. Kawasaki, T. Nishiue, Y. Takaki, C. Ohta, and H. Tamaki, "Control of transmission power and carrier sense threshold to enhance throughput and fairness for dense WLANs," in Proceedings, 30th ICOIN, 2016, pp. 51 – 56.

[109] S. Da-Shan, G. J. Foschini, M. J. Gans, and J. M. Kahn, "Fading correlation and its effect on the capacity of multielement antenna systems," IEEE Trans. on Communications, vol. 48, no. 3, pp. 502 – 513, March 2000.

[110] I. S. Gradshteyn and I. M. Ryzhik, *Table of Integrals, Series and Products, 7th Edition.* Elsevier Academic Press: ISBN-13: 978-0-12-373637-6, 2007.

[111] R. Corless and et. al., "On the Lambert W function." *Advances in Computational Mathematics*, vol. 5, pp. 329 – 359, 1996.

[112] G. Smith. (2013, November) Dynamic sensitivity control v2: Dsp group, california, tech. report. Accessed: 2018-11-05. [Online]. Available: https://mentor.ieee.org/802.11/dcn/13/11-13-1012-04-0wng-dynamic-sensitivity-control.pptx

[113] W. Yu and R. Lui, "Dual methods for nonconvex spectrum optimization of multicarrier systems," *IEEE Trans. on Communications*, vol. 54, no. 7, pp. 1310–1322, Jul. 2006.

[114] P. Zhouyue and F. Khan, "An introduction to millimeter-wave mobile broadband systems," *IEEE Comm. Mag.*, vol. 49, no. 6, pp. 101–107, June 2011.

[115] B. Naga and et. al., "Network densification: The dominant theme for wireless evolution into 5G," *IEEE Commun. Magazine*, vol. 52, no. 2, pp. 82 – 89, Feb. 2014.

[116] C. Subramanya and et. al., "5G multi-RAT multi-connectivity architecture," in *IEEE ICC Workshops: W01-Third Workshop on 5G Architecture (5GArch)*, Kuala Lumpur, Malaysia, May 2016.

[117] L. Yingzhe and et. al., "Modeling and analyzing the coexistence of Wi-Fi and LTE in unlicensed spectrum," *IEEE Trans. on Wireless Comm.*, vol. 15, no. 9, pp. 6310 – 6323, Sept. 2016.

[118] C. Bolin and et. al., "Coexistence of LTE-LAA and Wi-Fi on 5 GHz with corresponding deployment scenarios: A survey," *IEEE Communications Surveys & Tutorials*, vol. 19, no. 1, pp. 7–32, July 2016.

[119] L. Jiandong and et. al., "Share in the commons: Coexistence between LTE unlicensed and WI-FI," *IEEE Trans. Wireless Comm.*, vol. 23, no. 6, pp. 16 – 23, Dec 2016.

[120] J. G. Andrews and et. al., "Modeling and analyzing millimeter wave cellular systems," *IEEE Trans. Comm.*, vol. 65, no. 1, pp. 403–430, Jan. 2017.

[121] W. E. W. (2019) Erf: From mathworld: A wolfram web resource. Accessed: 2019-04-29. [Online]. Available: http://mathworld.wolfram.com/Erf.html

[122] H. Martin, "On distances in uniformly random networks," *IEEE Trans. on Information Theory*, vol. 51, no. 10, pp. 3584 – 3586, Oct. 2005.

[123] L. Xiaofeng, Q. Ni, W. Li, and H. Zhang, "Dynamic user grouping and joint resource allocation with multi-cell cooperation for uplink virtual MIMO systems," IEEE Trans. on Wireless Comm., vol. 16, no. 6, pp. 3854 – 3869, June 2017.

[124] C. V. Trinh, E. Bjornson, and E. G. Larsson, "Joint power allocation and user association optimization for massive MIMO systems," IEEE Trans. on Wireless Comm., vol. 15, no. 9, pp. 6384 – 6399, September 2016.

[125] Z. Haijun, S. Huang, C. Jiang, K. Long, V. C. M. Leung, and H. V. Poor, "Energy efficient user association and power allocation in millimeter-wave-based ultra dense networks with energy harvesting base stations," IEEE J. Selected Areas in Communications, vol. 35, no. 9, pp. 1936 – 1947, September 2017.

[126] Y. Zhaohui, J. S. W. Xu, H. Xu, and M. Chen, "Association and load optimization with user priorities in load-coupled heterogeneous networks," IEEE Trans. on Wireless Comm., vol. 17, no. 1, pp. 324 – 338, January 2018.

[127] Y. Lei and D. Yuan, "Load optimization with user association in cooperative and load-coupled LTE networks," IEEE Trans. on Wireless Comm., vol. 16, no. 5, pp. 3218 – 3231, May 2017.

[128] D. H. Made, W. S. Jeon, and D. G. Jeong, "A joint user association and load balancing scheme for wireless LANs supporting multicast transmission," in Proceedings of the 31st Annual ACM Symposium on Applied Computing, Pisa, Italy, April 2016.

[129] M. Duarte, C. Dick, and A. Sabharwal, "Experiment-driven characterization of full-duplex wireless systems," *IEEE Trans. on Wireless Communications*, vol. 11, no. 12, pp. 4296–4307, Dec. 2012.

[130] C. Tepedelenlioglu, A. Abdi, and G. B. Giannakis, "The Ricean K-factor: Estimation and performance analysis," *IEEE Trans. on Wireless Comm.*, vol. 2, no. 4, pp. 799–810, July 2003.

[131] A. Italo and M. Kountouris, "Full-duplex MIMO small-cell networks: Performance analysis," in *Proc., 2015 IEEE Global Communications Conference (GLOBECOM)*, San Diego, U.S.A, Dec. 2015.

[132] J. Zhu, X. Guo, L. L. Yang, W. S. Conner, S. Roy, and M. M. Hazra, "Adapting physical carrier sensing to maximize spatial reuse in 802.11 mesh networks," *Wireless Commun. and Mobile Computing - Special Issue: Emerging WLAN Application and Technologies archive*, vol. 4, no. 8, pp. 933 – 946, Dec. 2004.

[133] J. Nocedal and S. Wright, *Numerical Optimization, 2nd ed.* Springer, New York, NY, U.S.A, 2006.

[134] L. Yan and et. al., "Joint design of user association and power allocation with proportional fairness in massive MIMO HetNets," *IEEE Access*, vol. 5, no. 12, pp. 6560 – 6569, April 2017.

[135] K. Shen and W. Yu, "Distributed pricing-based user association for downlink heterogeneous cellular networks," *IEEE J. Selected Areas in Comm.*, vol. 32, no. 6, pp. 1100 – 1113, June 2014.

Appendix A

Appendix to Chapter 3

A.1 Proof of Equation 3.37

$$\mathbb{P}\left(\frac{h_{x_i y_i} P_t \|x_i - y_i\|^{-\alpha}}{\sigma^2 + \sum\limits_{x_j \in \tilde{\Phi}_a, i \neq j} h_{x_j x_i} \cdot P_t \cdot \|x_j - x_i\|^{-\alpha}} > \gamma_{x_i - y_i}\right) \tag{A.1}$$

$$= \mathbb{P}\left(h_{x_i y_i} > \gamma_{x_i - y_i}\left(\sigma^2 + \sum_{x_j \in \tilde{\Phi}_a, i \neq j} h_{x_j x_i} \cdot P_t \cdot \|x_j - x_i\|^{-\alpha}\right) \cdot P_t^{-1} \|x_i - y_i\|^{\alpha}\right)$$

since $h_{x_i y_i}$ is an exponential random variable of the channel, we have

$$= \mathbb{E}\left[\exp\left(-\gamma_{x_i - y_i} \sigma^2 \|x_i - y_i\|^{\alpha} P_t^{-1}\right)\right.$$
$$\left.\exp\left(\gamma_{x_i - y_i} \|x_i - y_i\|^{\alpha} P_t^{-1} \sum_{x_j \in \tilde{\Phi}_a, i \neq j} h_{x_j x_i} P_t \|x_j - x_i\|^{-\alpha}\right)\right], \tag{A.2}$$

clearly, the first exponential term is a function of all known parameters, therefore, (A.2) can be written as an expectation w.r.t the interference term. That is, taking expectation over all the interference sources in $\tilde{\Phi}_a$ and the channel gains $h_{x_j x_i}$ of the

interference channels as follows:

$$= \exp\left(-\gamma_{x_i-y_i}\sigma^2\|x_i-y_i\|^{\alpha}P_t^{-1}\right)$$
$$\mathbb{E}_{\tilde{\Phi}_a,h_{x_jx_i}}\left[\exp\left(\gamma_{x_i-y_i}\|x_i-y_i\|^{\alpha}P_t^{-1}\sum_{x_j\in\tilde{\Phi}_a,i\neq j}\frac{h_{x_jx_i}\cdot P_t}{\|x_j-x_i\|^{\alpha}}\right)\right] \tag{A.3}$$

using the following *probability generating function* of a point process Φ ([40, Eqn 4.54 p. 125]):

$$G(v)=\mathbb{E}\left(v(x_1),v(x_2),\dots\right)=\mathbb{E}\left(\prod_{x\in\Phi}v(x)\right),$$

Equation (A.3) can be written as:

$$\Lambda\cdot\mathbb{E}_{\tilde{\Phi}_a}\left[\prod_{x_j\in\tilde{\Phi}_a,i\neq j}\mathbb{E}_{h_{x_jx_i}}\left[\exp\left(\gamma_{x_i-y_i}\|x_i-y_i\|^{\alpha}\frac{h_{x_jx_i}}{\|x_j-x_i\|^{\alpha}}\right)\right]\right], \tag{A.4}$$

where $\Lambda=\exp\left(-\gamma_{x_i-y_i}\sigma^2\|x_i-y_i\|^{\alpha}P_t^{-1}\right)$ and by taking the expectation w.r.t the channel gains $h_{x_jx_i}$, i.e., $\mathbb{E}_{h_{x_jx_i}}[\cdot]$, Eqn. (A.4) becomes:

$$\Lambda\cdot\mathbb{E}_{\tilde{\Phi}_a}\left[\prod_{x_j\in\tilde{\Phi}_a,i\neq j}\frac{1}{1+\gamma_{x_i-y_i}\left(\frac{\|x_i-y_i\|}{\|x_j-x_i\|}\right)^{\alpha}}\right]$$
$$=\Lambda\cdot\mathbb{E}_{\tilde{\Phi}_a}\left[\exp\left(-\sum_{x_j\in\tilde{\Phi}_a,i\neq j}\ln\left(1+\gamma_{x_i-y_i}\left(\frac{\|x_i-y_i\|}{\|x_j-x_i\|}\right)^{\alpha}\right)\right)\right] \tag{A.5}$$

and by Jensen's inequality, $\left(\mathbb{E}\left[g(x)\right]\geq g\left[\mathbb{E}(x)\right]\right)$, Eqn. (A.5) is equivalent to:

$$\Lambda\cdot\exp\left(\mathbb{E}_{\tilde{\Phi}_a}\left[-\sum_{x_j\in\tilde{\Phi}_a,i\neq j}\ln\left(1+\gamma_{x_i-y_i}\left(\frac{\|x_i-y_i\|}{\|x_j-x_i\|}\right)^{\alpha}\right)\right]\right), \tag{A.6}$$

with the aide of Campbell's theorem, $\mathbb{E}\left(\sum_{x\in\Phi} f(x)\right) = \lambda \int_{\mathbb{R}^2} f(x)\mathrm{d}x$, (Eqn. 4.10 p. 114 in [40]), Eqn. (A.6) can be approximated as:

$$\Lambda \cdot \exp\left(\tilde{\lambda}_a^{-1} \int_{\mathbb{R}^2} \ln\left(1 + \gamma_{x_i - y_i}\left(\frac{\|x_i - y_i\|}{\|x_j - x_i\|}\right)^{\alpha}\right)\right), \tag{A.7}$$

which proves Equation (3.37). □

A.2 Proof of Proposition 3.1

Given the PPP Φ_a of APs with density λ_a, for each point $x_i \in \Phi_a$ is associated a mark $\eta \sim U[0,1]$ independent of any other point. A MHC point process Φ_{as} (containing all points of STA-AP associations) is generated by a *dependent thinning* of PPP Φ_a. A point x_i is retained in the MHC thinning Φ_{as} if it has the lowest mark compared to all points in a circle $B(x_i, Z)$ centered at AP location x_i with radius Z, where Z is the minimum distance between APs. The Palm probability of retaining a typical point x_i in Φ_{as},

$$p = \frac{1 - e^{-\lambda_a \pi Z^2}}{\lambda \pi Z^2}, \tag{A.8}$$

and the density of Φ_{as} is $\lambda_{\text{as}} = p\lambda_a$, which can be written as $\lambda_{\text{as}} = \frac{1-e^{-\lambda\pi Z^2}}{\lambda_a \pi Z^2}\lambda_a = \frac{1-e^{-\lambda_a \pi Z^2}}{\pi Z^2}$. STA at point y_i associated with AP at point x_i forms a circle $(B(y_i, \|y_i - x_i\|))$ centered at y_i with radius $\|y_i - x_i\|$. Let $N_{\text{S}}(B(y_i, \|y_i - x_i\|))$ represent the number of points in each $B(y_i, \|y_i - x_i\|)$ in Φ_{as} and $N(B(y_i, \|y_i - x_i\|))$ be the number of points in the original PPP Φ_a. The probability that a point in Φ_a is not retained in Φ_{as} is $\tilde{p} = 1 - p$. By definition, the number of points in any set $B \subset \mathbb{R}^2$ is a Poisson

R.V. with mean $\lambda|B|$, i.e. [40],

$$P\left(\Phi\left(B\right)=k\right)=e^{-\lambda|B|}\frac{\left(\lambda|B|\right)^{k}}{k!}. \tag{A.9}$$

Let $P[(B\left(y_i,\|y_i-x_i\|\right))=0]$ represent the probability that no other AP offers strongest SINR other than the AP located at point j and using (A.9):

$$\begin{aligned}
&P[N_{\mathrm{S}}\left(B\left(y_i,\|y_i-x_i\|\right)\right)=0]=\sum_{k=0}^{\infty}P[N\left(B\left(y_i,\|y_i-x_i\|\right)\right)=k]\times\tilde{p}^{k}\\
&=\sum_{q=0}^{\infty}e^{-\lambda_a\pi\|y_i-x_i\|^2}\times\frac{\left(\lambda_a\pi\|y_i-x_i\|^2\right)^{q}}{q!}\left(1-p\right)^{q}\\
&=\exp\left(-\lambda_a\pi\|y_i-x_i\|^2\right)\times\exp\left(\lambda_a\pi\|y_i-x_i\|^2\right)-\exp\left(\pi\|y_i-x_i\|^2\lambda_{as}\right),
\end{aligned}$$

therefore,

$$\begin{aligned}
f\left(\|y_i-x_i\|\right)&=\frac{\partial}{\partial d_{jk}}\left(P[N_{\mathrm{S}}\left(B\left(y_i,\|y_i-x_i\|\right)\right)=0]\right)\\
&=2\pi\lambda_{as}\|y_i-x_i\|\exp\left(-\pi\lambda_a\|y_i-x_i\|\right). \quad \square
\end{aligned}$$

Appendix B

Appendix to Chapter 4

B.1 Proof of Lemma 4.2

To prove Equation (4.32), we begin by deriving the probability that STA_n achieves target SINR γ. From (4.18), the probability $\mathbb{P}\left[\text{SINR}_n \geq \gamma\right]$ is:

$$= \left|\mathbf{W}_n^H \boldsymbol{\Theta}_n \mathbf{R}_n \mathbf{W}_n\right|^2 \geq \gamma \left(\left| \sum_{\kappa \in \mathcal{K}, \kappa \neq n | \mathcal{K} \subset \mathcal{N}} \mathbf{W}_n^H \left(\mathbf{R}_\kappa \cdot \boldsymbol{\Theta}_\kappa + \mathbb{E}\left[\mathbf{n}_o \mathbf{n}_o^H\right] \right) \mathbf{W}_n \right|^2 \right) \tag{B.1}$$

$$= \left|\mathbf{W}_n^H \boldsymbol{\Theta}_n \mathbf{R}_n \mathbf{W}_n\right|^2 \geq \left| \gamma \left(\sum_{\kappa \in \mathcal{K}, \kappa \neq n | \mathcal{K} \subset \mathcal{N}} \mathbf{W}_n^H \left(\mathbf{R}_\kappa \cdot \boldsymbol{\Theta}_\kappa + \mathbb{E}\left[\mathbf{n}_o \mathbf{n}_o^H\right] \right) \mathbf{W}_n \right) \right|^2 \tag{B.2}$$

$$= \left|\mathbf{W}_n^H \boldsymbol{\Theta}_n \mathbf{R}_n \mathbf{W}_n\right|^2 \geq \left| \mathbf{W}_n^H \left(\sum_{\kappa \in \mathcal{K}, \kappa \neq n | \mathcal{K} \subset \mathcal{N}} \gamma \mathbf{R}_\kappa \cdot \boldsymbol{\Theta}_\kappa \right) \mathbf{W}_n \right|^2 + \gamma \mathbb{E}\left[\mathbf{n}_o \mathbf{n}_o^H\right] \cdot \left\|\mathbf{W}_n^H\right\| \tag{B.3}$$

$$= \mathbb{E}\left[\exp\left(-\gamma \left\|\mathbf{W}_n\right\|^2 \left| K_r \sigma_{n_o}^2 \mathbf{I}_{K_r} \right|^2 \right) \right. \tag{B.4}$$

$$\left. \exp\left(-\gamma \left| \mathbf{W}_n^H \underbrace{\left(\sum_{\kappa \in \mathcal{K}, \kappa \neq n | \mathcal{K} \subset \mathcal{N}} \left| e^{j 2 \theta_\kappa} U_t \mathcal{E}_x \mathbf{I}_{U_t} \right|^2 \cdot \mathbf{R}_\kappa \right)}_{P_I} \mathbf{W}_n \right|^2 \right) \right]$$

$$= \exp\left(-\gamma \left\|\mathbf{W}_n\right\|^2 \left| K_r \sigma_{n_o}^2 \mathbf{I}_{K_r} \right|^2 \right) \tag{B.5}$$

$$\mathbb{E}_{P_I}\left[\exp\left(-\gamma\left|\mathbf{W}_n^H\left(\sum_{\kappa\in\mathcal{K},\kappa\neq n|\mathcal{K}\subset\mathcal{N}}\left|e^{j2\theta_\kappa}U_t\mathcal{E}_x\mathbf{I}_{U_t}\right|^2\mathbf{R}_\kappa\right)\mathbf{W}_n\right|^2\right)\right]$$

$$= \exp\left(-\gamma\left\|\mathbf{W}_n\right\|^2\left|K_r\sigma_{n_o}^2\mathbf{I}_{K_r}\right|^2\right)\exp\left(-\gamma\left|\mathbf{W}_n^H\left(\sum_{\kappa\in\mathcal{K},\kappa\neq n|\mathcal{K}\subset\mathcal{N}}\left|e^{j2\theta_\kappa}U_t\mathcal{E}_x\mathbf{I}_{U_t}\right|^2\mathbf{R}_\kappa\right)\mathbf{W}_n\right|^2\right) \tag{B.6}$$

$$= \exp\left(-\gamma\left\|\mathbf{W}_n\right\|^2\left|K_r\sigma_{n_o}^2\mathbf{I}_{K_r}\right|^2\right)$$
$$\cdot\exp\left(-\gamma\left|\mathbf{W}_n^H\left(\left|e^{j2\theta_\kappa}U_t\mathcal{E}_x\mathbf{I}_{U_t}\right|^2\mathbb{E}_{\kappa\in\mathcal{N}\setminus n}\left[\sum_{\kappa\in\mathcal{K},\kappa\neq n|\mathcal{K}\subset\mathcal{N}}\mathbf{R}_\kappa\right]\right)\mathbf{W}_n\right|^2\right) \tag{B.7}$$

where (B.3) follows from substituting Eqn. (4.20) into (B.1), (B.4) is obtained from the exponential property of the CSI, (B.5) follows from the fact that (B.4) is an expectation of the interference power P_I received from other concurrently transmitting STAs. The expectation of the interference power w.r.t to each interference channel $\mathbf{H}_\kappa$ of source κ is captured in (B.6) where $\mathbf{R}_\kappa = \mathbb{E}\left[\mathbf{H}_\kappa\mathbf{H}_\kappa^H\right]$ is given by Eqn. (4.22), the expectation of the correlation matrix of the interference source. Then (B.7) is an expectation of interference power over a set $\mathcal{K}$ of stochastic interference points and by substituting $\mathbf{R}_\kappa$ in (B.7) with Eqn. (4.22), we have

$$= \Psi\cdot\exp\left(-\gamma\left|\mathbf{W}_n^H\left(\left|e^{j2\theta_\kappa}U_t\mathcal{E}_x\mathbf{I}_{U_t}\right|^2\cdot\mathbb{E}_{\kappa\in\mathcal{N}\setminus n}\left[\sum_{\kappa\in\mathcal{K},\kappa\neq n|\mathcal{K}\subset\mathcal{N}}J_0\left(\Delta\psi_y\frac{2\pi}{\omega}\right)\right]\right)\mathbf{W}_n\right|^2\right)$$
$$= \Psi\cdot\exp\left(-\gamma\left|\mathbf{W}_n^H\left(\left|e^{j2\theta_\kappa}U_t\mathcal{E}_x\mathbf{I}_{U_t}\right|^2\cdot\lambda_n\cdot\int_0^\infty J_0\left(\Delta\psi_y\frac{2\pi}{\omega}\right)\right)\mathbf{W}_n\right|^2\right) \tag{B.8}$$

where $\Psi = \exp\left(-\gamma\left\|\mathbf{W}_n\right\|^2\left|K_r\sigma_{n_o}^2\mathbf{I}_{K_r}\right|^2\right)$, (B.8) is obtained by applying *Slivnyak-Mecke*'s theorem, $\mathbb{E}\sum_{x\in\Phi}f\left(x,\Phi\setminus x\right) = \lambda\int_{\mathbb{R}^d}\mathbb{E}f\left(x,\Phi\right)dx$ [40], [28]. Then by simplifying the $\int_0^\infty J_0\left(\cdot\right)$ term using the integral transformation [110, Eqn. 6.554.1], (B.8) evaluates to a closed-form expression, which proves Equation (4.32). □

Appendix C

Appendix to Chapter 5

C.1 Proof of Lemma 5.1

For WiGig APs to detect only Wi-Fi signals, the first condition in Eqn. (5.7) is the Palm probability of retaining x_j in $\tilde{\Phi}_{WG}$ following contention process and can be re-written as:

$$\begin{aligned} p_{x_j \in \tilde{\Phi}_{WG}} &= \mathbb{P}\left\{x_j \in \tilde{\Phi}_{WG} \middle| m(x_j) < m(\tilde{x}_j) \forall \tilde{x}_j \in \Phi_{WG} \setminus x_j\right\} \\ &= \mathbb{P}\left\{x_j \in \tilde{\Phi}_{WG} \middle| m(x_j) = t, P^{rx}_{(\tilde{x}_j, x_j)} < \Gamma_{WG}, \forall \tilde{x}_j \in \Phi_{WG} \setminus x_j\right\} \\ &= \int_0^1 \mathbb{P}\left(\frac{P_{\tilde{x}_j} G_{\tilde{x}_j, x_j} \left(\frac{c}{4\pi f_c}\right)^2}{\|\tilde{x}_j - x_j\|^{\alpha} t} < \Gamma_{WG}\right) dt = \\ &\int_0^1 1 - \exp\left(-\frac{\Gamma_{WG} \|\tilde{x}_j - x_j\|^{\alpha}}{P_{\tilde{x}_j} \left(\frac{c}{4\pi f_c}\right)^2} t\right) dt = \frac{1 - \exp\left(-\lambda_{WG} \Theta\right)}{\lambda_{WG} \Theta}, \end{aligned} \tag{C.1}$$

and using polar coordinates and given a volume b_2 of a unit ball $\mathcal{B}(x_j, \mathcal{R})$ centered at x_j in $\mathbb{R}^2$, $\Theta = b_2 \mathcal{R}$ and is:

$$\Theta = 2\pi \int_{\mathbb{R}^+} 1 - \left(1 - \exp\left(-\frac{\Gamma_{WG} \|\tilde{x}_j - x_j\|^{\alpha}}{P_{\tilde{x}_j} \left(\frac{c}{4\pi f_c}\right)^2}\right)\right) \|\tilde{x}_j - x_j\| \, \mathrm{d} \, \|\tilde{x}_j - x_j\| \tag{C.2}$$

$$\Theta = -\exp\left(-\frac{\Gamma_{WG}\left\|\tilde{x}_j - x_j\right\|^{\alpha}}{P_{\tilde{x}_j}\left(\frac{c}{4\pi f_c}\right)^2}\right) \Big/ \alpha \cdot \frac{\Gamma_{WG}}{P_{\tilde{x}_j}\left(\frac{c}{4\pi f_c}\right)^2}, \iff \alpha = 2. \tag{C.3}$$

Eq. (C.3) is obtained by simplifying Eq. (C.2) with the help of [110, Eqn 2.33.12]. The closed-form expression in Eq. (C.3) is valid if $\alpha = 2$, and since $\alpha = 2$ is the path loss exponent for mmWave environment as specified in IEEE 802.11ad [33], [22], Eq. (C.3) holds. By substituting Eqn. (C.3) into Eqn. (C.1), we have a desired expression for the first condition in (5.7). The second condition $\mathbb{P}\{P^{rx}_{(y_i,x_j)} < \Gamma^{ed}_{WG}\}$ implies that a WiGig AP x_j does not detect any active NR-U transmission above a threshold Γ^{ed}_{WG} through energy detection, which is derived as

$$\mathbb{P}\left\{P^{rx}_{(y_i,x_j)} < \Gamma^{ed}_{WG}\right\} = \mathbb{P}\left(\frac{P_{y_i}G_{x_j,y_i}\left(\frac{c}{4\pi f_c}\right)^2}{\left\|x_j - y_i\right\|^{\alpha}} < \Gamma^{ed}_{WG}\right) \tag{C.4}$$

$$= \mathbb{P}\left(G_{x_j,y_i} > \frac{\Gamma^{ed}_{WG}}{P_{y_i}\left(\frac{c}{4\pi f_c}\right)^2}\left\|x_j - y_i\right\|^{\alpha}\right) \tag{C.5}$$

$$= \mathbb{E}_{\Phi_{NR}}\left[\prod_{y_i}\left(1 - \exp\left(-\frac{\Gamma^{ed}_{WG}}{P_{y_i}\left(\frac{c}{4\pi f_c}\right)^2}\left\|x_j - y_i\right\|^{\alpha}\right)\right)\right] \tag{C.6}$$

$$= \exp\left(-\lambda_{NR}\int_{\mathbb{R}^2}\exp\left(-\frac{\Gamma^{ed}_{WG}}{P_{y_i}\left(\frac{c}{4\pi f_c}\right)^2}\left\|x_j - y_i\right\|^{\alpha}\right)\mathrm{d}\left\|x_j - y_i\right\|\right) \tag{C.7}$$

$$= \exp\left(-\lambda_{NR}\frac{1}{2}\sqrt{\pi\left(\frac{\Gamma^{ed}_{WG}}{P_{y_i}\left(\frac{c}{4\pi f_c}\right)^2}\right)^{-1}}\operatorname{erf}\left(\sqrt{\frac{\Gamma^{ed}_{WG}}{P_{y_i}\left(\frac{c}{4\pi f_c}\right)^2}}\left\|x_j - y_i\right\|\right)\right) \tag{C.8}$$

where (C.6) follows from the exponential property of $G(\cdot)$ given in Eqn. (5.3) and is a random variable characterized by Chi-Square distribution with $2N$ DoF, (C.7) is obtained by applying *Slivnyak-Mecke*'s theorem $\mathbb{E}\sum_{x\in\Phi} f(x, \Phi \setminus x) = \lambda \int_{\mathbb{R}^d} \mathbb{E}f(x, \Phi)\, dx$ [40] and (C.8) is obtained using [110, Eqn 2.33.16] where $\operatorname{erf}(\cdot)$ is the error function. Putting Eqns (C.1)

and (C.4) together proves Eqn. (5.7) and it is apparent that the probability of a WiGig AP transmitting depends on winning contention and detecting no active NR-U gNB within the CSR; the CAP of a WiGig AP is reduced when coexisting with NR-U gNBs □.

C.2 Proof of Lemma 5.3

$$\mathcal{P}_{NR} = \mathbb{E}\left[\sum_{y_i\in\Phi_{NR}} \mathbb{1}_{\mathrm{SINR}_{NR}>\gamma}\right] = \mathbb{P}\left(\mathrm{SINR}_{NR}\geq\gamma\right) = \mathbb{P}\left(\frac{P_{y_i}G_{o,y_i}\left(\frac{c}{4\pi f_c}\right)^2}{\|y_i\|^{\alpha}} \geq \gamma BW\sigma_o^2\right.$$

$$\left. +\gamma\sum_{\hat{y}_i\in\tilde{\Phi}_{NR}\setminus y_i} P_{\hat{y}_i}G_{\hat{y}_i,y_i}\left(\frac{c}{4\pi f_c}\right)^2 + \gamma\sum_{x_j\in\tilde{\Phi}_{WG}} P_{x_j}G_{y_i,x_j}\left(\frac{c}{4\pi f_c}\right)^2\right) \tag{C.9}$$

$$= N_o\mathbb{E}_{\tilde{\Phi}_{NR}}\left[\prod_{\hat{y}_i} e^{-\gamma\frac{P_{\hat{y}_i}G_{\hat{y}_i,y_i}\left(\frac{c}{4\pi f_c}\right)^2}{\|\hat{y}_i-y_i\|^{\alpha}}}\right]\mathbb{E}_{\tilde{\Phi}_{WG}}\left[\prod_{x_j} e^{-\gamma\frac{P_{x_j}G_{y_i,x_j}\left(\frac{c}{4\pi f_c}\right)^2}{\|y_i-x_j\|^{\alpha}}}\right] \tag{C.10}$$

$$= N_o\exp\left(-\tilde{\lambda}_{NR}\int_{\mathbb{R}^2} e^{-\gamma\frac{P_{\hat{y}_i}G_{\hat{y}_i,y_i}\left(\frac{c}{4\pi f_c}\right)^2}{\|\hat{y}_i-y_i\|^{\alpha}}}\,\mathrm{d}\,\|\hat{y}_i-y_i\|\right) \tag{C.11}$$

$$\exp\left(-\tilde{\lambda}_{WG}\int_{\mathbb{R}^2} e^{-\gamma\frac{P_{x_j}G_{y_i,x_j}\left(\frac{c}{4\pi f_c}\right)^2}{\|y_i-x_j\|^{\alpha}}}\,\mathrm{d}\,\|y_i-x_j\|\right)$$

$$= N_o\exp\left(-\frac{\tilde{\lambda}_{NR}}{2}\sqrt{\frac{\pi}{\gamma P_{\hat{y}_i}G_{\hat{y}_i,y_i}\left(\frac{c}{4\pi f_c}\right)^2}}\mathrm{erf}\left(\sqrt{\gamma P_{\hat{y}_i}G_{\hat{y}_i,y_i}\left(\frac{c}{4\pi f_c}\right)^2}\right)\right) \tag{C.12}$$

$$\cdot\exp\left(-\frac{\tilde{\lambda}_{WG}}{2}\sqrt{\frac{\pi}{\gamma P_{x_j}G_{y_i,x_j}\left(\frac{c}{4\pi f_c}\right)^2}}\mathrm{erf}\left(\sqrt{\gamma P_{x_j}G_{y_i,x_j}\left(\frac{c}{4\pi f_c}\right)^2}\right)\right)$$

where $N_o = \exp\left(-\gamma BW\sigma_o^2\right)$, (C.10) follows from the exponential property of the received power and the independence of $\tilde{\Phi}_{NR}$ and $\tilde{\Phi}_{WG}$, (C.11) is obtained by applying *Slivnyak-Mecke*'s theorem [40]. Since $\alpha = 2$, (C.12) is obtained using [110, Eqn 2.33.16]. The *Proof* of $\mathcal{P}_{WG}$ in Eqn. (4.32) is similar. □